Seismic Microzonation and Vulnerability of Highway Bridges in Montreal

by

Alejandro Gaspar DE LA PUENTE ALTEZ

October 2005

Department of Civil Engineering and Applied Mechanics
McGill University, Montreal, Canada

A thesis submitted to the Faculty of Graduate Studies and Research in partial fulfillment of the requirements for the degree of Doctor of Philosophy

© Alejandro Gaspar de la Puente Altez, 2005

Library and Archives Canada

Published Heritage Branch

395 Wellington Street
Ottawa ON K1A 0N4
Canada

Bibliothèque et Archives Canada

Direction du Patrimoine de l'édition

395, rue Wellington
Ottawa ON K1A 0N4
Canada

Your file Votre référence
ISBN: 978-0-494-25127-0
Our file Notre référence
ISBN: 978-0-494-25127-0

NOTICE:
The author has granted a non-exclusive license allowing Library and Archives Canada to reproduce, publish, archive, preserve, conserve, communicate to the public by telecommunication or on the Internet, loan, distribute and sell theses worldwide, for commercial or non-commercial purposes, in microform, paper, electronic and/or any other formats.

The author retains copyright ownership and moral rights in this thesis. Neither the thesis nor substantial extracts from it may be printed or otherwise reproduced without the author's permission.

AVIS:
L'auteur a accordé une licence non exclusive permettant à la Bibliothèque et Archives Canada de reproduire, publier, archiver, sauvegarder, conserver, transmettre au public par télécommunication ou par l'Internet, prêter, distribuer et vendre des thèses partout dans le monde, à des fins commerciales ou autres, sur support microforme, papier, électronique et/ou autres formats.

L'auteur conserve la propriété du droit d'auteur et des droits moraux qui protège cette thèse. Ni la thèse ni des extraits substantiels de celle-ci ne doivent être imprimés ou autrement reproduits sans son autorisation.

In compliance with the Canadian Privacy Act some supporting forms may have been removed from this thesis.

While these forms may be included in the document page count, their removal does not represent any loss of content from the thesis.

Conformément à la loi canadienne sur la protection de la vie privée, quelques formulaires secondaires ont été enlevés de cette thèse.

Bien que ces formulaires aient inclus dans la pagination, il n'y aura aucun contenu manquant.

Canada

Abstract

Ground Ambient Noise (GAN) readings were recorded across the island of Montreal and the recordings were processed using the horizontal-to-vertical spectral ratio technique. One-dimensional non-linear soil dynamic analyses were performed over a large database of boreholes in Montreal using the computer program SHAKE. The resulting predominant frequencies of vibration were used as the main parameter to define the seismic microzonation of the island of Montreal. The frequencies are mapped and used to identify twelve zones with potential seismic amplification problems. The largest ratio was obtained in the zone located at the eastern tip of the island of Montreal where long-period motions are predominant in the deep clay deposits.

The Incremental Dynamic Analysis (IDA) technique was used to study the seismic vulnerability of two typical lifeline highway overpass bridges in Montreal. The moment resisting frame components of the two bridges were studied and evaluated for different cases reflecting the condition of the concrete columns and their reinforcement, in accordance with the Canadian Highway Bridge Design Code (CHBDC). The frames were subjected to a wide range of earthquakes as part of the IDA study. The insufficient shear reinforcement of some frame elements of both bridges predicted a premature shear failure, which controlled the seismic behaviour of the frames. The predicted failures occurred at a lower spectral acceleration level than the acceleration specified by the CHBDC for both lifeline bridges.

A minimum-intervention retrofitting approach was devised for each one of the overpass bridges. In both cases, provisions were made to ensure that flexural yielding would occur before shear failures of the critical elements. The retrofitted frames are predicted to sustain higher levels of spectral acceleration in excess of 0.8 g.

Résumé

De multiples mesures du bruit de fond (GAN) ont été effectuées sur le territoire de l'île de Montréal afin de caractériser la réponse dynamique des dépôts de sols superficiels en fonction du rapport des composantes spectrales horizontales et verticales. Des analyses dynamiques unidimensionnelles et non-linéaires ont été effectuées avec le logiciel SHAKE à partir d'une base de données de forages géotechniques pour l'île de Montréal. Les fréquences fondamentales obtenues avec les deux types d'analyse ont été utilisées afin de définir la microzonation sismique de l'île de Montréal. Les fréquences fondamentales ont été utilisées afin d'identifier 12 zones susceptibles d'amplifier les secousses sismiques. La zone la plus sévère correspond à des dépôts profonds d'argile à l'extrémité est de l'île.

Une analyse dynamique par incréments a été utilisée pour évaluer la vulnérabilité sismique de deux viaducs essentiels typiques à Montréal. Les composants du cadre rigide de deux viaducs ont été analysés et évalués pour différentes conditions représentatives de la condition du béton et de l'armature des colonnes suivant les critères du Code canadien sur les ponts (CHBDC, Canadian Highway Bridge Design Code). Les cadres ont été soumis à une large gamme de séismes dans le cadre de l'analyse dynamique par incréments. Les analyses indiquent que plusieurs éléments des deux viaducs sont déficients en cisaillement. Il en résulterait une défaillance prématurée des viaducs en cisaillement lors d'un séisme pour une accélération spectrale inférieure à celle spécifiée dans le code pour les lignes de vie.

Des solutions de mitigation minimales ont été développées pour chacun des deux viaducs. Dans les deux cas, les renforcements ont été conçus afin de favoriser une déformation plastique en flexion des éléments critiques au lieu d'une rupture par cisaillement. Les modèles indiquent que les solutions envisagées permettront aux viaducs de résister à des séismes avec des accélérations spectrales supérieures à 0.8g.

Table of Contents

List of Tables

List of Figures

Acknowledgements

No amount of words can express enough gratitude and appreciation to the large number of people that was involved in this project. In particular, the author would like to mention the following people:

Prof. Luc Chouinard and Prof. Denis Mitchell, for their invaluable counselling, guidance, and patience during these years

Philippe Rosset, for his ideas, initial work, constructive critics, and commentaries on the seismic microzonation part

John Adams and the Geological Survey of Canada, for their support with equipment for the seismic microzonation part

To the City of Montreal, for providing the borehole database and city maps used in this research; and the Ministère des transports du Québec for the drawings of the overpass bridges

Ricardo Madriz, for his help during the field measurements and borehole collecting, as part of his Master's program

To my office colleagues, for making the journey of a Ph.D. a rather enjoyable experience

The entire Staff of the Department of Civil Engineering and Applied Mechanics, who helped solve those little problems that students always have

To my Family and friends of Peru, who always found a way to keep me going

To the Natural Sciences and Engineering Research Council of Canada (NSERC) and the Fonds québécois de la recherche sur la nature et les technologies, for the financial support and research funds received

A mi padre que me inculcó ser mejor, siempre. A mi madre que siempre estuvo ahí para ayudarme a serlo.

To my father who told me to be better, always. To my mother who always was there to help me do it.

Chapter 1

Introduction

1.1 Background

Although major earthquakes in Eastern Canada might have been relatively frequent in the nineteenth century, they were relatively infrequent in the twentieth century. This may have led to a lack of concern in earthquake engineering in Eastern Canada. However, a recent event like the Saguenay Earthquake of 1988 has reminded the community about the destructive potential of earthquakes. The Montreal Urban Community, with its 3.5 million population (city and suburbs), was rated second-place in the nation (after Vancouver) on a scale of urban seismic risk, as shown in Figure 1-1 (Adams *et al*, 2002). The surface geology of the island is composed of quaternary glacial-fluvial deposits of till, clay and sand over bedrock (Prest and Hode Keyser, 1977). In addition, thick layers of soft soils are located close to existing and ancient riverbeds and can greatly amplify seismic waves, as recognized by many authors (e.g.: Reiter, 1990). This effect, soil amplification, has been observed for some buildings in Montreal during the last Saguenay Earthquake (Mitchell *et al*, 1989), where a masonry building founded on a 17-m layer of clay was damaged. There is a need to estimate the potential for damage to infrastructure, and hence seismic microzonation is important to determine where such damage could be greater. Microzonation gives estimates of the dominant frequency of soil deposits and the amplification factor for ground motion for different regions. Therefore, microzonation is an important step in performing a seismic hazard analysis of the Montreal Urban Community.

As an island and a major urban centre, Montreal is a hub for highways and it is dependant on its lifelines, such as bridges. Most of these bridges were built in the early

1960s or 1970s, when seismic codes were not well developed, with many of these bridges lacking proper seismic design and having poor reinforcement detailing (Griezic, 1996). Deficiencies in these older bridges include inadequate amounts of shear and confinement reinforcement, poor anchorage details of transverse reinforcement and the use of lap splices in potential plastic hinge regions. In addition, several of these bridges are in a poor state due to the cumulative deterioration due to poor quality concrete, inadequate concrete cover and from years of service under severe environmental conditions (Basheer *et al*, 1996). The current state of these bridges is an additional concern relative to their performance during a severe earthquake.

The objective of the proposed research is to assess the seismic performance of typical existing bridges in Montreal and to make recommendations relative to possible mitigation plans. Two very different bridges were selected: St. Jean Boulevard bridge crossing the CN and CP railway lines, and the St. Jean Boulevard bridge crossing Autoroute 40.

1.2 Problem Definition

The surficial soil deposits on the island of Montreal can amplify seismic waves and hence it is necessary to investigate this important aspect. In addition, the seismic hazard, in terms of the Uniform Hazard Spectrum (UHS) approach has been implemented to provide more realistic assessment of the seismic hazard of major urban centres (NBCC, 2005).

The potential damage to the city's infrastructure needs to be estimated using this newly defined hazard. The first problem addressed in this research is to set the groundwork for seismic microzonation, which is the first step towards a complete seismic hazard analysis for Montreal.

1.3 Research Objectives

The objectives of this research program are:

✓ To contribute to the seismic microzonation of the city of Montreal

✓ To investigate the seismic vulnerability of representative highway overpass bridges using the provisions of the 2000 Canadian Highway Bridge Design Code (Canadian Standards Association, 2000)

1.4 Organization of the Thesis

There are two main research topics in this thesis: The Seismic Microzonation of Montreal, and the Seismic Vulnerability of Overpasses. To accomplish this, the thesis discusses in the first two chapters the previous relevant research work and tools that have been developed. The third chapter discusses the methodology employed in assessing the microzonation of Montreal. The fourth chapter presents the results and comments of the maps that are the results of the preliminary microzonation work. The fifth chapter presents the seismic evaluation and retrofit studies for the bridge crossing the CN and CP railway lines. Chapter 6 presents the studies carried out on the St-Jean overpass crossing Autoroute 40. The conclusions, recommendations and suggestions for future research are presented in the seventh chapter of this thesis.

Finally, two appendices are included, that describe the two computer programs that were developed and used in this thesis. These include *Excel Shake*, to process in an easier way the boreholes database using *SHAKE91* (Idriss and Sun, 1992), and *Ruaumoko Helper*, to create the input file for the structural analysis using Ruaumoko 3D (Carr, 2001) and to perform the Incremental Dynamic Analysis.

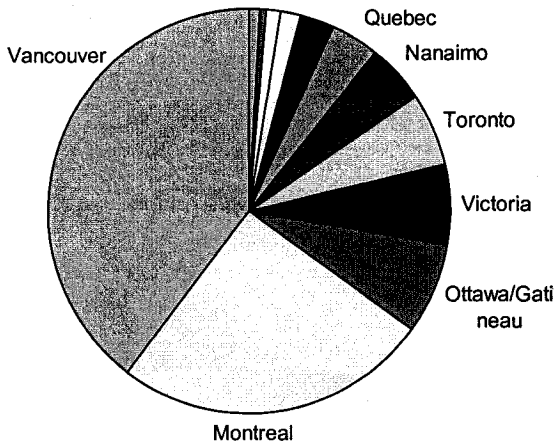

Figure 1-1 Vulnerability Index (*Population x Probability of Damage*) for major cities in Canada (after: Adams *et al*, 2002)

Chapter 2

Literature Review

This research is motivated by the desire to a more effective way to assess the potential damage of earthquakes on important infrastructure of the city of Montreal. The first step is to conduct a seismic microzonation study of the island. All the microzonation methods involve an assessment of the influence of the soil layers, either by vibration measurements or by soil amplification predictions. For this study, both methods were used for assessing the site effects. In this chapter, the seismicity and geology of the region will be reviewed first, followed by a review of the two methods used for the microzonation studies. Bridges are key structures of the infrastructure that might be damaged in the event of an earthquake. The second part of the chapter reviews the techniques and procedures for the analysis of two older bridges, including the novel Incremental Dynamic Analysis (IDA) method and its application to this research.

2.1 The Seismic Hazard of the Region of Montreal

As pointed out by many authors, the eastern part of the North America continent has relatively moderate seismicity. About one-half of the Canadian landmass has too few earthquakes to define reliable source zones, and on prior maps, the hazard computed for these regions came only from distant external sources (Adams *et al*, 1999). The 1988 Saguenay Earthquake raised questions concerning the validity of the underlying source model for large events and the adequacy of the knowledge concerning Eastern North America source spectra (Atkinson and Boore, 1995). Since 1988, new research has been carried out to improve the seismic models of the region. A new model based on the

Cornell-McGuire probabilistic approach (Cornell, 1968; McGuire, 1995) along with new ground motion relations that were revised after the Saguenay Earthquake of 1988 (Atkinson and Boore, 1995) have been used for the development of the Uniform Hazard Spectra (UHS) (Adams *et al*, 1999) for eastern Canada. Figure 2-1 shows the 5% damped horizontal component spectra for the 50 and 84 percentile for annual probabilities of exceedance of 2% and 10% in 50 years for the "robust approach". This Uniform Hazard Spectrum approach involves combining the effects from different sources that give a uniform probability of exceedance for all the ordinates of the spectrum. The UHS maps along with the spectral values for different locations in Canada have been adopted by the Canadian National Committee on Earthquake Engineering in developing the 2005 Edition of the National Building Code of Canada (Adams and Atkinson, 2003; Adams *et al*, 1999).

2.1.1 Ground Motion Records

Strong ground motion records for the Montreal area are not available and hence records from other sources or records generated through simulation must be used. Atkinson and Beresnev (1998) generated compatible ground-motion time histories based on the new seismic hazard maps that are compatible with the Uniform Hazard Spectra (UHS), for several major cities. The target UHS for these time history simulations are the GSC 5% damped horizontal-component spectra for "firm ground" (Class B, close to Basal Till) sites for an annual probability of 1/500 and 1/2475. These artificially simulated accelerogram records provide a realistic representation of ground motion for the epicentral distances and magnitudes that contribute most strongly to the hazard and probability level of the selected cities (in this case Montreal) (Atkinson and Beresnev, 1998). For each city, horizontal components are generated for a moderate earthquake located nearby, and horizontal components are generated for a larger earthquake farther away. These accelerograms respectively match the short- and long-period ends of the target UHS (Atkinson and Beresnev, 1998). A suite of earthquakes is needed because a disadvantage of Probabilistic Seismic Hazard Analysis is that the concept of a "design earthquake" is

lost due to its integrative nature (McGuire, 1995). Probabilistic Seismic Hazard Analysis calculates a combined probability of exceedance that incorporates the relative frequencies of occurrence of different earthquakes and ground-motion characteristics by integrating over all possible earthquake occurrences and ground motions (McGuire, 1995). If different seismic sources dominate the hazard at different frequencies, then contributions to the hazard come from significantly different magnitudes, distances, and the number of standard deviations, so that a single design earthquake is not appropriate (McGuire, 1995).

Numerous studies have shown that simulated records and real records are functionally equivalent, for use in linear and non-linear structural analyses (i.e., Tremblay and Atkinson, 2001). Although real records can have several characteristics that simulated records do not have, new earthquake records may not resemble historical records. The advantage of the simulation approach lies in generalizing the gross features of past events that are repeatable (Atkinson and Beresnev, 1998; Filiatrault *et al*, 2004; Tremblay and Atkinson, 2001). The unrestricted use of real records from a different area (i.e., California) may not be appropriate. One alternative is to use records from regions of similar tectonic environment (i.e., intraplate regions for Eastern Canada), which present a problem of scaling; another is to use simulated records. Simulated time histories include the main characteristics of past events that are repeatable, such as average amplitudes and frequency content as a function of magnitude and distance, while accounting for the features of ground motion which are random (Filiatrault *et al*, 2004; Tremblay and Atkinson, 2001).

The scaling of earthquake records is a major issue among researchers; there is no consensus on scaling limits. Some recommend a limit of two or less on scaling factors in order to avoid distortion of the spectral properties of the records (Vanmarcke, 1979). Others have scaled records to a factor of 11 (Luco and Bazzurro, 2004) . Luco and Bazzurro (2004) propose a bias (defined by the ratio between the median response to

scaled records and the median response to unscaled records) as a measure of the influence of scaling on the nonlinear response of structures to the scaled records. They suggest the use of statistical biases to correct the response of structures, however the use of this approach is not necessary for the application of the Incremental Dynamic Analysis method. For soil dynamic analysis, there is no mention of scaling limits except that some researchers have used relatively low scaling factors for studying this effect.

2.1.2 Geology of Montreal

The city of Montreal is situated around a region with predominantly sedimentary rocks belonging to the Upper Cambrian and Ordovician periods, which in turn rest on a Precambrian basement. On top of these old rock formations, younger layers of soil and rock from the Wisconsinan Glacial Sub-stage of the Quaternary Period form the majority of the stiff soil deposits of the region. These deposits are known as tills (from older to younger): Malone Till, Middle Till Complex and Fort Covington Till. See Table 2-1 for more details and Prest and Hode Keyser (1977) for a comprehensive geological review.

Late glacial and post-glacial events, through land glacial uplifting, rapid deglaciation and sea flooding, deposited debris of soft material in several parts of the St Laurent River Valley, which resulted in patches of Leda Clay and Saxicava Sand through the area. The land rise that defined the island of Montreal allowed, through erosion, the accumulation of more material carried by rivers and streams. Pond clay, marl and peat were deposited where ponds, abandoned rivers and bogs areas remained. This added a new dimension in the complexity of the soil deposits of the island of Montreal and surrounding areas, as shown by a very simplified surficial deposits map in Figure 2-2.

2.2 Microzonation and Site Effects

The general objectives of seismic microzonation are to quantify urban seismic hazard and risk (loss potential) by accounting for the local variations in shaking levels due

to near-surface geological differences (Jacob, 1999). These differences can influence the amplitudes and the spectral content of ground motions and, thereby, the shaking level of buildings and lifelines, and hence control the expected losses.

A recent work in determining the frequency-dependent amplification inherent in hard rock sites across Canada has been done under the assumption that it can be estimated from the ratio of the horizontal-to-vertical (H/V) components of ground motion (Siddiqqi and Atkinson, 2002). The records from an array of strong and weak motion recorders are used to determine site responses (Martirosyan *et al*, 2002). This idea is the same proposed by Nakamura for microtremors and is the core for the field analysis of the microzonation work, which is also applied elsewhere (e.g.: Aguilar *et al*, 2004; Motamed and Ghalandarzadeh, 2004; Studer *et al*, 2004; Tuladhar *et al*, 2004).

An early demonstration of site effects occurred in an earthquake in India in 1819, where different damage was observed in similar structures located on different soils (Seed and Idriss, 1982). Since then, the site response or site effect has become a well-documented phenomenon of earthquake ground motion amplified by local site (near surface) conditions (Field *et al*, 1990). Montreal's first registered earthquake was in 1732 resulting in collapsing of dwellings due to site amplification and poor construction techniques (Reiter, 1990). So great are the effects of local site conditions that the propensity for earthquake damage at some locations may be much more dependant upon these conditions than on the proximity of nearby earthquake sources. In many cases, once a general knowledge of nearby and regional earthquake sources is available it may be more beneficial, from the perspective of risk avoidance, to concentrate on local site studies rather than on refined source-related geological and seismological studies (Reiter, 1990). Often site effects are considered through coefficients applied to foundation factors in the base shear equation (Finn and Wightman, 2003) but when more information is available, a more comprehensive study is applicable.

Others (Jacob, 1999; Zembaty and Rutenberg, 2002) have performed a site effect assessment by using directly the formula of $T = 4H/V_h$, where T is the period of vibration of the soil, H is the soil depth, and V_h is the maximum shear wave velocity. Relationships of shear wave velocity versus depth were developed by using geotechnical data. These data consist of standard penetration test (SPT) blow counts and standard soil descriptions from construction-related soil borings of the city under study. Many of these relationships were determined independently of the depth. Also, the use of microtremors can help determine the shear wave profile if other parameters of the soil profile are known (Arai and Tokimatsu, 2004; Tokimatsu *et al*, 2004; Wathelet *et al*, 2004).

The best procedure for determining the site response of a particular location is to observe the ground motion during an actual event. It is therefore desirable to develop alternate methods of characterizing site amplification in high-noise urban environments and in regions such as Eastern North America where the level of seismicity is low, yet the potential for a large event is still significant. One alternate approach to wait-for-the-next-big-event involves determining the physical properties of the local setting by conducting borehole and/or seismic profile studies. Then, measured parameters can be used in theoretical models to predict the site response (Field *et al*, 1990). Although this can be very expensive in terms of carryout the geotechnical surveys, a city of median size (like Montreal) has a database of existing boreholes that could be useful for this analysis.

Another approach involves recording some ground microtremors at the site of interest. Microtremors are omnipresent low-amplitude oscillations (1 to 10 microns) that arise predominantly from oceanic, atmospheric and human disturbances. Previous work on recording microtremors had involved the use of portable seismometers to record ambient noise across a geological determined zone. In the case of the meadows of New York city (Field *et al*, 1990), resonant frequencies predicted by one-dimensional modelling of the valley centre site response show excellent agreement with observations. Also it is pointed out (Field *et al*, 1990) that those easily obtained microtremor measurements can

contribute valuable microzonation and site response information towards a study of regional earthquake hazard.

There are several experimental methods for estimating site effects. Those are the standard spectral ratio (or SSR), H/V ratio or "Nakamura" technique and the H/V spectral ratio (see Lacave *et al*, 1999). It is noted that the Nakamura method (Nakamura, 1989) is one of the most inexpensive and convenient techniques to estimate fundamental frequencies of soft deposits (Lacave *et al*, 1999). Numerical methods are useful when the geotechnical characteristics are known. A good example of a robust and simpler method is the one used by SHAKE (See for more details Schnabel *et al*, 1972). This program performs an analysis over a soil column that is excited by an incoming planar S wave. Then, the required parameters for each layer are the shear-wave velocity, density, damping and thickness (Lacave *et al*, 1999). Other programs perform complex analyses that require more knowledge of the actual non-linear material behaviour (the stiffness and damping versus the strain). Other advanced methods (2-D and 3-D modelling, boundary- and domain-based techniques) require very detailed geotechnical or geophysical investigations for the site to provide the constitutive properties needed as input parameters (Lacave *et al*, 1999). However, there is on-going research about the use of microtremors and the determination of subsurface structures, shear-wave profiles and other geotechnical parameters (Arai and Tokimatsu, 2004; Studer *et al*, 2004; Tokimatsu *et al*, 2004; Uebayashi *et al*, 2004).

2.2.1 Description of the Nakamura Method applied to Ground Ambient Noise

Ground Ambient Noise (GAN) is generated by surface sources such as traffic and other human activities, but also results from oceanic waves and wind-structure interactions (Rosset *et al*, 2003). Nakamura (1989) proposed that this noise can be utilized to estimate the predominant frequency and the amplification factor of natural soil deposits without having detailed soil characteristics. He demonstrated that the spectral ratio between horizontal and vertical ambient noise records is related to these parameters. It was

observed that the ratio between the horizontal and vertical motions of some earthquakes gave a number consistent with the soil characteristics of the site (i.e., rock, firm soil, soft soil) where such earthquakes were recorded, therefore the hypothesis that the Rayleigh-type surface waves that compose the ambient noise might play a factor. The transfer function for site effect ($S_E = H_S/H_B$) is divided by the transfer function for Rayleigh wave effect ($A_S = V_S/V_B$) to exclude source contribution ($S_M = S_E/A_S$), where H and V are the spectra for the horizontal and vertical components respectively of the ambient noise records at the surface S or the basement B (Rosset *et al*, 2002). It was demonstrated that the spectra of the horizontal H_B and vertical V_B components are equivalent at the basement or $H_B/V_B \cong 1$ (Nakamura, 1989; Theodulidis *et al*, 1996), therefore site effects can be expressed as the spectral ratio of the horizontal and vertical components of ambient noise at the surface of a site ($S_M = H_S/V_S$).

The Nakamura Method implies that an estimate of the soil response at a site can be obtained by recording about 10 to 15 minutes of ambient noise with a single 3-component seismometer (components: North-South, East-West, and vertical). This recording is divided into time windows of smaller length and for each one; smoothed spectra of the two horizontal components are combined ($H = \sqrt{H_{N-S}^2 + H_{E-W}^2}$) and the combined values are divided by the smoothed spectrum of the vertical component V. The newfound spectra of each window are combined and the average and standard deviation are calculated (Rosset *et al*, 2002; Rosset *et al*, 2003). Software called SPCRATIO was developed to facilitate this task (Rosset, 2002). This software with some variations was used in this project.

Three main hypotheses apply regarding ambient noise and this technique (Nakamura, 1989): (1) Ambient noise is generated by reflection and refraction of shear waves within superficial soil layers and by surface waves. (2) Local superficial sources of noise do not affect ambient noise at the bottom of the unconsolidated structure or

basement. (3) Soft soil layers do not amplify the vertical component of ambient noise. Although the theory and hypotheses are not unanimously accepted by the scientific community (Lacave *et al*, 1999), comparisons with other techniques have proven the validity and efficiency of the method (Lermo and Chavez-Garcia, 1994; Nakamura, 2000) (Atakan *et al*, 2004; Bard and SESAME participants, 2004; Theodulidis *et al*, 2004).

This method continues to be one of the most popular methods for microzonation when ground ambient noise is the predominant or least expensive source of information (Aguilar *et al*, 2004; Motamed and Ghalandarzadeh, 2004; Tuladhar *et al*, 2004).

The method is also used for site characterisation because of its capability of identifying soil responses, whether it is with strong motion records or microtremors. Other variations of this method involve the use of the 5% response spectrum of each component instead of the frequency spectrum to compute the H/V ratio (Zhao *et al*, 2004), having in this way a natural smoothing on the spectra.

There are drawbacks to Nakamura's method. Although the fundamental frequency is well predicted for soft and medium stiff soils, the amplification factor can be somewhat higher (Lacave *et al*, 1999), compared with other methods, such as numerical modeling. More research on the amplification issue (Tokeshi *et al*, 2004) and the application of the method in general is being carried out by others (Atakan *et al*, 2004; Bard and SESAME participants, 2004; Mucciarelli and Gallipoli, 2004).

2.2.2 Numerical method for soil amplification and SHAKE

Another way to estimate site effects and to complement the limitations of the empirical approach (i.e., amplification factor) is to perform a numerical analysis on a model of the layers of soil and then to subject it to an input ground motion. The parameters of interest are the fundamental frequency and the amplification factor of the site. Different types of models can be employed, some requiring complex sets of geotechnical data, for example two- or three-dimensional models. However, one-dimensional models are often the most convenient alternative when the soil layer structure

is not very complex (i.e. horizontal layers) and the geotechnical data only consist of borehole reports with limited dynamic soil properties.

SHAKE91® (Idriss and Sun, 1992; Schnabel *et al*, 1972) is the most used software that analyzes horizontally layered soils that can be characterized with data from a single borehole. However, its original interface is not user friendly, demanding the creation of an input file in text format for each analysis. Although more user-friendly interfaces were developed like *EERA*® (Bardet *et al*, 2000) and *SHAKE2000*® (Ordonez, 2004), an interface capable of handling a customized database (Madriz, 2004; Rosset *et al*, 2003) with hundreds of borehole data over dozens of earthquake records was developed (Excel-Shake: De la Puente and Rosset, 2002). A set of batch commands is issued to perform calculations for a group of sites and input ground records, and to store selected results in a new worksheet or external file. For a detailed explanation, see Appendix A – Excel Shake.

The numerical model idealizes the soil profile from the borehole information as a system of homogeneous, viscous-elastic sub-layers of infinite horizontal extent, each with its parameters of shear modulus, damping ratio, unit weight, and thickness, practically independent from the frequency range of interest. Shear waves, which are propagated vertically from the underlying half space bedrock to the surface produce horizontal motions that satisfy the wave equation (Schnabel *et al*, 1972):

$$\rho \frac{\partial^2 u}{\partial t^2} = G \frac{\partial^2 u}{\partial x^2} + \eta \frac{\partial^3 u}{\partial x^2 \partial t} \qquad 2\text{-}1$$

where G is the shear modulus, ρ is the density, η is the viscosity, and $u = u(x,t)$ is the horizontal motion. This is a function of the amplification of both the incident (E) and reflected wave (F), which travel in the x- or vertical direction:

$$u(x,t) = Ee^{i(kx+\omega t)} + Fe^{-i(kx-\omega t)} \qquad 2\text{-}2$$

where $k^2 = \frac{\rho\omega^2}{G(1+2i\beta)}$ is the complex wave number and β is the damping factor ($\beta = \omega\eta/2G$). The shear stress, τ, on a horizontal plane is defined by:

$$\tau(x,t) = G\frac{\partial u}{\partial x} + \eta\frac{\partial^2 u}{\partial x \partial t} = ikG(1+2i\beta)\left(Ee^{i(kx+\omega t)} + Fe^{-i(kx-\omega t)}\right)e^{i\omega t} \qquad 2\text{-}3$$

The shear stress and the displacements must be continuous between the transitions of one layer to the next. With this condition is found that the amplitudes E and F of the incident and reflected waves of the layer $m+1$ are a function of the amplitudes of the layer m located above:

$$\begin{aligned} E_{m+1} &= 1/2\,E_m(1+\alpha_m)e^{ik_m h_m} + 1/2\,F_m(1-\alpha_m)e^{-ik_m h_m} \\ F_{m+1} &= 1/2\,E_m(1-\alpha_m)e^{ik_m h_m} + 1/2\,F_m(1-\alpha_m)e^{-ik_m h_m} \end{aligned} \qquad 2\text{-}4$$

where $\alpha_m = \dfrac{\rho_m G_m(1+2i\beta_m)}{\rho_{m+1} G_{m+1}(1+2i\beta_{m+1})}$ is the complex impedance ratio, which is independent of the frequency, and h_m is the thickness of the m layer.

At the surface, there is no shear stress ($\tau_1=0$) thus $E_1=F_1$ or the amplitudes of the incident and reflected waves are always equal at the free surface. The recursion of the formulas of amplitude E_{m+1} and F_{m+1} (Equation 2-4), starting from the surface, the following relationship is obtained (Schnabel *et al*, 1972):

$$\begin{aligned} E_m &= e_m(\omega)\,E_1 \\ F_m &= f_m(\omega)\,E_1 \end{aligned} \qquad 2\text{-}5$$

These two transfer functions $e_m(\omega)$ and $f_m(\omega)$, which are a function of the impedance ratio as well, can be used to generate other transfer functions, such as the transfer function $A_{n,m}(\omega)$ between the displacements at any two layers n and m:

$$A_{n,m}(\omega) = \frac{e_m(\omega) + f_m(\omega)}{e_n(\omega) + f_n(\omega)} \qquad 2\text{-}6$$

Therefore, if the motion is known in any other layer (i.e., the half-space basement) the motion and any other parameter can be computed for other layers (Schnabel *et al*, 1972).

In this way, given an earthquake applied to the bedrock, the amplification of motion or acceleration at the surface can be estimated, thus making possible to estimate the soil amplification phenomena for the site and motion selected.

2.3 Structural Modeling and Seismic Analysis of Overpasses

A significant amount of research is being carried out to assess and minimize the vulnerability of bridges to major seismic events. For more recent structures, this vulnerability is reduced due to the major improvements in seismic design and detailing of bridge codes. However, older bridges, designed before the recent code improvements, are typically more vulnerable. In Montreal, the majority of the overpasses were built in the 1960s and 1970s, many of them with deficiencies that affect their ductility, such as: inadequate bar anchorage, splicing in critical locations, inadequate confinement and shear reinforcement, poor anchorage details, and inadequately detailed beam-column joints and column-footing joints (Griezic, 1996). In many cases, severe deterioration of the concrete cover and significant corrosion of the reinforcing steel have resulted in additional deficiencies (see Figure 2-3).

2.3.1 The Canadian Highway Bridge Design Code

The Canadian Highway Bridge Design Code (CHBDC) (Canadian Standards Association, 2000) specifies a design event corresponding to a probability of exceedance of 10% in 50 years (equivalent to a return period of 475 years) for the vast majority of bridges. Existing bridges, depending on their importance (lifeline, emergency route or other), at least must satisfy this performance criterion.

The Code presents methods for performing the analysis that depend on the importance of the bridge, the number of spans, and its seismic performance zone. These analysis methods include: (1) limited evaluation, (2) a single-mode elastic method, and, (3) a multimode elastic method. The evaluation method compares the ductility provided by the elements to the ductility required by the code. Depending on the importance of the bridge (emergency-route or greater), the number of spans and the Seismic Performance

Zone, general guidelines are provided for use of time-history methods and static pushover analyses with the formation of plastic hinges in structural members.

2.3.2 Methods for Seismic Analysis of Bridges

Seismic screening is a simplified method for ranking bridges for more detailed evaluations. This screening is carried out by ranking the bridges using a combination of three parameters (Priestley *et al*, 1996): seismicity, vulnerability and importance. Seismicity is governed mainly by site effects (Prest and Hode Keyser, 1977; Reiter, 1990). Vulnerability is governed mainly by the year of construction, and Importance can be estimated though the cost associated with bridge closure or potential for loss of life (Priestley *et al*, 1996).

In general, three main types of seismic analyses can be performed (Priestley *et al*, 1996):

(1) Capacity/Demand Ratio Analyses: It is the basic method suggested by the CHBDC. A capacity/demand ratio less than one indicates the need for retrofitting.

(2) Plastic Collapse Mechanism (Pushover) Analyses. This method is a progressive inelastic force-deformation analysis that accounts for the strength and ductility of the members. The method is not appropriate for structures having different bents or for bridges that are irregular. Only a 3-D analysis is appropriate for those cases.

(3) Inelastic Time-History Analyses. This is the most sophisticated method of analysis available. It requires careful modelling of the hysteretic response of the structural components and a very good representative suite of detailed ground motions (acceleration-time inputs). One of the best methods for evaluating the results from many time-history analyses is the Incremental Dynamic Analyses approach. The ground motions are selected to be representative of regional and local effects. They are used for time-history analysis only. The objective is to subject the structure to different events and to develop all possible sequences of failure (Shome, 1999). Non-linear analysis models can be either two-dimensional or three-dimensional. The versatility of the models is highly dependent of the

computer programs available (such as DRAIN-2DX, DRAIN-3DX, Oversees, RUAUMOKO, etc.) and of their capabilities of modeling material non-linearity and soil-structure interaction. This research will be done using RUAUMOKO (Carr, 2001).

2.3.3 Nonlinear analysis using Ruaumoko 3D

Numerous existing bridges are being analyzed using a variety of techniques and computer programs. The most detailed form of analysis involves non-linear dynamic analysis, based on the general equations of motion (Newmark, 1959). Examples of these programs include DRAIN-2DX, DRAIN-3DX, Oversees, RUAUMOKO, as well as others. This research program was carried out using RUAUMOKO 3D (Carr, 2001), mainly because it offers the following advantages:

- ✓ can model elements (i.e. frame elements) using different flexibility and materials rules
- ✓ over 40 different hysteresis rules are available, such as, for the nonlinear springs at the ends of elements
- ✓ moment amplification due to $P - \Delta$ is included
- ✓ different formats for the excitation input may be used
- ✓ a graphical interface is provided to help understand the response
- ✓ the input can be handled in a batch mode with minimum user intervention

2.4 Incremental Dynamic Analysis (IDA)

One of the advantages that the increase of computer power has provided is the feasibility of using more powerful methods of analysis and obtaining the results in a shorter period of time. The Incremental Dynamic Analysis (IDA) is a method that through repeated analyses presents graphically the demands and capacities of structures subjected to a variety of acceleration-time records. The method can be summarized as follows (Vamvatsikos and Cornell, 2002):

(1) A non-linear model of the structure is developed and a vector of performance parameters is selected (such as: inter-story drift, curvature, etc.). This vector of performance parameters contains what is called "Damage Measurement" (DM) indices that characterize the response of the structural model due to a prescribed seismic input. Typical DM quantities are: interstorey drifts, curvatures of elements, node rotations, maximum base shear, damage indices, shears, moments, etc.

(2) A set of ground motions is selected. These should represent the hazard governing the zone where the structure is located.

(3) A scaling factor (SF), which is a scalar that multiplies the original accelerogram to a desired level, is selected, based on the type of Intensity Measurement (IM) function chosen for the analysis and seismic records. The most common parameters that can be scaled are the Peak Ground Acceleration (PGA), Peak Ground Velocity (PGV), and the 5% damped Spectral Acceleration at the structure's first-mode period ($S_a(T_1,5\%)$). Thus, by scaling a single accelerogram to increasing levels, scaled records are produced, each with its own IM. The more levels of scaling used, the more resolution is obtained in the study. The upper limit on scaling should correspond to an earthquake that causes the collapse of the structure.

(4) For each of the scaled records of every accelerogram, a non-linear dynamic analysis is performed on the structure using the previous scaled accelerogram as input motion. The vector of performance parameters is extracted from the results of each analysis, and is matched with the IM selected for the IDA.

(5) A set of curves (one for each original record employed) is plotted from the previous stored results. The plots are generally DM versus IM. Any single point of the curves constitutes an individual result with a unique "scaled" earthquake and DM quantity associated with that. A median curve is calculated from the set of curves to simplify the results of the analysis.

This repetitive process has been automated to work in batch mode with the computer program Ruaumoko using an application developed in Excel. For a detailed explanation, see Appendix B – Ruaumoko Helper.

The major advantage of the method is that the results provide an easy interpretation of the demands imposed on the structure. The curves reflect a linear relationship between the S_a and the corresponding DM, until the yielding DM index is reached (at S_a^{yield}), which is when any element reaches the end of its elastic behaviour. After this point and toward the end of the curve consecutive yielding events of different elements cause changes in the slope *IM/DM*. Figure 2-4 illustrates this behaviour for the DM index of Maximum Interstory Drift Ratio. Softening is produced by the successive yielding of elements that contribute directly to the lateral stiffness that governs the Maximum Interstory Drift Ratio. If few elements are involved or the yielding mechanism is relatively easy to calculate, the resultant graph would resemble a pushover analysis. Hardening is produced as a result of changes in the yielding mechanism when weak response cycles in the early part of the response time-history become strong enough to cause yielding, thus altering the properties of the structure for the subsequent stronger cycles. A severe case of hardening also known as "structural resurrection" (Vamvatsikos, 2002; Vamvatsikos and Cornell, 2002) occurs when the earthquake scaled at a lower level causes the collapse of the structure, but when scaled at a higher level the structure survives.

The major disadvantage of this method is, for large structures (i.e., many degrees of freedom), it is very computationally demanding. There are advances to solve this problem by computing alternative IDA median curves using inelastic spectra, ductility factors, a force-displacement pushover analysis result, and equivalent single-degree-of-freedom models (Fajfar, 2000). The method developed by Dolsek and Fajfar (2004), called IN2, results in an alternate IDA curve that substitutes for a standard IDA curve in the probabilistic framework for seismic design and assessment of structures. However, the

application of this novel method is reserved for future research. The standard IDA approach is used in this thesis.

The ultimate application for IDA would be the use of hundreds of earthquakes, from a wide range of magnitudes and epicentral distances, to simulate an appropriate mean annual frequency of exceeding a structural demand measure, via Probabilistic Seismic Hazard Analysis (Luco and Cornell, 2001; Mackie and Stojadinovic, 2002; McGuire, 1995; Shome, 1999). This approach may render the method impractical, until faster computers and better algorithms are developed in the future.

2.5 Summary

Site effects are likely to occur where soft soil deposits are located. There are several methods to perform a seismic microzonation. The empirical method based on Nakamura's ground ambient noise analysis is an inexpensive, yet accurate method used by many researchers. The numerical method, based on the non-linear dynamic analysis of a column of soil, presents another approach to calculate the microzonation parameters and to overcome the limitations of the empirical method. Pilot studies have demonstrated this possibility (Madriz, 2004; Rosset *et al*, 2003).

Advances in computer technology and the development of the Incremental Dynamic Analysis method (Vamvatsikos and Cornell, 2002) provide an opportunity for more realistic assessments of the seismic performance of bridges.

Table 2-1 Geological Time and Rock Units – Montreal Area (after: Prest and Hode Keyser, 1977)

Eon	Era	Period	Stage	Sub-Stage	Years B.P.[1]	Geological Unit
Phanerozoic	Cenozoic	Quaternary	Holocene (Recent)	(Present) Postglacial	0 10,000	Bog, pond, river deposits
			Pleistocene	Wisconsinan (Glacial)	12,500	Champlain Sea deposits
					25,000	Fort Covington Till
					55,000	Middle-Till Complex
					70,000	Malone Till
					125,000	
				Sangamon (Interglacial)	250,000	(Deposits presumably removed by successive glaciations and erosions)
				Other Glacials and Interglacials	1.8 million	
		Tertiary			6.5 million	
	Mesozoic	Cretaceous			135 million	Monteregian intrusives
		Jurassic			195 million	
		Triassic			225 million	
	Paleozoic	Permian			280 million	
		Pennsylvanian			325 million	
		Mississippian			345 million	
		Devonian			395 million	Limestone blocks in Breccia
		Silurian			440 million	
		Ordovician			505 million	Trenton, Black River, Chazy, Beekmantown – Mainly, limestone, dolomite and shale
		Cambrian			570 million	
(Precambrian)	Proterozoic				2,500 million	Anorthosite – (in Carterville) Granitic and other gneisses, schist, crystalline limestone, slate, etc. – (in Oka area and the Laurentians to the north) Some of these rocks have been folded and metamorphosed several times
	Archean[2]				3,700 million	(oldest dated rocks in the world)
					4,500 million	(presumed age of the earth)

1 B.P. – "Before Present". The ages given are those generally accepted by the Geological Survey of Canada; they are based on a variety of radiometric-age determinations (^{14}C, K/Ar, Pb/Sr, U/Th/Pb) and partly on bio-chronological evidence.

2 Subdivided by some authors into Pre-Archean and Archean, the latter being applied to the time of dated rocks only.

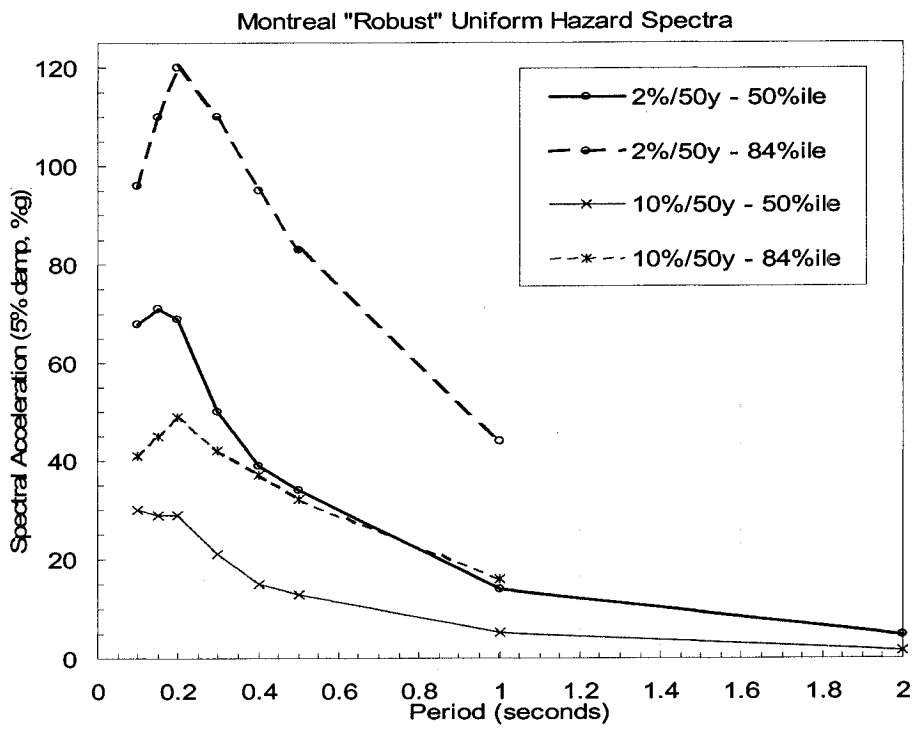

Figure 2-1 Montreal "Robust" Uniform Hazard Spectra (Data after: Adams *et al*, 1999)

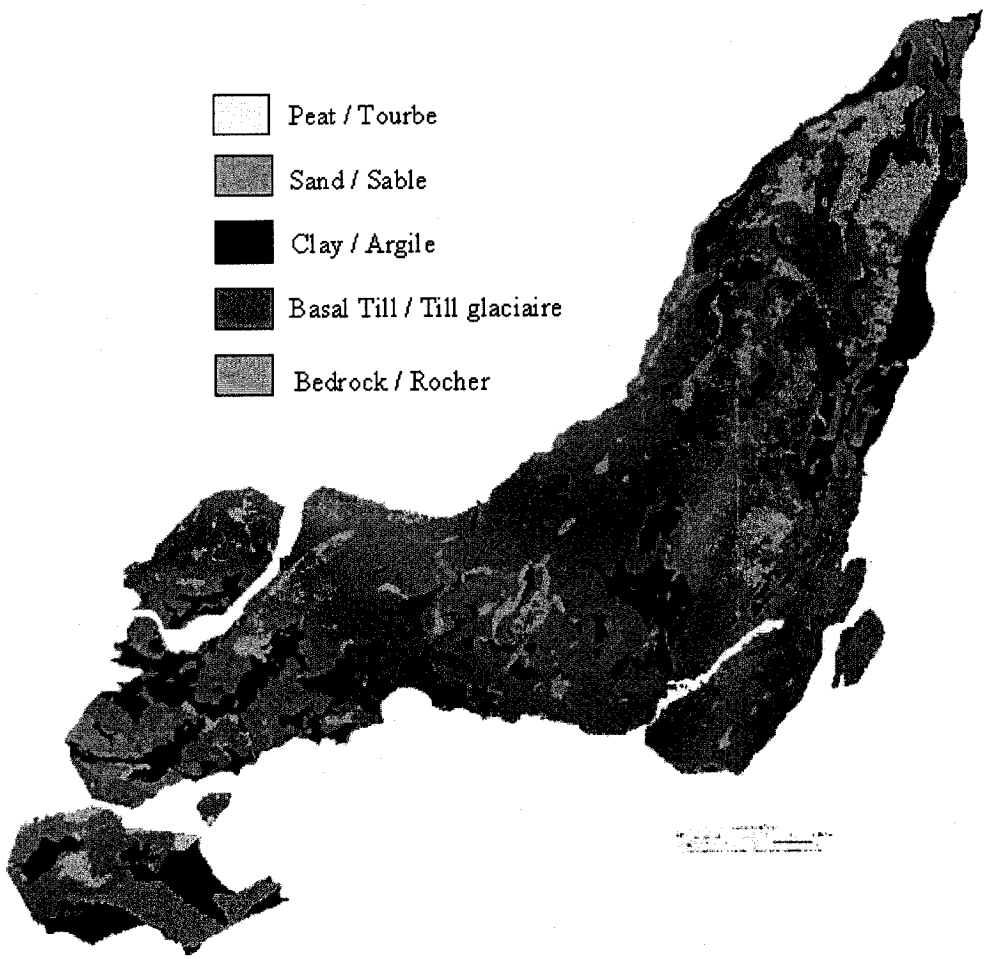

Figure 2-2 Simplified geological map of surface quaternary deposits (adapted from: Prest and Hode Keyser, 1977; Rosset *et al*, 2003)

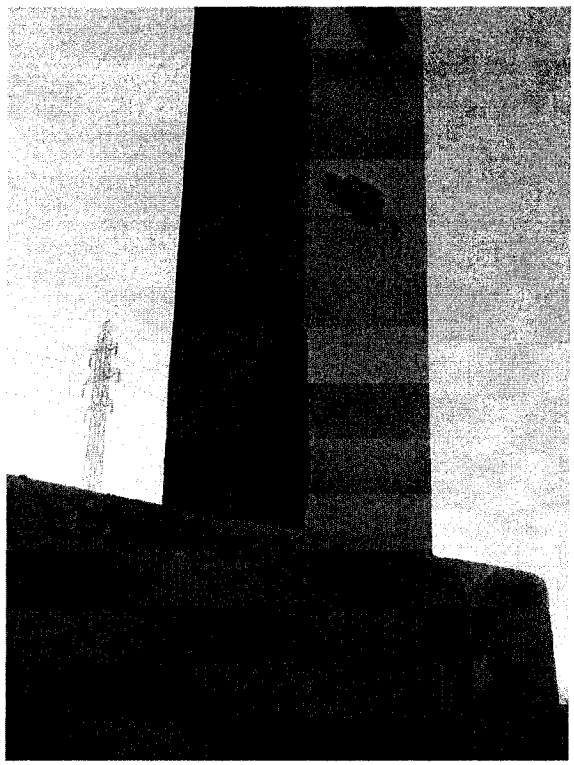

Figure 2-3 Deterioration in one of the edge columns of St-Jean Blvd. crossing Railroad bridge

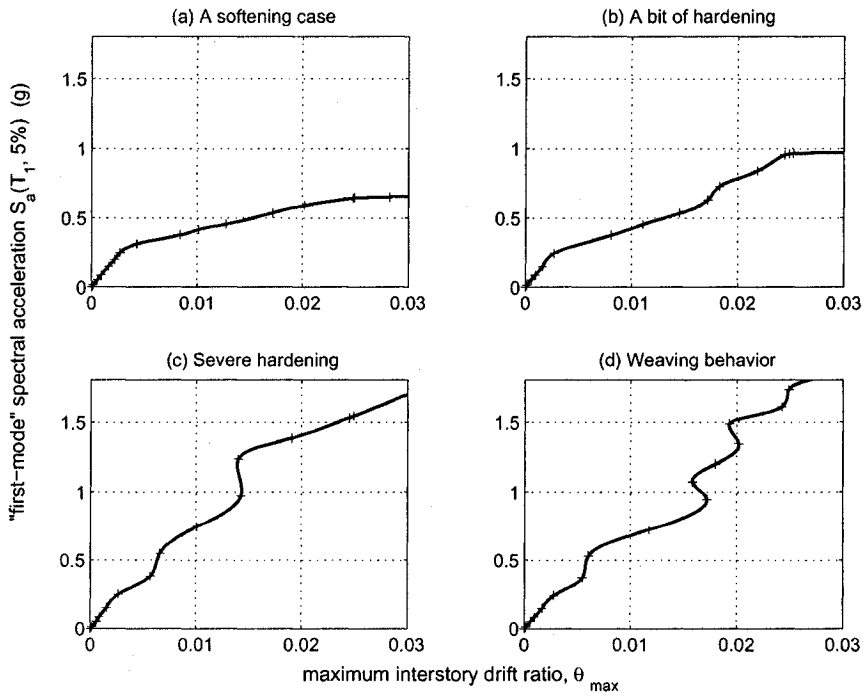

Figure 2-4 IDA curves of a T_1 = 1.8 sec, 5-storey steel braced frame subjected to 4 different records (after: Vamvatsikos and Cornell, 2002)

Chapter 3

Methodology for the Microzonation of Montreal

The focus of this chapter is to describe the methodology followed to execute the seismic microzonation of the island of Montreal. Field and numerical work was carried out in parallel over 800 locations in order to develop maps for the predominant frequency and response spectra acceleration. First the procedures and instruments used for performing the fieldwork are described as well as the software used to perform pre-processing and post-processing of the data. This is followed by a description of the methodology used to compile borehole data, as well as pre- and post-processing to perform numerical analyses at multiple locations.

3.1 Ground Ambient Noise Recordings

A pilot study during 2001 - 2002 demonstrated the feasibility of using ground ambient noise (GAN) recordings to estimate the fundamental frequency of vibration and amplification factor at specific sites (Rosset *et al*, 2002; Rosset *et al*, 2003). This work has been extended to cover the entire island of Montreal.

3.1.1 Field work methodology

In order to cover the entire island and to develop a rational sampling strategy, the island was divided into approximately 70 zones of 3 km x 3 km (Figure 3-1). A target number of recordings was defined for each of the zones. This number of recordings varies from 2 in zones where surface soil deposits are predominantly Basal Till or Rock, to 25, in zones where surface soil deposits are predominantly clay or sand. Although it is recommended to perform a minimum of 9 to 10 recordings per square kilometre (or 80 to

90 recordings per zone, Rosset *et al*, 2003), the densities of 2 to 25 recordings per zone were used due to limitations of resources and time. The initial selection of recording densities was based on the surficial soil deposit maps and depth to bedrock maps by Prest and Hode-Keyser (1977). The justification for the low density of recordings in zones with predominantly Basal Till and Rock, with low amplification and high frequency, is anticipated. Both of these features usually are favourable in terms of seismic hazard. The higher density of recordings in zones with predominance of clay and sand is justified because of higher acceleration and lower frequencies, which usually correlate with extensive damage from experience of past earthquakes.

Even if the density of recordings is not optimal, it is sufficient to develop a useful first wide microzonation map for Montreal, and in guiding higher densities of recordings for future field investigations.

Ground Ambient Noise is generated by surface sources such as traffic and other human activities, but also from wind-structure interactions. The opinions of experts differ in relation to the type of waves of microtremors that influence the frequency peak found in the Horizontal-to-Vertical Spectral Ratio (HVSR) technique. For example some argue that all body and surface waves except Rayleigh waves found in microtremors are responsible (Nakamura, 1989; Nakamura, 2000), while others conclude that Rayleigh-waves are the responsible for such peaks (Field *et al*, 1990; Lermo and Chavez-Garcia, 1994). Note that the passage of vehicles or other source of noise near a recording station will affect negatively the results. For this reason, records were obtained mainly during the night using the experience learned from the previous pilot study (Rosset *et al*, 2003). The main recommendations for performing fieldwork are as follows:

- Field recordings should be performed during night hours, from 9 to 4 am, and from Sunday to Thursday. This schedule is optimal to avoid periods of intense urban activity noise on the results for the quality of records.

- A vehicle should be used to carry the equipment to the selected locations and to power up the battery of the seismometer recorder. Figure 3-2 shows the typical arrangement of the equipment and vehicle.
- A crew of two operators should perform the measurements to ensure the completion of the recording schedule in a timely and efficient manner.
- Each measurement session should be planned beforehand by selecting the target zone(s) and approximate locations for recordings, using as reference a map on surface geology made by the Geological Survey of Canada (Prest and Hode Keyser, 1977). Sixteen to twenty sites can be surveyed in a typical session.
- The data obtained during these sessions should be compiled in a survey worksheet, containing the following information: Page Header: Local Date, Local Time, Zone(s) surveyed, Operator Names, Seismometer ID, Hard disk ID, Name of File, Ambient Air Temperature, Odometer count (from car), Sensor Date and Time. Table Body Header: Site ID, Time (GMT) of beginning and end of recording, Location of site (Intersections and Landmarks), Comments (such as: windy, noisy, truck passing, etc), Soil Conditions on geological map (depth to bedrock, surface soil deposit), post-processing file name and status.

A typical field recording takes approximately 20 minutes to complete, with 10 to 12 minutes of effective signal recording on disk. The recommended step-by-step procedure is as follows:

(1) Drive to the determined site.

(2) Park close to a flat area for the placement of the sensor. The surface must be hard enough to support the sensor without any settlement. Asphalt and concrete sidewalks are adequate surfaces.

(3) Operator 1 manipulates the sensor. The sensor is first removed from its box. It is aligned cardinally and levelled on the spot. Although the orientation of the sensor does have little relevance with the HVSR method, it is preferable to be consistent within

zones by following the standard North-South orientation. Note that sensors have to be manipulated with care during transportation and deployment since these are highly sensitive pieces of equipment and can be easily damaged. Operator 2 lays out the cable that connects the recorder to the sensor and places visual aids to warn incoming traffic.

(4) Operator 1 registers data on the Survey Sheet. Operator 2 manipulates the recorder. Recordings should commence a minimum of two minutes after the unit has been deployed to ensure that the internal dampers of the sensor are stabilized. The time on the recorder at the beginning of the recording is noted by Operator 1. Operator 2 verifies all three channels are operational.

(5) The minimum that a record length should be is 10 to 12 minutes. During this period, any unusual activity that might affect the recording signal should be noted in the Survey Sheet (e.g. heavy trucks, pedestrians, strong winds, etc).

(6) When the recording is completed, the sensor is returned to its protective container and the cable is carefully rolled. Note that the cable is fragile and kinks in the cable should be avoided.

(7) Return to the vehicle and proceed to the next site.

3.1.2 Instrumentation

The instruments, on loan from the Geological Survey of Canada, comprised of: A Digitizer or Recorder Computer model ORION (Nanometrics Inc., 2001), and a Sensor Güralp CMG-40T (Guralp, 2000). The settings used for recordings are listed in Table 3-1 and the most important technical specifications are listed in Table 3-2.

The ORION Recorder consists of a portable computer, a LCD panel for the user interface, a removable SCSI hard disk, and a battery (Figure 3-3(c)). These components are protected by a sturdy waterproof case outfitted with power inlets (AC and DC), GPS antennae, and two ports for up to six channels. A cable connects one of the ports to the Sensor. Figure 3-3(a) and (d) show the general layout of the complete station when

deployed in a stand-alone mode. The ORION station was normally powered using the DC adapter of the vehicle.

The Sensor CMG-40T is a lightweight portable velocimeter seismometer sensor, capable of recording motion along three perpendicular axes: Two Horizontals (North-South and West-East) and one vertical (Up-Down). It was designed for fast deployment and is encased in a water resistant stainless steel container. It requires minimal setups, and uses a bubble level for basic levelling within three degrees. It does not require any setups relative to mass clamping, precise levelling or mass centering.

Note that the equipment used in the project is specifically designed to be portable. It is a rapid-deployment seismic station, for example installed at places with minimal infrastructure after a strong earthquake to monitor aftershocks. However, it is not designed specifically for multiple deployments in a single day. Instruments specifically designed for this purpose are now commercially available (e.g. solid state sensors) and would be preferable for more extensive field surveys.

3.1.3 Data processing and Analysis

After each field session, data that have been recorded are first processed to convert the recordings from the Nanometrics proprietary ringbuffer format to an ASCII format. The records from the ORION station are continuous in time. In consequence, there are several gaps in the records corresponding to the downtime between successive sites. The downtime consists of the travel time between points, set-up time to install the equipment and to allow the dampers to stabilize the sensor. The post-processing steps are as follows: (1) Unused data disk space in the external ORION SCSI disk is trimmed. (2) The trimmed data record is copied to the laptop computer via a SCSI card, and converted to ASCII format. This task was automated using a program specifically created for this purpose using a Visual Basic Application in *Excel*© (Figure 3-4). Note that this post-processing is also useful to correct matching records for each site.

The recordings are finally processed using an application created in the MATLAB© environment called SPCRATIO (Rosset, 2002), based in the original works of Frischknecht *et al* (1998), and refined during the pilot research project on the microzonation of Montreal (Rosset *et al*, 2003)(Figure 3-5).

The internal features of the program are described in the Figure 3-6 (Rosset, 2002). First, a file to be processed is selected. The data in ASCII format is read by the program, which automatically detrends the signal of each of the three components using the DC-offset value registered by the recorder along the rest of the data, and tapers the ends of the records to have an equal length in each component. The program displays time series of the three acceleration components. Using this information, the user first validates the record, and can eliminate bad segments by choosing the desired segment of data. Using the remaining records, the program separates the signal into successive segments of 40.96 seconds, which correspond to 2^{12} points recorded at a rate of 100 samples per second. This usually results in 10 to 15 windows for each of the three components of the record. The windows were smoothed at the end using a Hanning function to reduce uncertainties due to truncation of the original data. Next, each time record is processed using a Fast Fourier Transform. These spectra are smoothed using a moving average method weightening with a Parzen window. Next, each smoothed spectrum is analyzed using the Horizontal-to-Vertical Spectral Ratio (HVSR) method, originally developed by Nakamura (1989). Each resulting curve is displayed together with the average and standard deviation. Locations with soft soil deposits usually have clearly indicated peaks. The program identifies the frequency corresponding to the maximum value on the mean. This value is recorded in an output file for mapping purposes.

SPCRATIO was modified to run in batch mode to process sequentially records from several sites. Note that in this case the first 30 seconds of records were systematically eliminated to avoid problems associated with the stabilization of dampers. In addition, the entire average spectrum of each site is saved in an output file for analysis at a later stage.

3.2 Numerical Analysis

The parameters of interest for microzonation such as the predominant frequency of vibration, amplification factor and many others can also be obtained numerically. Although there are many alternatives for modelling soil deposits at specific sites, the simplest one-dimensional model is often reliable (Lacave *et al*, 1999). The most popular program to perform one-dimensional dynamic soil analysis is *SHAKE* (Idriss and Sun, 1992). The program requires information relative to the soil layers, including thickness, dynamic soil properties, and input earthquakes.

The parameters of interest that can be obtained from the analysis are the fundamental frequency, maximum amplification factor, and maximum acceleration at the surface.

3.2.1 Borehole information and Soil Parameters

Borehole data was obtained from the City of Montreal and compiled by Madriz (2004) and by Rosset *et al* (2003). The database is a compilation of boreholes from municipalities and the government (in microfiche form). In addition, soil profiles were obtained at specific locations from miscellaneous geotechnical reports (i.e., Previllon *et al*, 1979). The original database has more than 26000 boreholes but less than 14000 reach the bedrock. Of these, less than 2000 have enough information to be used in conjunction with *SHAKE* (Madriz, 2004).

The boreholes describe the type of soil in each layer as clay, sand, silt, rock, till, in various combinations thereof. For the purposes of the analysis, the types of soils were grouped into seven encompassing categories: (1) Rock, (2) Clay, (3) Sand, (4) Peat, and three varieties of Till based on the surface geology of Montreal (Prest and Hode Keyser, 1977). The database of boreholes contained limited information on soil properties. Input

parameters, such as the unit weights, shear wave velocities, as well as dynamic soil parameters are those recommended by Rosset *et al* (2003) (Table 3-3 and Figure 3-7).

3.2.2 SHAKE analysis

The version of SHAKE that was used for the analysis is *SHAKE91* (Idriss and Sun, 1992). This program in its original form performs a complete analysis for one site at a time. Since more than 2000 sites had to be analysed in the project, a pre-processor was developed to allow the analysis of several sites in a single run as well as for multiple earthquake scenarios. A post-processor was also added for the compilation of results. Appendix A – Excel Shake shows a detailed explanation of the capabilities and internal workings. Figure 3-8 shows some screenshots of the interface. Up to ten layers of soil can be modeled using distinct soil parameters stored in the database and auxiliary sheets (Figure 3-7 and Table 3-3).

The column of soil is subjected to an array of ground motion records scaled to three specific levels: PGA = 0.16g, UHS 10%/50 years, UHS 2%/50 years. The PGA = 0.16g corresponds to an acceleration level in the same range than the 0.20g specified in the CHBDC, but close to the 10% in 50 years level of the Uniform Hazard Spectra (UHS). The two hazard levels of 10% of exceedance in 50 years and 2% of exceedance in 50 years will help to understand the soil amplification phenomena under the levels specified by the UHS. The results of those analyses are presented and discussed in the next chapter.

3.2.3 Earthquake Records

The ground motion records were selected for this analysis to obtain estimates of soil response for earthquakes with different frequency contents. Rosset *et al* (2003) classified the records in four scenarios according to their frequency contents: Low Period Scenario, with High Frequency; Intermediate Period Scenario, with Intermediate Frequency; Long Period Scenario, with Low Frequency; and Broadband Period Scenario, with Broadband Frequency. The earthquake records used in the analysis are all from

intraplate regions. These are: the Saguenay Earthquake of 1988 (high frequency, Tinawi *et al*, 1990), the two Kocaeli and Duzce Turkish earthquakes of 1999 (intermediate frequency content). In addition, the two Californian earthquakes El Centro of 1940 and Loma Prieta of 1989 (low frequency content) are used (Table 3-4).

A set of synthetic earthquakes that match approximately the Uniform Hazard Spectra for Montreal (Adams *et al*, 1999) were produced by Atkinson and Beresnev (1998). Figure 3-9 shows the unscaled response spectra of these records. The unscaled records from the Saguenay event produced response spectra that are lower than the UHS of 10% in 50 years (Figure 3-9(b)) except in the low period range where they are close. The Atkinson's Artificial Records were developed to reach the level of 2% in 50 years of the UHS (Figure 3-9(c) and (d)). Table 3-5 indicates the predominant characteristics of the records of these events.

Three scaling factors were used on each of the records in the numerical analysis. The target levels are: (1) Peak Ground Acceleration of 0.16*g*, (2) Uniform Hazard Spectra of 2% of exceedance in 50 years, (3) Uniform Hazard Spectra of 10% of exceedance in 50 years. Table 3-5 shows the scaling factor employed to match the UHS. These three levels will help understand the changes in the ground acceleration level when the seismic hazard is increased.

The earthquake records used in the dynamic analysis for the microzonation were also used in the Incremental Dynamic Analysis of the second part of the thesis, the seismic analysis of two overpasses.

3.3 Mapping Procedure

The results obtained from the processing of the ground ambient noise and the borehole data are assigned to coordinates (Quebec MTM NAD 83) for mapping purposes. The maps show iso-lines of fundamental frequency or depth to bedrock. The computer

program *SURFER*, (version 6.04, Golden Software Inc, 1996) was chosen as mapping software for its numerous interpolation methods as well for its availability in this research. The program generates a regularly spaced grid from the irregularly spaced data to interpolate. The values assigned to each grid node are calculated accordingly to the interpolation method selected, generally trying to estimate the value on the interpolation surface at locations where no data exists.

There are several interpolation methods, but only three methods were tried: Kriging (Stein, 1999), Inverse Distance to a Power, and Triangulation with Linear Interpolation (*SURFER* User Manual, Golden Software Inc, 1996). The Kriging method was considered due to its successful use by other researchers in interpolating data with good spatial correlation. However, the interpolated grid showed negative values or values greater than the maximum allowed frequency of 25 Hz for the fundamental frequency from the GAN and SHAKE data sets. This is probably because the spatial correlation function is not constant as a function of location across the island of Montreal. Only the results of the Inverse Distance to a Power and Triangulation with Linear Interpolation methods are presented and discussed in the next chapter. The grid spacing was set at 484m and 466 m for the X (West-East) and Y directions (South-North) respectively. For the region considered in the analysis, this translated to 80 grid lines in the X direction and 72 grid lines in the Y direction. Default SURFER parameters (no anisotropy, average of duplicates) were used in both interpolation methods. A power factor of 2.00 and a quadrant search ellipse (data per sector 6, minimum total data 5, maximum empty sectors 4) with a radius of 3000 m were used in the Inverse Distance of a Power Method.

The final aspect of the contour lines is determined by the level of smoothing chosen in SURFER at the time of plotting the contour lines from the grid.

The HVSR graphs of the GAN recordings show the predominant frequency peaks of each site. However, when two or more peaks of similar magnitude but at different frequencies are observed, a manual selection of the maximum peak may be required. This

selection consists of comparing the predominant peaks of adjacent sites, and if a trend is observed in the area (i.e., all peaks above 10 Hz), therefore the peak closer to the local area trend may be the one that corresponds to the fundamental frequency of the site.

The average fundamental frequency calculated from the *SHAKE* analysis of three different scenarios was mapped using the same procedure as used with the GAN recordings. Previous research work determined that there is not enough information to infer an correlation in any specific direction related to the maximum frequencies of amplification (Madriz, 2004).

3.4 Summary

The methodology used in the seismic microzonation of the island of Montreal is presented in this chapter. Two different approaches have been used to find the predominant frequency of vibration of the soil at various sites. The first approach involves the recording of Ground Ambient Noise (GAN) and its processing using the Horizontal to Vertical Spectral Ratio (HVSR, Nakamura, 1989), based on a procedure validated by a previous research (Rosset *et al*, 2002; Rosset *et al*, 2003). This fieldwork methodology was extended on 700 recordings in approximately seventy 3 km by 3 km zones. The records, performed with an Orion portable seismometer, were distributed accordingly to the predominant surface soil deposit of the area, namely two records in zones predominantly with Rock or Basal Till and over twenty records in zones predominantly with clay, peat or sand. A more detailed survey methodology is also presented where recommendations for performing fieldwork and the data post processing are given. The software, called SPCRATIO (Rosset, 2002), was used for the post processing and final computation of the HVSR spectra of the GAN records.

The second approach involves the one-dimensional modeling of columns of soil of borehole data, compiled mainly from the City of Montreal (Madriz, 2004; Rosset *et al*,

2003) . Non-linear dynamic analyses were performed using the computer program *SHAKE* (Idriss and Sun, 1992) with the assistance of the interface application *Excel-Shake* (De la Puente and Rosset, 2002) for performing batch calculation and data extraction. Seventeen different earthquakes (Table 3-4 and Table 3-5) were used in the analyses and the results were combined to provide the maps shown in the next chapter.

A mapping procedure is also described. The mapping, using the software *SURFER* (Golden Software Inc, 1996), was done with two interpolation methods: Triangulation with Linear Interpolation and Inverse Distance to a Power Methods.

The results of the microzonation from the two approaches, as well as the mapping, are presented in the next chapter.

Table 3-1 Settings of Recorder ORION for the research

Recorder type	ORION s/n 228 (Nanometrics Inc.)
Number of Channels	3
Sample Rate	100 Hz
DC Filter Frequency	100 Hz
Acquisition Mode	Continuous Mode
Recording Method	No Overwrite
Corner Frequency	0.0033 Hz

Table 3-2 Device Specifications for sensor Guralp and the portable seismometer recorder ORION

Sensor	Type	Triaxial velocimeter
	Model	Guralp CMG-40T s/n T4786 (Guralp)
	Corner Frequency	0.0033 Hz
	Flat Response	0.03 to 50 Hz
Recorder	Type	ORION s/n 228 (Nanometrics Inc.)
Input Channels	Sensor channels	3 standard, 6 optional
	Type	Differential
	Sensitivity	2.55 $\mu V/bit$, default
	Dynamic Range	132 db rms-rms
Digitizer	Type	24 bits delta-sigma
	Anti-Aliasing Analog Filter	3rd order Bessel – 3 dB at 3.7 kHz
	Digital Filter	-140 db at output Nyquist
	Hardware Sample rate	256 kHz
	Sample Instant	Simultaneous
	Sample rates	10, 20, 40, 50, 80, 100, 125, 200, 250, 500 and 1000
	Acquisition Mode	Continuous, Event, and Window mode
	Recording Method	Ring buffer or No Overwrite
Data Cartridge	Storage Space	2 GBytes

Table 3-3 Type of deposits and soil assignments (Prest and Hode Keyser, 1977; Rosset *et al*, 2003)

Type of Deposit	Name of Soil	Type of Soil and Rock	Soil Type		Initial Damping	Unit Weight kg/m^3 (kcf)			Shear Wave Velocity m/s (ft/s)		
			Type	Label		Min	Max	Used	Min	Max	Used
Rock	Limestone of Trenton	Limestone	Rock I	ROCK1	0.1	2620 (0.1634)	2777 (0.1732)	2706 (0.1688)	-	-	2286 (7500)
	Shale of Utica	Shale	Rock II	ROCK2	0.1	2640 (0.1646)	2710 (0.1690)	2645 (0.165)	-	-	2103 (6900)
Glacial Deposit	Malone Till	Boulders + sand – silt	Basal Till I	BT1	0.05	2160 (0.1347)	2480 (0.1547)	2379 (0.1484)	-	-	975 (3200)
	Intermediate Till	Sand – gravel – silt – cobbled	Basal Till II	BT2	0.05	2000 (0.1247)	2240 (0.1397)	2140 (0.1335)	-	-	792 (2600)
	Fort Covington Till	Undifferentiated till	Basal Till III	BT3	0.05	1640 (0.1023)	2380 (0.1484)	2061 (0.1286)	360 (1181)	760 (2493)	457 (1500)
Marine Deposit	Offshore sediments	Clay-Silt, marine shells	Clay Silt	CS	0.05	1520 (0.0948)	1920 (0.1198)	1704 (0.1063)	100 (328)	300 (984)	152 (500)
Fluvial Deposit	Saint Laurent Deposits	Sand-Gravel	Sand	S	0.05	1780 (0.1110)	2360 (0.1472)	2036 (0.1270)	350 (1148)	600 (1968)	396 (1300)
Late Deposit	Bog-Pond deposit	Peat-muck-filled ground	Peat	P	0.05	-	-	1988 (0.124)	-	-	304 (1000)

Table 3-4 Main characteristics of real and synthetic earthquakes used as input ground motions (Modified from: Rosset *et al*, 2003)

Event	Date and Hour	Magnitude	Depth	Faulting type	Station	Coordinates of station	Epicentral Distance
Saguenay	25 Nov 1988 23:46:04	$M_N = 6.5$ $M_S = 6.0$ $M_B = 5.7$	29 km	Thrust with a strike – slip component	Chicoutimi-Nord Site 16	48.4902 N 71.0123 W	43 km
					St-Andre Site 17	48.3248 N 71.9917 W	64 km
					La Malbaie Site 8	47.6553 N 70.1527 W	92 km
					Tadoussac Site 5	48.1432 N 69.7189 W	109 km
					Quebec Site 2	46.7782 N 71.2749 W	150 km
Kocaeli	17 Aug 1999 03:02	$M_W = 7.4$ $M_S = 7.8$	16 km	Right lateral strike – slip	Gebze, Kocaeli	40.820 N 29.440 W	42 km
Duzce	12 Nov 1999 16:57:20	$M_W = 7.1$ $M_L = 7.2$ $M_S = 7.3$	14 km	Right lateral strike – slip	Murdunu, Duzce	40.463 N 31.182 W	34 km
Imperial Valley	18 May 1940 08:37	$M_W = 6.9$	≈ 10 km	Right lateral strike – slip	Diamond Heights	N/A	N/A
Loma Prieta	18 Oct 1989 00:05	$M_W = 6.9$ $M_L = 6.7$ $M_S = 7.1$	17 km	Right lateral strike – slip and reverse slip	Belmont, BES	37.518 N 122.267 W	64 km
Atkinson's Artificially Generated	(Atkinson and Beresnev, 1998)	$M_W = 6.0$	--	--	1, 2, 3, 4	--	30 km
		$M_W = 7.0$	--	--	1, 2, 3, 4	--	70 km

Table 3-5 Main Characteristics of the Records used in this analysis

Earthquake	Filename	Frequency Content	Sampling [samples per sec]	Length [sec]	Scaling Factor for UHS 2%/50yrs	Scaling Factor for UHS 10%/50yrs
Quebec, Saguenay	81125S02.txt	High	200	20.04	5.00	2.60
Tadoussac, Saguenay	81125S05.txt	High	200	20.48	13.00	8.00
La Malbaie, Saguenay	81125S08.txt	High	200	20.44	2.00	1.20
Chicoutimi-Nord, Saguenay	81125S16.txt	High	200	20.48	3.00	2.00
St-Andre, Saguenay	81125S17.txt	High	200	20.48	5.00	4.50
Loma PrietaEQ	BES-EW.txt	Low	200	20.475	0.85	0.40
El Centro, California	ElcentroH.txt	Low	50	53.74	0.50	0.16
Kocaeli, Turkey	GBZ-NS.txt	Medium	200	20.475	0.87	0.30
Duzce, Turkey	MDR-NS.txt	Medium	200	20.475	1.35	0.70
Atkinson's Artificial M6 1	AtkM6_1.txt	Broad	100	8.88	1.02	0.40
Atkinson's Artificial M6 2	AtkM6_2.txt	Broad	100	8.88	0.93	0.36
Atkinson's Artificial M6 3	AtkM6_3.txt	Broad	100	8.88	1.08	0.42
Atkinson's Artificial M6 4	AtkM6_4.txt	Broad	100	8.88	0.87	0.34
Atkinson's Artificial M7 1	AtkM7_1.txt	Broad	100	24.07	0.88	0.34
Atkinson's Artificial M7 2	AtkM7_2.txt	Broad	100	24.07	0.87	0.34
Atkinson's Artificial M7 3	AtkM7_3.txt	Broad	100	24.07	0.95	0.37
Atkinson's Artificial M7 4	AtkM7_4.txt	Broad	100	24.07	0.93	0.36

Figure 3-1 Zonal division of the island of Montreal (Map after: Prest and Hode Keyser, 1977)

Figure 3-2 Arrangement of instrumentation and vehicle

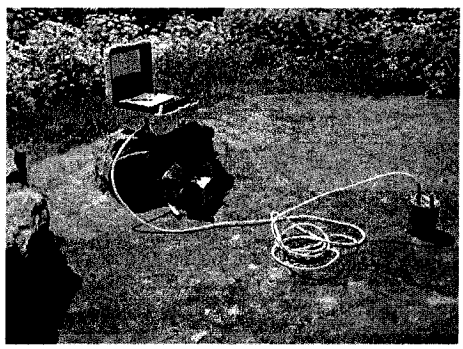

(a) Orion recorder with Guralp sensor on soil

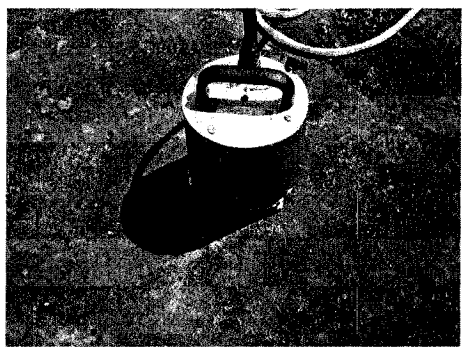

(b) Guralp sensor

(c) Orion LCD panel display

(d) Orion recorder with Guralp sensor on asphalt

Figure 3-3 Arrangement of Orion recorder with Guralp Sensor on the field

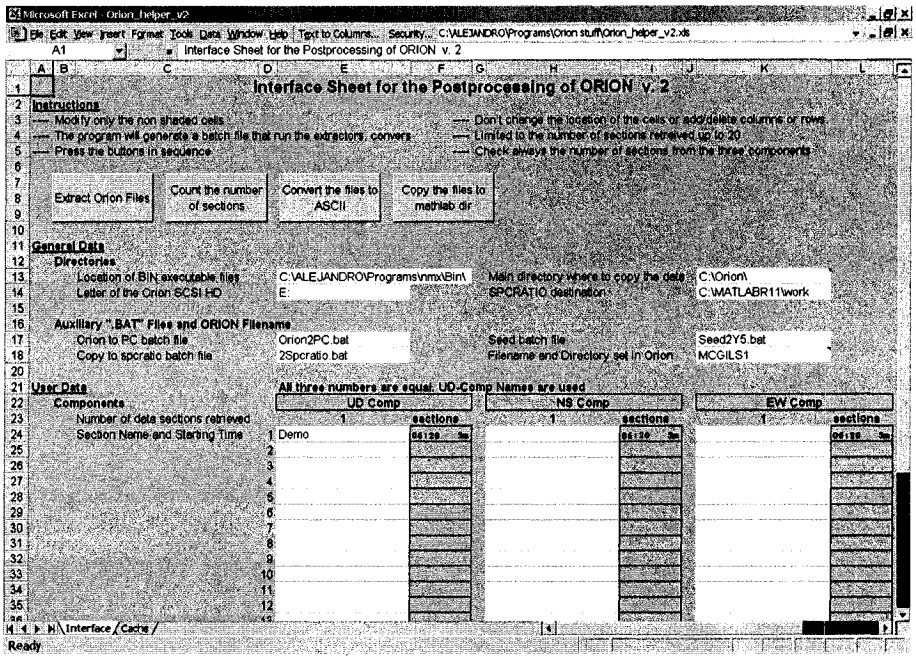

Figure 3-4 Screenshot of *Orion Helper*, post-processing program for ORION records

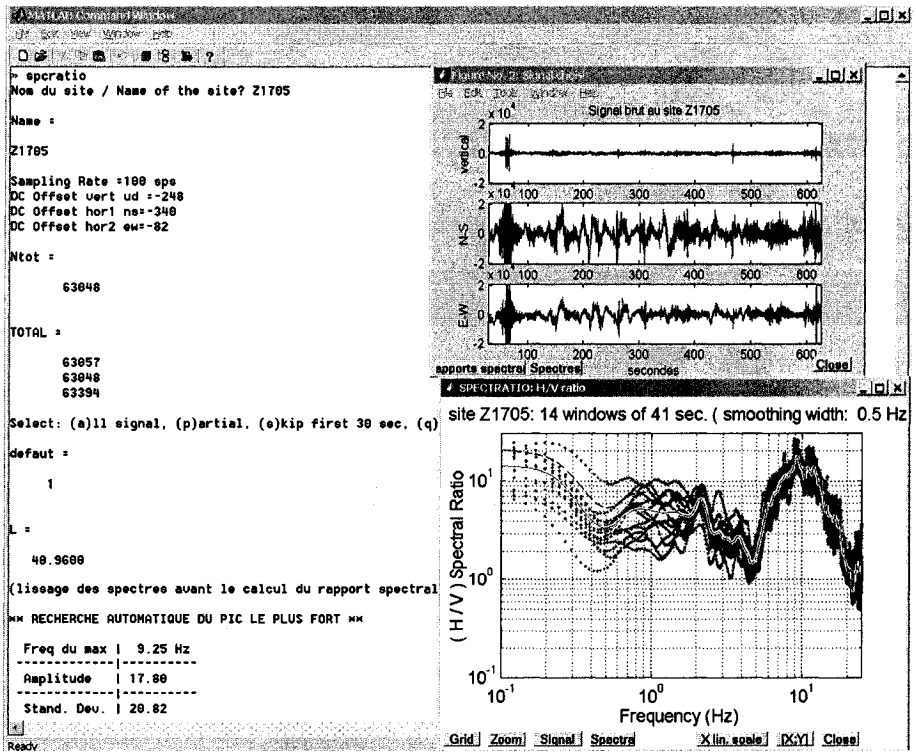

Figure 3-5 Screenshot of SPCRATIO (Rosset, 2002), application in MATLAB© used to process the signals using the HVSR method

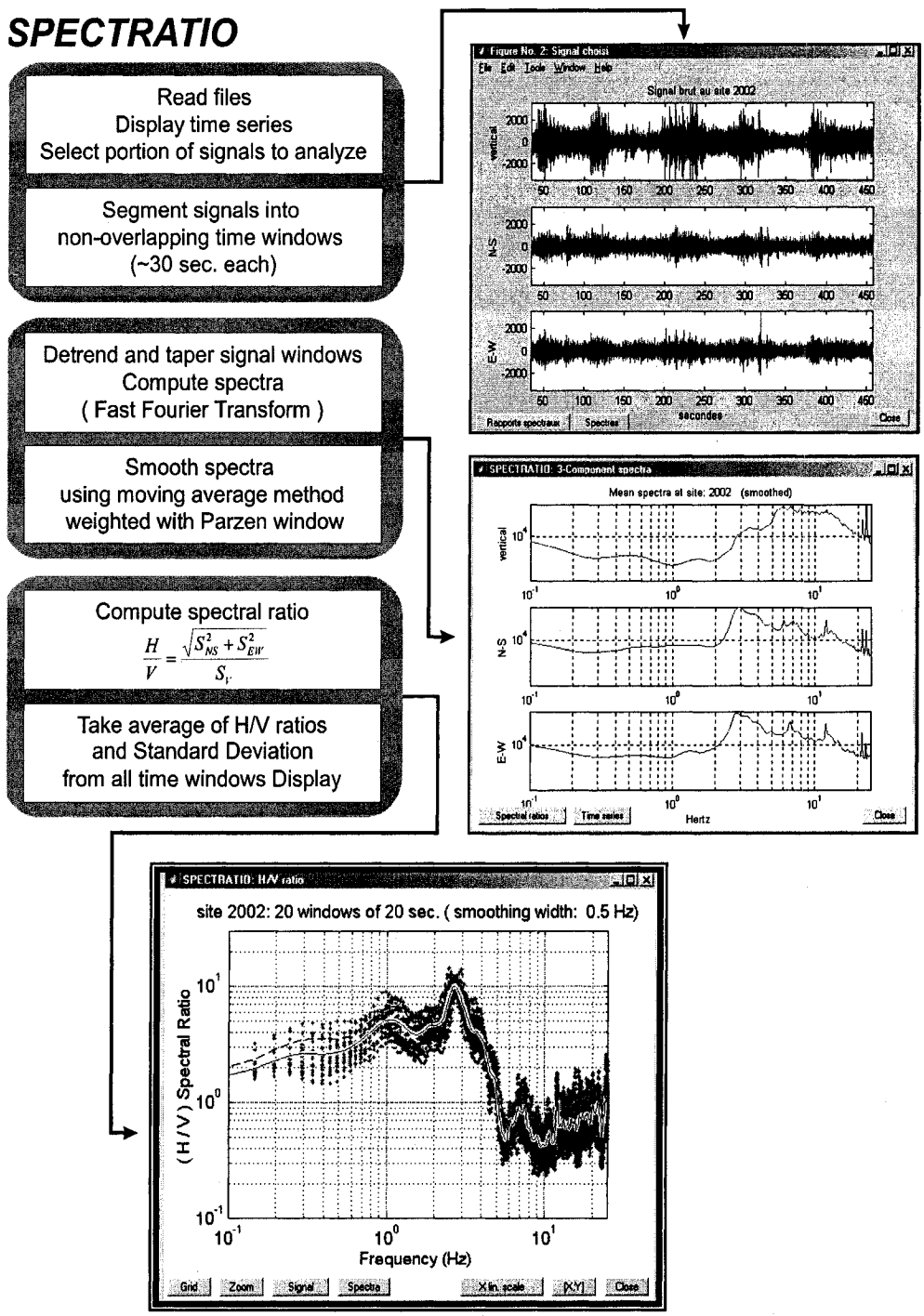

Figure 3-6 Procedure for calculating the HVSR from the records of ambient noise (After: Rosset, 2002)

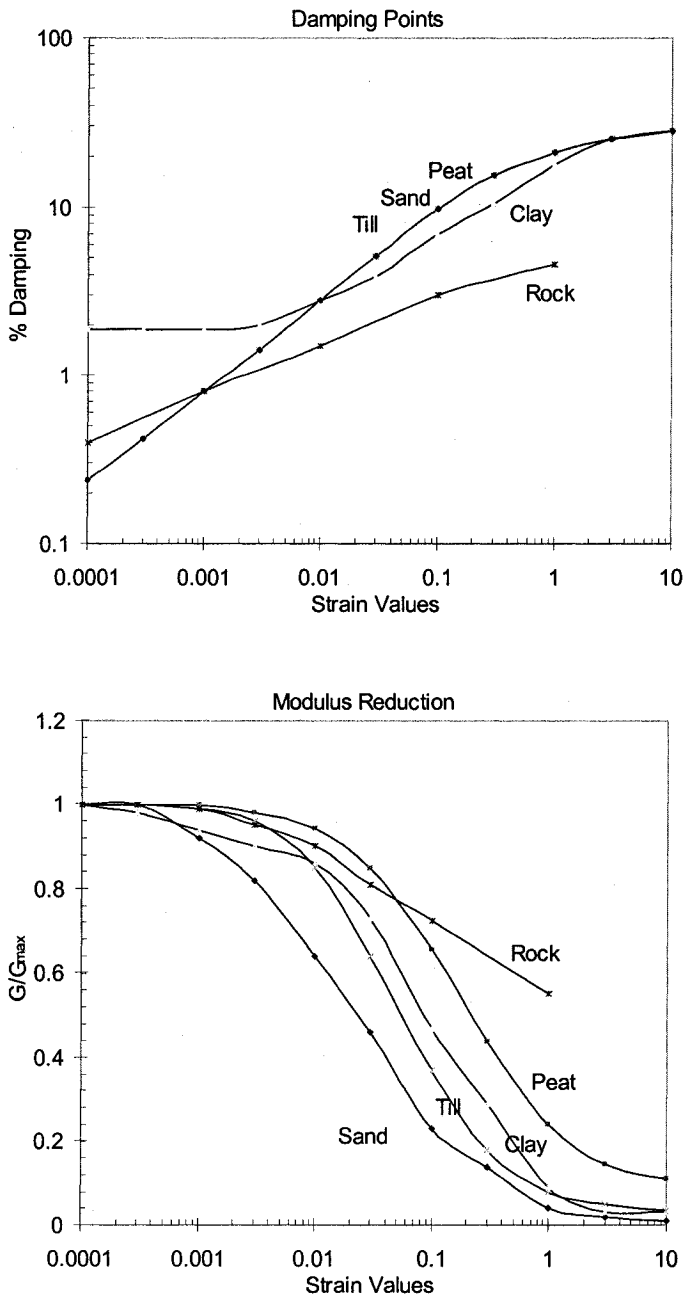

Figure 3-7 Dynamic Soil Parameters Curves (Normalized Shear Modulus and Damping Ratio) employed in the non-linear analysis with SHAKE (Rosset *et al*, 2003)

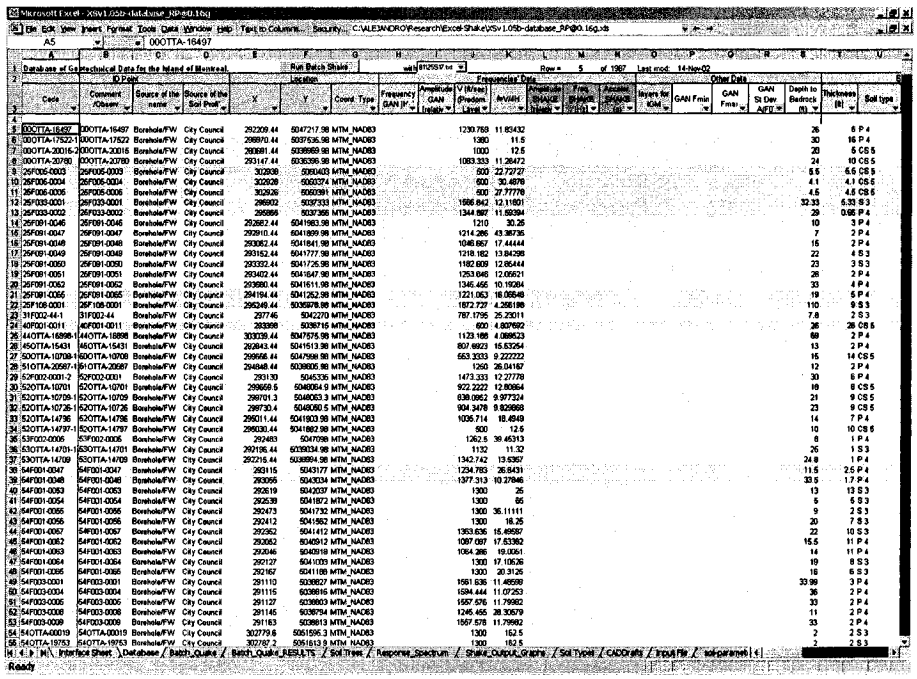

(a) Database

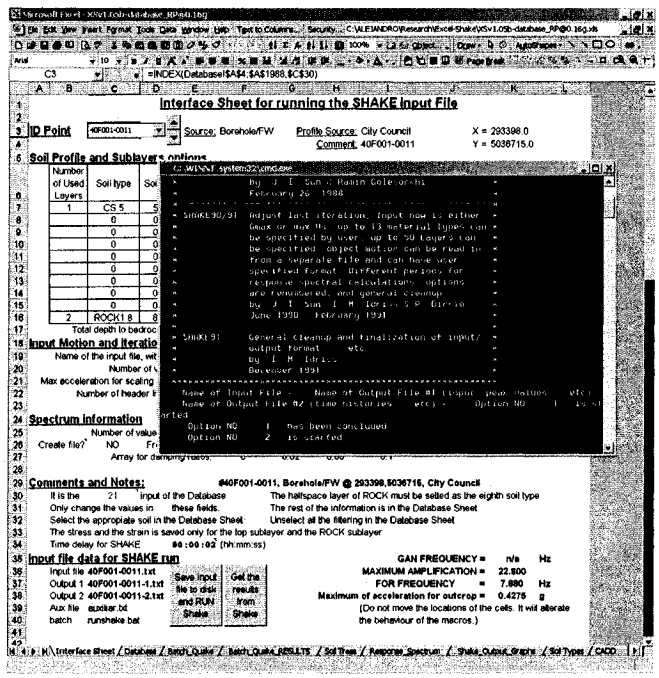

(b) Execution

Figure 3-8 Screenshots of *Excel-Shake* (De la Puente and Rosset, 2002)

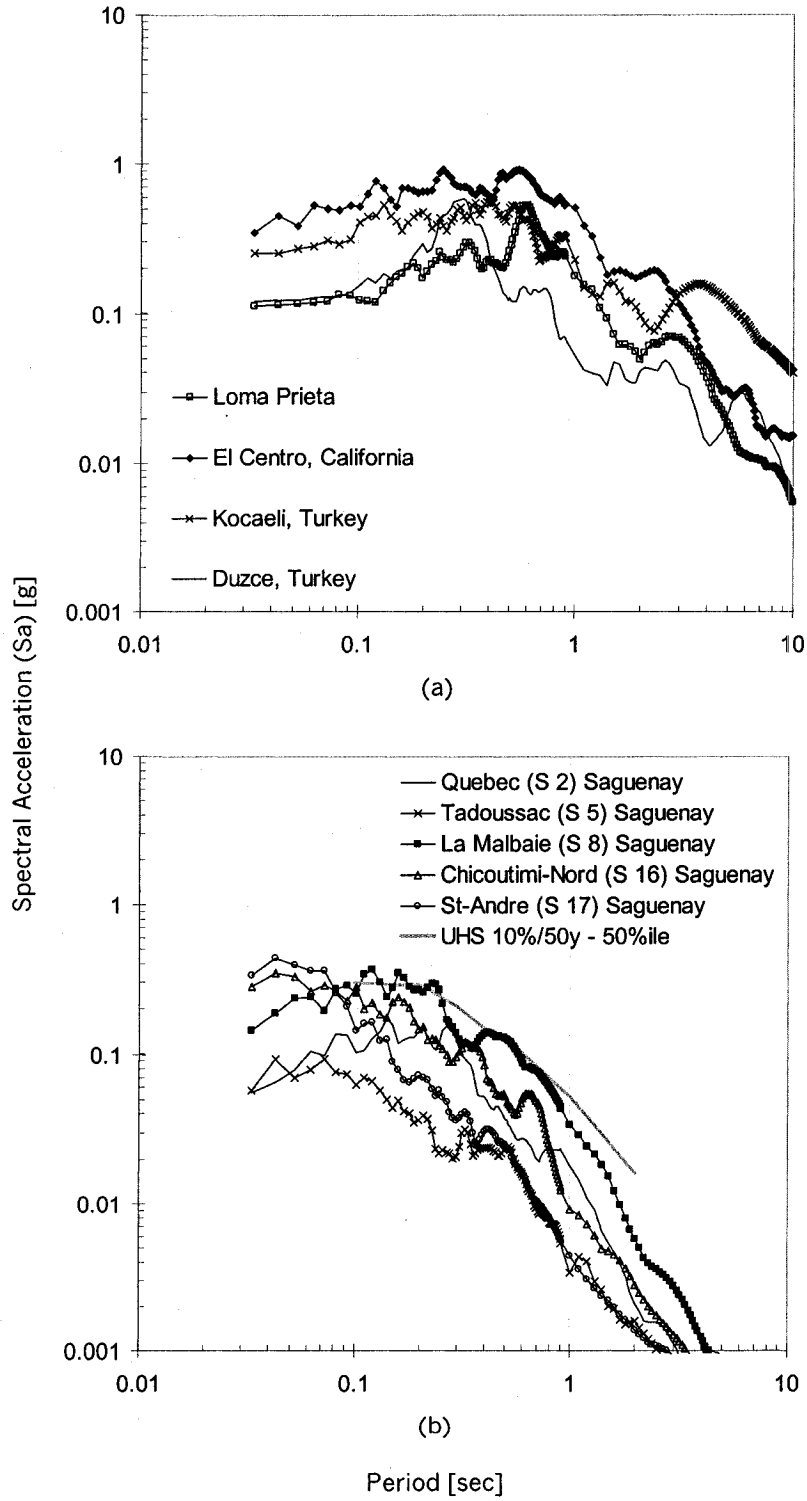

Figure 3-9 Unscaled Response Spectra at 5% damping for the Earthquake Records used with *SHAKE* and *RUAUMOKO*.

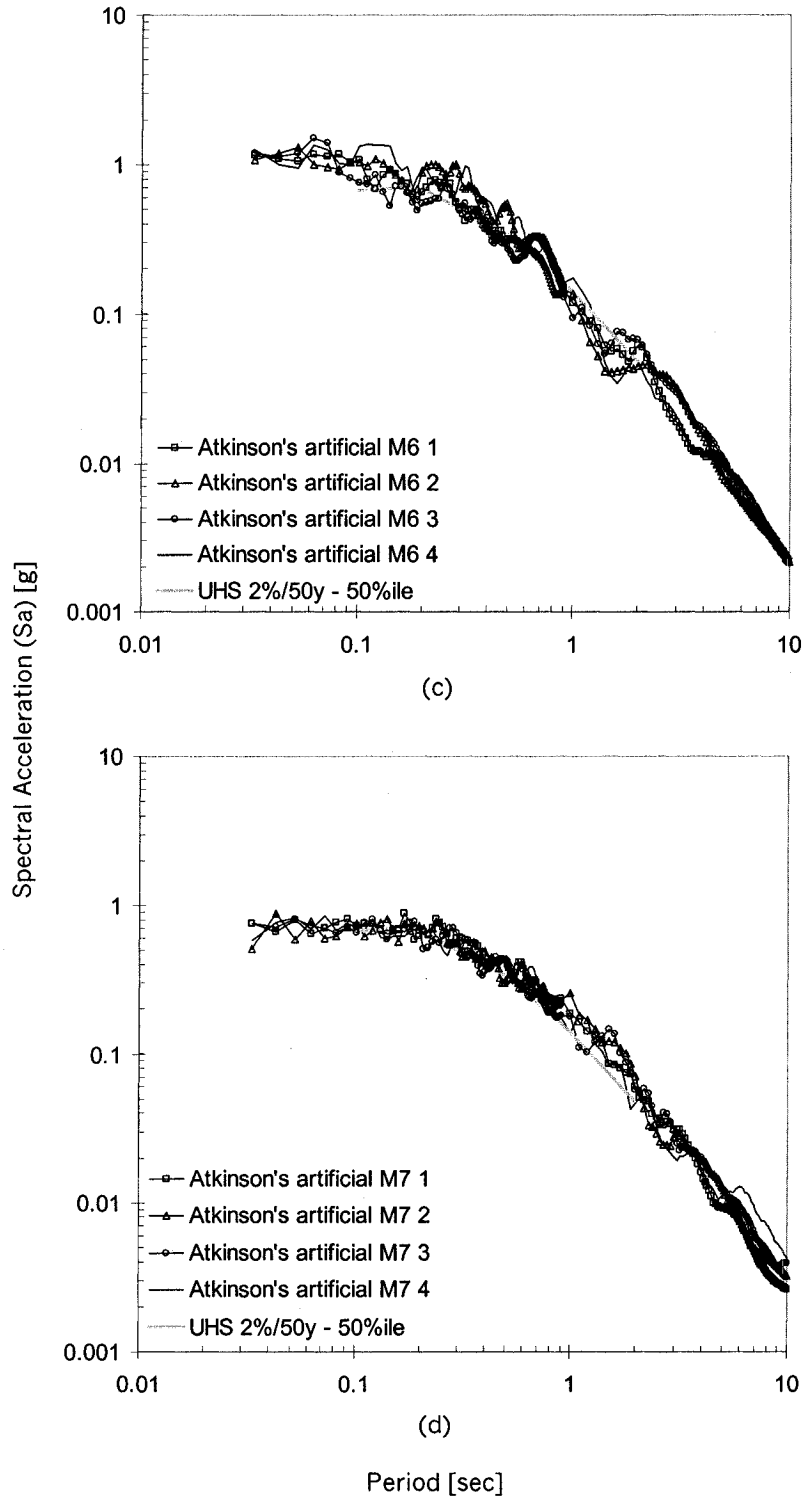

Figure 3-9(cont.) Unscaled Response Spectra at 5% damping for the Earthquake Records used with *SHAKE* and *RUAUMOKO*.

Chapter 4

Microzonation Mapping

The present chapter describes the results of the analyses and measurements towards the microzonation of the city of Montreal. First, a description of the mapping process is presented. Second, the surficial soil deposit and depth to bedrock maps obtained from borehole data are presented. Third, the predominant frequency maps for three cases are presented and discussed: (1) GAN recording analysis, (2) SHAKE borehole numerical analysis, and (3) a combination of both cases. Finally, twelve zones with potential seismic amplification problems are identified and further discussed.

4.1 Mapping Process

As described in the previous chapter, grid data was generated using the program *SURFER* (Golden Software Inc, 1996). Various research projects on microzonation (i.e., Frischknecht *et al*, 2005) have produced maps using diverse interpolation methods with varying grid spacings, which usually depend on the size of the area to map and the desired resolution. The resulting number of grid lines usually ranges from 40 to 140 in each direction. The most common interpolation method used in microzonation is Kriging (See: Stein, 1999). Kriging is an interpolation procedure that assumes that observations are spatially correlated and that correlation is proportional to the distance pairs of points. However, this assumption and the form of the correlation function have to be validated in each particular case. In the application of Kriging to the fundamental frequency data, some of the interpolated values resulted in negative natural frequencies or values outside the maximum allowed frequency (25 Hz).

On the other hand, other methods, such as Triangulation or Inverse Distance methods produce interpolated values that remain within the allowable range of values while still identifying significant and meaningful trends in the data.

A variety of grid sizes was used in combination with the various interpolation schemes. The average spacing for the original data is 488 m (total area of the island: 470.14 km^2, 1973 points) and grid sizes varying between 25 and 780 m were investigated. Large grid spacings often resulted in internal error messages by *SURFER*, mainly due to memory problems. Results were found to be relatively insensitive to grid size for spacings smaller than 25m. In this application, a grid size of 484 x 466 m, based on the number of grid lines (80 x 72), was used for all the cases.

No anisotropy in any method was considered in the interpolated maps. Although soil deposition along the axis of the St-Laurent river would suggest a stronger correlation structure parallel to the St-Laurent river, the empirical correlation was found not be statistically significant. This can be explained by the complexity of soil deposition processes and the relatively small amount of data from which the correlation function is estimated. Interpolations performed with an anisotropy ratio of 1.3 and an orientation angle of 30 degrees gave similar results to the isotropic case.

Figure 4-1 shows the histogram of residuals for the three types of interpolations: (1) Triangulation with Linear Interpolation (Triang), (2) Inverse Distance to a Power (IDP), and (3) Kriging (Krig). Residuals are defined as the difference between an observation and the interpolated grid value at the same location. The methods produce similar histograms, and cannot be differentiated based on the histograms alone. Figure 4-2 shows the spatial distribution of the residuals for the case of SHAKE and GAN data combined and the Triangulation method. The figure indicates that there are no spatial trends in the residuals, which would be indicative of biases introduced by the interpolation procedure.

Triangulation with Linear Interpolation does not require the specification of any parameter to obtain interpolated values and control their degree of spatial smoothness.

Inverse Distance to a Power (IDP) requires the specification of a 'search radius'. Since the relevance of fundamental periods should decrease rapidly as a function of distance from a point of interest, a small search radius was specified. The spacing between data points is a function of the sampling plan adopted for this research. As explained previously, the Island of Montreal was divided into 70 squares of approximately 3 km by 3 km. Using this partition, the maximum distance between two points would be 6 km. However, using a more realistic distance corresponding to the midpoints of adjacent cells, the maximum value selected for the search radius was 3 km (Figure 3-1).

In a few cases, boreholes or GAN recordings that are located in proximity were attributed the same coordinates and were treated as duplicates by the software. In such cases, only one point was retained corresponding to the average value of the duplicates.

Note that the locations of GAN recordings are more or less uniformly distributed across the island which is favourable to an interpolation technique such as Linear Triangulation which is local since it uses only the closest three points to interpolate. However, one disadvantage of Linear Triangulation is that it does not extrapolate beyond the array of grid points, unlike the IDP.

Figure 4-3 shows boundaries between municipalities and districts as well as the main highways on the island to help in the localisation and interpretation of the interpolated maps.

4.2 Surface Geology Maps

Figure 4-4 shows a reproduction of a historical map of the Island of Montreal showing the location of streams, rivers and possibly lakes as of 1872 (Johnston, 1872). The old map was digitized by matching contour lines of the island and some inaccuracy in the position of the various features is to be expected. Most of the historical streams, rivers and lakes have been drained, channelled or covered and are not apparent nowadays.

However, their location often correlates with soft soil deposits. One particularly striking example is the thick soft soil deposits along the Turcot Interchange corresponding to the location of the historical Lac à la loutre. The approximate location of the ancient streams and rivers is superimposed in all subsequent maps of predominant frequency.

Figure 4-5 shows two maps for depth to bedrock, obtained from borehole and profile data. A total of 1973 boreholes were used in the mapping procedure. Data coverage is not uniform across the island and is highly biased towards the location of existing infrastructures such as highways and sewer lines. The maps were obtained with the two interpolation methods described previously. It can be observed that deeper soil deposits are located near the southeast shore and the easternmost tip of the island. When compared with the ancient river map of Figure 4-4, it can be observed that the depth to bedrock is not well correlated with the location of ancient streams and rivers, with the exception of the river in the vicinity of the Lachine Channel (Zone G1 in Figure 4-11), which is also the location of the ancient Lac à la loutre.

Figure 4-6 shows the location of the boreholes around the island indicating the predominant surficial soil deposit and the ancient rivers. Surficial deposits are quite variable as a function of location and do not correlate well with fundamental frequency. The correlation with the latter is much better with the predominant surficial deposit over the entire soil column (Figure 2-2, Prest and Hode Keyser, 1977).

4.3 Predominant Frequency Maps

Three sets of maps were prepared for the predominant frequency, each using the two grid interpolation methods described previously. The first set shows the results of the ground ambient noise recordings (Figure 4-8), the second set shows the results of the numerical analysis made with *SHAKE* (Figure 4-9), and the third set shows the results of both analyses combined (Figure 4-10).

4.3.1 GAN Analysis Maps

The predominant frequencies of vibration from GAN (Figure 4-7) are mapped in Figure 4-8 using the two grid interpolation methods. Both methods show similar contour lines for most of the island, with values of frequency less than 10 Hz. The value of 10 Hz is selected for its engineering relevance since it corresponds to the upper limit for the natural frequency of common one-storey buildings. Most of the differences in contour lines are observed in the zones G2, H, C, and A (Figure 4-11). Figure 4-8 also shows the locations of ancient rivers and streams (Figure 4-4) superimposed over the predominant soil frequency maps. As mentioned before, ancient streams and rivers may have carried sediments that formed soft soil deposits that have a fundamental frequency below 10 Hz. Correlations between ancient rivers and low fundamental frequencies can be observed mainly in Zones A and G1. This correlation is more evident in Zone A for the map created with the Triangulation grid interpolation method (Figure 4-8(a)) than the map created with the IDP method (Figure 4-8(b)). This may be attributed to a weakness of the IDP method relative to isolated data points when interpoint distances are close to the search radius. In such cases, a single observation may dominate interpolated values at several grid points resulting in a "bull's eye" pattern. Other areas of the island do not show a correlation between low natural frequencies and location of ancient stream and river deposits. This may be attributed to the removal of soft soil deposits during construction, the location of ancient rivers in zones of shallow bedrock, or lack of data in the vicinity of the ancient rivers.

4.3.2 Numerical Analysis (SHAKE) Maps

Figure 4-9 shows the predominant frequency of vibration using borehole data and numerical analysis with *SHAKE* for the same two interpolation methods. The frequency used for interpolation is the average of the predominant frequencies for three earthquake-scaling scenarios: (1) Peak Ground Acceleration equal to 0.16g, (2) Uniform Hazard

Spectra exceedance of 10% in 50 years, and (3) Uniform Hazard Spectra exceedance of 2% in 50 years (Table 3-5).

As in the previous case, both methods show similar contour lines along the island of Montreal. However, a comparison of fundamental frequency maps from GAN and SHAKE shows major differences in Zones A and B. This difference is attributed to the lack of borehole data in these areas. Ancient streams and rivers (Figure 4-4) do not correlate well with the SHAKE results, except in the area of deep soil deposits of Zone G1. The map of Figure 4-9(a) created with the Triangulation method appears to indicate some correlation with ancient rivers in the Southwest and Northeast corners of Zone I. The correlation is not as strong in the map created with the Inverse Distance to a Power method (Figure 4-9(b)).

4.3.3 Combined GAN-SHAKE Maps

The interpolation map using GAN data is based on observations that are more or less uniformly distributed in space (Figure 4-7), especially in the areas where Rock or Basal Till are present. The interpolation map using SHAKE data is constrained by the location of the boreholes and the corresponding 'gaps' in their spatial distribution. As shown in previous sections, the fundamental frequencies from GAN and SHAKE appear to be well correlated for soft soil deposits despite the fact that the waveforms associated with the two methods are not identical (Rayleigh or Shear wave: Lermo and Chavez-Garcia, 1994; Nakamura, 2000). The correlations may not be as strong for other types of soils; however, these are not as critical for seismic hazards. Consequently, it may be beneficial to combine both maps in order to increase the sample size and improve spatial coverage (Figure 4-10). The resulting frequency map interpolated with the Triangulation method (Figure 4-10(a)) shows better correlation with ancient streams and rivers than the map interpolated with the Inverse Distance to a Power method (Figure 4-10(b)). The size of the area corresponding to low frequency content in Zone B is reduced because of the mixture of low and high frequency points in these areas.

4.4 Zones of Seismic Amplification Map and Response Spectra

The maps obtained with the Triangulation method was used to delimit zones of soft to medium soil deposits that are susceptible to amplification of ground motions. Twelve zones are identified on the basis of contour lines for frequencies below 10 Hz (Figure 4-10(a) and Figure 4-11).

Table 4-1 shows the average fundamental frequencies for the three earthquake scenarios considered. It can be observed that there is a shift to the low frequencies in the predominant frequency in the UHS 2%/50 yrs scenario in relation to the PGA = 0.16g and UHS 105/50yrs scenarios. This frequency shift is normally expected with larger earthquakes (i.e., Dimitriu *et al*, 1999).

Four zones (C, H, J, and K) with average fundamental frequencies less than 6 Hz were selected. The median response spectra of each zone were calculated for the three earthquake scenarios (Figure 4-12). A large increase in spectral accelerations is observed between periods of 0.3 to 0.7 seconds for zones J and K (Figure 4-12(c) and (d)) relative to the spectral accelerations from the UHS for Montreal. Table 4-2 summarizes the amplification factors of UHS spectral acceleration for return periods of 475 years (10% in 50 years) and 2475 years (2% in 50 years) at the average fundamental frequency of each zone (Table 4-1).

Figure 4-13 shows the percentile distribution in the form of box plots, of the fundamental frequencies of the zones defined in Figure 4-11 and listed in Table 4-1, for the three earthquake scenarios. The box plot shows the median, the 25% and 75% quartiles, non-outliers range, outliers, and extreme values. The ranges for outliers and extreme values are respectively obtained by multiplying the 25% and 75% ranges by 1.5 and 3.0.

The box plots of the three earthquake scenarios (Figure 4-13(a), (b), and (c)) and the average frequency (Figure 4-13(d)) are very similar, with the exception of a few outliers in Zone D. The figure indicates that frequencies within the 12 zones of Figure 4-11 are

predominantly below 10Hz, which is indicative of softer soils. Conversely, frequencies for the rest of the island are predominantly above 10Hz, which is indicative of stiffer soils.

A significant number of outliers can be observed for zones G1 and G2. This is due to the relatively large number of boreholes located in these zones, compared with the others. These outliers correspond to locations within the zones with stiffer soils. Another observation is there is a trend of decreasing median frequencies from west to east for zones E, F, G1, G2, H, J, and K. The zones G1 and G2 are located near Mt-Royal, while zones J and K are located in Montreal-East near the shore of the river. The zones are fairly homogeneous as indicated by the relatively small range of frequencies between the 25% and 75% quartiles.

Based on the box plots of Figure 4-13, it is possible to expect seismic amplification around the low frequency range (0 – 5 Hz) in the easternmost tip of the island of Montreal.

4.5 Summary

Potential site-effects for the island of Montreal have been studied and mapped, by combining results from a field approach (GAN) and a numerical modeling procedure (SHAKE). The predominant frequency of vibration of the soil has been chosen as the main parameter to characterize potential site-effects. Different mapping techniques were investigated resulting in the selection of the Inverse Distance to a Power (IDP) and the Triangulation Interpolation methods as the most appropriate.

Characteristic features of the surface geology of the island, such as ancient streams and rivers and depth to bedrock, are presented in Figure 4-4 and Figure 4-5, respectively. The depth to bedrock is not well correlated with the location of ancient streams and rivers, with the exception of the Lac à la loutre.

The predominant frequency of vibration maps from the GAN records (Figure 4-8) and the average of the predominant frequency for the three earthquake scenarios from

SHAKE analyses (Figure 4-9) are compared with the location of ancient streams and rivers (Figure 4-4). A significant correlation is obtained for soil deposits located in zones A and G1 (Figure 4-11).

Further comparisons between GAN and SHAKE results give the appearance of disagreement in zones A and B (Figure 4-11), however, these are mainly due to the scarcity of data in these zones and poor overlap of information. Further investigations with additional boreholes or GAN surveys are recommended to decrease the uncertainty on predominant frequencies in these zones.

Figure 4-10 shows maps that combine the results from the GAN and SHAKE analyses. Results from the SHAKE analyses are constrained by the availability of borehole data and in consequence tend to be spatially clustered despite a very large number of data points. Results from the GAN surveys correspond to pre-selected locations and in consequence are much more uniformly distributed. As before, the interpolation procedure that produces the better results appears to be the Triangulation method based on correlations with surface geology features. Only contour lines for frequencies smaller than 10 Hz are mapped in order to clearly delineate the twelve zones of soft to medium soil deposits most important for seismic amplification (Figure 4-11).

Box plots of the frequencies from the SHAKE analysis are shown in Figure 4-13 for each of the zones and for each of the three earthquake scenarios and the average scenario. The majority of the boreholes located in these zones have a fundamental frequency less than 10 Hz, while the majority of the boreholes in the remaining part of the island have frequencies above 10Hz.

The median response spectra acceleration of the four zones (C, H, J and K) with the lowest average predominant frequency (less than 6 Hz) is shown in Figure 4-12. These zones were selected because of the presence of soft soil and the possibility of damage to typical buildings. Table 4-2 shows the spectral acceleration evaluated at the average predominant frequency for each of the four zones. The maximum amplifications are

observed in Zone K, which is located at the eastern tip of the island of Montreal and where deep clay deposits are predominant. Zones J and K (Table 4-1) have predominant fundamental periods of respectively 0.29 and 0.74 seconds corresponding to the natural periods of two or more storey buildings.

Table 4-1 Statistics for the predominant frequency (Hz) for twelve zones of soft to medium soils

Zones	Average Freq. PGA = 0.16g	Average Freq. UHS 10%/50yr	Average Freq. UHS 2%/50yr	Average Freq. all scenarios (Hz)	Aver. Period all scenarios (sec)
A	7.56	7.63	6.83	7.34	0.136
B	10.22	10.30	9.45	9.99	0.100
C	6.07	6.15	5.54	5.92	0.169
D	8.37	8.63	8.03	8.34	0.120
E	8.87	8.92	8.25	8.68	0.115
F	9.33	9.41	8.63	9.12	0.110
G1	8.86	8.92	8.30	8.70	0.115
G2	8.13	8.20	7.56	7.96	0.126
H	5.20	5.30	4.69	5.06	0.198
I	8.27	8.35	7.71	8.11	0.123
J	3.54	3.64	3.19	3.45	0.290
K	1.38	1.44	1.24	1.35	0.739
Rest	16.92	16.95	16.24	16.70	0.060

Zones	St. Dev. Freq. PGA = 0.16g	St. Dev. Freq. UHS 10%/50yr	St. Dev. Freq. UHS 2%/50yr	St. Dev. Freq. all scenarios (Hz)	Number of records
A	3.16	3.13	2.98	3.09	19
B	6.38	6.35	6.62	6.44	16
C	2.86	2.84	2.67	2.79	56
D	5.78	5.79	6.07	5.86	19
E	0.87	0.89	0.80	0.85	23
F	2.33	2.35	2.18	2.28	33
G1	4.89	4.87	4.83	4.86	182
G2	4.67	4.64	4.58	4.62	170
H	2.05	2.06	1.73	1.92	76
I	5.01	4.99	4.85	4.94	83
J	2.08	2.07	1.89	2.01	67
K	0.30	0.32	0.26	0.29	26
Rest	6.92	6.88	7.14	6.97	1203

Table 4-2 Amplification of response spectral acceleration (g) for zones C, H, J and K

Zones	Acceleration PGA = 0.16g	Acceleration. UHS 10%/50yr	Acceleration UHS 2%/50yr	Increase factor UHS 10%/50yr	Increase factor UHS 2%/50yr
C	0.72	0.71	1.36	2.459	1.946
H	0.93	0.87	1.63	3.003	2.487
J	0.56	0.50	0.94	2.238	1.960
K	0.56	0.39	0.65	4.534	3.432

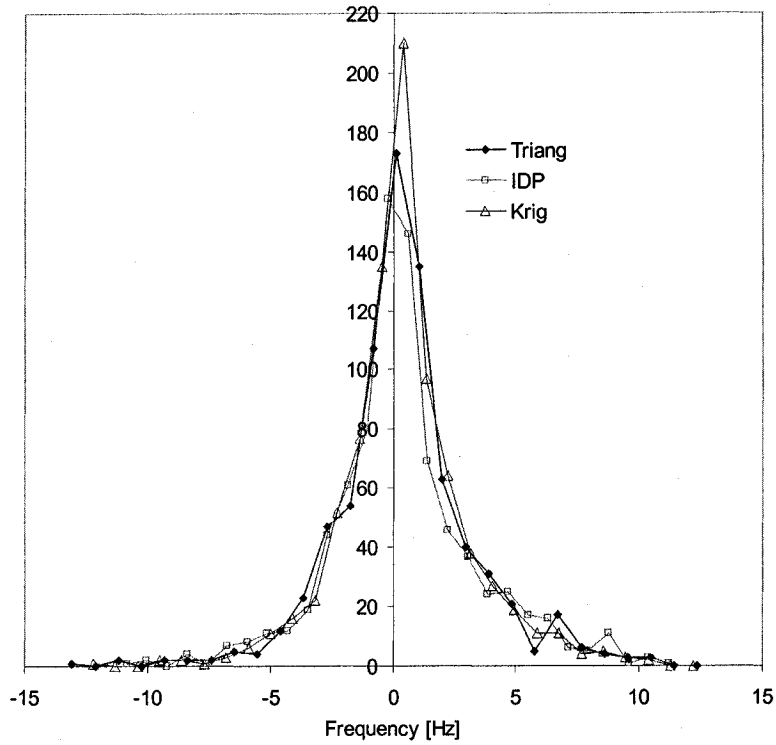

(a) GAN records

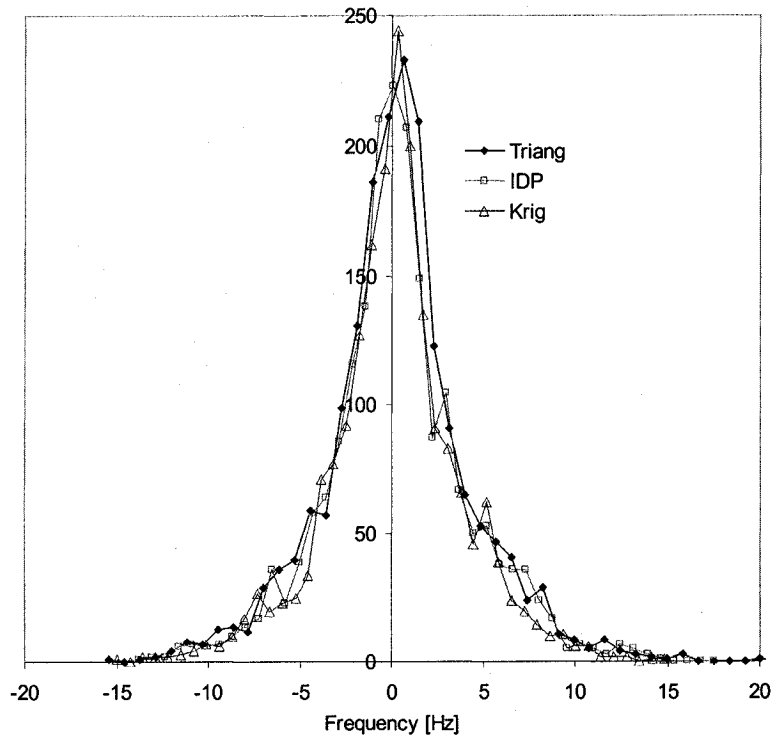

(b) SHAKE analysis results

Figure 4-1 Histograms of residuals for various interpolation schemes

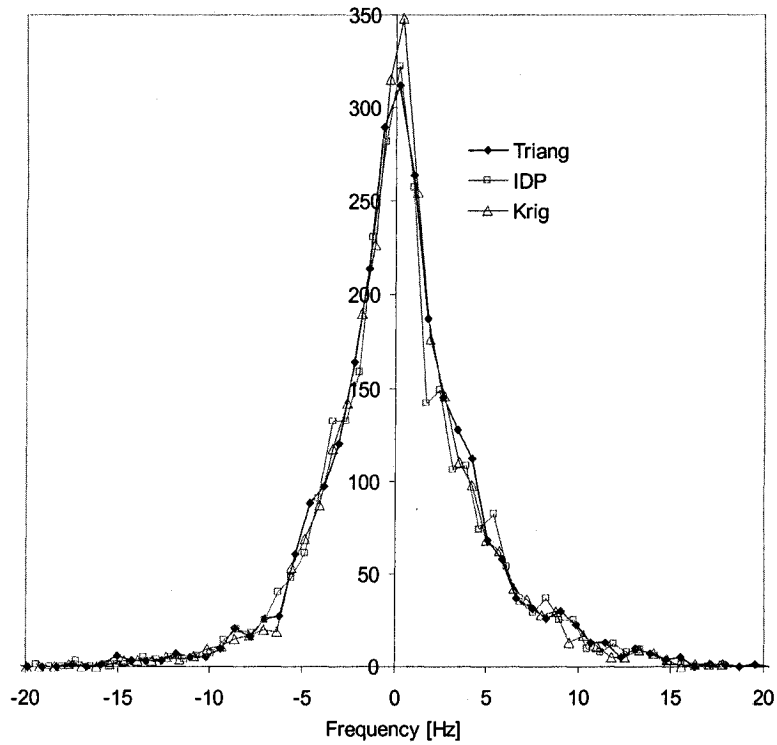

(c) SHAKE and GAN combined

Figure 4-1(cont.) Histograms of residuals for various interpolation schemes

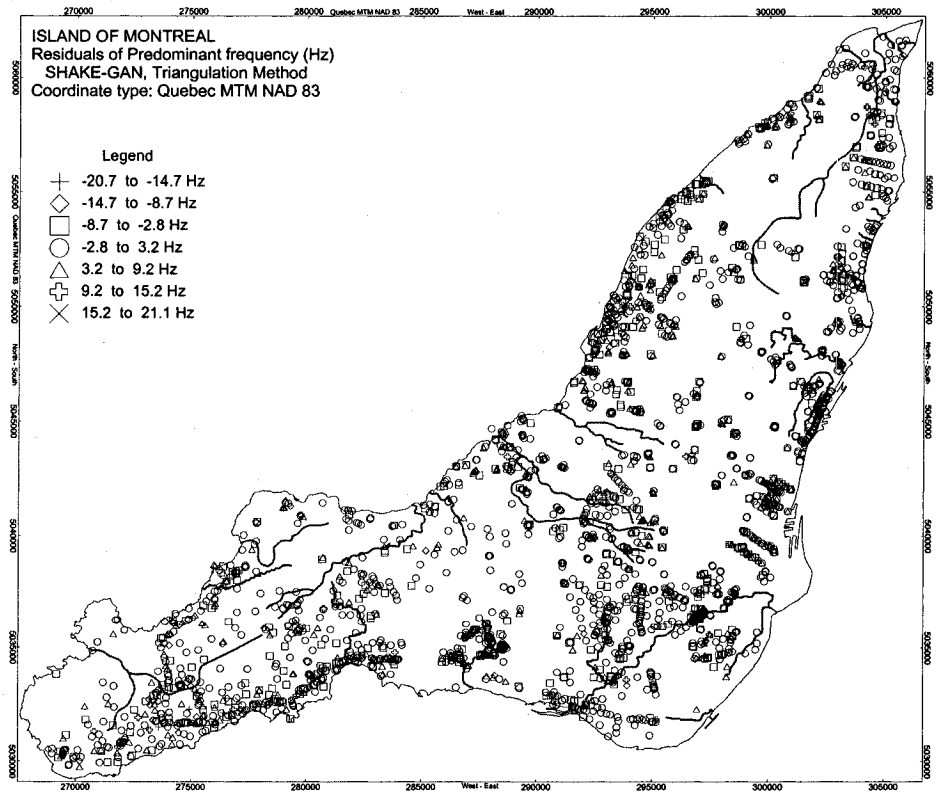

Figure 4-2 Spatial distribution of the residuals for the SHAKE-GAN results using Triangulation interpolation

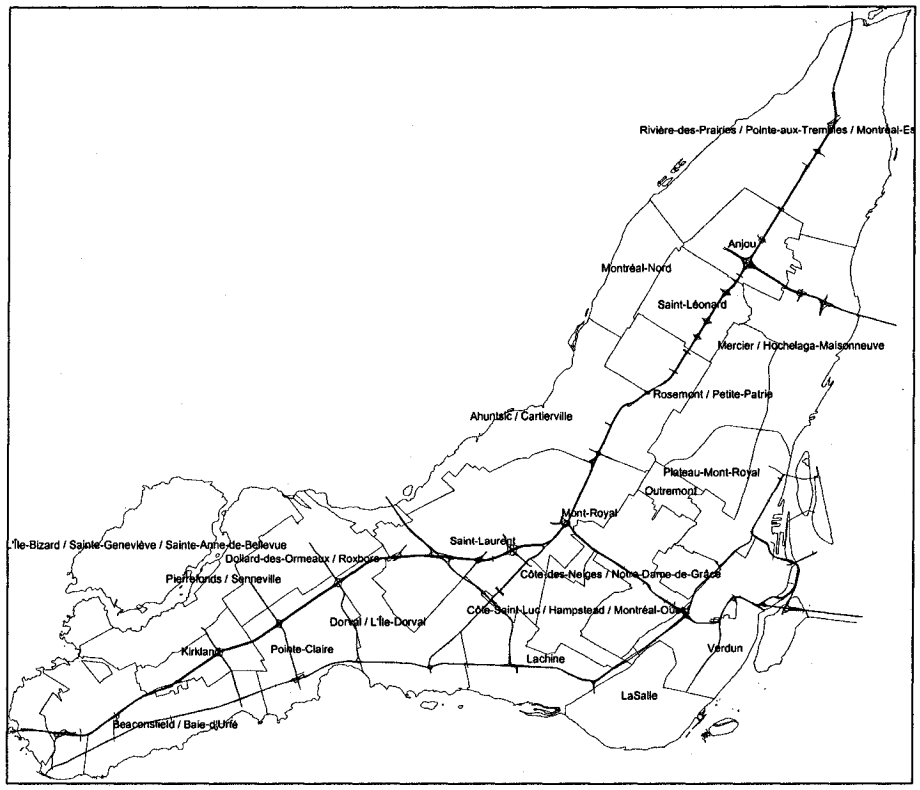

Figure 4-3 Municipalities and districts of the island of Montreal (2002) and major highways.

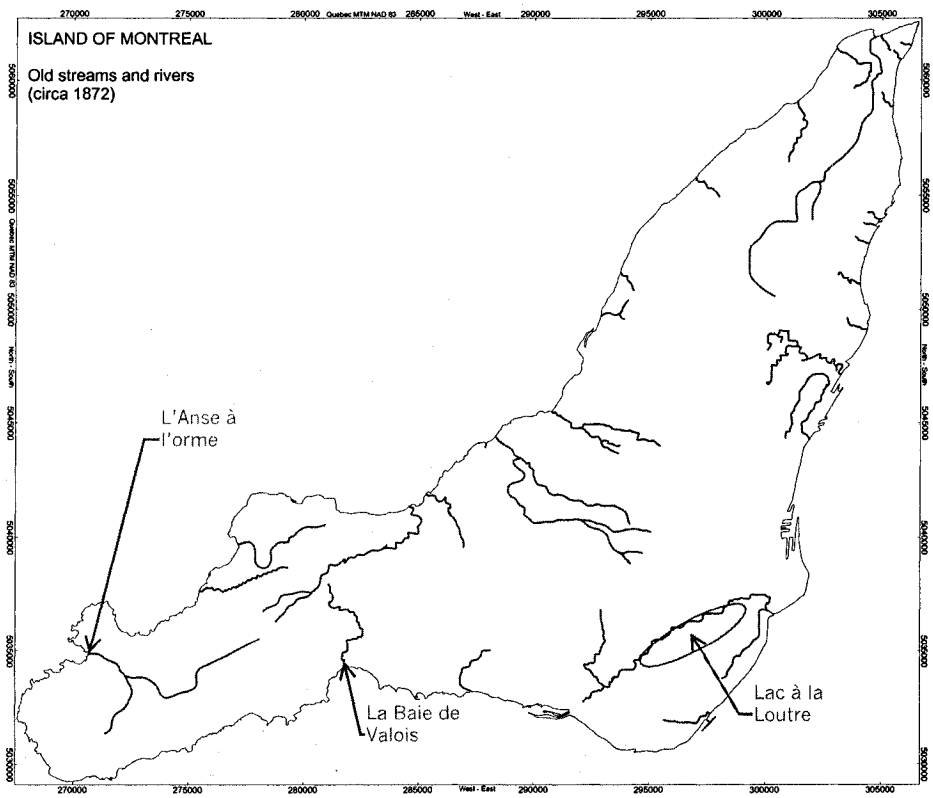

Figure 4-4 Ancient streams and rivers of the island of Montreal (After: Johnston, 1872)

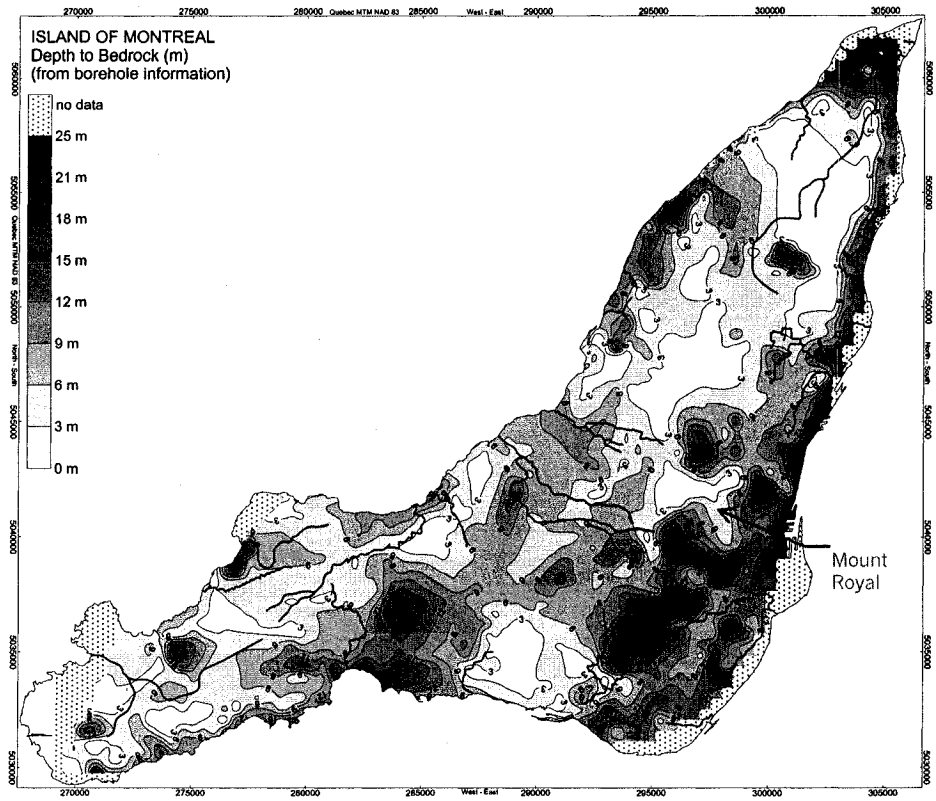

(a) Triangulation grid interpolation method

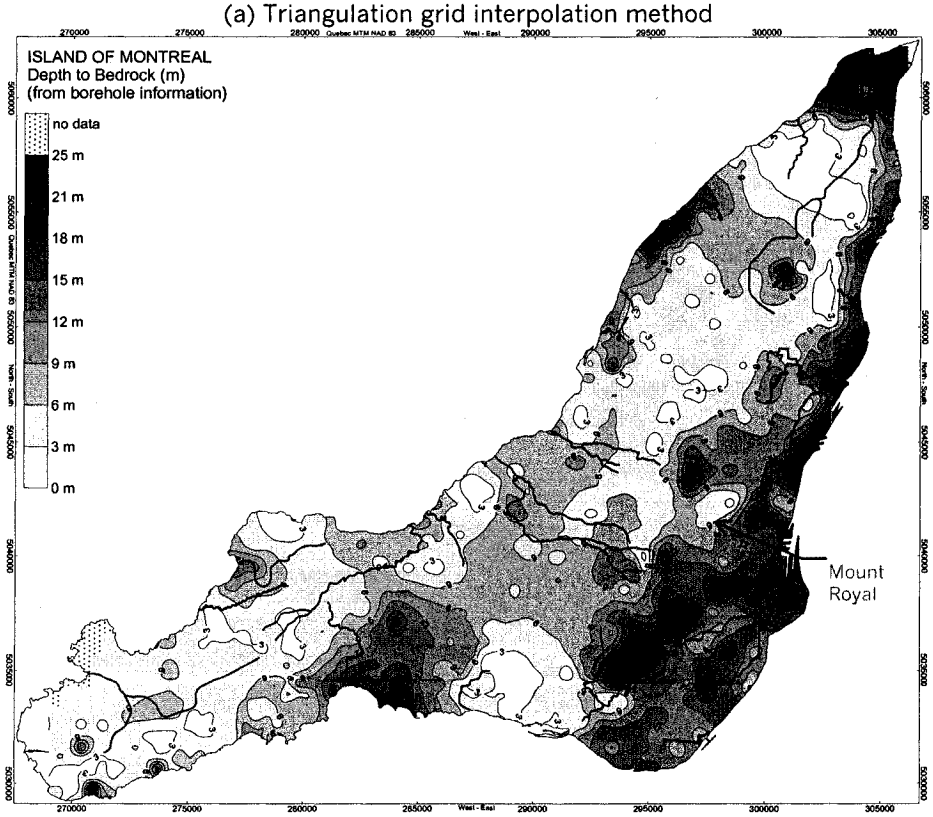

(b) Inverse distance to a power grid interpolation method

Figure 4-5 Depth to bedrock (m) estimated from borehole data

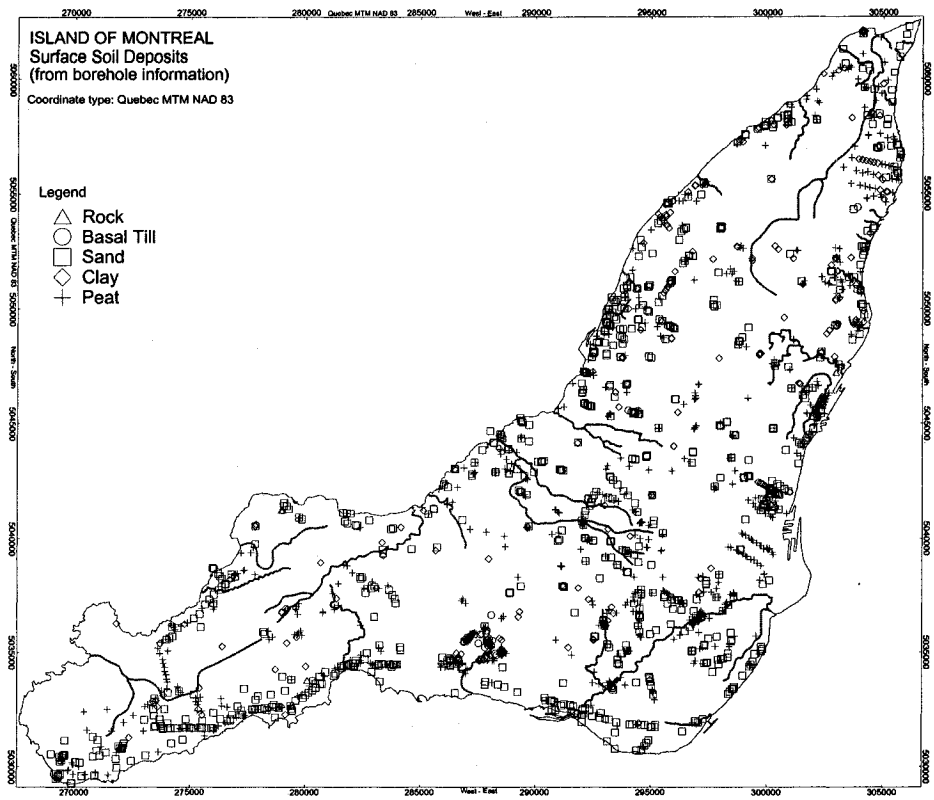

Figure 4-6 Surface soil deposits map from borehole data

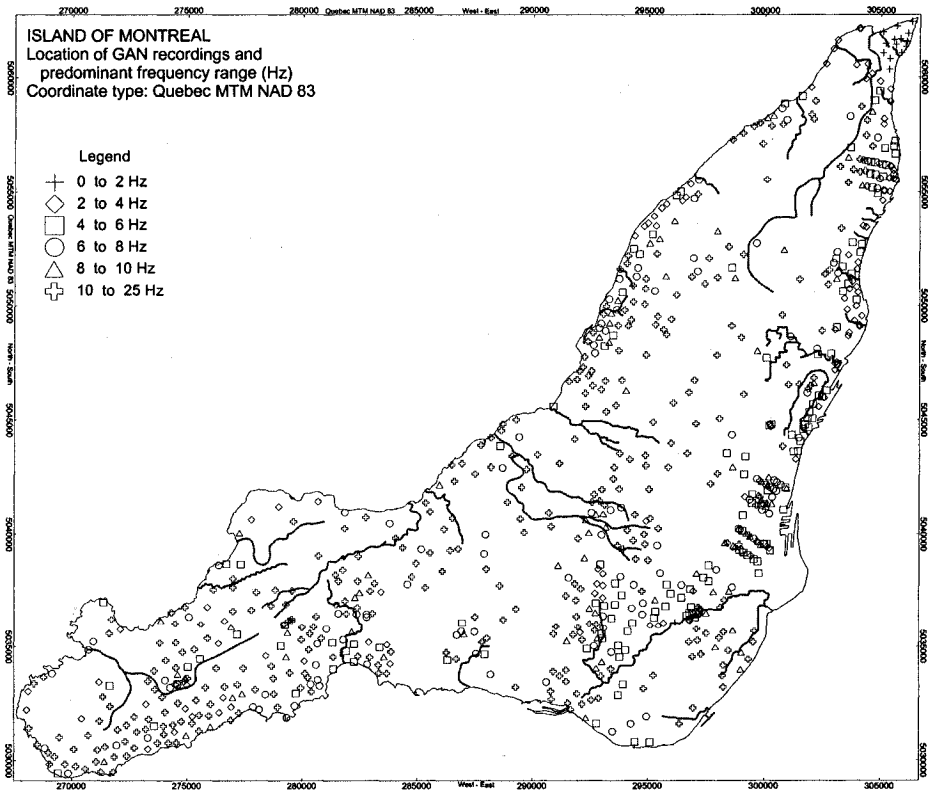

Figure 4-7 Location of GAN records and predominant frequency range

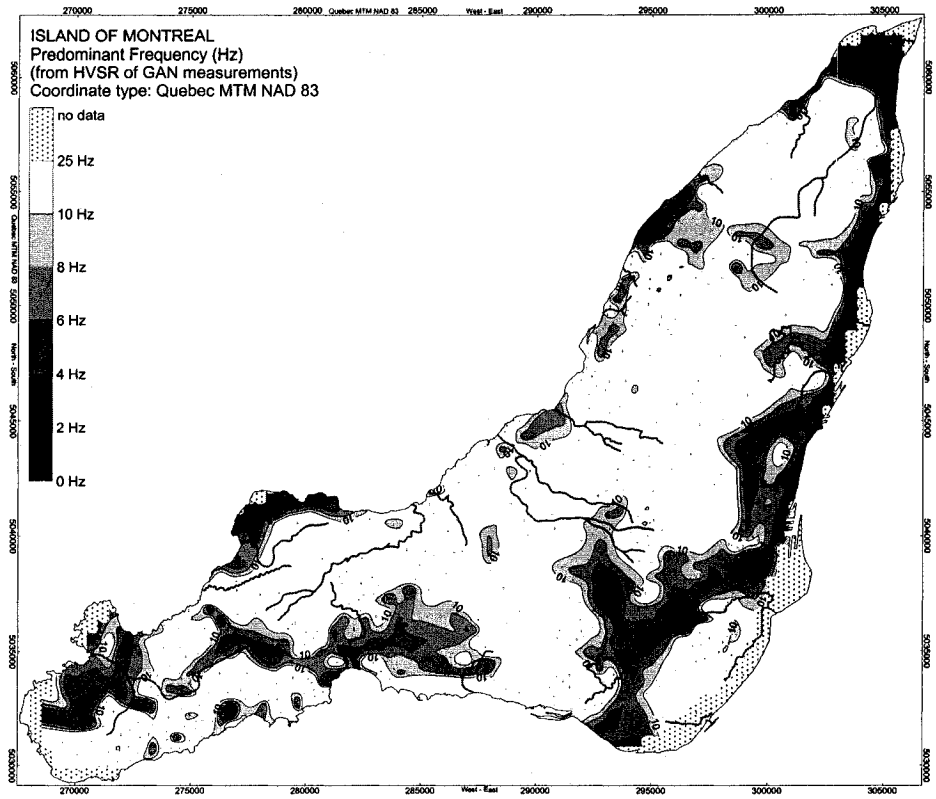

(a) Triangulation grid interpolation method

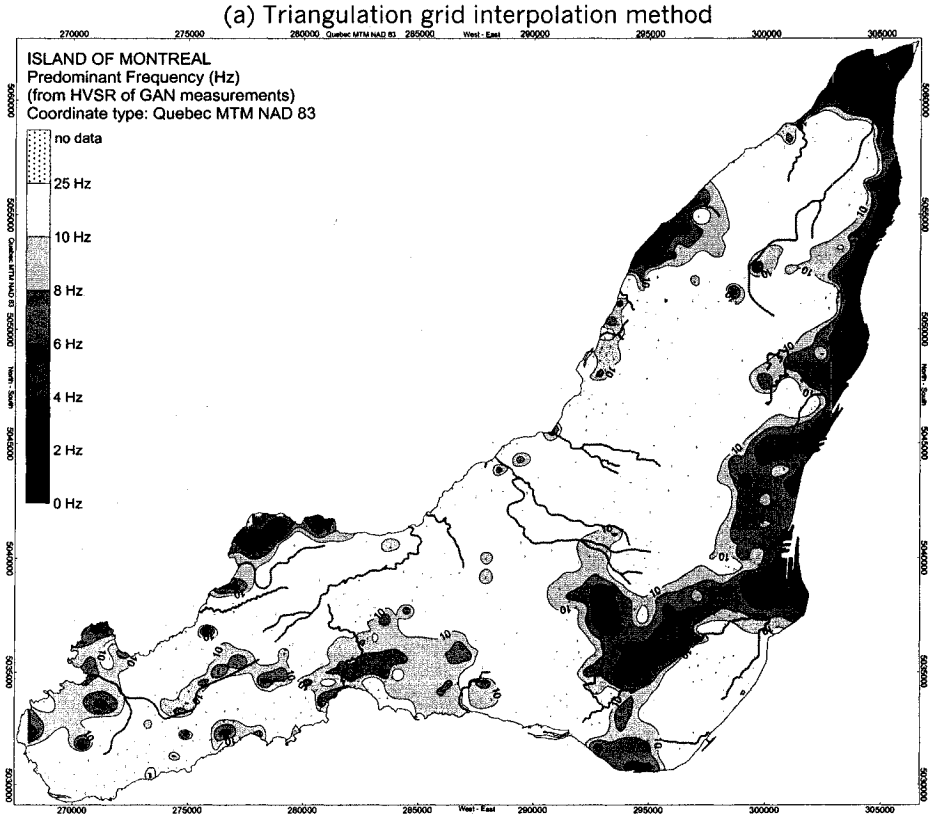

(b) Inverse distance to a power grid interpolation method

Figure 4-8 Predominant frequency from GAN records

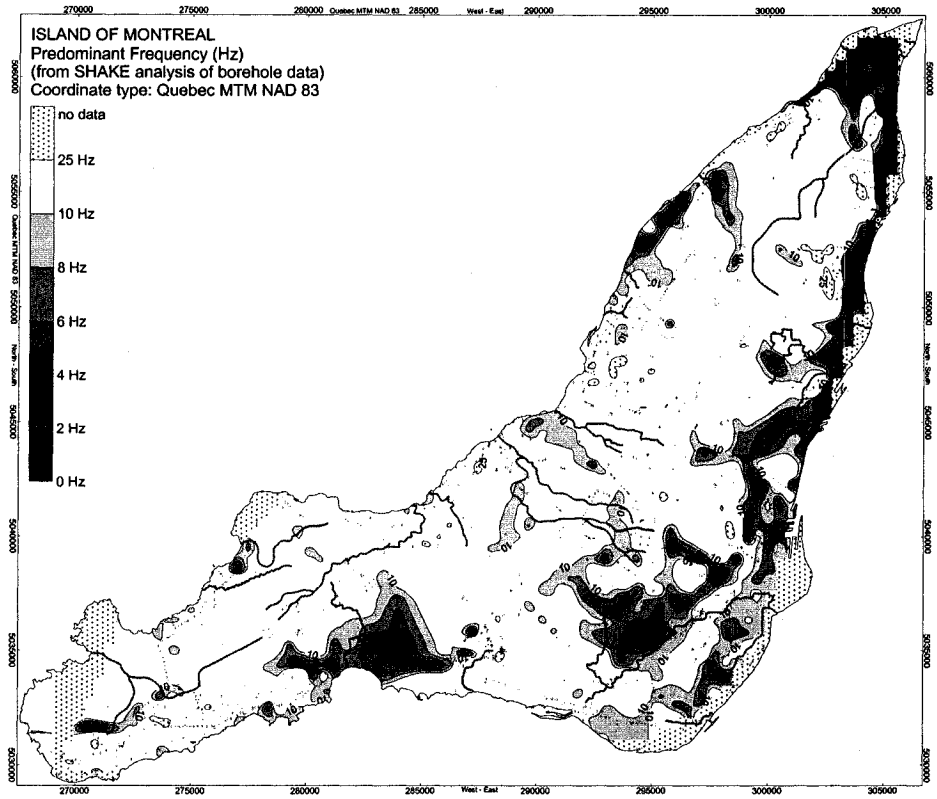

(a) Triangulation grid interpolation method

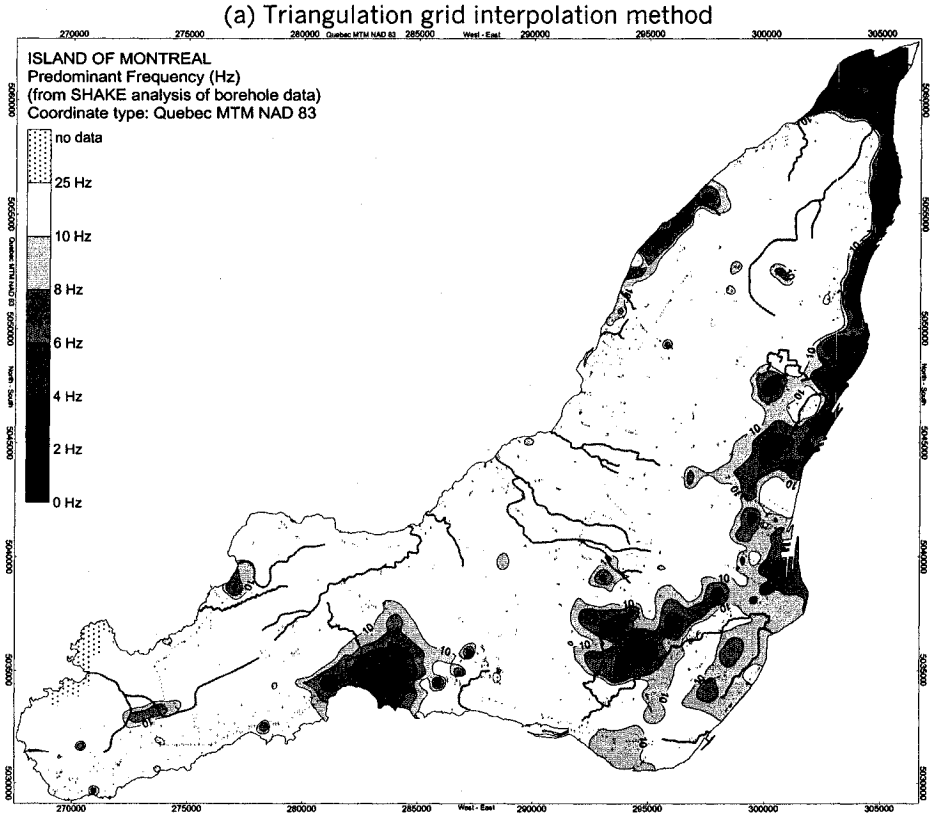

(b) Inverse distance to a power grid interpolation method

Figure 4-9 Average predominant frequencies from SHAKE analysis

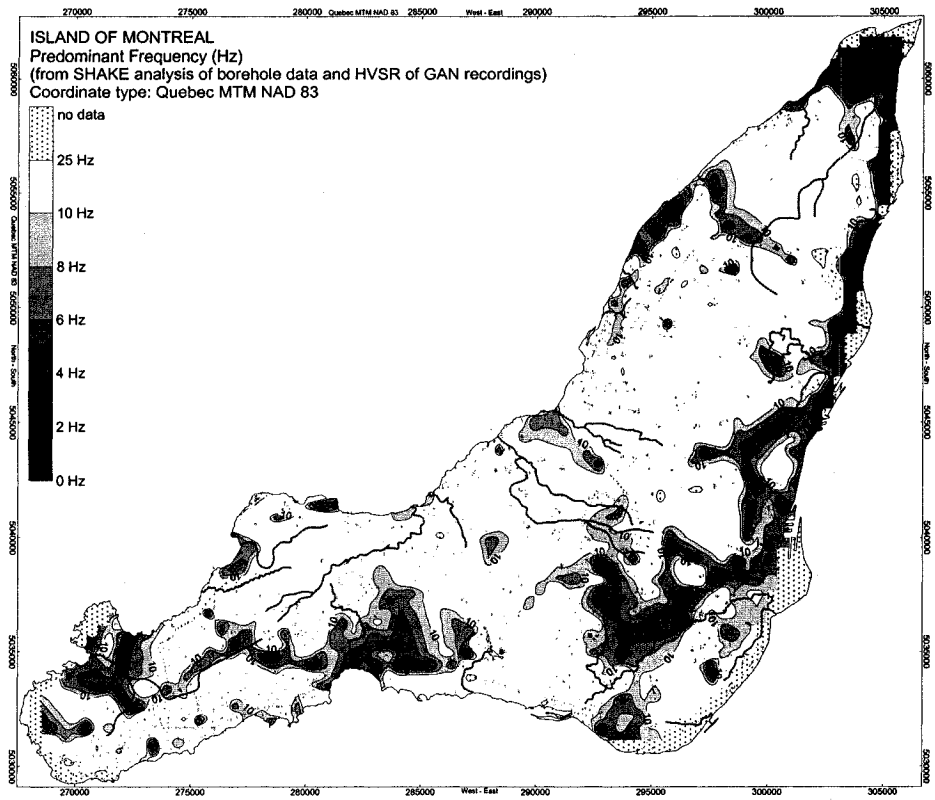

(a) Triangulation grid interpolation method

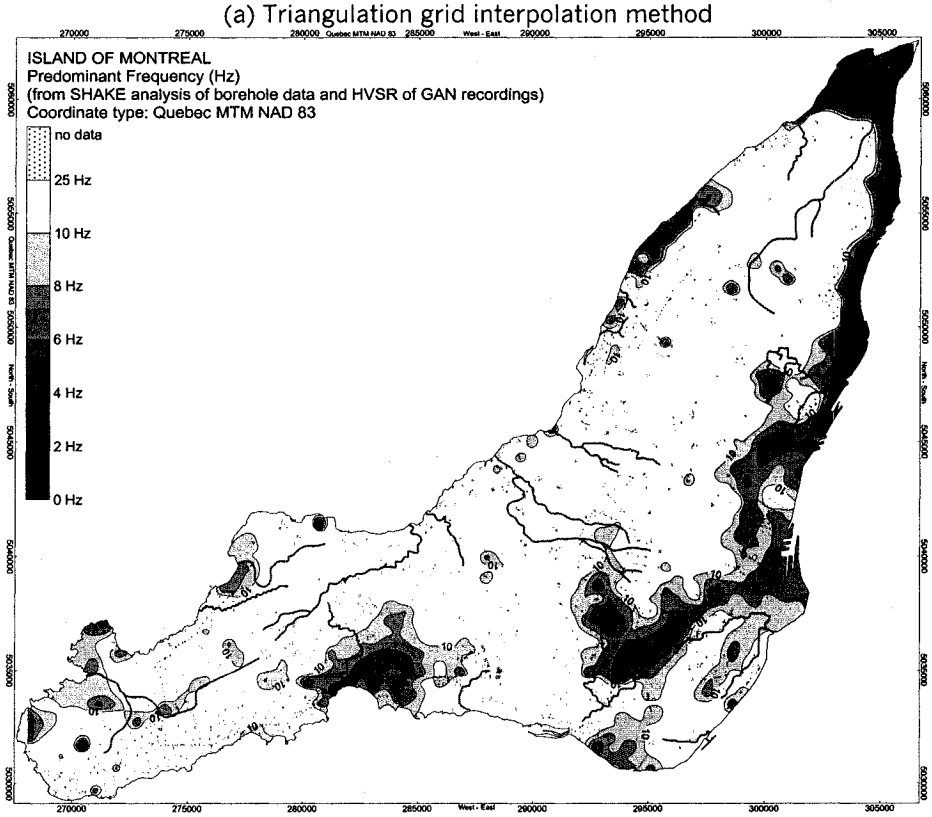

(b) Inverse distance to a power grid interpolation method

Figure 4-10 Predominant frequencies from SHAKE and GAN analyses

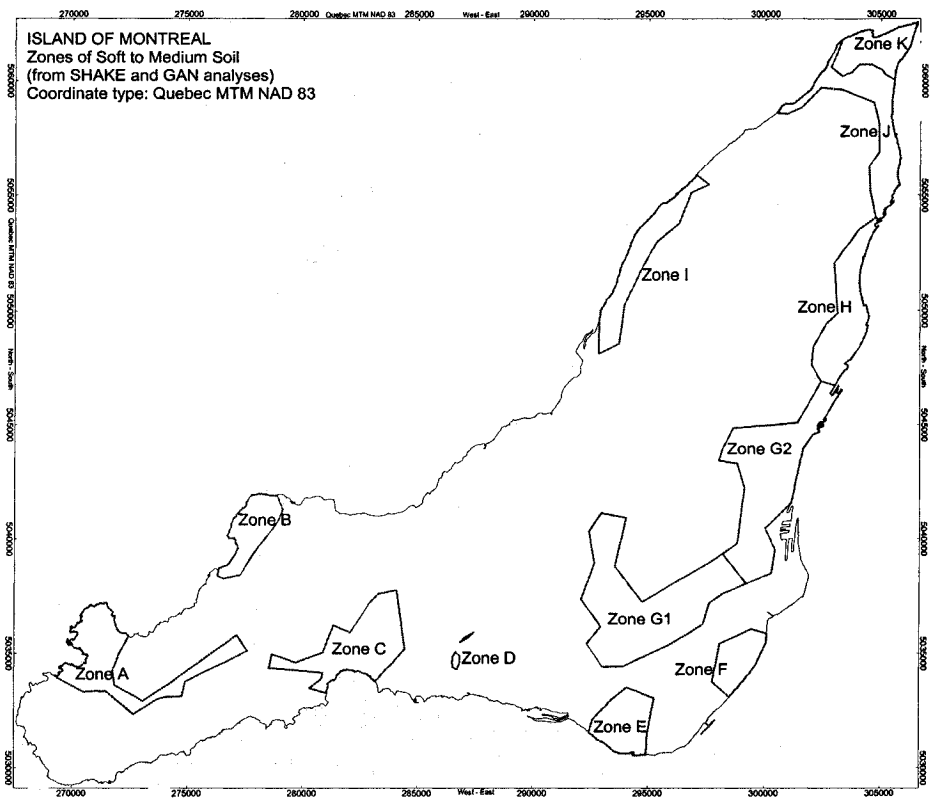

Figure 4-11 Major zones of soft to medium soil deposits.

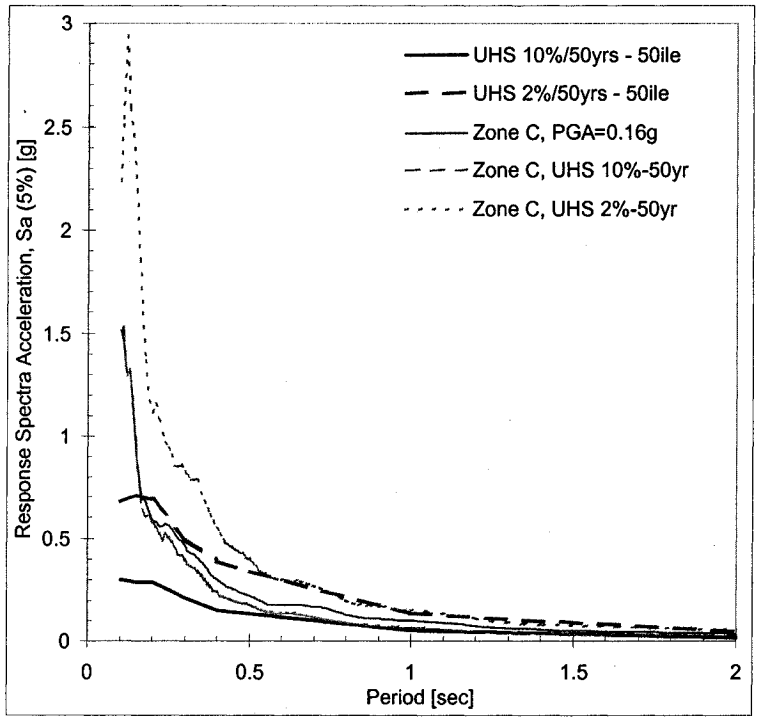

(a) Response Spectra Acceleration for Zone C

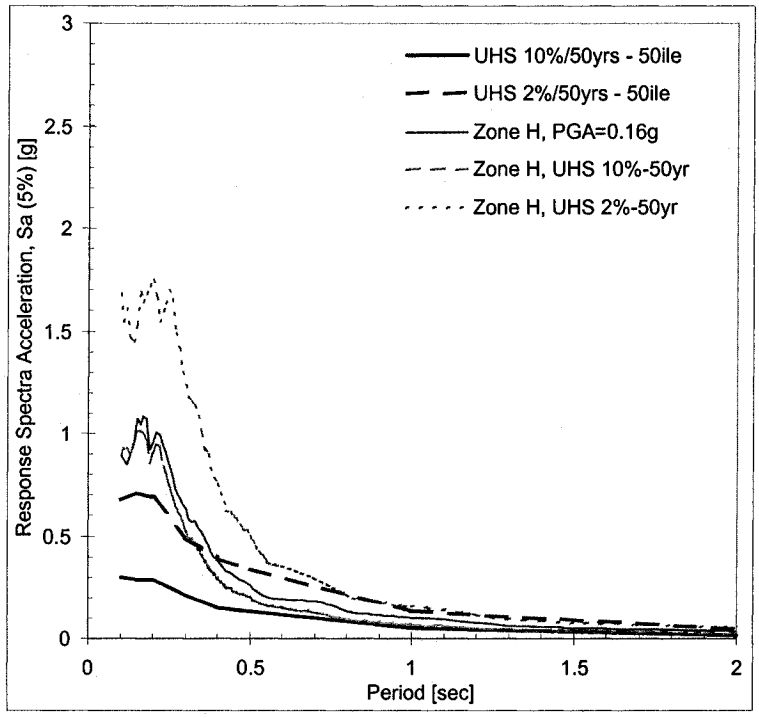

(b) Response Spectra Acceleration for Zone H

Figure 4-12 Response spectra acceleration of selected zones for three earthquake scenarios

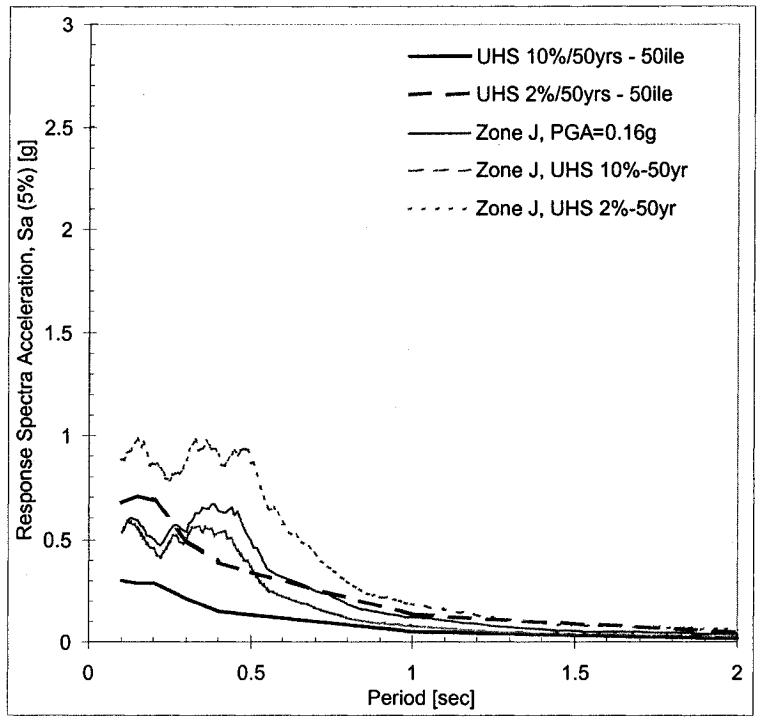

(c) Response Spectra Acceleration for Zone J

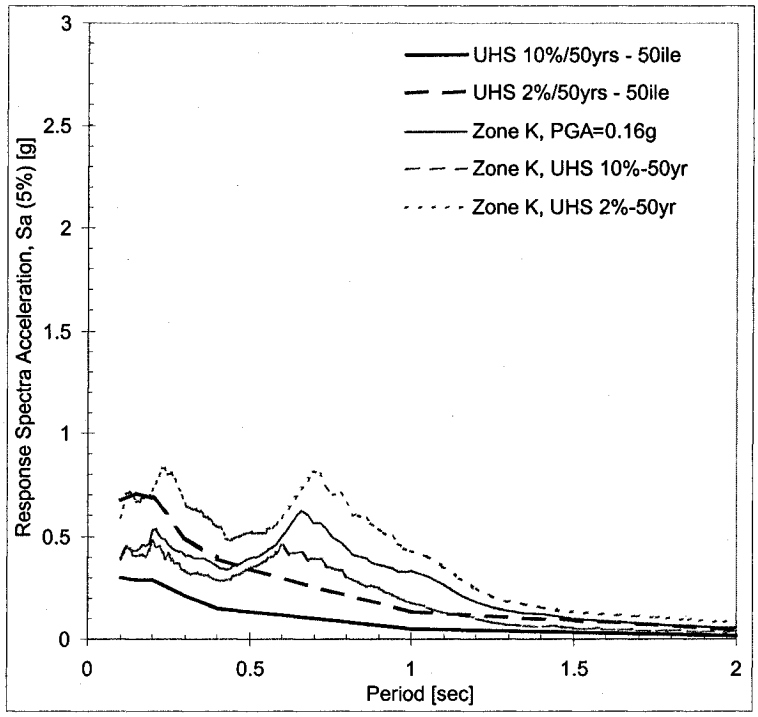

(d) Response Spectra Acceleration for Zone K

Figure 4-12(cont.) Response spectra acceleration of selected zones for three earthquake scenarios

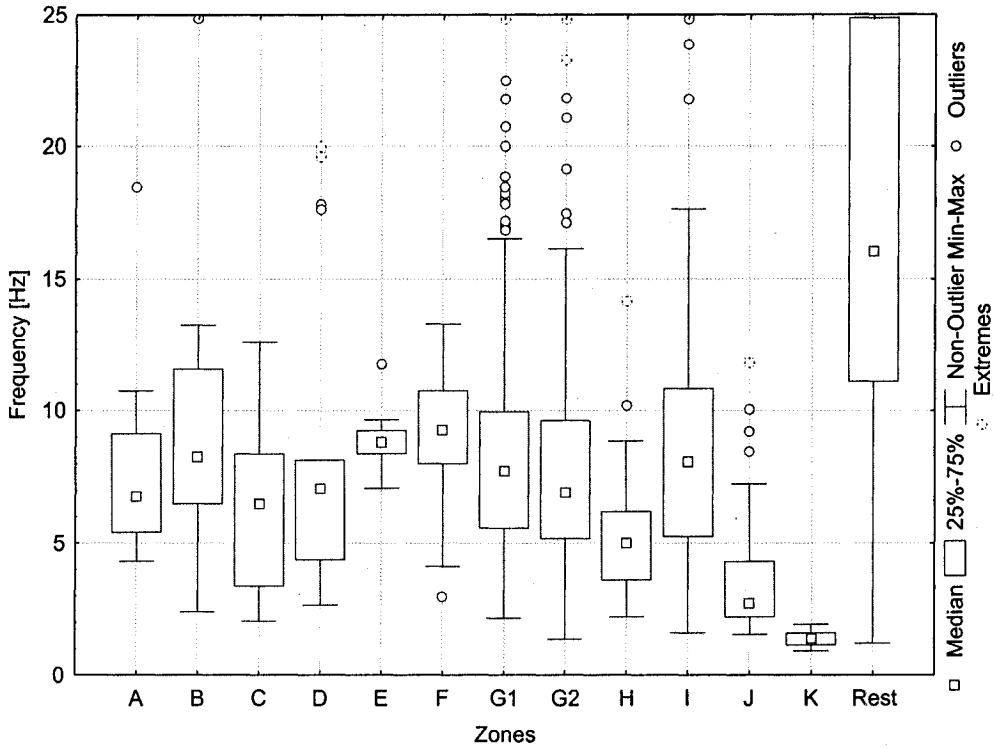

(a) PGA = 0.16 g scenario

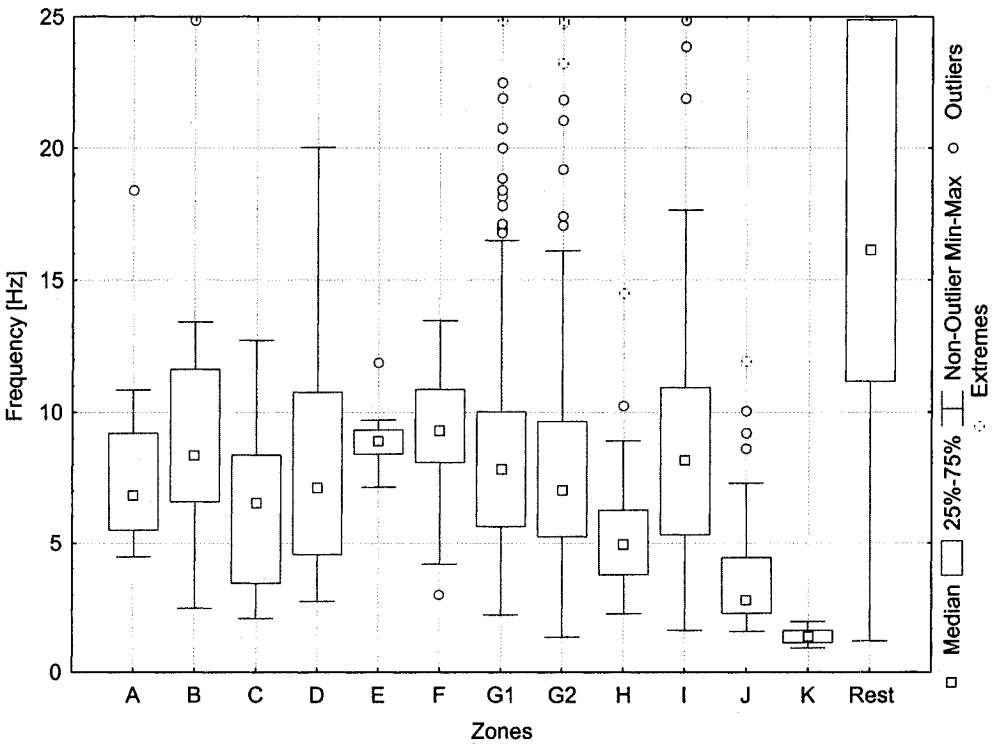

(b) UHS 10% in 50 years scenario

Figure 4-13 Box plots (quartiles) of predominant frequency for different zones

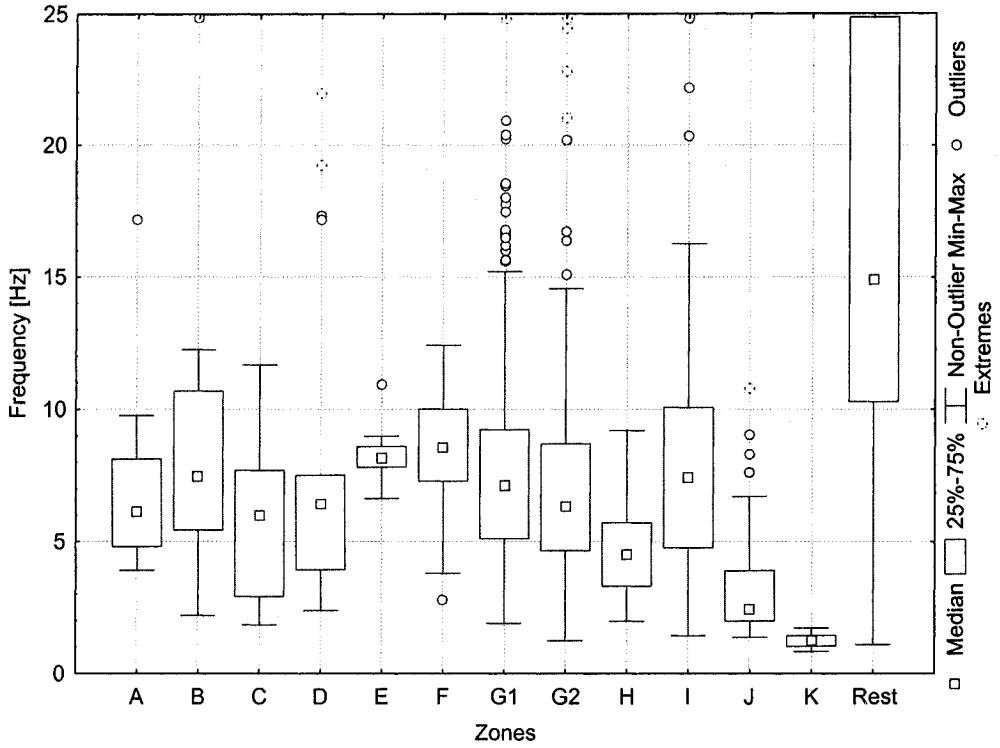

(c) UHS 2% in 50 years scenario

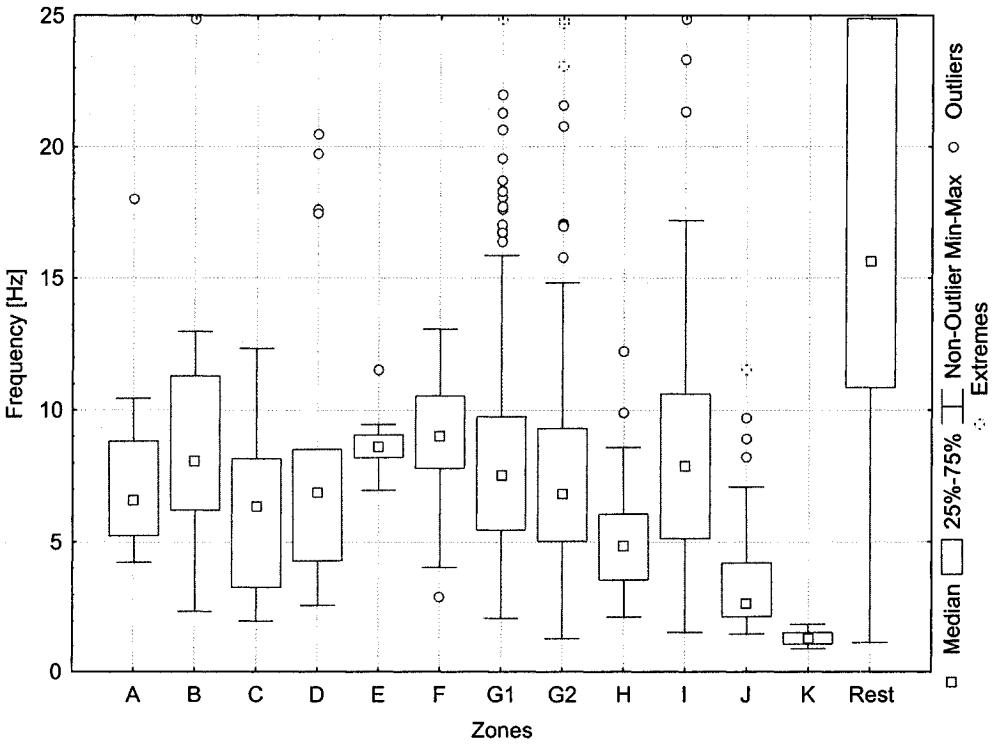

(d) Average frequency of all three scenarios

Figure 4-13(cont.) Box plots (quartiles) of predominant frequency for different zones

Chapter 5

Seismic Evaluation and Retrofit Strategy for the St-Jean Blvd. Overpass Crossing Railway Lines

This chapter describes the procedure followed for the seismic evaluation for the St-Jean Blvd. overpass crossing the CN and CP railway lines. A non-linear model of the main moment-resisting frames of the overpass was created. The model was subjected to time-history ground motions as part of an Incremental Dynamic Analysis. The responses of the key frame elements are presented for three different cases of deterioration in the columns. Seventeen different ground motions were scaled (60 different scaling factors) and a vector of performance parameters was recorded for each case. The program *Response 2000* (Bentz, 2001) was used to determine the non-linear parameters of the main concrete elements of the frame. The program Ruaumoko 3D (Carr, 2001) was used to perform the non-linear dynamic analysis. An application in *Excel*® was developed to perform these operations systematically (Appendix B – Ruaumoko Helper). Finally, a retrofitting strategy is suggested based on the results of the analysis.

5.1 Bridge Description

The St-Jean Boulevard bridge crossing the Canadian National and Canadian Pacific railway lines near Autoroute 20, is considered a lifeline bridge. The definition of a lifeline bridge in the Canadian Highway Bridge Design Code (CHBDC, Canadian Standards Association, 2000) is a bridge that carries or crosses a route that must remain open to all traffic after the design earthquake. A lifeline bridge must also be usable by emergency

vehicles immediately after a large earthquake (say, a 1000-year return period). If the bridge were to be unusable after a major event, the traffic interruption would result in a detour of about 10 km and would affect access to Lakeshore General Hospital. In addition, severe damage or collapse of the bridge would result in the interruption of traffic on the four railroad tracks belonging to the Canadian Pacific Railway and the Canadian National Railway. For the case of lifeline bridges, advanced analysis methods such as non-linear time-history analyses are typically used.

The code specifies importance factors depending of the bridge classification: I = 3.0 for lifelines, I = 1.5 for emergency-routes, and I = 1.0 for other bridges. Although the importance factor of 3.0 can be used for lifeline bridges, the code advises the use of sophisticated methods for the analysis of these bridges. For comparison purposes, the importance factor of 1.5 is used as a minimum requirement for this bridge.

5.1.1 Superstructure

Figure 5-1 shows the geometry of the bridge. The details of the bridge were obtained from the structural drawings dated 1961. The bridge superstructure consists of a reinforced concrete deck supported by a grid of steel beams. Its three spans (21.3, 26.2 and 21.3 m) are supported by two concrete abutments, one at each end, and two concrete moment resisting frames. These frames each consist of twelve columns supported by a wall. The columns are interconnected at their tops by a cap beam, as shown in Figure 5-2. There is a 25 mm gap between the superstructure and the abutments, hence longitudinal displacements greater than 25 mm are limited by the stiff abutments. Therefore, the seismic evaluation was carried out for the transverse direction only. Due to the symmetry of the bridge, it is assumed each of the two frames will share equally the lateral loads.

5.1.2 Description of Structural Components

The load of each of the steel beams from the concrete deck is directly supported by one concrete column, which transmits the load directly to a wall and then to the

foundation. The square-shaped concrete columns contain a longitudinal reinforcement ratio of 3.52% and a volumetric ratio of transverse reinforcement of 0.557%, with #4 ties spaced at 12", as shown in Figure 5-5. This level of transverse reinforcement, combined with its deterioration level is of concern. The overall member performance is analyzed later. The deterioration level observed in the columns (see Figure 2-3) consists of exposed steel reinforcement with significant loss of cover. The CHBDC requires that all forms of deterioration be considered in the seismic evaluation. Figure 5-6 shows a spalled concrete section for such analysis of the columns. In addition, the effect of corrosion on the longitudinal and transversal steel reinforcement was considered. It was assumed to have a reduction of 10% of the gross steel area to account for this effect.

The top of each column is connected to a cap beam composed of eleven segments. This beam carries only longitudinal reinforcement (1.464%) without any transverse reinforcement, and hence is expected to have a brittle failure mode. Figure 5-7 shows the section of the as-built beam.

5.1.3 Material Information

Section 14.6 of the Canadian Highway Bridge Design Code (CHBDC) recommends several methods for determining the strength of the materials used: a review of the original construction plans and documents, analysis of samples from the bridge structure, estimation considering the date of construction, and other approved methods. The technical information for this overpass comes from drawings dated 1961, but no specific information about the quality of the concrete or strength of the steel reinforcement is mentioned. Non-destructive testing such as the Schmidt Hammer Test was inappropriate because the frame elements and foundation walls (Figure 5-2) are covered by a layer of concrete parging making it impossible to test directly on the structural concrete. There was no authorization to take core samples from the structure. The code recommends that for cases where specifications are not available and where samples can not been obtained, to assume values for concrete and steel reinforcement, depending on the age of the

structure. For concrete elements above the foundation, concrete strengths varying from 20 to 25 *MPa* are suggested. A value for the concrete compressive strength of 25 MPa was assumed for the evaluation.

The minimum recommended yield strength value for steel reinforcement for a structure built between 1956 and 1978 is 275 *MPa* for structural grade and 345 *MPa* for intermediate grade. A yield-strength of 300 *MPa* was chosen for the evaluation. The assumed stress-strain relationships are shown in Figure 5-8.

5.2 Site-Specific Soil Conditions

The CHBDC computes the effect of site conditions by introducing a site coefficient, S, in the calculation of the elastic seismic response coefficient C_{sm} (Equation 5-5). The determination of S is based upon soil profiles characterized by the stiffness of the soil (shear wave velocity). These soil profiles range from Type I (mainly rock) to Type IV (mainly soft deep clays). A value of S can be chosen based on the profiles or by engineering judgement, conservatively representing the local site amplifications.

Chapter 4 proposes a set of seismic microzonation maps for the island of Montreal. However, if site-specific information is available, detailed studies can be carried out. In the case of the St-Jean Boulevard overpass crossing the CN and CP railways, ground ambient noise (GAN) was recorded at several locations close to the bridge (Figure 5-9). Their Horizontal-to-Vertical Spectral Ratios (HVSR) are presented in Figure 5-10. According to the Nakamura technique (Nakamura, 1989), the peak frequency of the HVSR graphs corresponds to the fundamental frequency of vibration of the soil column. From Figure 5-10, it can be observed that the peak frequencies are around or greater than 10 Hz, which correspond to stiff soils (Dense Sand, Basal Till, or Rock). The borehole 63OTTA-23421 (whose location shown in Figure 5-9) shows the bedrock close to the surface. The results from the GAN recordings and the borehole are confirmed by the structural drawings, which

indicate rock at the base of the foundations. Therefore, a rock foundation was assumed in evaluating this bridge.

5.3 Structural Idealization of Bridge Frame

The moment-resisting frame (half of it depicted in Figure 5-2) was idealized by 69 elements divided into six types (Figure 5-3). Of those 69 elements, 23 have possible non-linear behaviour. These elements correspond to the 12 columns and the 11-segments of the cap beam that links their tops. A steel beam grid (*33WF141* principal beams, *18W50* and *15C33.9* diaphragm beams) supports the concrete deck and is connected to the moment-resisting frame by rocker supports (Figure 5-4). It is assumed the only forces transmitted to the concrete moment-resisting frame are shears and axial loads. This effect is achieved by introducing an internal hinge at the bottom end of the steel elements that connect the superstructure to the concrete frame. The mass of the superstructure is assumed to be located at the level of the deck.

5.4 Sectional Analysis of the Bridge Elements

The structure has been idealized into 69 elements, from which 23 have possible non-linear behaviour. These elements are reinforced concrete columns and beams that are assumed to resist the entire lateral load applied to the system. The correct modeling of the nonlinearities of these elements is a key point in the seismic evaluation of the bridge. The modeling is strongly tied with the capabilities of the available tools, in this case Ruaumoko 3D (Carr, 2001).

5.4.1 As-Built Column

The level of deterioration of the columns is an important factor that affects the ultimate resistance. Initially, a typical column behaves as a double-fixed cantilever, 4.877

m long. The length corresponds to the column height between the bottom of the cap beam and the top of the wall. The columns were analyzed with *Response 2000* with and without the spalling of the concrete cover as shown in Figure 5-6. In addition, the influence of corrosion of the reinforcing bars was also studied. The corrosion was modelled by assuming a ten percent reduction of the area of the steel reinforcement.

The failure mode of the element can be either shear or flexure. It is noted that for these relatively long columns, the shear capacity is adequate and flexure is critical (see Figure 5-11). The complete response is calculated by *Response 2000* using the following procedure: (1) moment-shear iterations are performed varying the loads until the failure occurs; (2) a moment-shear envelope curve that encompasses the maximum values is plotted; (3) an increasing lateral load or pushover load is applied until the moment-shear envelope line is reached. For the columns analyzed, the predicted failure mode is principally flexure. Figure 5-12 shows the pushover load-deflection responses for the three cases. In all of the cases, a constant applied axial load per column was taken as 454 *KN* (gravity load effect).

The variation of the axial load in the columns may change substantially the value of the general yielding moment for the section. Higher compressive loads will increase the yielding moment, but will decrease the ductility. On the other hand, lower compressive loads will decrease the general yielding moment and increase the ductility of the section. This effect is illustrated by the predicted moment-curvature responses in Figure 5-13.

Ruaumoko normally requires the definition of the axial load versus yielding moment diagram for each of the members with non-linear behaviour. *Response 2000* calculates the interaction diagram of axial load versus maximum moment of a section (Figure 5-14). The general yielding moment and curvature should be determined (Park, 1989) to model the stiffness before and after yielding.

Figure 5-15 shows the predicted hysteresis responses for an unspalled section and a section with corroded reinforcement for a selected earthquake ground motion. The

Takeda hysteresis model was used (Figure 5-16), with the Emori unloading pattern, an unloading stiffness factor (α) of 0.25 and a reloading stiffness factor (β) of 0.3. In determining the initial loading stiffness for the response of the columns, a cracked section was assumed up to general yielding. A reduction in strength or degradation is accounted for at a pre-selected curvature. Figure 5-13 shows the degradation in strength for the three cases considered. Note the degradation rate is more pronounced with higher axial loads. Since the columns are subjected to variable axial loads during an earthquake, a unique value cannot be used for the analysis. Hence, an average degradation factor of 0.87 was assumed and is used in the Ruaumoko analysis. These dynamic parameters are used in the Incremental Dynamic Analysis (Table 5-1), whose results are shown later in this chapter.

5.4.2 As-Built Beam

The as-built beam has only longitudinal steel reinforcement (Figure 5-7). The lack of transverse reinforcement makes the beam susceptible to shear failures (Figure 5-18(a) and (b)). The geometry of the beam and its interaction with the adjacent columns will make it experience only nodal forces: axial load, moment, and shear, without any distributed load (Figure 5-17), with a moment-to-shear ratio of about 0.893m at the column faces. The moment curvature relationship evaluated with this ratio is shown in Figure 5-18(c).

The maximum beam shear, V, is a function of the applied nodal moments, M, and the clear length between the columns, L, given by the relationship $V = 2M/L$. For this beam without stirrups, the shear strength is controlled by the concrete resistance. Because shear failure occurs before flexural yielding the ultimate shear capacity will dictate the maximum loads in the beam. The maximum shear resistance using a simplified code expression can be approximated as:

$$V_u \approx 0.166\sqrt{f'_c}\, b\, d = 0.166\sqrt{25} \times 457 \times 406 = 154\,\text{kN} \qquad 5\text{-}1$$

where: b is the width of beam (*mm*), and d is the distance (*mm*) from the top compression fibre to the centroid of bottom steel and f'_c is the compressive strength of the concrete (*MPa*).

Using the relationship between the shear and the moment at the column faces gives a maximum beam moment at the occurrence of shear failure of:

$$M = VL/2 = 154 \times 1786/2 = 138\,\text{kN.m} \qquad 5\text{-}2$$

A companion research project was carried out by Itagawa (2005) and involved the testing of a two-column half-scale frame structure that simulated the details of this bridge bent. This experimental project clearly showed that the beam fails in shear before any plastic hinges could form in the beam or the columns. It was concluded that the prediction of shear failure from *Response 2000* gave better predictions than the approach using Equation 5-1. The predictions of the response of the full-scale beams of this structure were made using *Response 2000* and a moment-to-shear ratio of 0.893 to include the interaction of moment and shear. The *Response 2000* prediction gave a maximum shear of 128 kN. It is noted that this prediction is lower than that given by Equation 5-1. It is believed that the *Response* prediction more accurately accounts for the details of the flexural reinforcement and the size effect for this 457 mm deep beam. The corresponding maximum moment in the beam (see Equation 5-2) is 114 kN.m. These more accurate predictions were used in the non-linear dynamic analyses. Figure 5-18 shows the *Response 2000* predictions. The hysteresis response used for the non-linear dynamic analyses was chosen to severely degrade and decay after this peak load (Figure 5-19).

5.5 CHBDC Predictions

The Canadian Highway Bridge Design Code provides recommendations for the seismic evaluation and retrofitting of existing bridges using a static analysis approach. The

ratio between the ductility provided R_{prov} and ductility required R_{req} must be greater or equal to 1.00 (Eq. 5-3) otherwise retrofitting is required.

$$\frac{R_{prov}}{R_{req}} \geq 1.00 \qquad 5\text{-}3$$

The ductility required is defined by the ratio between the seismic effects as if all members are elastic (S), and the member capacity after the dead load has been accounted (C):

$$R_{req} = \frac{S}{C} \qquad 5\text{-}4$$

The seismic effects (shear or moment) on a member are proportional to the dead and earthquake load ($S \sim 1.0D + 1.0EQ$). The earthquake load is defined by the elastic seismic response coefficient C_{sm} multiplied by the total seismic weight of the structure W:

$$C_{sm} = \frac{1.2AIS}{T_m^{2/3}} \leq 2.5AI \qquad 5\text{-}5$$

For the Montreal region, the zonal acceleration ratio A is 0.20. The site coefficient S for a rock site is 1.0 (Soil Profile I, rock). From a static analysis, the fundamental period was found to be T = 0.629 sec. Therefore the elastic seismic response coefficient C_{sm} is:

$$C_{sm} = \frac{1.2 \times 0.20 \times 1.5 \times 1}{0.629^{2/3}} = 0.4905 \leq 2.5 \times 0.20 \times 1.5 = 0.75 \qquad 5\text{-}6$$

The total earthquake load applied to the entire bridge (both frames) is approximately $EQ \sim 0.4905 \times 15802\text{kN} = 7750\,\text{kN}$ on the two frames (24 columns), or 322.9 kN applied on nodes 25 to 36 (Figure 5-3). From a static analysis using this lateral force, the shear and moment at base of the column (near middle) are 329.9 kN and 871.8 kN.m, respectively. For the edge beam, the moment is 654.6 kN.m and the shear is 495 kN.

For the evaluation of this bridge, the member capacities are defined by:

$$C \sim \begin{matrix} M_n - M_D \\ V_n - V_D \end{matrix} \qquad 5\text{-}7$$

where: M_n and M_D are the nominal moment resistance and moment action due to dead load. V_n and V_D are the nominal

shear resistance and shear action due to dead load.

The dead load effects are negligible (shear and the moment) when applying an axial dead load on this structure; hence, M_D and V_D are zero. The nominal flexural and shear resistances of the as-built column are 463 kN.m and 189.8 kN, respectively (Figure 5-11, Figure 5-12). As found in the previous section, the beam fails in shear at a predicted nominal resistance of 128 kN and a corresponding maximum moment of 114 kN.m. Therefore, in accordance with the evaluation procedure given in the CHBDC (Canadian Standards Association, 2000) the required ductility for the column and beam are:

$$\text{Moment in Columns: } R_{req} = \frac{S}{C} = \frac{871.8}{463} = 1.883$$

$$\text{Moment in Beam: } R_{req} = \frac{S}{C} = \frac{654.6}{114} = 5.742$$

$$\text{Shear in Columns: } R_{req} = \frac{S}{C} = \frac{329.9}{189.8} = 1.738 \qquad 5\text{-}8$$

$$\text{Shear in Beam: } R_{req} = \frac{S}{C} = \frac{495}{128} = 3.867$$

It is evident from these values that the element with the highest ductility required is the as-built beam. Because the beam has no transverse reinforcement and is predicted to fail in shear, it is valid to assume that its ductility provided is close to 1.00. Therefore, the beam requires retrofit.

5.6 Incremental Dynamic Analysis (IDA)

5.6.1 Scaled Time-Histories

The selection of design earthquakes can be a challenging task, especially for a structure that has deficiencies at many locations and has several modes of vibration. The advantage of the Incremental Dynamic Analysis is it repeatedly analyzes a structure with a set of earthquakes scaled within a range, and the overall performance is recorded. The more numerous the earthquakes are, the better the structure is tested. The original scale

factor is not of great importance, or the intensity associated with the source and distance. This is because since the record will be scaled up or down, the intensity becomes of secondary importance to earthquake frequency content. Theoretically, if a very large number of earthquakes is used, it is possible to predict the maximum response at determinate levels of input ground acceleration. In summary, the IDA approach permits a graphical display of the "Intensity Measurement" (IM) versus the "Damage Measurement" (DM) of a structure under a set of earthquakes (Vamvatsikos and Cornell, 2002). The set of earthquakes used are the same used in the first part of the thesis and are listed in Table 3-4 and Table 3-5.

The scaling of the earthquakes used in an IDA is normally associated with the structure, often with its first elastic fundamental period. In this research, the scaling procedure and its interaction within IDA is carried out as follows: (1) the response spectrum of the earthquake (5% damping) is evaluated at the first elastic fundamental period of the structure; (2) one value of a range of target response spectra acceleration (S_a) is selected. In this research, the range is from 0.015 g to 1.6 g; (3) a scale factor is defined as the ratio between the target S_a and the value first evaluated from the earthquake; (4) the input ground motion used is the original record multiplied by the scale factor; (5) the structure is analyzed (using Ruaumoko) and the DM values are extracted and recorded from the results file along with the associated target spectral acceleration (or IM) and scale factor; (6) the process is repeated again from step 2, until the full range has been covered; and (7) the entire process is repeated with another earthquake record.

5.6.2 Performance Parameters

The behaviour of a structure can be described by appropriate performance parameters. For the case of buildings, the maximum interstorey drift is often used to determine the level of performance of the building. For the case of bridges, the vector of performance parameters is less related to the overall structure and more to critical elements that might undergo yielding or brittle failures. The critical elements of this bridge

are the columns and beams. Due to the overturning effect, the elements located to the edge of the structure are subjected to a higher variation of axial loads than the elements closer to the middle. To study this effect, three elements were selected as control elements: two columns: elements 1 and 5, and one beam: element 13. Their locations are shown in Figure 5-3(a).

In this research, the selected performance parameters are:

(1) Maximum Curvature:

Curvatures can be evaluated at the two ends of a frame element. For the case of the columns, their top end is connected to the concrete beam and the superstructure, while their bottom-ends are connected to the wall support. For lateral loading, hinging is expected to occur at the base of the column before hinging at the top of the column. It is predicted that the beams will fail in shear before significant yielding in the columns and hence after shear failure the columns will behave as cantilevers. The maximum curvature at the bottom end of Element 1 (edge column) and Element 5 (middle column) are used as performance indicators. For the case of the beams, their expected moment-curvature behaviour is quasi-linear until a brittle shear failure occurs (Figure 5-18(c)). Element 13 (edge beam) is the most critical beam element. The maximum curvature at both ends of the edge beam is used as a performance indicator.

(2) Maximum and Minimum Axial Force:

The expected overturning effect in the bridge will produce a compressive or tensile force in the columns depending on the direction of the inertial horizontal forces. It is of interest to track the changing axial forces in the columns to see if they experience tensile axial forces. The edge columns are more susceptible to this effect than the middle columns. Ruaumoko gives the maximum axial force as tension (positive) and the minimum axial force as compression (negative). These predicted axial loads were used as performance indicators.

It was noted that when the maximum curvatures reached about 0.04 radians/m, the structural response tended to be unstable and collapse was assumed.

5.6.3 Predicted behaviour of key elements

The results of an Incremental Dynamic Analysis are displayed in a Damage Measurement (X-axis) vs. Intensity Measurement (Y-axis) format. The collection of curves is a result of plotting one curve per earthquake used, and a set of percentile curves (16%, 50% and 84%) to summarize the analysis. Figure 2-4 shows four different cases for the IDA curves. 'Softening' occurs when the structure yields as the spectral acceleration increases, giving a response similar to a force-displacement analysis. The 'hardening' case occurs when the element apparently recovers due to internal redistribution of loads due to a change in stiffness. 'Weaving' behaviour is a combination of both and it is due to the nature of the earthquake timing that triggers yielding at certain levels and hardening at others. All of these cases are present in this analysis. Another type of case called 'structural resurrection' (Vamvatsikos and Cornell, 2002) is also present in this analysis. This case is when; at a certain acceleration level, the element under study experiences large curvature levels associated with collapse, but at a larger acceleration levels the curvatures are back to normal levels, hence showing a recovery or 'structural resurrection'.

Three key elements are under observation (Figure 5-3(a)): Element 5, or the column closest to the middle; Element 1, or an edge column, located at the outermost end of the frame; and Element 13, or the edge beam, is the outermost beam segment that connects to an edge column.

The results of the three cases considered for the as-built bridge analysed are summarized below:

(1) Unspalled Column Section:

Figure 5-20(a) and Figure 5-21 show the IDA results of maximum curvature for edge beam and the two columns, respectively. The consolidation of these values is shown in Figure 5-24(a), which contains the median values of maximum curvature for the three

key elements and an additional beam segment (element 14). It can be observed that around the same acceleration level the edge beam softens, the edge column hardens, triggering dispersion of the curves with increasing acceleration. It is noted that the 16, 50 and 84 percentiles of the IDA values were determined by calculating the curvatures associated with a constant acceleration level for different earthquakes and repeating these calculations for different acceleration levels.

Figure 5-25(a) shows the axial force variation for the three elements. As expected, the variation in the axial load of an edge column increases with increasing acceleration levels. The variation of axial load in a middle column is negligible until high values of spectral acceleration are reached.

The predicted behaviour of the frame with an unspalled column section results in premature shear failure of the beam. This shear failure is followed by the formation of a pin connection in the beam, with the columns becoming more flexible and the columns experiencing some inelastic response at their bases shortly thereafter. It is apparent from Figure 5-24(a) that the beam shear failure and the subsequent large deflections of the frame constitute failure. This occurs at a spectral acceleration level of 0.15g, much below the CHBDC code of 0.49g, even for 'emergency- route' bridges (I = 1.5). It is noted that the predicted median IDA (50% IDA) indicates beam shear failure with subsequent flexural yielding of the 'pin-connected' columns at their bases. Due to the variation of the axial loads in the edge columns, they yield first. The beam shear failure occurs considerably below the UHS 2% in 50yrs (50th percentile) level. It is important to realize that there is considerable dispersion in the IDA values for different seismic input levels.

(2) Spalled Column Section:

Figure 5-20(b) shows the results of the predicted maximum curvatures for the edge beam and Figure 5-22 shows the results of predicted maximum curvatures for the middle and edge columns. The predicted median IDA values for the three key elements and an additional beam segment (element 14) are combined in Figure 5-24(b). Similar to the

unspalled case, the edge column element hardens at the same level of acceleration when the edge beam softens. The dispersion of the maximum response also increases with increasing acceleration.

Figure 5-25(b) shows the variation of axial force for the three key elements, with the variation of the axial load in edge columns increasing with increased spectral acceleration.

The predicted behaviour of the frame with a reduced column section (Figure 5-24 (b)) greatly exceeds the UHS 2%/50yrs (50^{th} percentile) level of 0.288g but with a large variation in the response at these levels, including the variation of axial load. The overall response is of the same magnitude as the case before, but with column yielding at a slightly lower acceleration level.

(3) Spalled and Corroded Column Section:

Figure 5-20(c) and Figure 5-23 shown the results of the predicted maximum curvatures for the edge beam and the middle and edge columns, respectively. The predicted median values of these elements and a middle beam (element 14) are summarized in Figure 5-24(c). As expected the response is similar to the unspalled and spalled cases up to the point when beam fails in shear (i.e., at a curvature of 0.0033 rad/m). It is evident that the 'spalled-corroded' results in yielding at the column bases at a reduced acceleration level.

Figure 5-25(c) gives the predicted variation of axial forces for the three selected elements. Their behaviour is similar to the first two cases.

The predicted behaviour of the frame with a reduced column section with corroded reinforcement significantly exceeds the UHS 2%/50yrs (50^{th} percentile) level. The predictions indicate that there is a large variation in the responses at these levels, including the variation of axial load. The strength parameters for the columns used in this case are believed to represent more accurately the current condition of the structure and hence these response characteristics are used in the analysis of the retrofitted case.

5.6.4 Summary of predicted behaviour of the moment resisting frame, failure definition

The maximum curvature values of the edge beam soften at approximately the same level as the maximum curvature values of the edge column start to harden. The hardening of the middle column occurs at a slightly higher level of spectral acceleration. It is also observed that the dispersion of values begins to increase with increased spectral acceleration after the failure of the beam. This premature shear failure of the edge beam results in 'pin-connected' columns at the top and a more flexible frame, with larger moments at the column bases. This is accompanied by an increase in the period of the structure. However, at higher acceleration levels, there is a very large dispersion of the values, with this dispersion increasing with increases in acceleration levels. The phenomenon of 'structural resurrection' (Vamvatsikos and Cornell, 2002) was also observed in Figures 5-20 to 5-23. The brittle shear failure in the beam and the large dispersion of the results makes it difficult to predict the behaviour of the frame at a particular higher spectral acceleration level. Earthquakes with spectral acceleration levels above about 0.15g (median response) are predicted to cause brittle shear failure of the beams and hence the frame should be retrofitted. Figure 5-24 compares the responses of the Element 13 (edge beam) and Element 14 (beam near middle). It is clear that the edge beam is more critical because it has higher moments and shears than an interior beam.

5.7 Retrofitting Strategy and Predicted Response

It was shown that the early shear failure of the concrete beam dominates the overall response of the frame. The objective is to improve the performance of the frame with minimum retrofit. The retrofitting strategy is based on the reduction of the response dispersion by strengthening the reinforced concrete beam. If the beam becomes stronger than the columns then yielding will occur in the columns rather than in the beams. To accomplish this, the beams must be capable of resisting the moments and shears

corresponding to the probable moments in the column at the beam-column joint. The probable moment resistance of the column, as defined by the CHBDC (Clause 4.4.10.4.3), is taken as 1.3 times the nominal moment resistance of the column. The nominal resistance was evaluated with an average axial load of 454 kN.

There are two important joints to consider: One is a beam column joint with two beams framing into the joint (all interior columns) and the other is the joint with only one beam framing into the joint (edge column). Because all of the columns have the same reinforcement and all of the beams have the same reinforcement, the most critical case is an edge beam–column connection.

5.7.1 Details of Retrofitted Beam

The factored moment resistance, M_r, of the retrofitted beam must be equal or greater than the probable moment resistance, $M_{p\,col}$, of the column. For determining $M_{p\,col}$, the unspalled column section is used. Table 5-2 summarizes these moments and calculations, which were done using *Response 2000*. The value of the nominal resistance of the column $M_{n\,col}$ was determined with an axial load level corresponding to the dead load of the bridge (see Table 5-2). Hence the probable resistance of the column is:

$$M_{p\,col} = 1.3 M_{n\,col} = 1.3 \times 461.9 = 600.5\ \text{kNm} \qquad 5\text{-}9$$

The required factored moment resistance in the beam is therefore:

$$M_r = M_{p\,col} = 600.5\ \text{kNm} \qquad 5\text{-}10$$

Due to the geometry of the frame structure, the additional longitudinal reinforcement can only be added to the sides of the beam. Four 30M and two 35M bars are placed in three layers as shown in Figure 5-26(b). To ensure that the added reinforced concrete is fully composite with the existing beam, horizontal bars with a fixed head on one end and a threaded head at the other end are used (see Figure 5-26(b)). Additional 15M U-stirrups are added to increase the shear resistance. To facilitate placement self-levelling concrete, with a minimum specified compressive strength of 60 MPa is used.

The retrofitted beam with the additional 4-30M and 2-35M bars has a factored flexural resistance (see Table 5-2) of 656.8 kN.m, which exceeds the required M_r.

Once the resisting moment has been calculated, the beam must be reinforced to have enough shear capacity to ensure flexural yielding. For beams in frames subjected to lateral load, the required factored shear resistance is defined by the following relationship:

$$V_r = \frac{2M_{p\,beam}}{L} \qquad 5\text{-}11$$

where: $M_{p\ beam}$ is the probable moment resistance of the beam, equal to 1.3 times the beam nominal moment resistance; and L is the distance between column faces.

The nominal resistance of the beam was determined using *Response 2000* for a moment-to-shear ratio of 0.893 and resulted in a nominal moment resistance of 743.4 kN.m. Hence, the probable resistance is $M_{p\,beam} = 1.3 \times 743.4 = 966.4\,\text{kN.m}$. Therefore the required factored shear resistance for an edge beam is:

$$V_r = \frac{2M_{p\,beam}}{L} = \frac{2 \times 966.4}{1.786} = 1082\,\text{kN} \qquad 5\text{-}12$$

If double-legged 15M stirrups at a spacing of 80 mm are used in the edge beams, then the factored shear resistance is:

$$\begin{aligned} V_r = V_c + V_s &= \phi_c \times 0.166\sqrt{f'_c}\,bd + \phi_s \times A_v f_y d/s \qquad 5\text{-}13 \\ &= 0.75 \times 0.166\sqrt{38.9} \times 757.2 \times 470.7 \\ &\quad + 0.9 \times 2 \times 200 \times 400 \times 470.7/80 = 276.8 + 847.2 = 1124\,\text{kN} \end{aligned}$$

The retrofitted beam with the 15M stirrups at a spacing of 80 mm has a factored shear resistance (see Table 5-2) of 1124 kN, which exceeds the required V_r.

For interior beams, because of the lower shear demand, 15M stirrups at a spacing of 150 mm (see Table 5-2) are required.

It was decided to use the same longitudinal reinforcement for all of the beams. However due to the great differences in the shear demand between an edge beams and interior beams, two different stirrup spacings were used (see Table 5-2).

The horizontal shear force at the joints can be estimated as:

$$V_{jh} = \frac{M_{p\,col}}{0.9d} = \frac{600.5 \times 1000}{0.9 \times 525} = 1271\,\text{kN} \qquad 5\text{-}14$$

In addition, the vertical shear force at the joint can be estimated as:

$$V_{jv} = \frac{M_{p\,col}}{0.9d} = \frac{600.5 \times 1000}{0.9 \times 406} = 1643\,\text{kN} \qquad 5\text{-}15$$

In determining the amount of horizontal shear reinforcement in the joint, the use of 15M double-legged horizontal bars at a spacing of 55 mm gives a shear resistance of:

$$\begin{aligned} V_r = V_c + V_s &= \phi_c \times 0.166\sqrt{f_c'}bd + \phi_s \times A_v f_y d/s \qquad 5\text{-}16 \\ &= 0.75 \times 0.166\sqrt{38.9} \times 757.2 \times 406 \\ &\quad + 0.9 \times 2 \times 200 \times 400 \times 406/55 = 238.7 + 1063.0 = 1301.7\,\text{kN} \end{aligned}$$

In determining the amount of vertical shear reinforcement in the joint, the use of 15M double-legged horizontal bars at a spacing of 55 mm gives a shear resistance of:

$$\begin{aligned} V_r = V_c + V_s &= \phi_c \times 0.166\sqrt{f_c'}bd + \phi_s \times A_v f_y d/s \qquad 5\text{-}17 \\ &= 0.75 \times 0.166\sqrt{38.9} \times 757.2 \times 525 \\ &\quad + 0.9 \times 2 \times 200 \times 400 \times 525/55 = 308.7 + 1374.5 = 1683.2\,\text{kN} \end{aligned}$$

Therefore, a grid of 15M double-legged stirrups spaced at 55 mm in both directions provides factored shear resistances of 1302 kN and 1683 kN for the horizontal and vertical directions, respectively.

The added joint reinforcement must be properly anchored in the added concrete and the added reinforced concrete must be adequately attached to the existing concrete. The interface shear reinforcement, assuming that 25M T-headed bars are used and a roughened surface between the new reinforced concrete and the existing concrete can be determined as described below.

The resultant shear on the interface between the new and old concrete can be conservatively determined from the horizontal and vertical shear components on the joint, as:

$$V_{interface} = \sqrt{V_{jh}^{\,2} + V_{jv}^{\,2}} = \sqrt{1271^2 + 1643^2} = 2077\,\text{kN} \qquad 5\text{-}18$$

The factored cohesive resistance on the two interface planes at a joint is given by

$$V_{cohesion} = \phi_c c A_{interface} = 0.75 \times 0.50 \times 2 \times 607 \times 457 = 208\,\text{kN} \quad 5\text{-}19$$

Therefore, the number of pairs of 25M horizontal anchors required is given by:

$$N = \frac{V_{interface} - V_{cohesion}}{\phi_c A_v f_y \mu} = \frac{(2077 - 208) \times 1000}{0.75 \times 4 \times 500 \times 400 \times 1.0} = 3.11 \quad 5\text{-}20$$

Hence, due to the conservatively nature of these calculations, three sets of four pins through the joint region are provided, as shown in Figure 5-26.

Figure 5-26 shows the details of the proposed retrofitted beam: an elevation view of the reinforcement, a section at midspan, and a section at a joint.

5.7.2 Behaviour of Retrofitted Frame

Figure 5-27 shows: the shear–moment, force–displacement, moment–curvature, and axial load–moment interaction diagrams of the retrofitted beam. Figure 5-27(c) shows the moment–curvature relationship (sectional response) for a moment-to-shear ratio of 0.893 m (or *L/2*). Figure 5-27(d) shows the moment–axial load interaction diagram of the retrofitted beam for the cases of ultimate moment and general yielding moment, as used in Ruaumoko. It is noted that the retrofitted beam is able to develop general flexural yielding without major shear distress. The retrofitted beam reaches general yielding at a moment of 694 kN.m at a curvature of 0.0061 rad/m. This represents significant improvement from the existing beam, which would suffer shear failure at an equivalent moment of 114 kN.m at a curvature of 0.0035 rad/m (Figure 5-18(c)). The predicted moment–axial load response as calculated by Ruaumoko for one earthquake case with a PGA of 0.80g is shown in Figure 5-27(d). This seismic input is representative of an earthquake with a spectral acceleration of 1.007g, that is, similar to the spectral acceleration of the CHBDC with an importance factor of 3.0 (Period = 0.6045 sec). It can be observed that the moment oscillates between a positive and a negative value without reaching general yielding. Figure 5-28 shows the hysteresis diagram used for this case. It can be observed from these two graphs that the moment–axial load and overall moment–

curvature relationship remain elastic during the analysis. Although the beam does not yield, the columns would have undergone yielding as discussed below.

A summary of the main parameters used in Ruaumoko for the case of the retrofitted beam is presented in Table 5-1. The parameters for the column were the same as the spalled–corroded case. Figure 5-29 shows the maximum curvature of the retrofitted beam. Figure 5-30 shows the maximum curvature of an edge and middle column after the retrofitting has been applied. It can be observed that the predicted IDA curves for the columns now have little dispersion and a common trend, independent of the type and scale of the earthquake used. In contrast to the results of the as-built analyses, hardening occurs in the beams after softening occurs in the columns. This is evident in Figure 5-31, which contains the median values of the curvature plots for the three types of elements under observation and an additional beam segment (element 14). It is noted that the as-built structure had beam shear failure at a spectral acceleration level of 0.15 g (Figure 5-24(c)) whereas the retrofitted structure has column yielding occurring at a spectral acceleration level of 0.35 g (Figure 5-31), with ability to archive spectral accelerations in excess of 0.8 g.

Figure 5-32 shows the median values for the variation of the axial loads for the three selected elements. It can be observed that the variation in axial load in the edge column is still significant; the relationship is linear over a greater range of spectral acceleration, reaching higher levels (above 0.35g). In contrast, the predicted response of the as-built frame (Figure 5-25) shows that the linear response ends at about 0.15 g.

For comparison, an ideal frame with a ductile beam was analyzed. It was assumed that the beam had the same dimensions and longitudinal reinforcement as the as-built beam, but also included 15M closed stirrups spaced at 50 mm as transverse reinforcement, such that the beam would have a ductile response. Figure 5-33 shows the median values of the curvature plots for the three elements under study. It is evident that the spectral acceleration levels at which the elements start to yield are similar to those for

the retrofitted frame case (above 0.30g). One major difference between the response of the ideal frame and the response of the retrofitted frame is that the edge beams in the ideal frame are weaker than the columns and hence yield before the columns yield.

5.8 Summary

One of the frames of the St-Jean Blvd. overpass crossing the CN and CP railways was evaluated using the Incremental Dynamic Analysis (IDA) approach. Three cases reflecting the condition of the concrete columns were studied: unspalled columns, spalled columns, and spalled columns with corroded reinforcement. The 12–column frame, in each case, was subjected to a wide range of earthquakes and scale factors, as part of the IDA approach, to evaluate and compare the response with the spectral acceleration levels specified by the CHBDC and UHS for Montreal. The lack of transverse reinforcement in the as-built beam required a careful evaluation of the shear strength. It was evident that the beam would fail in shear before yielding of the beams or the columns. An equivalent yielding moment versus axial load interaction diagram was calculated for the expected range of axial load on the beam (Figure 5-18(d)). Similar diagrams were developed in each case for the columns, but in these cases, the elements were reaching their yielding moment before failing in shear.

The maximum curvatures and axial loads of three representative elements (edge column, middle column, and edge beam) were collected during the IDA. A comparison between the median IDA curves in each case of the three elements showed that the early shear failure of the beam dominates the overall behaviour of the frame (Figure 5-24(a), (b), (c)). The spectral acceleration level at which the beams fail (approximately 0.15g) is much lower than the spectral acceleration level of the CHBDC, even for an emergency-route bridge (0.49g, I = 1.5). It is also lower than the level that corresponds to the 2% in 50 years (50th percentile) of the Uniform Hazard Spectra for Montreal (0.288g).

The chosen retrofitting strategy involves the strengthening of the concrete beam to avoid shear failure and to provide sufficient flexural resistance so that yielding occurs in the columns rather than in the beams (Table 5-2). The additional flexural reinforcement for the critical edge beam was used throughout the entire cap beam (Figure 5-7, Figure 5-26). However, a greater amount of shear reinforcement was provided in the edge beams due to the greater moment and shear demands in that beam. The overall behaviour of the retrofitted frame shows clearly the beams do not suffer any shear distress or any flexural yielding. The columns of the retrofitted frame can sustain higher levels of spectral acceleration before starting to yield (Figure 5-30, Figure 5-31).

In deciding upon the retrofitting strategy, an approach using minimum intervention was studied. The retrofit of the beam completely changes the performance of the frame. The as-built frame suffers a brittle shear failure at a predicted spectral acceleration of 0.15g whereas the retrofitted frame is predicted to experience general yielding of the columns at 0.35g, with the ability to undergo spectral accelerations in excess of 0.8g.

Although the localized spalling and corrosion of some of the column ties should be addressed with corrective measures, this study indicates that this minimal deterioration has not significantly affected the expected seismic performance.

Table 5-1 Main Parameters Used by Ruaumoko in the Analysis per case

Parameter \ Case	Unspalled Column Section	Spalled Column Section	Spalled/ Corroded Section	Retrofitted beam
Reinforced Concrete Column (Elements 1 to 12)				
Elastic Section Properties				
Cross Sectional Area [m^2]	0.2089	0.2089	0.2089	
Moment of Inertia [m^4]	0.00364	0.00364	0.00364	
Inertia Cracking Factor	0.6271	0.5732	0.5296	
Element Properties				
Member Hinge Lengths [m]	0.226	0.226	0.226	
Concrete Interaction Parameters (*)				
Factor for Flexural terms (α)	1.304	1.389	1.332	
Factor for Axial terms (β)	1.268	1.244	1.276	
Axial Compression Yield Force (PC) [KN]	-7243	-6665	-6463	
Axial Compression Force at Balance Point (PB) [KN]	-2047	1760	1775	
Yield Moment at Balance Point around the z-z axis (MBz) [KN.m]	568	506	477	
Axial Tension Yield Force (PT) [KN]	2360	2375	2146	
Strength Degradation Data				
Ductility at which degradation begins	5.92	6.43	7.10	
Ductility at which degradation stops	9.93	10.79	11.92	
Reduction in strength due to degradation	0.85	0.88	0.88	
Ductility at 0.01 strength	13.95	15.15	16.74	
Reinforced Concrete Beam (Elements 13 to 23)				
Elastic Section Properties				
Cross Sectional Area [m^2]		0.2089		0.4598
Moment of Inertia [m^4]		0.00364		0.01413
Inertia Cracking Factor		0.3625		0.3146
Element Properties				
Member Hinge Lengths [m]		0.226		0.226
Concrete Interaction Parameters (*)				
Factor for Flexural terms (α)		1.065		1.335
Factor for Axial terms (β)		1.025		1.56
Axial Compression Yield Force (PC) [KN]		-6061		-19901
Axial Compression Force at Balance Point (PB) [KN]		-2006		5969
Yield Moment at Balance Point around the z-z axis (MBz) [KN.m]		288		1595
Axial Tension Yield Force (PT) [KN]		1139		1751
Strength Degradation Data				
Ductility at which degradation begins		1.01		9.14
Ductility at which degradation stops		3.56		17.81
Reduction in strength due to degradation		0.001		0.29
Ductility at 0.01 strength		n/a		19.59

Note: (*) The yield interaction surface is $\left\{\frac{P-PB}{PC,PT-PB}\right\}^{\beta}+\left\{\frac{Mz}{MBz}\right\}^{\alpha}+\left\{\frac{My}{MBy}\right\}^{\alpha}=1$ (Carr, 2001).

Table 5-2 Summary of Calculations for Beam Retrofitting

Moments at Column			
Nominal Moment	$M_{n\,col}$	461.9	KN.m
Probable Moment ($M_{p\,col}=1.3\,M_{n\,col}$)	$M_{p\,col}$	600.5	KN.m
Moments at Beam			
Required Factored Moment for Edge Beam	M_r	600.5	KN.m
Required Factored Moment for Middle Beam	M_r	300.2	KN.m
Resisting Moment (calculated with *Response 2000*)			
Positive bending	M_r	629.2	KN.m
Negative bending	M_r	656.8	KN.m
Nominal Moment of Retrofitted Beam			
Positive bending	$M_{n\,beam}$	708.5	KN.m
Negative bending	$M_{n\,beam}$	743.4	KN.m
Probable Moment of Retrofitted Beam ($M_{p\,beam}=1.3\,M_{n\,beam}$)	$M_{p\,beam}$	966.4	KN.m
Distance d from top to bottom centroid of steel longitudinal steel reinforcement	d	473.4	mm
Distance d from bottom to top centroid of steel longitudinal steel reinforcement	d	470.7	mm
Distance d used in shear calculations	d	470.7	mm
Shear force for edge beam			
Required Shear Force $V = 2M_{p\,beam}/L$	V	1082.2	KN
Averaged concrete strength for the retrofitted beam section	f'_c	38.9	MPa
Contribution from Concrete $V_c = \phi_c \times 0.166\sqrt{f'_c}bd$	V_c	276.8	KN
Contribution from 15M @ 150mm U-stirrups	V_s	451.9	KN
Contribution from 15M @ 80mm U-stirrups	V_s	847.3	KN
Factored Shear Resistance (15M @ 150mm)	$V = V_s + V_c$	728.7	KN
Factored Shear Resistance (15M @ 80mm)	$V = V_s + V_c$	1124	KN
Bolts			
Surface's Roughness Factor	μ	1	
Combined Axial Force of 4-30M + 2-35M bars		1920	KN
Resisting force of 9 layers of 15M bolts		2160	KN

Figure 5-1 Lateral view of St-Jean Blvd. overpass crossing the CN and CP railway lines

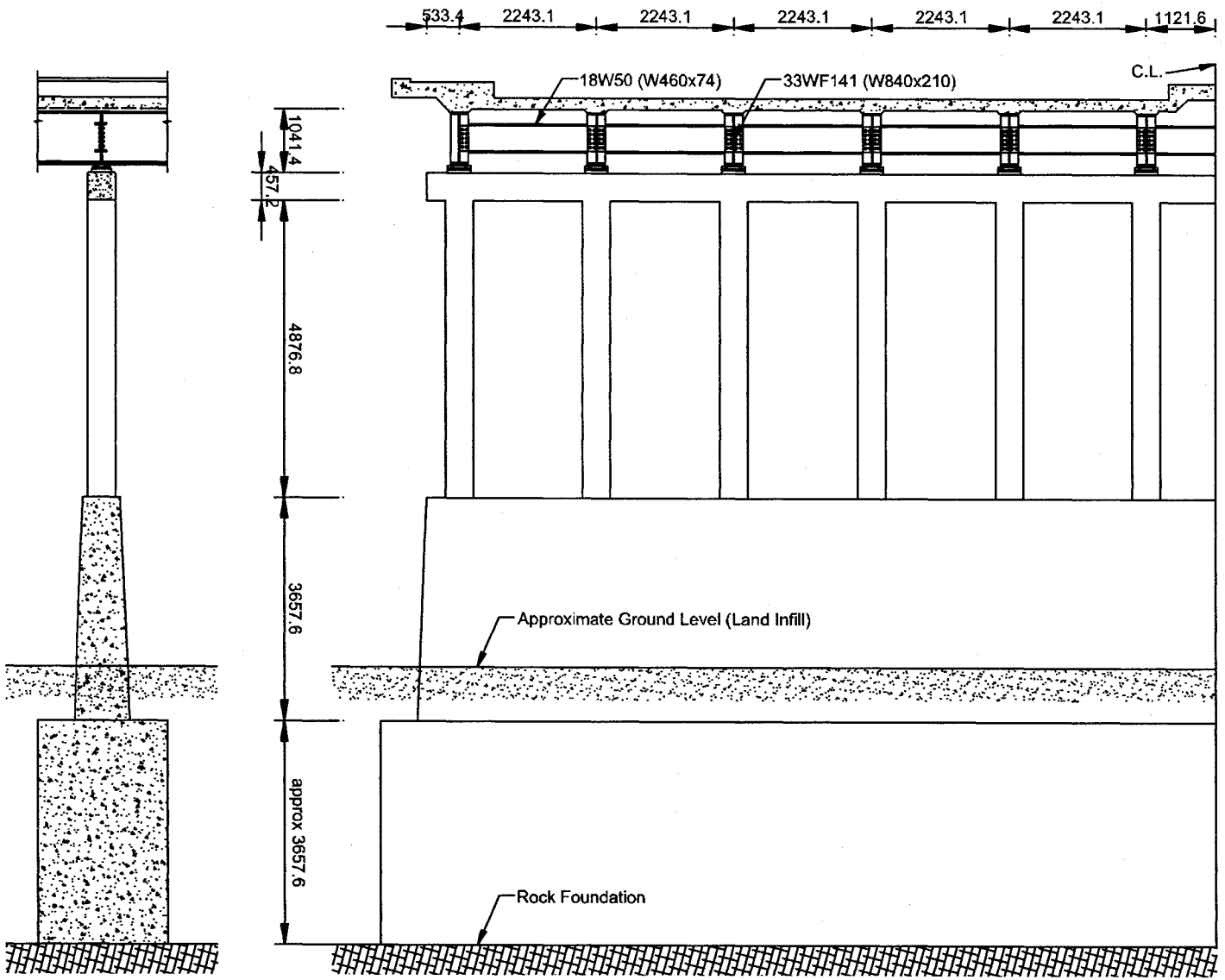

Figure 5-2 Elevation of moment-resisting frame

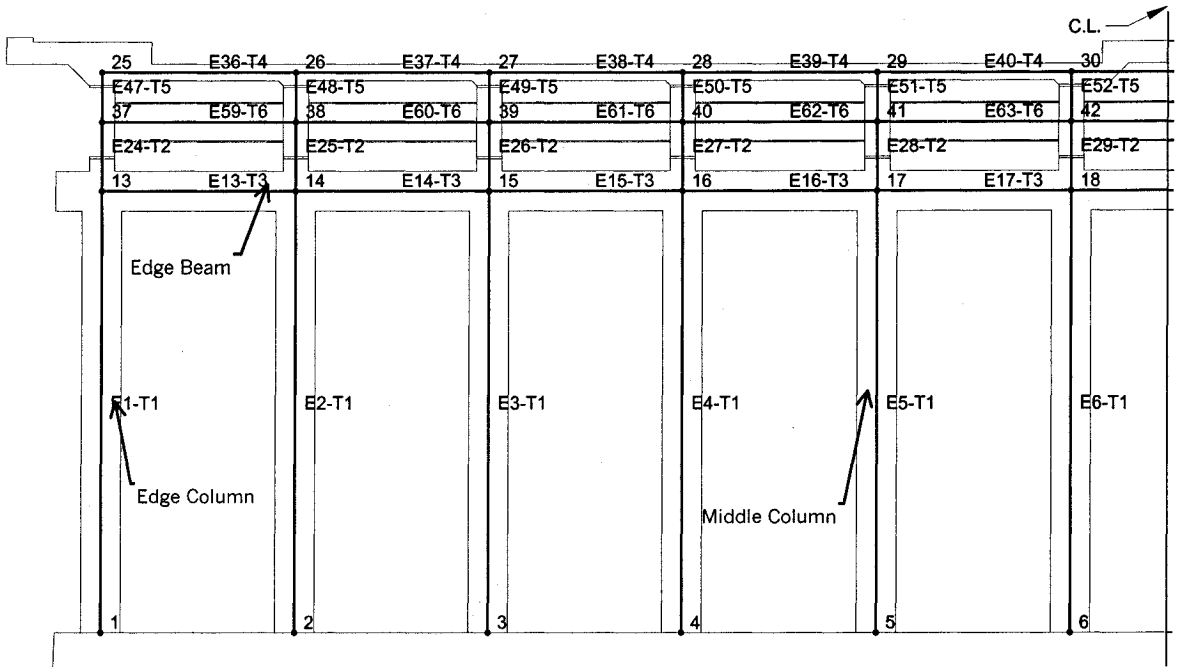

(a) Left side

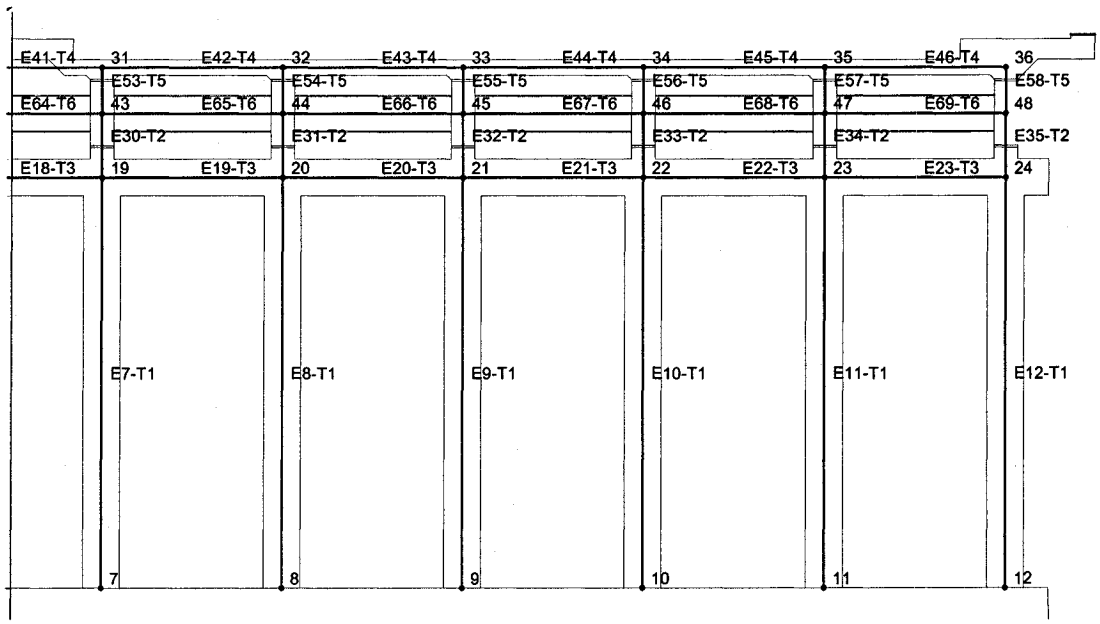

(b) Right side

Figure 5-3 Structural idealization of moment-resisting frame

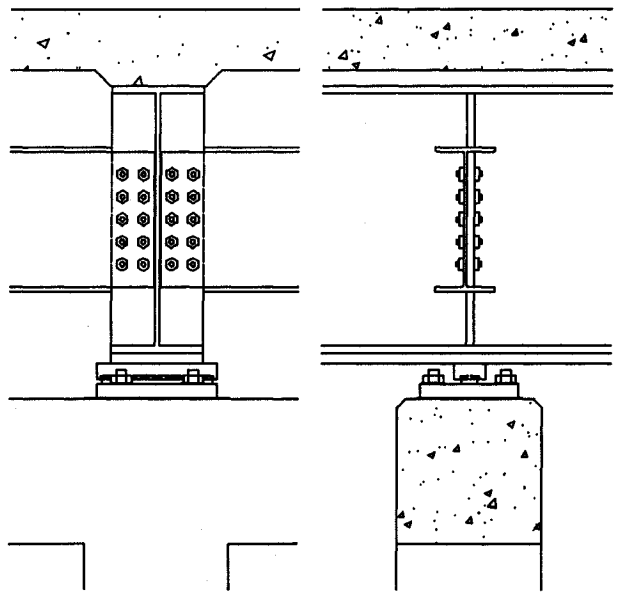

Figure 5-4 Details of support of steel beams

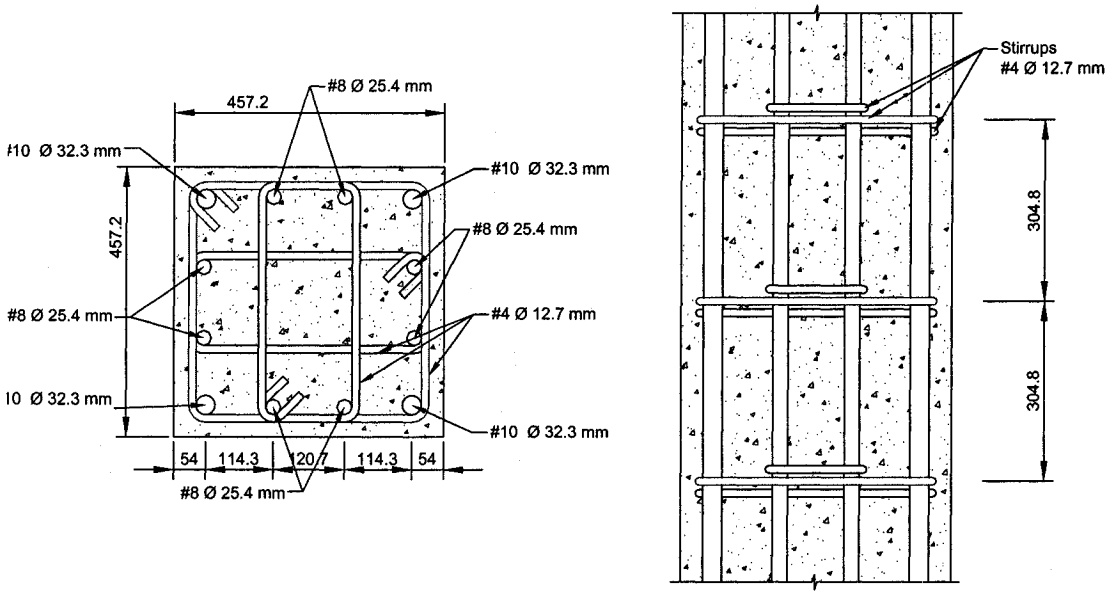

(a) Section (b) Elevation

Figure 5-5 Details of as-built column

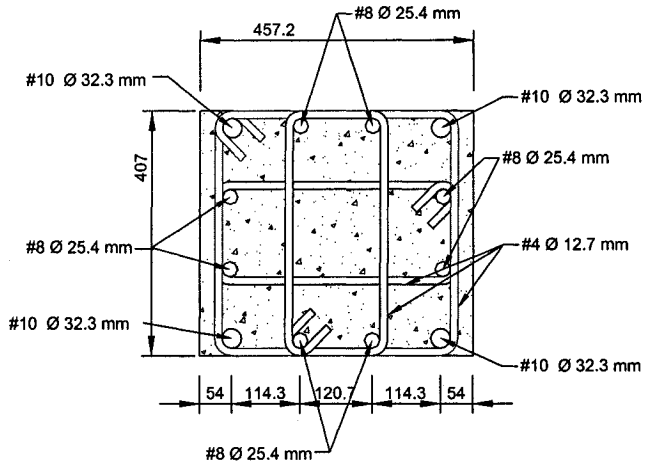

Figure 5-6 Reduced section of column due to spalling

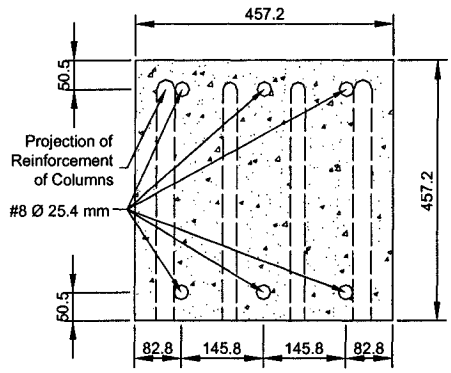

Figure 5-7 Details of as-built beam section

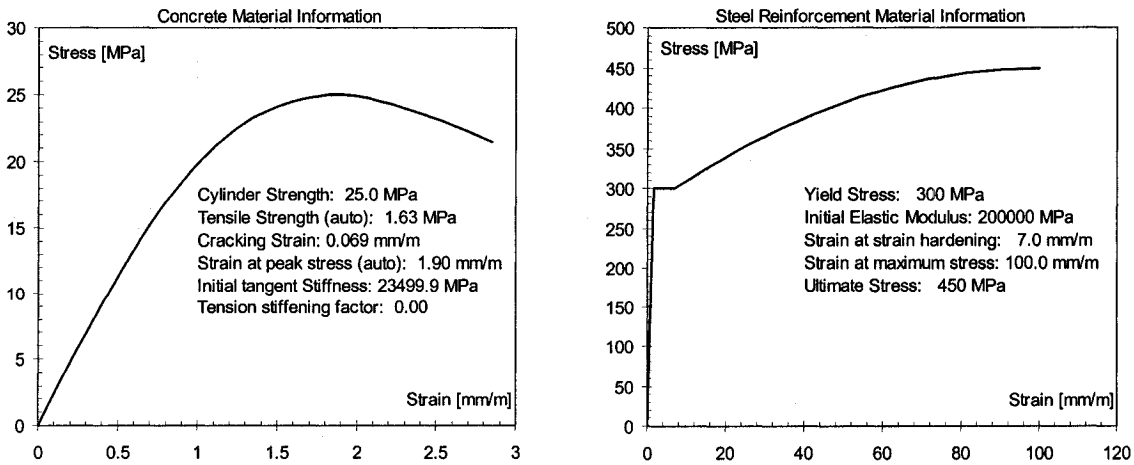

(a) Concrete (b) Steel Reinforcement

Figure 5-8 Assumed stress-strain relationships for as-built frame

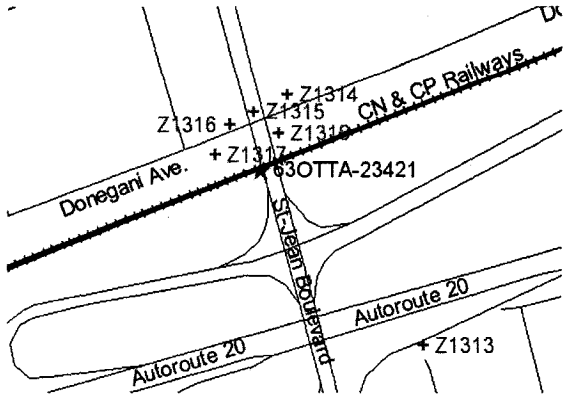

Figure 5-9 Location of GAN recordings and borehole near St-Jean overpass crossing Railway lines

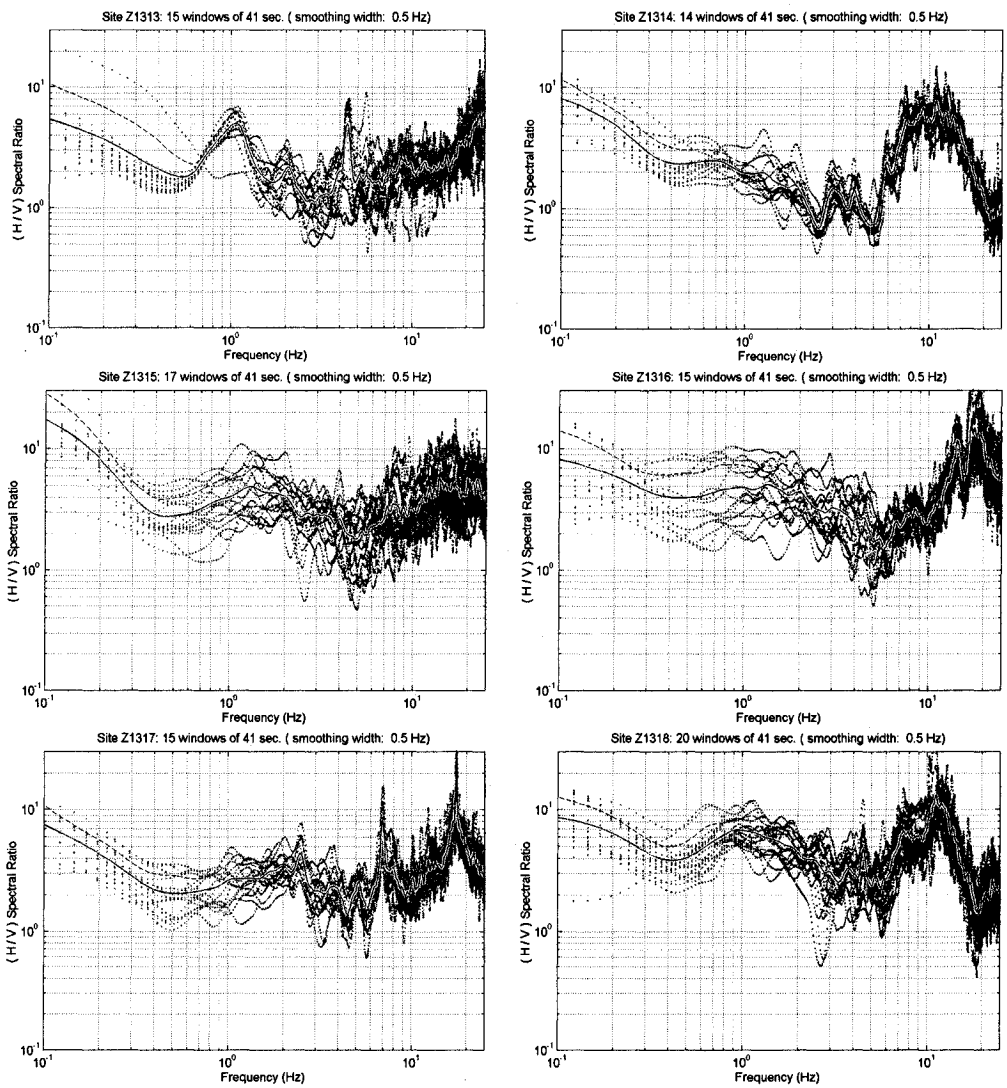

Figure 5-10 HVSR of GAN recordings near St-Jean overpass crossing Railway lines

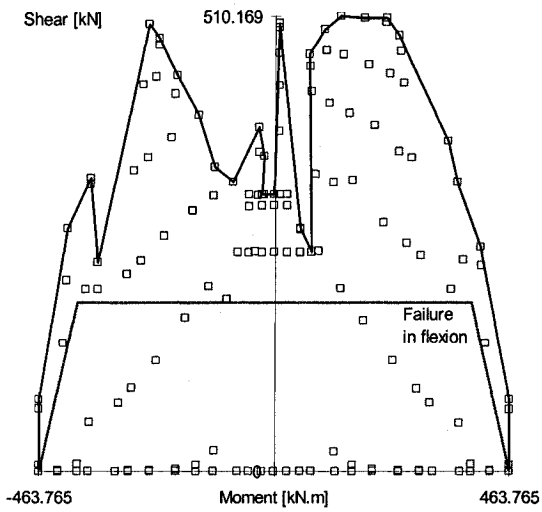

(a) Unspalled column

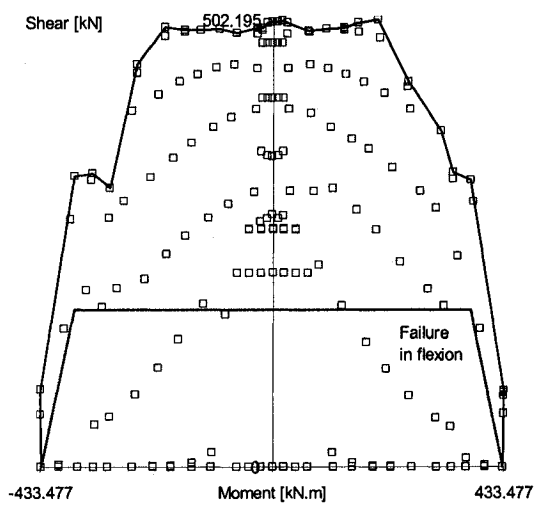

(b) Spalled column

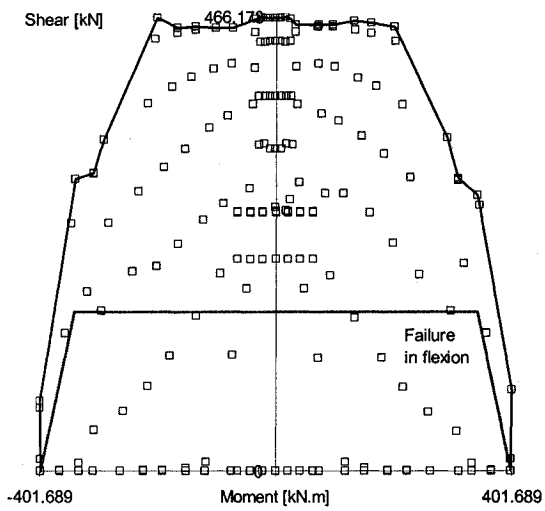

(c) Spalled-corroded column (10% reduced area steel reinforcement)

Figure 5-11 Predicted shear-moment diagram of as-built column with different section configurations

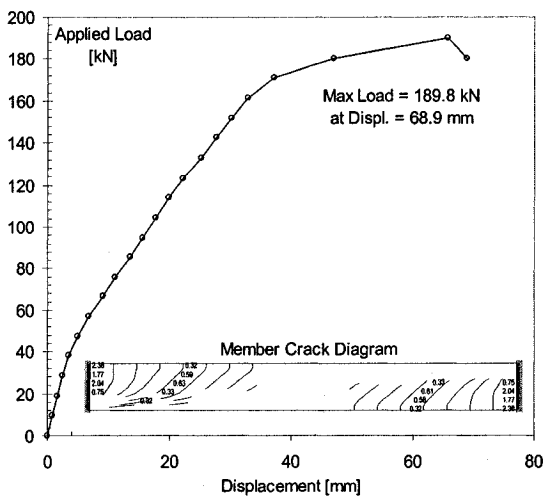

(a) Unspalled column

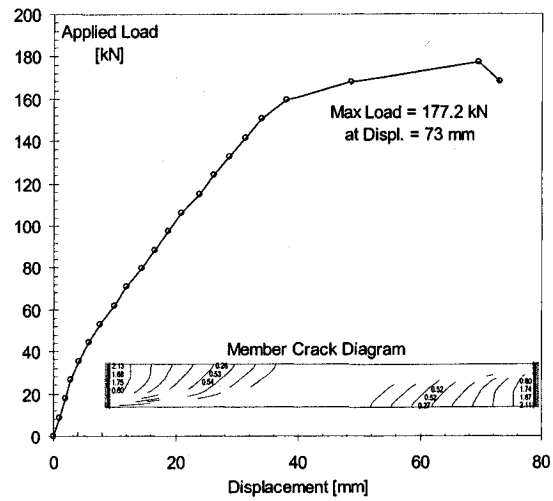

(b) Spalled column

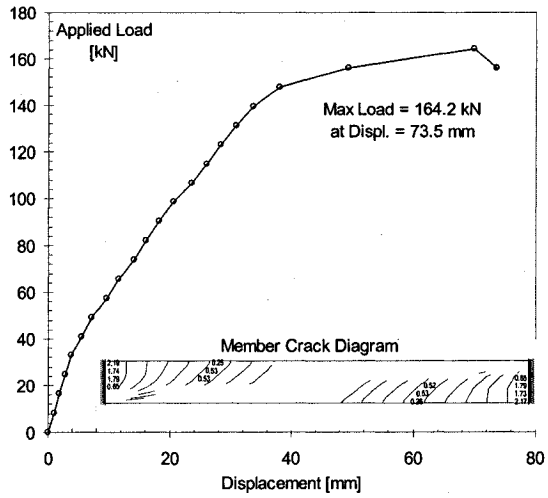

(c) Spalled-corroded column (10% reduced area steel reinforcement)

Figure 5-12 Predicted force-displacement response of as-built column with different section configurations

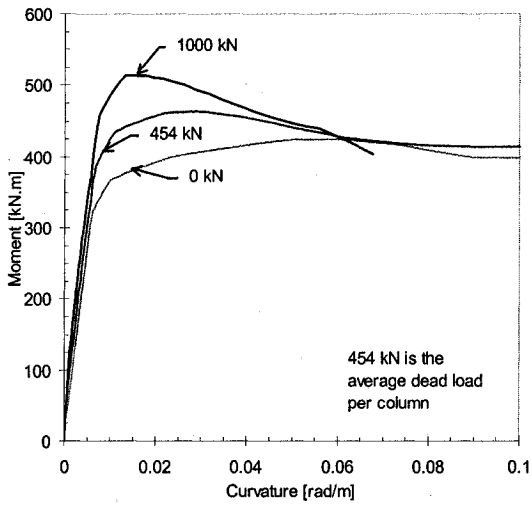

(a) Unspalled column

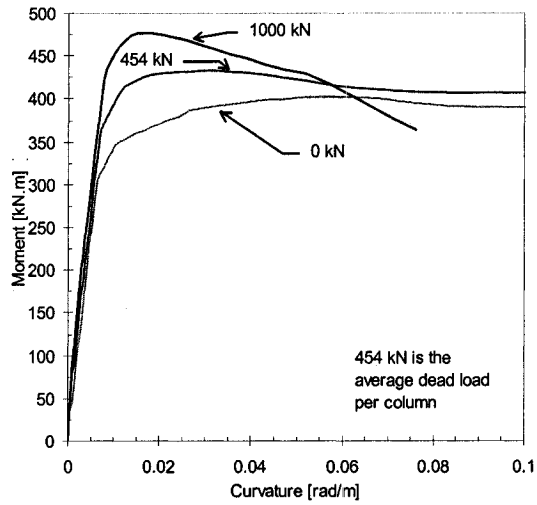

(b) Spalled column

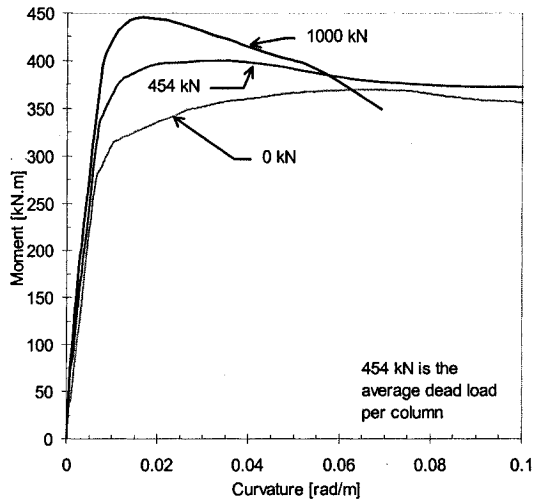

(c) Spalled-corroded column (10% reduced area steel reinforcement)

Figure 5-13 Predicted moment-curvature relationships of as-built column with different section configurations and different axial loads

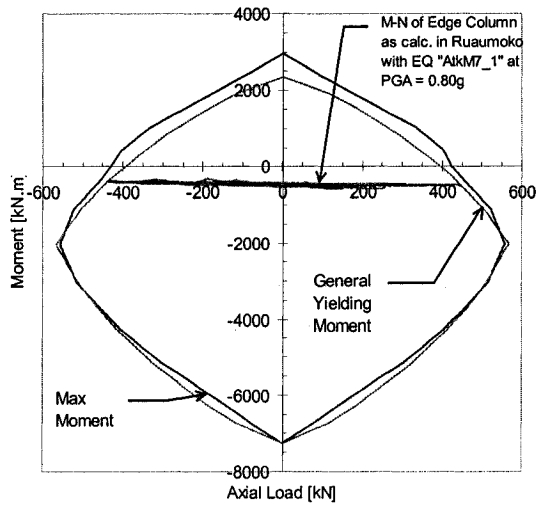

(a) Unspalled Column

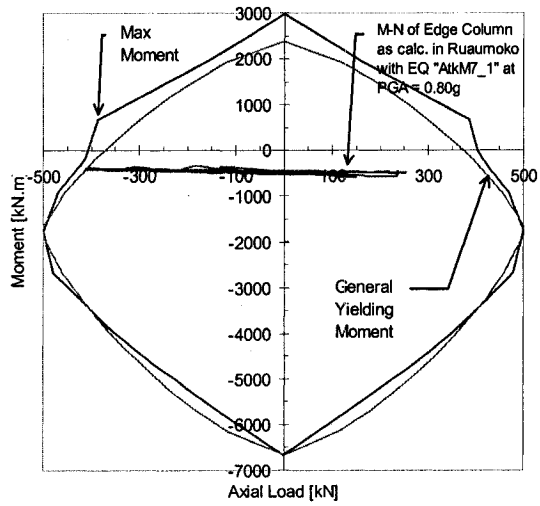

(b) Spalled Column

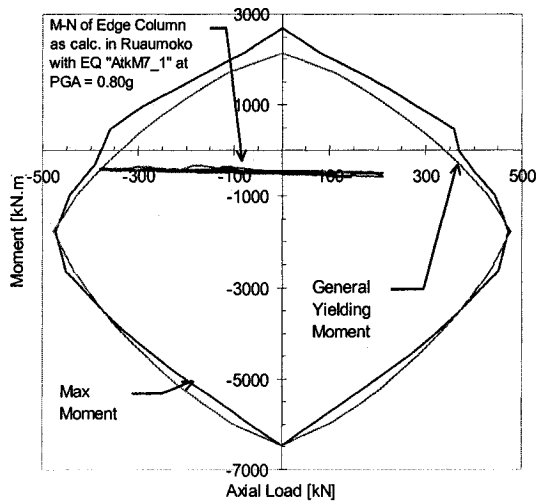

(c) Spalled-Corroded Column (10% Reduced Area Steel Reinforcement)

Figure 5-14 Predicted axial load–moment interaction diagram of as-built column with different section configurations

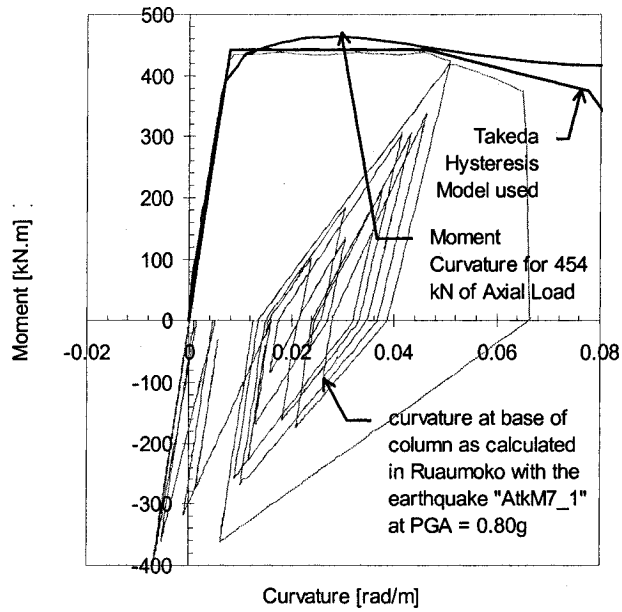

(a) Unspalled edge column case

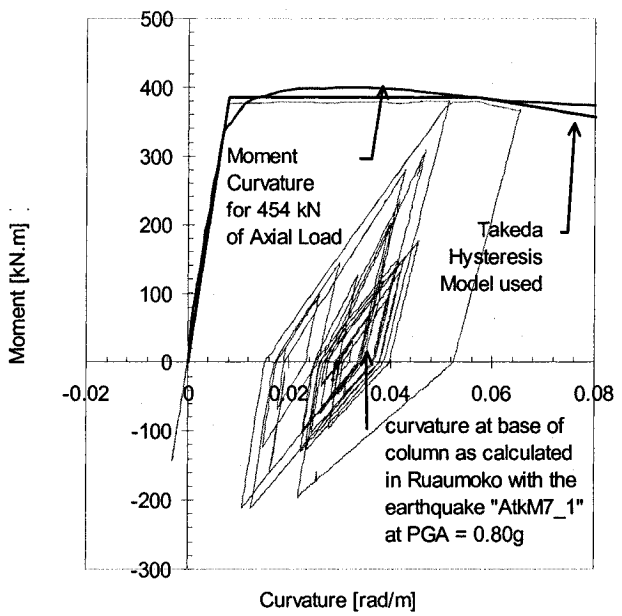

(b) Spalled-corroded edge column case

Figure 5-15 Hysteresis diagrams used in Ruaumoko and the moment-curvature from *Response* for column sections

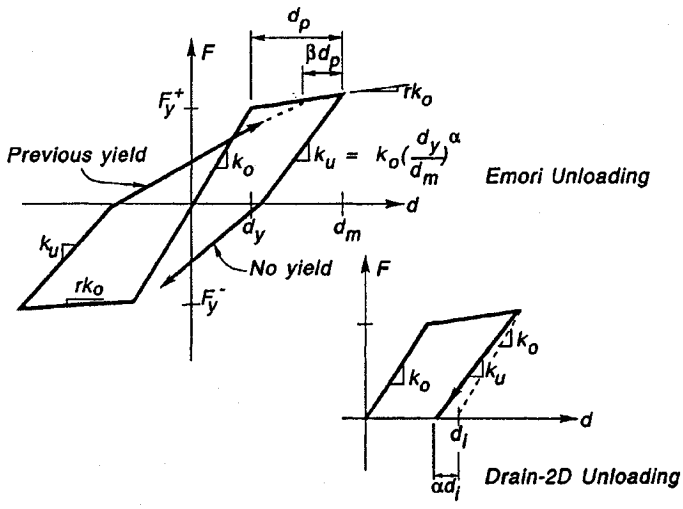

Figure 5-16 Takeda hysteresis model used in Ruaumoko
(After: Carr, 2001)

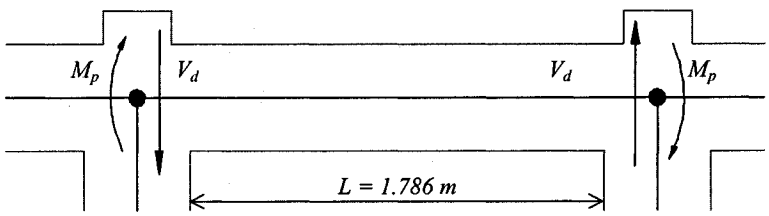

Figure 5-17 Member-end force diagram for beam element

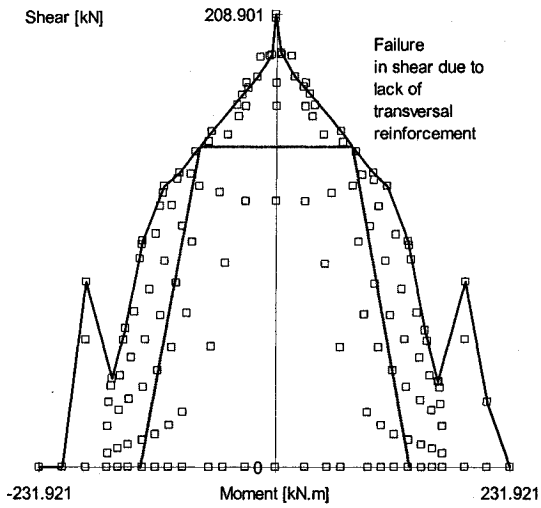

(a) Shear Moment Diagram

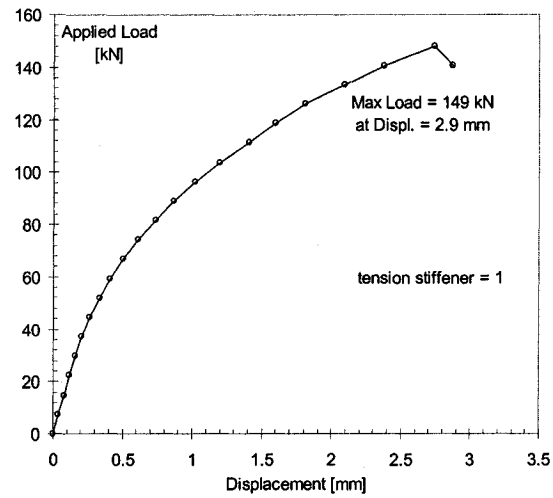

(b) Force Displacement Diagram

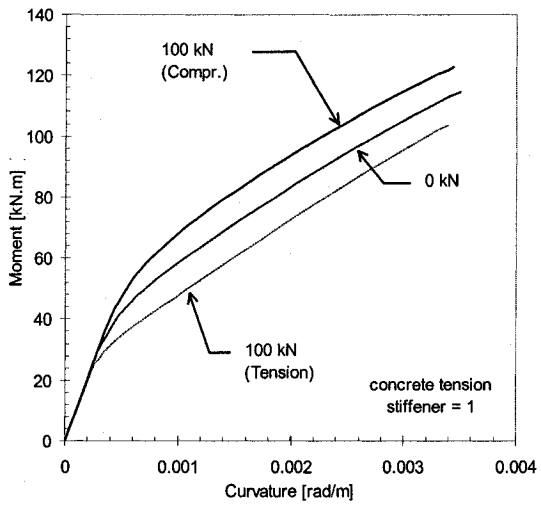

(c) Moment Curvature Relationships
M/V = 0.893 m

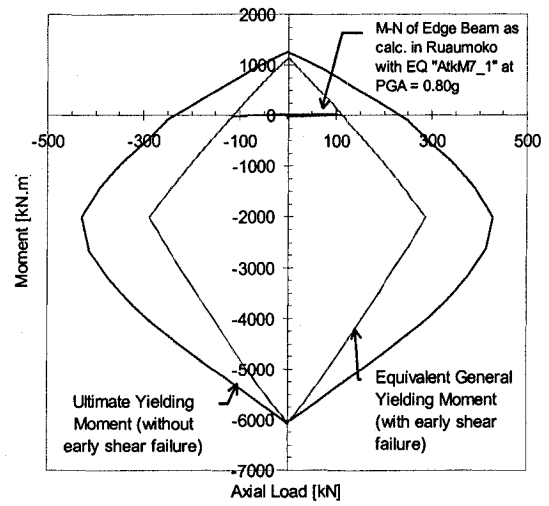

(d) Axial Load–Moment Interaction Diagram

Figure 5-18 Predicted member responses of as-built beam. Note the beam has no transverse reinforcement as shown in Figure 5-7

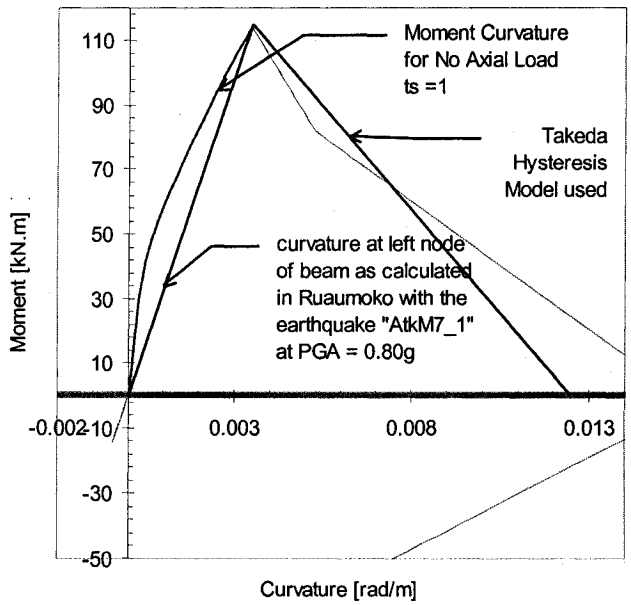

Figure 5-19 Hysteresis diagrams used in Ruaumoko and the moment-curvature from *Response* for an edge beam section (as-built)

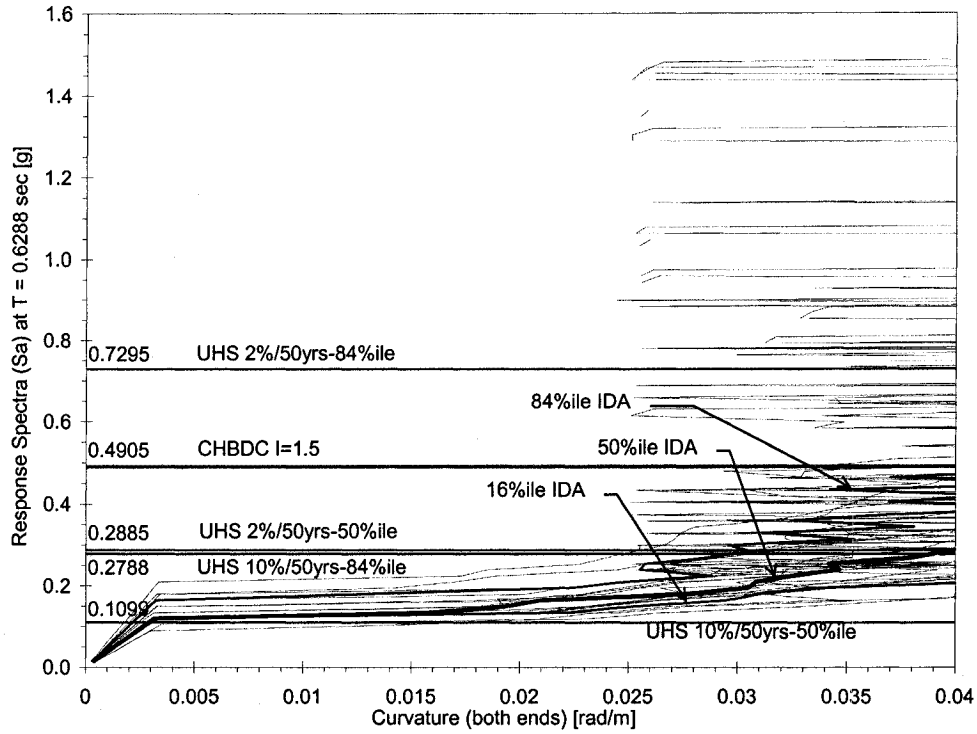

(a) Unspalled Column Case

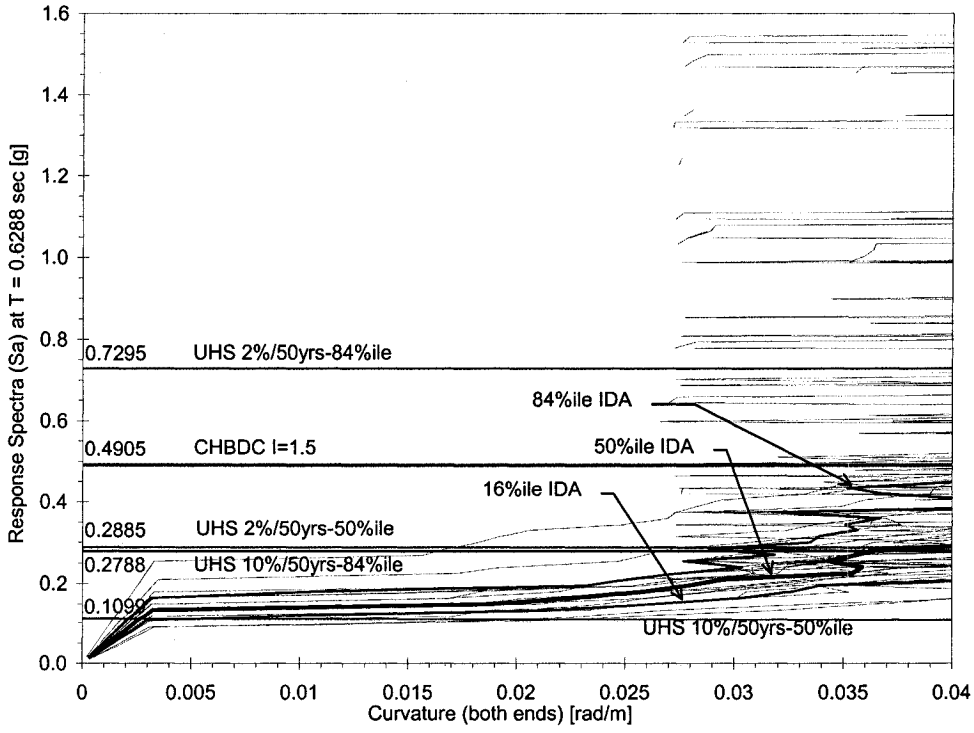

(b) Spalled Column Case

Figure 5-20 Predicted IDA curvatures at edge beam (element 13) for different cases (as-built)

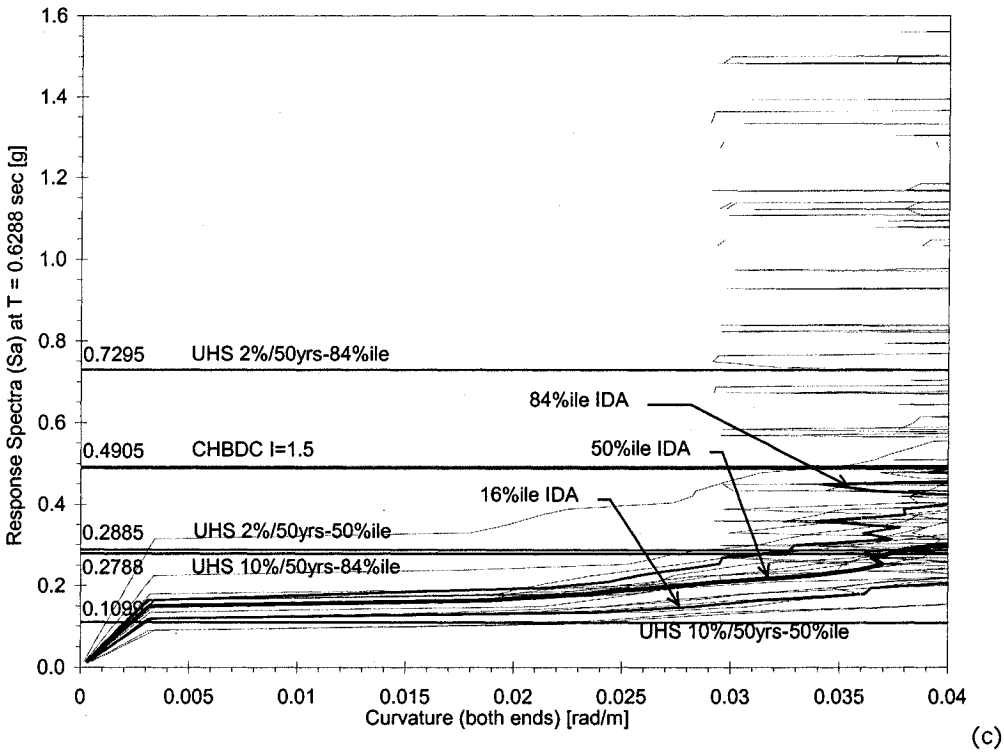

Figure 5-20(cont) Predicted IDA curvatures at edge beam (element 13) for different cases (as-built)

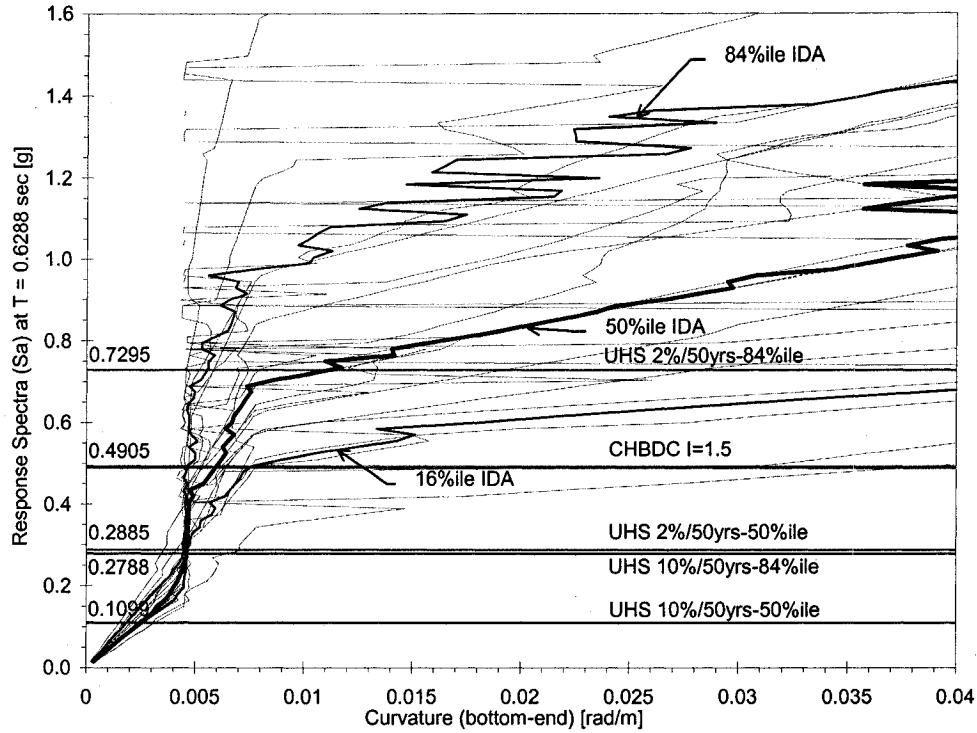

(a) Curvature of middle column (Element 5)

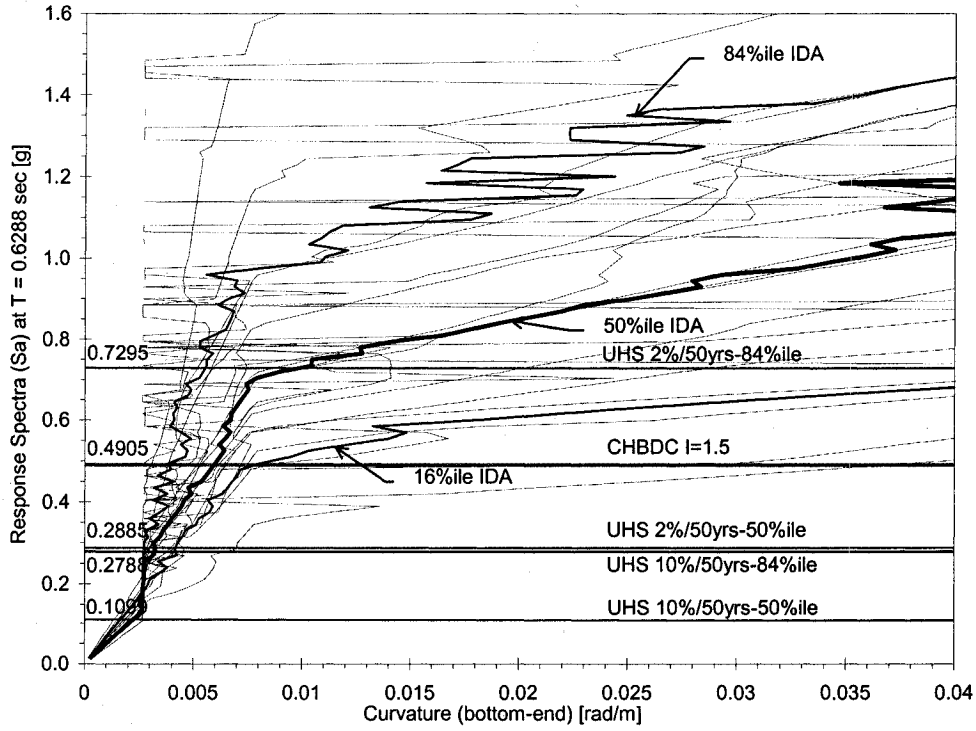

(b) Curvature of edge column (Element 1)

Figure 5-21 Predicted IDA curvatures at bottom of columns, unspalled column case (as-built)

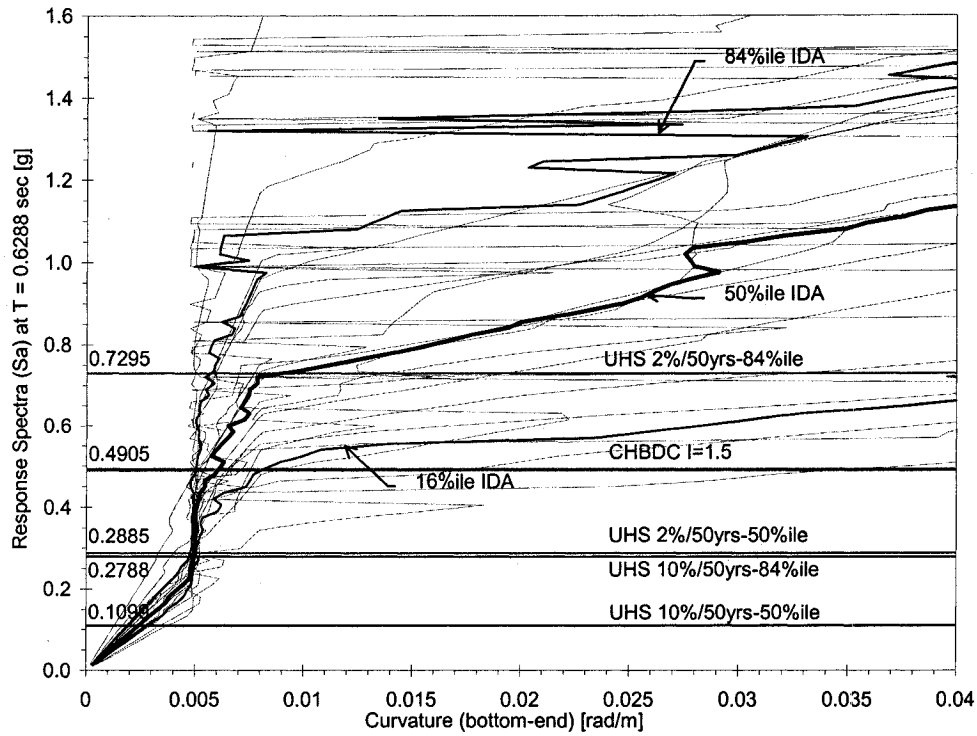

(a) Curvature of middle column (Element 5)

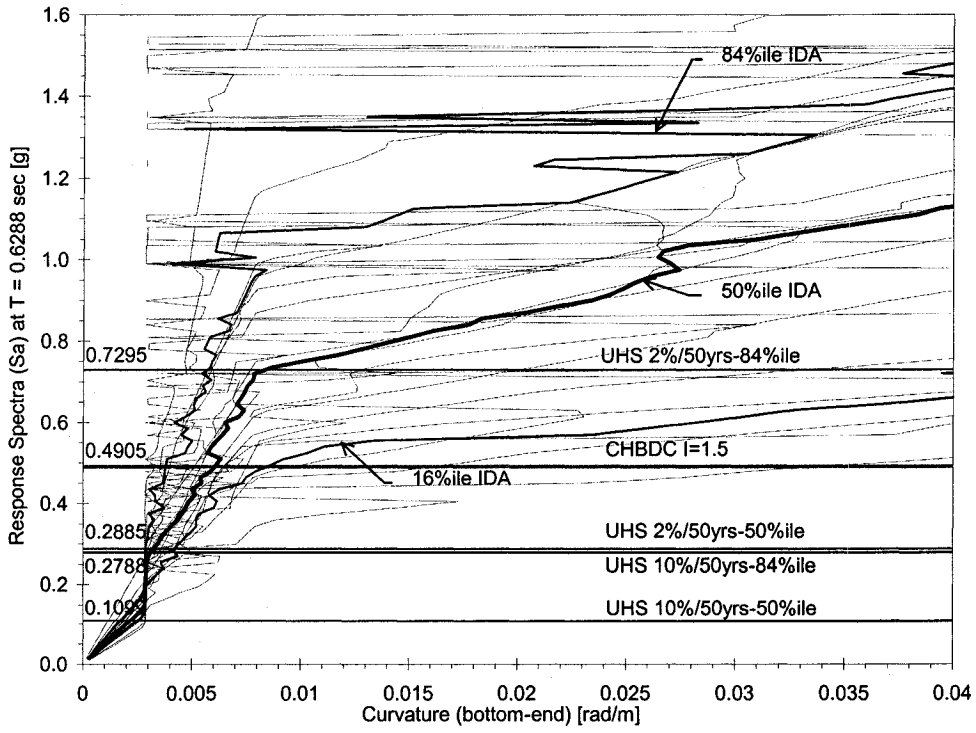

(b) Curvature of edge column (Element 1)

Figure 5-22 Predicted IDA curvatures at bottom of columns, spalled column case (as-built)

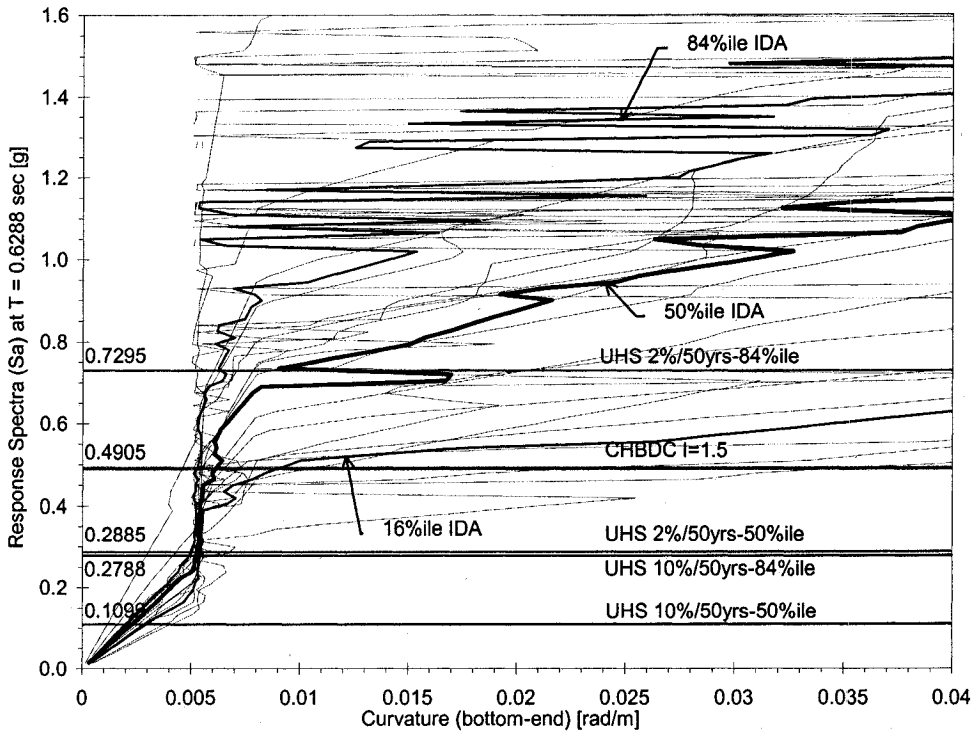

(a) Curvature of middle column (Element 5)

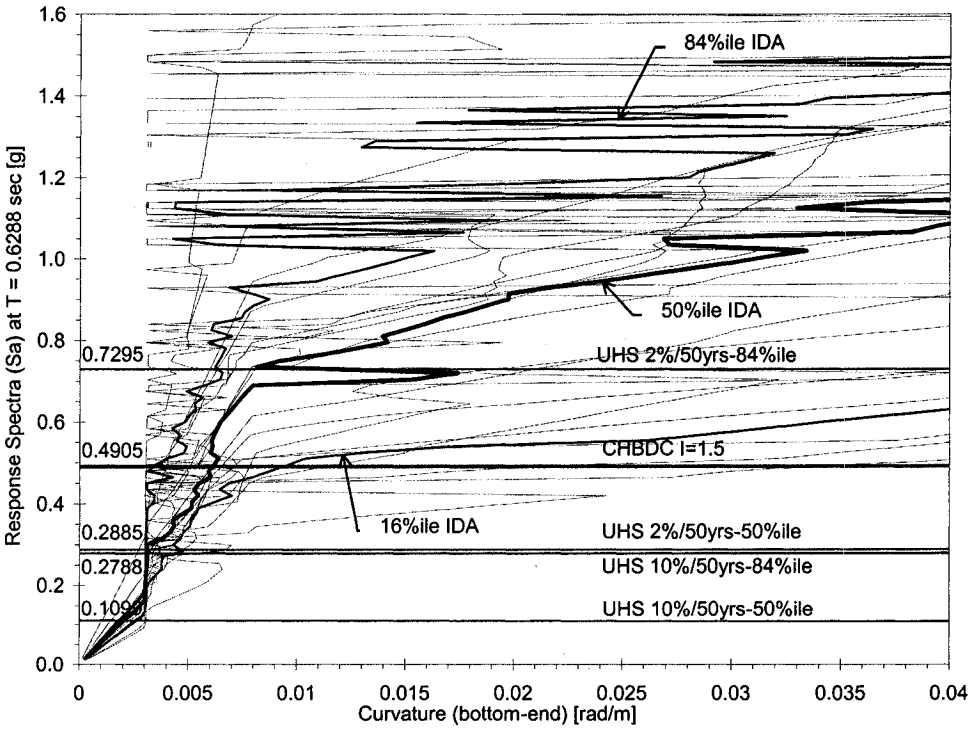

(b) Curvature of edge column (Element 1)

Figure 5-23 Predicted IDA curvatures at bottom of columns, spalled-corroded column case (as-built)

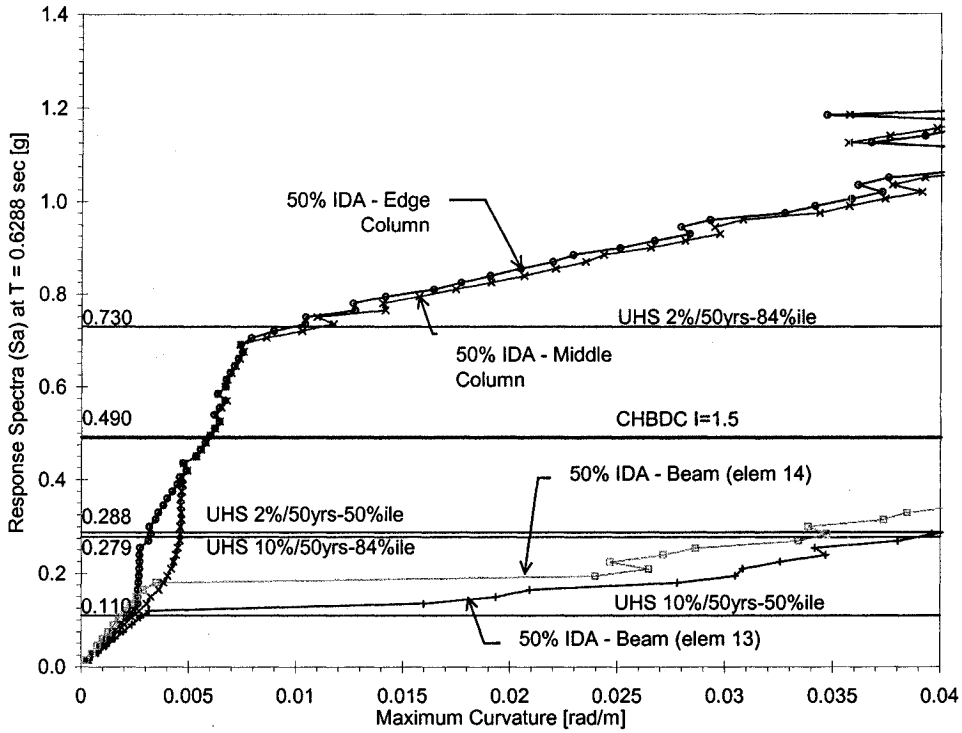

(a) Unspalled column case

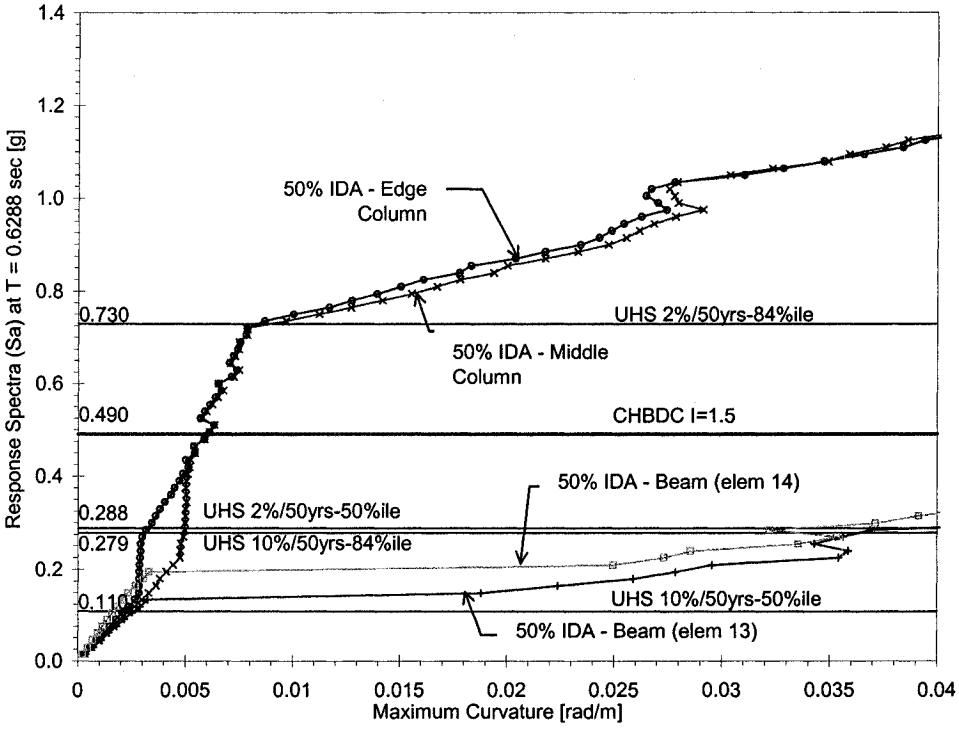

(b) Spalled column case

Figure 5-24 Predicted IDA median values of maximum curvatures for different cases (as-built)

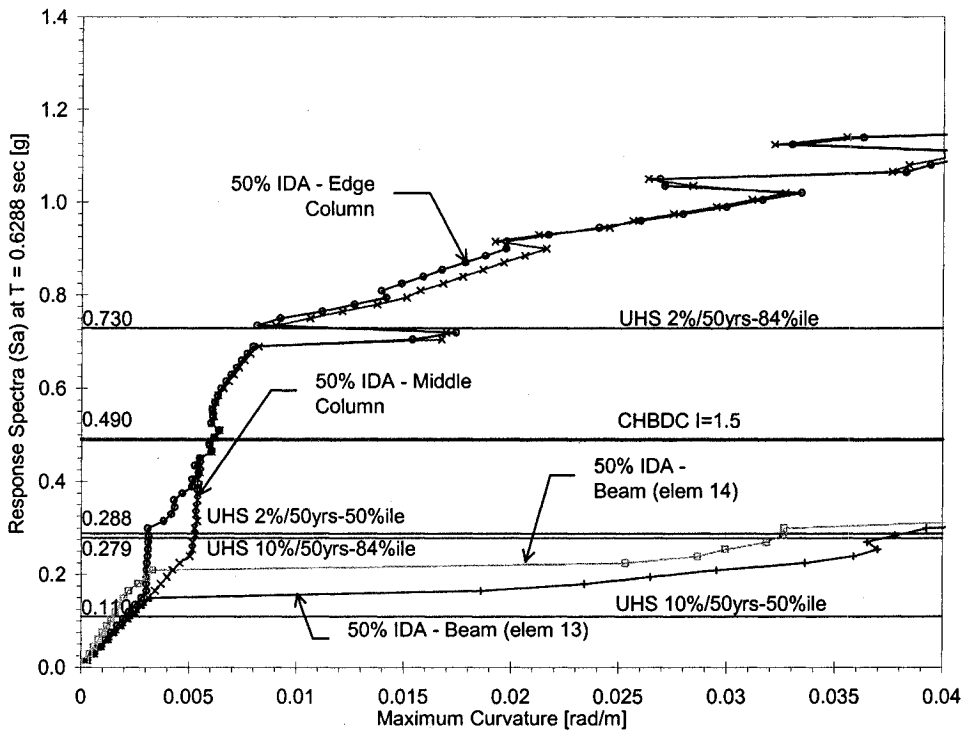

(c) Spalled-corroded case

Figure 5-24(cont) Predicted IDA median values of maximum curvatures for different cases (as-built)

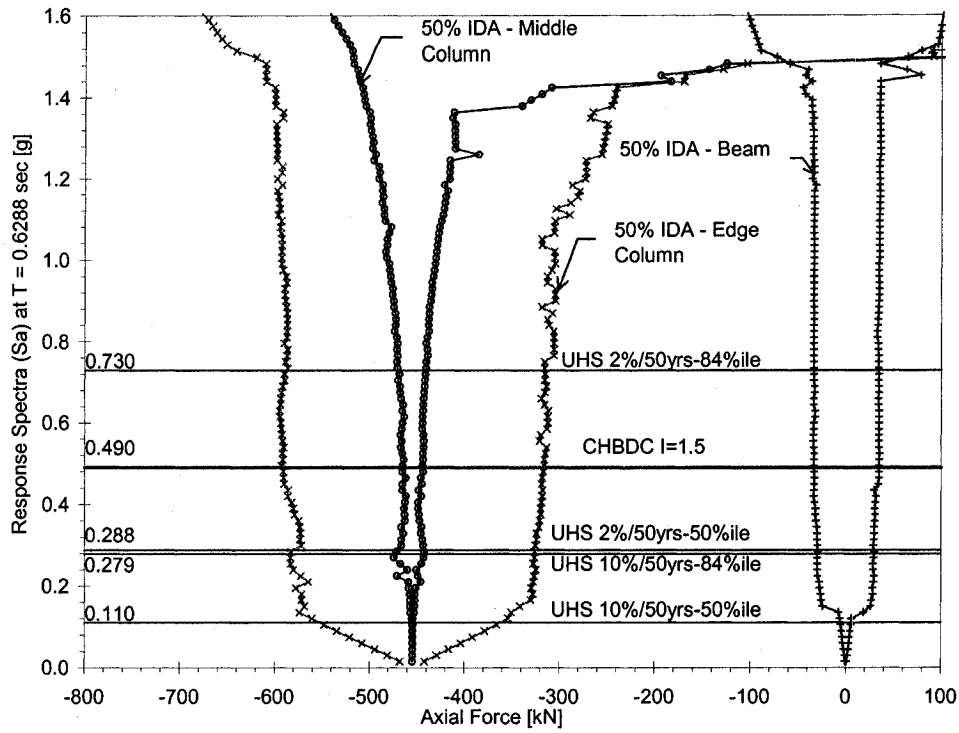

(a) Unspalled column case

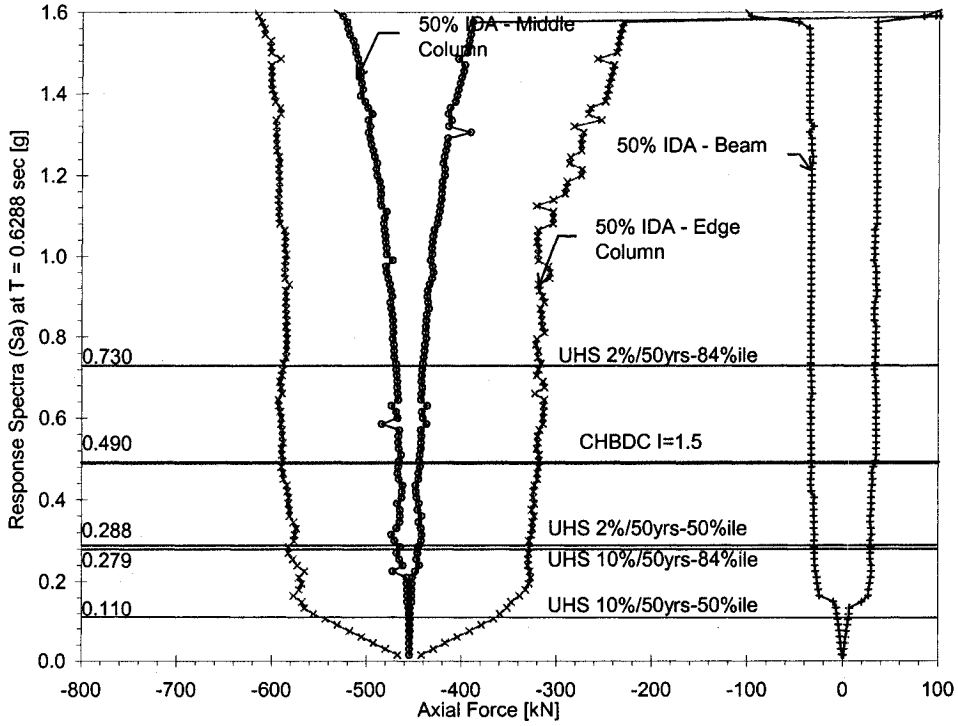

(b) Spalled column case

Figure 5-25 Predicted IDA median values of axial force variation for different cases (as-built)

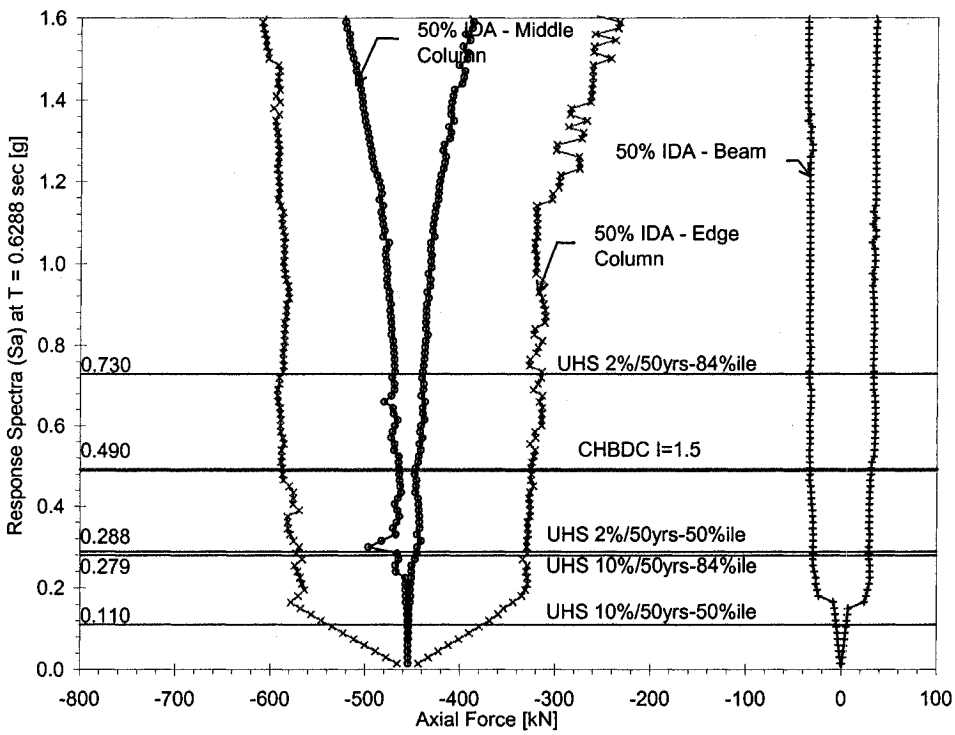

(c) Spalled-corroded case

Figure 5-25(cont) Predicted IDA median values of axial force variation for different cases (as-built)

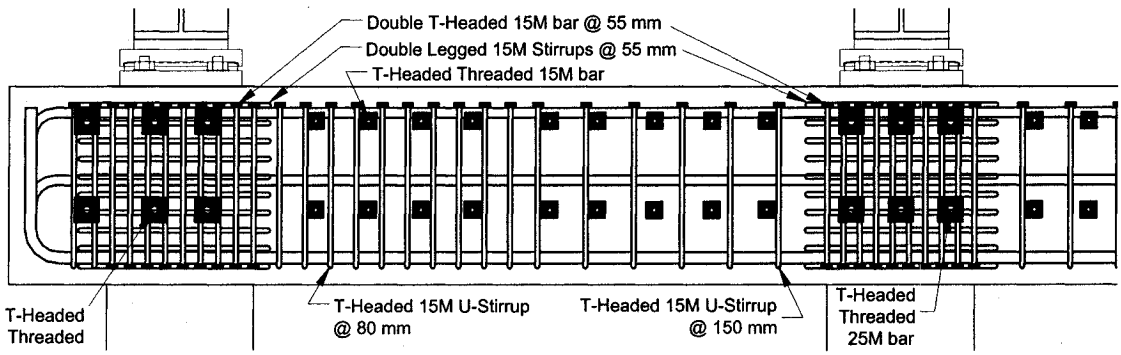

(a) Retrofitted beam elevation

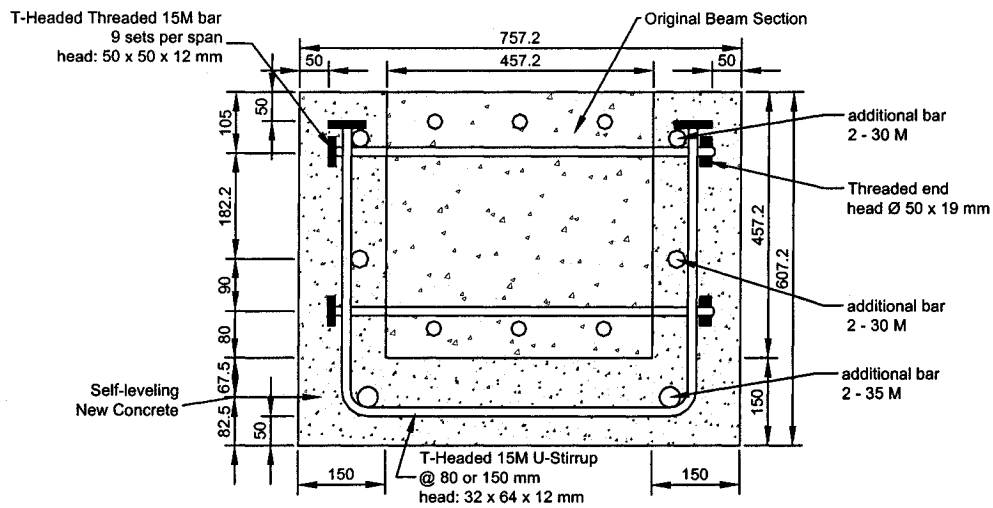

(b) Retrofitted beam detail

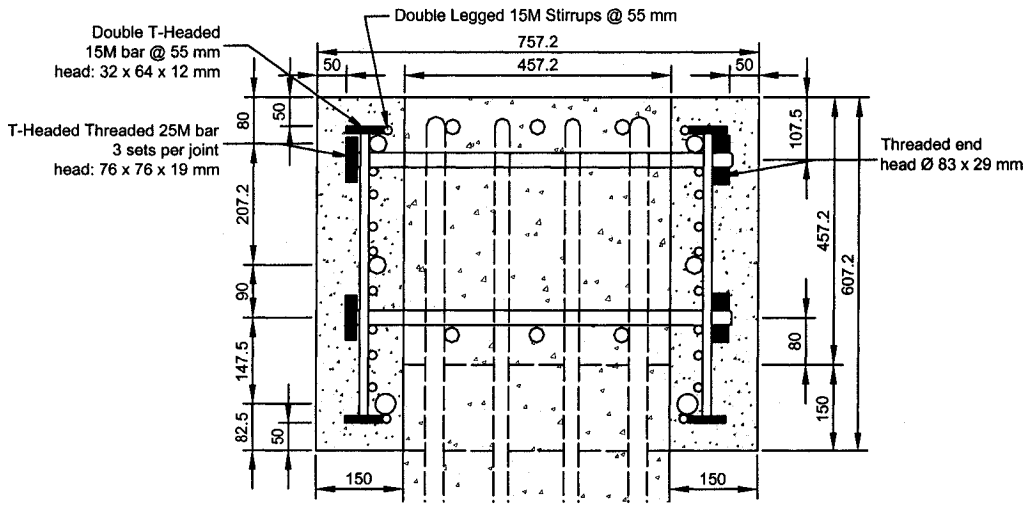

(c) Retrofitted beam detail at joint location

Figure 5-26 Details of Retrofitted Beam

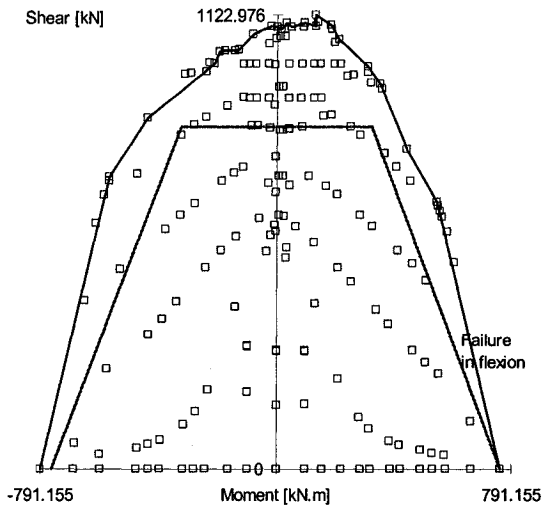

(a) Shear Moment Diagram

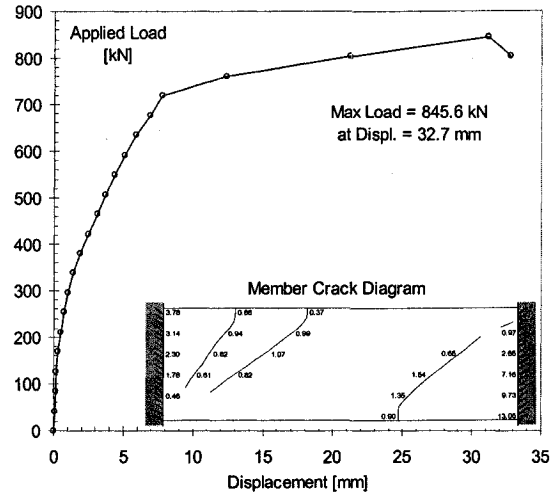

(b) Force Displacement Diagram

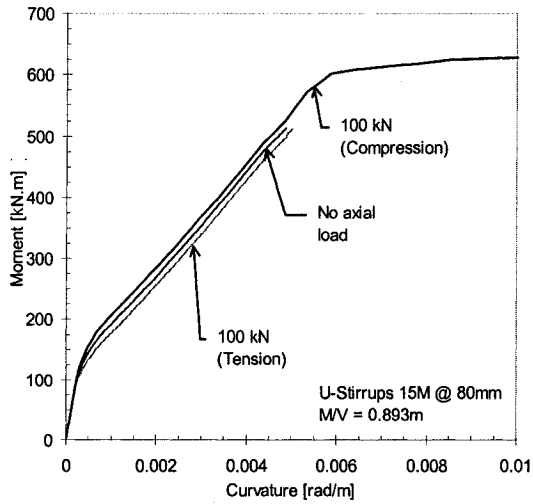

(c) Moment Curvature Relationships
M/V = 0.893 m

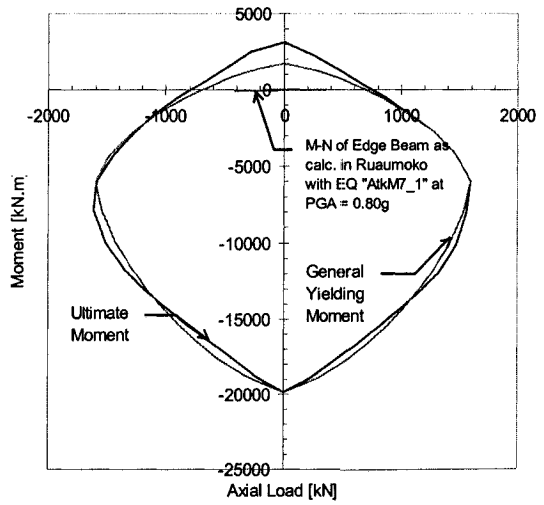

(d) Axial Load–Moment Interaction Diagram

Figure 5-27 Predicted member responses of the proposed retrofitted beam. Section details shown in Figure 5-26(b)

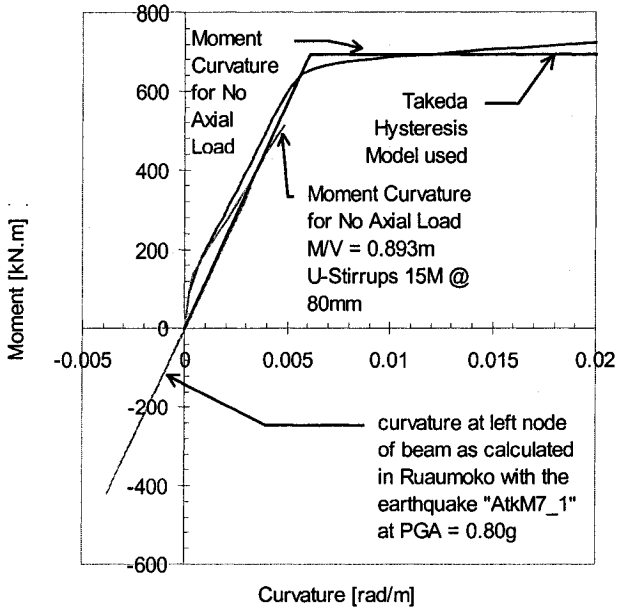

Figure 5-28 Hysteresis diagrams used in Ruaumoko and the moment-curvature from *Response* for an edge retrofitted beam

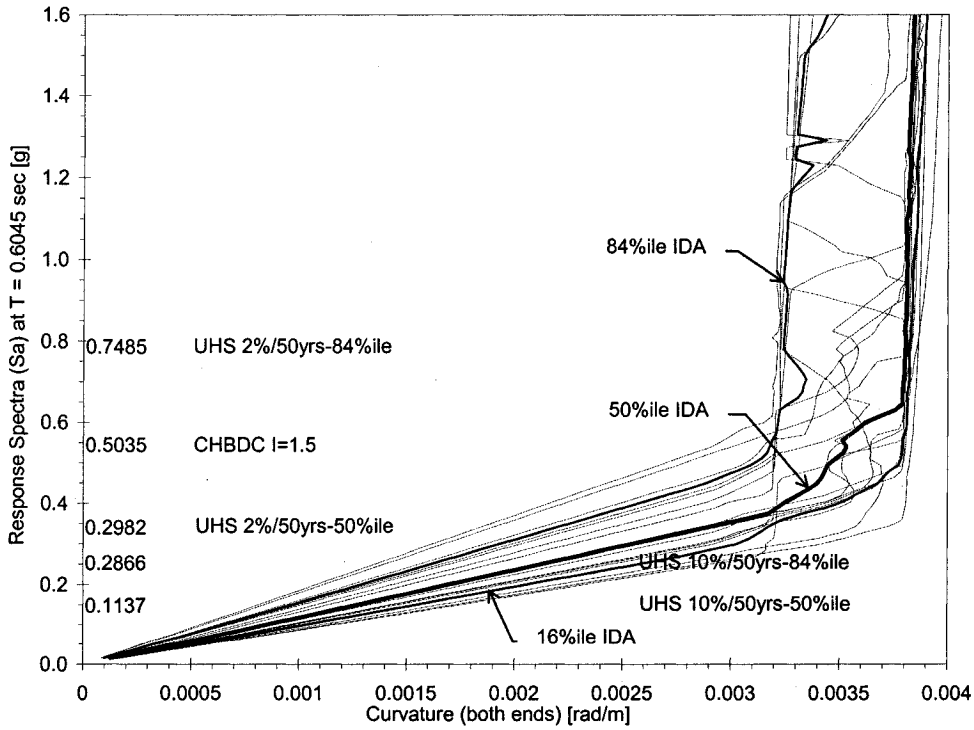

Figure 5-29 Predicted IDA curvatures at edge beam (element 13) for the retrofitted beam case

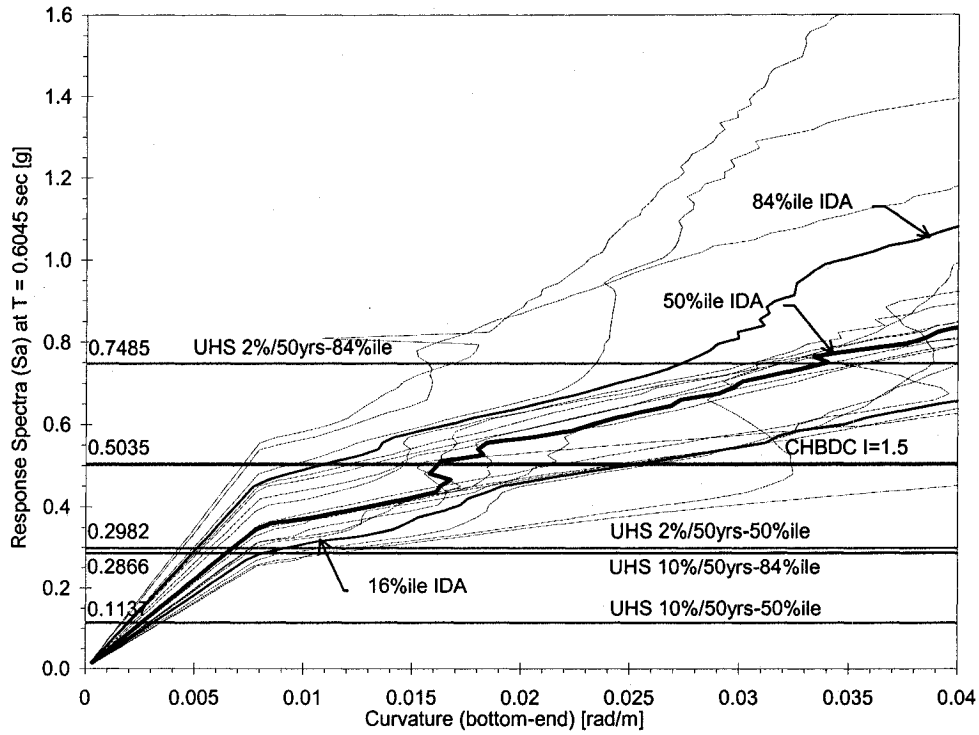

(a) Curvature of middle column (Element 5)

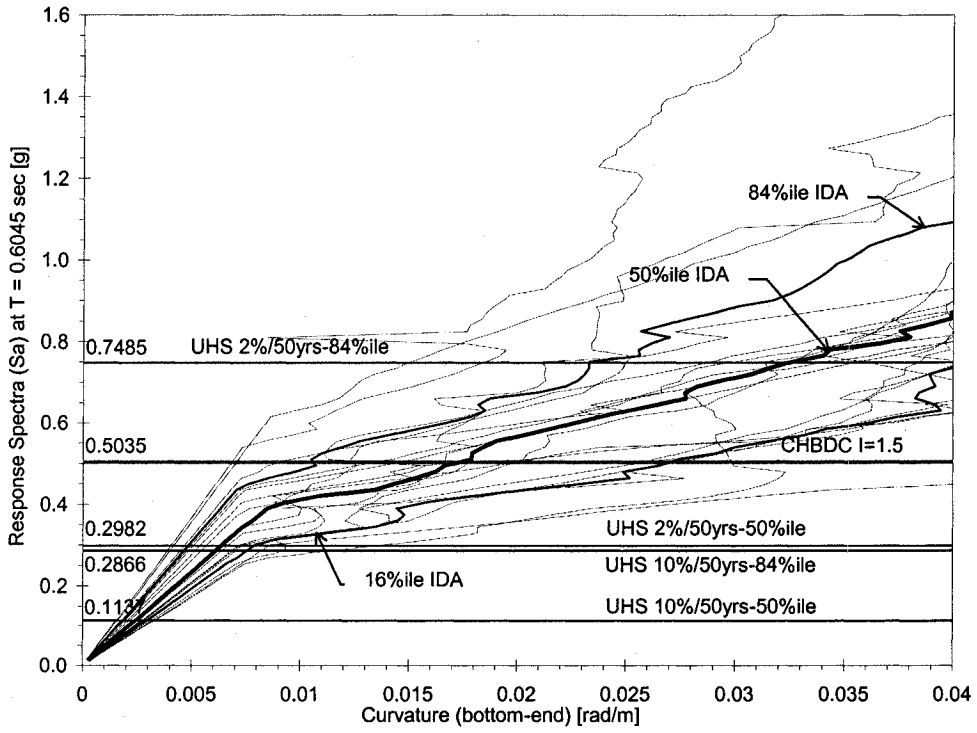

(b) Curvature of edge column (Element 1)

Figure 5-30 Predicted IDA curvatures at bottom of columns for the spalled-corroded column and retrofitted beam case

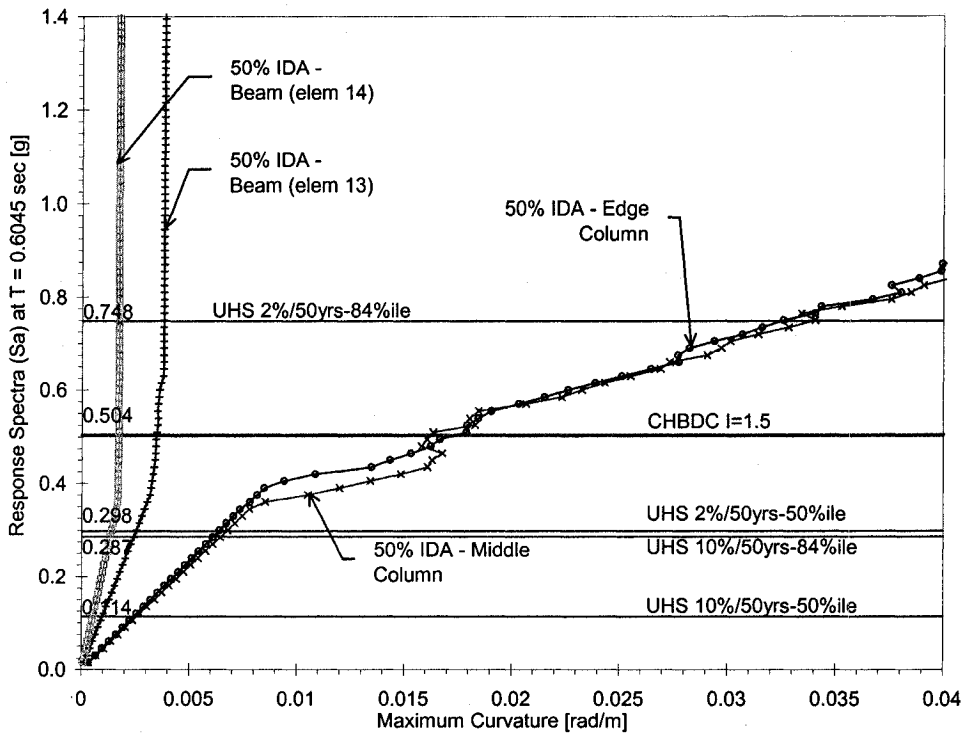

Figure 5-31 Predicted IDA median values of maximum curvatures for the spalled-corroded column and retrofitted beams case

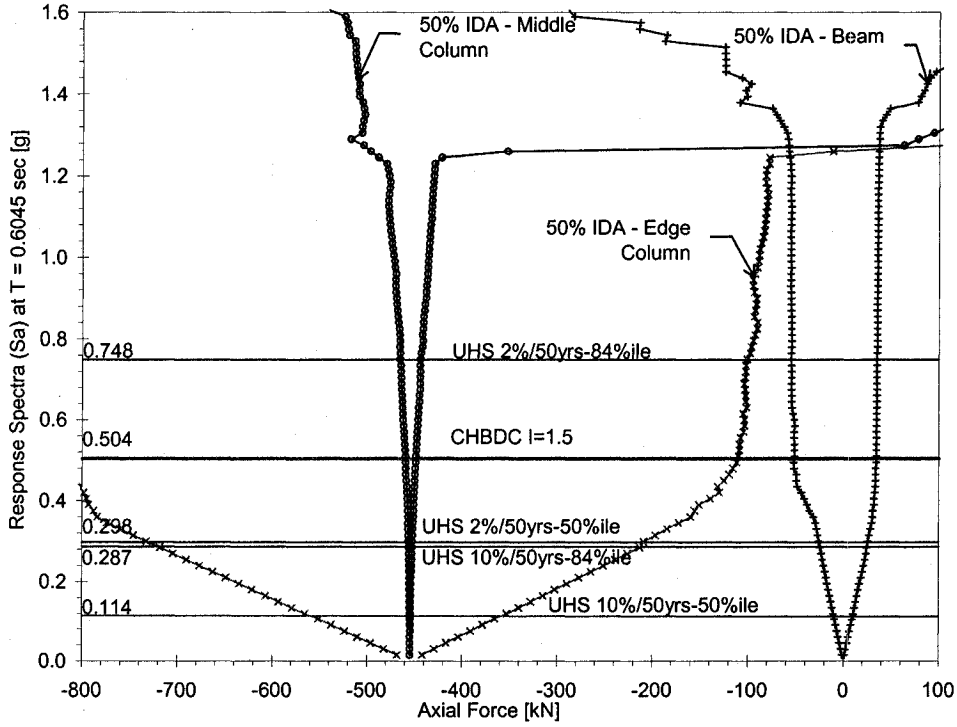

Figure 5-32 Predicted IDA median values of axial force variations for the spalled-corroded column and retrofitted beams case

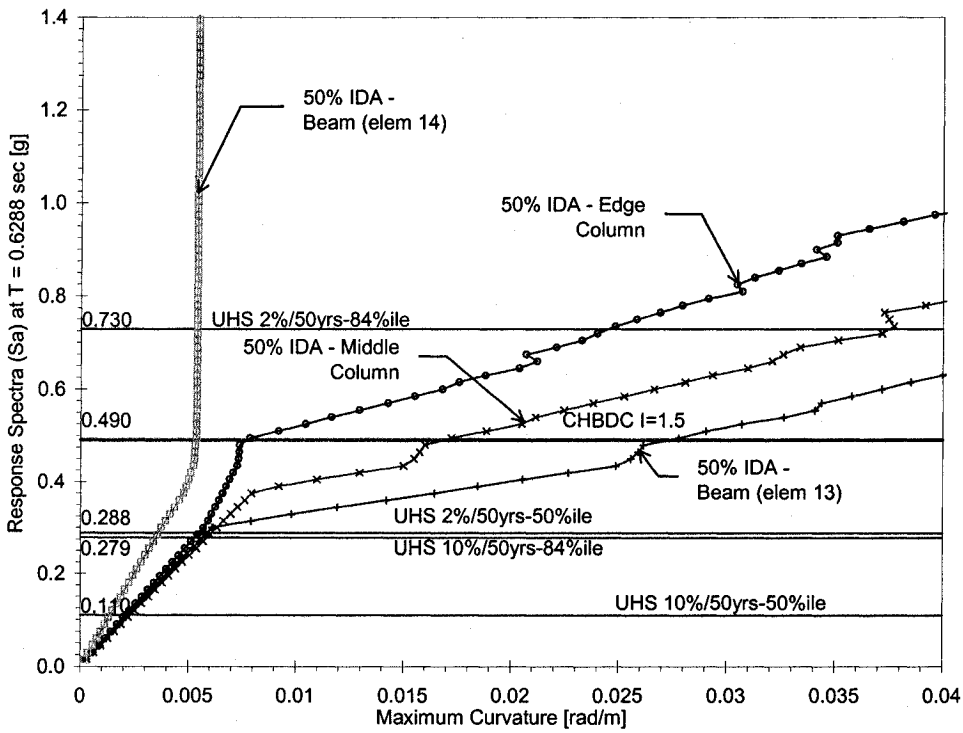

Figure 5-33 Predicted IDA median values of maximum curvature for the case of a properly designed and detailed ductile beam with spalled-corroded columns

Chapter 6

Seismic Evaluation of the St-Jean Blvd. Overpass Crossing Autoroute 40

6.1 Bridge Description

The St-Jean Boulevard Bridge crossing Autoroute 40 is considered a lifeline bridge. This importance category applies because the bridge crosses a major highway (Autoroute 40) that must remain operational. In addition, the closure of St-Jean Boulevard to emergency vehicles adds a significant detour that may hinder post-earthquake emergency efforts due to the presence of Lakeshore Hospital and a major fire station.

This overpass, shown in Figure 6-1, is one of several overpasses (Boulevard des Sources, Boulevard Saint-Charles, Ch. Sainte-Marie West and Ch. Sainte-Marie East overpasses) crossing Autoroute 40 that have similar geometry and reinforcement details.

It is believed that the general conclusions concerning the seismic assessment of the St-Jean Boulevard Bridge also apply to these other bridges.

6.1.1 Substructure and Superstructure

The bridge has four spans, as shown in Figure 6-2. The drawings are dated in the year 1961. The bridge is composed of two separate two-span structures, separated by a 25 mm gap. It is assumed that these two structures act independently with no accidental eccentricities. Each two-span structure is supported by an abutment, a seven-column moment resisting frame, and a frame consisting of seven columns pinned at their bases.

The superstructure is a voided slab with circular voids parallel to the bridge spans (Figure 6-2). These voids are interrupted by an integral cap beam at the frame locations, with two diaphragms at the third points of the span. The superstructure is structurally integrated with the supporting columns.

It is assumed that the 'rocking' supports at the abutments offer no resistance to lateral displacements. The bottom-pinned columns form a twin frame consisting of two sets of seven columns each, sharing the same foundation, but separated by a gap of 25 mm (1"). These rectangular columns have their sections reduced to a 356 mm (14") diameter section over a 25 mm height to form hinges at their bases. Designers typically assumed that these columns were pin-connected at their bases. Griezic *et al* (1999) demonstrated that these types of 'hinges' provide some moment resistance at their bases.

Because the seven-column moment resisting frame is located very close to the centre of mass of the two-span structure (see Figure 6-2), this moment resisting frame takes 99.3% of the lateral loading. The frame at the end of the two-span structure with bottom-pinned columns provides negligible resistance due to low stiffness and location. It is assumed the middle frame of each of the two-span structures resists 100% of the lateral load (Figure 6-3).

6.1.2 Description of Structural Components

The main moment resisting frame consists of seven columns (Figure 6-4) and one beam that is integral with the voided deck slab of the superstructure (Figure 6-5). Each column of this frame has a rectangular cross section with its weak axis parallel to the frame axis. The longitudinal steel reinforcement of the columns consists in 34-#11 bars (35.8 mm dia.) or 3.188% of the gross area. This reinforcement extends from the top of the foundation and it is anchored into the cap beam. The vertical reinforcement of the column is lap-spliced with vertical dowel bars that extend 914 mm into both the foundation and the column (Figure 6-4(a)). This lap-splice length corresponds to 26 bar diameters and is less than length required by the CHBDC for lap-splices in tension (about

35 bar diameters, Clause 8.15.9.3) for new construction. This reduced lap-length may result in limiting the stress of the reinforcement and slippage of the reinforcement.

Experimental research on the influence of lap-splices in columns at their bases indicates that the ductility can be significantly reduced with premature decay in moment resistance (Priestley *et al*, 1996). The presence of lap-splices in regions of expected plastic hinging can restrict the ability for yielding to spread over the height of the column (i.e., Griezic, 1996; Griezic *et al*, 1996). Furthermore, insufficient lap-length has been shown to cause severe bond distress in columns with insufficient confinement and premature shear failures (Griezic, 1996).

The transverse reinforcement of the column consists of three closed #4 ties: one peripheral tie and two smaller ties at a spacing of 305 mm (12"). The first column tie is located 76.2 mm (3") above the foundation and the last column tie is located 215.4 mm below the bottom of the cap beam (Figure 6-4).

The beam, shown in Figure 6-5, forms an integral part of the superstructure deck (Figure 6-2, Figure 6-3(a)). The longitudinal reinforcement consists of: 20-#11 (35.8 mm dia.) in the top layer, 4-#9 (28.7 mm dia.) in the middle layer, and 12-#11 in the bottom layer of the section. The transverse reinforcement consists of #6 (19 mm dia.) U-stirrups arranged as shown in Figure 6-5. The width of the beam varies from 1829 mm to 3658 mm, depending on the position of the ends of the circular voids in the superstructure (Figure 6-2). For modelling purposes, a rectangular section of 1829 mm width and 1067 mm height was used.

Figure 6-6 shows the condition of an exterior column of the frame under study. There are cracks on the surface, but no evidence of corrosion of the reinforcement is visible. However, this does not guarantee that corrosion has not started to affect the reinforcement. The CHBDC recommends that only the uncompromised parts of the section should be used for capacity analysis. In addition to considering an unspalled non-corroded column section, another case with a spalled column section having corroded reinforcement

is also considered. The corrosion effects are assumed to result in a 10% reduction of the gross steel area. Figure 6-4(b) shows the sections of the two cases considered.

6.1.3 Material Characteristics

The technical information for this overpass comes from drawings dated 1961. However, no specific information about the quality of the concrete or steel reinforcement is provided. The CHBDC (Section 14.6) provides several recommendations for determining the strength of the materials used when no specifications are found in the original plans and documents: analysis of samples from the structure, and estimation considering the date of construction. It was not possible to take core samples from the structure.

The code recommendation for cases where specifications are not available and where samples cannot be obtained, is to assume values for concrete and steel reinforcement that depends on the age of the structure. For concrete elements above the foundation, concrete strengths varying from 20 to 25 MPa are suggested. A value for the concrete compressive strength of 25 MPa was assumed for the evaluation.

For a structure built between 1956 and 1978, the minimum yield strength value for steel reinforcement recommended by the code is 275 MPa for structural grade and 345 MPa for intermediate grade. A yield-strength of 300 MPa was selected for the evaluation. The stress-strain relationships assumed for the evaluation are shown in Figure 6-7.

6.2 Site-Specific Soil Conditions

The seismic microzonation maps proposed in Chapter 4 provide site-specific soil conditions for different zones of the Island of Montreal. Local soil conditions for the St-Jean Boulevard overpass crossing Autoroute 40 were investigated. Ground Ambient Noise (GAN) recordings were obtained at several locations (Figure 6-8) and their Horizontal-to-Vertical Spectral Ratios were calculated (Figure 6-9). It is believed that traffic noise influenced the results of the HVSR making very difficult to identify a peak frequency in the

graphs. Despite this problem, in site Z1414, a clear peak in the fundamental frequency can be observed around 15 Hz. This site was located relatively far from the highway traffic. Although the peaks are not evident at the other sites, general trends can be observed in the high frequency segment (10 to 25 Hz). These observations suggest the presence of stiff soil between the surface and the bedrock.

The nearest borehole obtained from the database provided by the City of Montreal is B01384 (its location shown in Figure 6-8). The borehole has the bedrock at less than 1.80 m (6 ft) from the surface, with clay and sand deposits in between. The bridge drawings show the local soil profile based on three boreholes. They indicate bedrock at a depth of 5.6 to 6 m, relative to the original surface level, with varying layers of Clay and Basal Till up to the surface. The drawings also indicate that the bridge foundation is on rock.

The results from the GAN recordings and borehole information indicate the presence of stiff soil (Dense Sand, Basal Till, or Rock). Therefore, it is correct to assume the local soil conditions of this bridge correspond to a rock or firm soil site, and the site coefficient, S, (Equation 6-4) as 1.00.

6.3 Structural Idealization of Bridge Frame

The moment-resisting frame (Figure 6-3) was idealized by 13 elements to represent the columns and beams. The mass of the structure is assumed to be located at the beam or deck level, and to be distributed equally at each node (nodes 8 to 14, Figure 6-3(b)). A distributed load of 411.4 kN/m is applied on the beam elements to account for the dead load. Additionally, two vertical nodal loads of 376 kN are applied on top of the edge columns (node 8 and 14) to account for the weight of the barrier and edge cantilever. All mass nodes are defined to have the same lateral displacement to account for the large axial stiffness of the bridge deck.

6.4 Sectional Analyses of the Frame Elements

In order to evaluate the seismic performance of the frame, the response of its elements must be determined to model the non-linear response of the structure in Ruaumoko (Carr, 2001). The frame elements are discussed below:

6.4.1 As-Built Column

Although no corrosion is visible, surface cracks are present (Figure 6-6). It has been assumed that concrete cover spalling will occur during a major earthquake and that some corrosion is present in the reinforcing steel. Hence, two different cases for the as-built column were studied: an unspalled column, and a spalled column with 10% reduction in the steel reinforcement area (Figure 6-4(b)). These cases were analyzed with *Response 2000* for a double fixed-end cantilever column, 5.778 m long.

The as-built columns are predicted to fail in shear, as shown in Figure 6-10. Because of the geometry of the frame, the columns would behave as a double-fixed cantilever until they start to fail. Although the column is predicted to fail in shear, it is very close to flexural yielding. Figure 6-11 shows the predicted shear-displacement diagrams for the two cases, for an axial load of 1451 kN (average dead load) calculated with *Response 2000*. Equivalent moment-curvature diagrams are constructed for both cases (Figure 6-12). These moment curvature relationships were found from predicted shear-displacement diagrams with different axial loads, using Equation 6-1. The P-Delta effects were calculated to be less than 1.5% of the moment and were ignored in the analysis.

$$\phi_{equiv} = d\frac{6}{h^2}, \quad M_{equiv} = \frac{V h}{2} \qquad 6\text{-}1$$

where: d and V are the predicted displacement and shear; h is the free height of the columns (5778 mm)

Figure 6-13 shows the predicted axial load-moment interaction diagrams for the two types of column sections studied. In the graphs, the ultimate moment of the columns, considering only flexure are plotted, along with the equivalent yielding moment adjusted to account for the premature shear failure. The latter was developed for the range of axial loads believed to be present in the analysis (From 1000 kN in tension to -2500 kN in compression). The curve was fitted into the yield interaction surface equation (Table 6-1) used in Ruaumoko.

Figure 6-14 shows the predicted hysteresis responses for the two cases for a selected earthquake ground motion. The Takeda hysteresis model was used (Figure 5-14), with the Emori unloading pattern, an unloading stiffness factor (α) of 0.25 and a reloading stiffness factor (β) of 0.3. A reduction in strength or degradation is expected after the first equivalent 'yield' event, especially with columns with lap-splices in critical regions. Priestley *et al*, (1996) recommends reducing the strength at a predetermined ductility level to the residual moment at a ductility of about 8.0 (Table 6-1). For the lap-splice lengths provided (26 d_b), it was assumed that strength degradation started at a ductility level of 1.33. The residual moment was considered to be $1/20^{th}$ of the ultimate equivalent moment, that is somewhat lower than that recommended by Priestley *et al*, (1996). This accounts for the tension forces that the columns would experience during an earthquake. Table 6-1 summarizes the values used by *Ruaumoko* in the Incremental Dynamic Analysis (IDA), whose results are shown later in this chapter.

The tension stiffening factor used in *Response 2000* analysis was assumed to be 0.1. The CHBDC (Clause 4.7.4.13) considers a varying factor for the concrete contribution to shear varying between 0.0 and 1.0, proportional to the ratio of the applied axial load to the balanced axial load of the element. In this case, the predicted axial load varies from small tensions up to 30% of the balanced axial load. The assumed tension stiffening factor of 0.1 accounts for tensile loads and low axial compressions.

6.4.2 As-Built Cap Beam

The as-built cap beam is an integral part of the superstructure deck (Figure 6-2). The minimum width of 1829 mm (Figure 6-5) is used in the calculations of the predicted response of the member in *Response 2000*, as shown in Figure 6-15. The massive concrete beam is predicted to yield in flexure (Figure 6-15 (a) and (c)). The differences in the amount of positive and negative longitudinal reinforcement of the beam result in an asymmetric predicted flexural response. Only the lower strength values, shown in Figure 6-15 (c), were used in the determination of the yield interaction surface (Table 6-1) of Figure 6-15 (d).

The tension stiffening factor used in the *Response 2000* calculations was conservatively assumed to be 0.2. Although the axial load in the beam is spread through the entire deck, the massive amount of concrete of the beam suggests that the concrete contribution to shear can be higher than the value recommended by the code.

The predicted hysteresis response of the beam is shown in Figure 6-16. The Takeda hysteresis model was used, with the Emori unloading pattern, an unloading stiffness factor (α) of 0.25 and a reloading stiffness factor (β) of 0.3. A very ductile behaviour was chosen for the element (Table 6-1).

6.5 CHBDC Predictions

The Canadian Highway Bridge Design Code provides recommendations for the seismic evaluation and retrofitting of existing bridges using a static analysis approach. The ductility provided R_{prov} must be greater or equal to the ductility required R_{req} (Eq.6-2) otherwise retrofitting is required and hence:

$$\frac{R_{prov}}{R_{req}} \geq 1.00 \qquad 6\text{-}2$$

The ductility required is defined by the ratio between the seismic effects as if all members are elastic (S), and the member capacity (C) after the dead load has been accounted for:

$$R_{req} = \frac{S}{C} \qquad 6\text{-}3$$

The seismic effects (shear or moment) on a member are a function of the dead and earthquake loads. The earthquake load is defined by the elastic seismic response coefficient C_{sm} multiplied by the total seismic weight of the structure W:

$$C_{sm} = \frac{1.2AIS}{T_m^{2/3}} \leq 2.5AI \qquad 6\text{-}4$$

For the Montreal region, the zonal acceleration ratio A is 0.20. The site coefficient S for a rock site is 1.0 (Soil Profile I, rock). From a static analysis, the fundamental period was found to be T = 0.369 sec. Therefore the elastic seismic response coefficient C_{sm} is:

$$C_{sm} = \frac{1.2 \times 0.20 \times 1.5 \times 1}{0.369^{2/3}} = 0.7003 \leq 2.5 \times 0.20 \times 1.5 = 0.75 \qquad 6\text{-}5$$

The total earthquake load applied to one of the two-span structures is approximately $EQ \sim 0.7003 \times 20313\,\text{kN} = 14226\,\text{kN}$. Therefore, the seven columns of the fixed-end frame must carry all of this load, resulting in 2032 kN applied to nodes 8 to 14 (Figure 6-3). A static analysis using this force results in a shear of 2088 kN and a moment of 6090 kN.m for the middle column. The shear and moment for the edge beam are 2644 kN and 5141 kN.m, respectively.

For the evaluation of this bridge, the member capacities are defined by:

$$C \sim \begin{matrix} M_n - M_D \\ V_n - V_D \end{matrix} \qquad 6\text{-}6$$

where: M_n and M_D are the nominal moment resistance and moment action due to dead load. V_n and V_D are the nominal shear resistance and shear action due to dead load.

The column shears and moments due to dead load are negligible. In the beam, V_D and M_D are 741 kN and 312 kN.m, respectively.

As found in the previous section, the column fails in shear at a predicted nominal resistance of 1279 kN and a corresponding maximum moment of 3695 kN.m. The nominal shear resistance of the beam is due to the concrete contribution, the contribution of the vertical stirrups, and the contribution of the inclined reinforcement (Figure 6-5), and is estimated to be 3163 kN. The flexural resistance of the beam is 3442 kN.m (Figure 6-15). Hence, according with the procedure given by the CHBDC, the required ductility of the column and the beam are:

$$\text{Moment in Columns: } R_{req} = \frac{S}{C} = \frac{6090}{3695-0} = 1.648$$

$$\text{Moment in Beam: } R_{req} = \frac{S}{C} = \frac{5141}{3442-312} = 1.642$$

$$\text{Shear in Columns: } R_{req} = \frac{S}{C} = \frac{2088}{1279-0} = 1.633 \qquad 6\text{-}7$$

$$\text{Shear in Beam: } R_{req} = \frac{S}{C} = \frac{2644}{3442-741} = 1.092$$

It is noted that the values computed for the R_{req} are the maximum values for the columns and beams. The R_{req} for the shear failure of the beams was determined in a very conservative way, with a low tension stiffening factor. It is concluded that the beams have sufficient strength and ductility in shear and flexure. However, the columns do not have sufficient strength and ductility in shear. The shear-critical columns have an R_{prov} of about 1.00. Therefore, the column requires retrofit.

6.6 Incremental Dynamic Analysis

6.6.1 Scaled Time Histories

The selection and scaling of the earthquake records used in this analysis followed the same procedure used in the previous chapter. Seventeen ground motion records, from natural events to artificial simulations, were used in this analysis (Table 3-4 and Table 3-5). The results of the Incremental Dynamic Analysis (IDA) were associated to the spectral

acceleration of the earthquakes evaluated at the fundamental elastic period of the bridge (T = 0.3692 sec). The spectral accelerations S_a were scaled from 0.015g to 1.2 g.

6.6.2 Performance Parameters

For this bridge, the critical elements are the columns and the integral cap beams. Overturning effects make the columns located at the edge of the structure more susceptible to higher axial load variations than the columns closer to the middle. Three control elements were selected: two columns (elements 1 and 3), and a beam (element 8). Their locations are shown in Figure 6-3(b).

In this research, the selected performance parameters are:

(3) Maximum Curvatures:

The tops of the columns are connected to the concrete beam, and the bottoms are connected to the foundation beam. Failure is expected to occur at the bases of the columns before it occurs at their tops, when the structure is subjected to lateral loading. The beams are predicted to be stronger than the columns, and the columns are predicted to fail in shear. The columns will behave as double-fixed elements until shear failure. The maximum curvature at the bottom end of Element 1 (edge column) and Element 3 (middle column) are used as performance indicators. For the case of the columns, their expected moment-curvature behaviour is quasi-linear until a brittle failure occurs (Figure 6-12 (c)). Element 8 (edge beam) is the most critical beam element. The maximum curvature at both ends of this edge beam is used as a performance indicator. It was noted that when the maximum curvatures reached about 0.01 radians/m, the structural response tended to be unstable and collapse was assumed.

(4) Maximum and Minimum Axial Forces:

The expected overturning effect in the bridge will produce compressive or tensile forces in the columns, depending on the direction of the inertial horizontal forces. It is believed that the edge columns rather than the middle columns will experience some tensile forces and it is of interest to know their magnitude. Ruaumoko gives the maximum

axial force as tension (positive) and the minimum axial force as compression (negative). These predicted axial loads were used as performance indicators and their 50th percentile IDA curves are shown later.

6.6.3 Predicted behaviour of key elements

The response of three key elements was monitored (Figure 6-3(b)): Element 3, or one of the columns closest to the middle; Element 1, or an edge column, located at the outermost end of the frame; and Element 8, or the edge beam, is the outermost beam segment that connects to an edge column.

Two different cases are evaluated for the as-built structure:

(4) Unspalled Column Section:

Figure 6-17 and Figure 6-19(a) show the IDA curves of maximum curvatures for the edge and middle columns and the edge beam for the unspalled column section case. The median values of the IDA curves for the three elements are shown in Figure 6-20(a). It can be observed that about an acceleration level (0.60 g), the middle column (Element 3) starts to soften, followed by the edge column (Element 1), while the edge beam (Element 8) starts to harden. It also can be observed that the curve with the median values of maximum curvatures in the edge beam (Figure 6-19(a) and Figure 6-20(a)) indicates that the yielding curvature of about 0.002 rad/m was not exceeded (Figure 6-16). With the failure of the columns in shear, it is assumed that the structure fails.

It is noted that the 16, 50 and 84 percentiles of IDA values were determined from the curvatures of different earthquake records at different acceleration levels.

The median values for the IDA curves for the axial load variation on the two columns under study are shown in Figure 6-21(a). It is observed that the edge column (Element 1) would experience tension at a spectral acceleration level above 0.32 g. This is due to the comparatively lower initial axial loads on the edge columns compared to the interior columns. The middle column (Element 3) does not experience significant tension values, and has relatively small variations in the axial load. The variation of the axial load

in Element 2 (not shown) falls in between Element 1 and 3. It can also be observed that the variation in axial load increases linearly with increasing acceleration levels up to about 0.60 g, which corresponds to the same level where the IDA curvatures of the columns start to soften. The 0.60 g level in spectral acceleration is below the limit of 0.7 g imposed by the CHBDC for 'emergency-route' bridges (I = 1.5). The axial loads in the beams are negligible.

The predicted behaviour of the frame with unspalled column sections also results in a premature shear failure of the columns. Although the exact sequence of 'hinge' formation is difficult to predict as the columns change from double-fixed-ends to cantilever behaviour and then double-pinned end behaviour for significant ground motions. This change is accompanied by an increment of the fundamental period of the structure, hence the hardening of the beams.

As expected, there is considerable dispersion in the IDA curves for the selected elements and cases of 'structural resurrection' can be observed (Vamvatsikos and Cornell, 2002) for different earthquakes (Figure 6-17 and Figure 6-19(a)). This dispersion has the effect of moving the damage measurement values (curvature or axial load) to values in between a lower limit, usually near a yielding value, and a higher limit outside the scale, indicating a probable collapse of the structure.

(5) Spalled Column Section and Corroded Steel Reinforcement:

Figure 6-18 and Figure 6-19(b) show the IDA curves of maximum curvatures for the edge and middle columns, for the case of a spalled column section and corroded steel reinforcement. The median values of the IDA curves for the three elements are shown in Figure 6-20(b). It can be observed that the columns, first the edge column then the middle column, start to soften at a spectral acceleration level of around 0.60 g. At the same level, the beam starts to experience hardening due to the redistribution of forces associated with an increase in the fundamental period. The curvature values of the edge beam for different

earthquakes never exceed the yielding curvature limit determined for the beam: about 0.002 rad/m (Figure 6-19 (b)).

Figure 6-21(b) shows the median values of the maximum and minimum axial loads determined for each column. Similar to previous analyses, the edge column (Element 1) starts to experience tension at spectral acceleration levels greater than about 0.36 g, while the middle column, on average, does not experience tensile loads. This behaviour is due to the geometry of the frame as it is subjected to lateral forces and is also due to the fact that the edge columns have lower axial loads than the interior columns. The variation in axial loads increases linearly with increasing acceleration levels up to about 0.60 g, which corresponds to the same spectral acceleration level (and curvature) where the columns start to fail (Figure 6-14(b)).

The frame of the spalled corroded case has an overall behaviour very similar to the case where the columns are unspalled, but at slightly lower spectral accelerations. The columns fail prematurely in shear before any yielding occurs in the beams, creating a potential structural instability and hence collapse.

6.6.4 Summary of predicted behaviour of the moment resisting frame, failure definition

The maximum curvatures values of the edge beam start to harden at the same acceleration level as the maximum curvature values of the columns start to soften. The dispersion of the values and cases of 'structural resurrection' are apparent after the failure of the first column, making it difficult to predict the behaviour of the frame at high spectral acceleration levels. In addition, when the tangent slope of the IDA median curve after softening becomes too small, usually less than 20% of the elastic value, it can be considered that the element has reached its capacity point and may experience collapse soon afterwards (Vamvatsikos and Cornell, 2002).

In general, earthquakes with a spectral acceleration above 0.60 g (at T = 0.3692 sec) are predicted to cause a brittle shear failure in the columns and perhaps collapse. A brittle shear failure is unacceptable in columns; hence, the frame should be retrofitted.

6.7 Retrofitting strategy and Predicted Response

It was shown that the premature shear failure of the columns governs the overall response of the frame. The objective is to prevent such failure with a minimum of retrofit work. The column shear failure is attributed to insufficient shear reinforcement. If additional shear reinforcement is added in the direction of the weak axis of the column, it is possible to prevent a shear failure and develop yielding at the critical sections of the column. To accomplish this, sets of three T-headed bars are inserted into the columns to increase the overall shear resistance of the section. To obtain conservative values in the adequacy of the reinforcement, the spalled column section with the corroded steel reinforcement is used in the strength calculations.

6.7.1 Calculation and Details of Retrofitted Column

Figure 6-22 shows the details of the proposed additional shear reinforcement in the column. Three 25M T-headed bars (f_y = 400 MPa), spaced every 305 mm (12") are added in between the original ties. The program *Response 2000* is used to compute the effects of the additional reinforcement on the column section. Figure 6-23 shows the pushover analysis carried out for the column over a clear height of 5.778 m. The presence of additional shear reinforcement changes the mode of failure, experiencing flexural yielding at a nominal flexural resistance of 3456 kN.m and a corresponding shear of 1196 kN. The added six sets of 3-25M T-headed reinforcing bars were provided over a height of 1.675 m measured from bottom and top of the columns (see Figure 6-22). This height exceeds twice the dimension of the column in the direction of the lateral load. The portion of the column outside of these T-headed bars has a height of 2.428 m. Figure 6-23 shows the pushover analysis for this portion of the column. This analysis, which accounts for combined moment-shear and axial load, indicates that the column can resist a shear of 1438 kN. Hence, this portion of the column height is adequate without additional shear

reinforcement. Therefore, six sets of 3-25M T-Headed bars are recommended at each end of the columns, as shown in Figure 6-22(a).

6.7.2 Behaviour of Retrofitted Frame

Figure 6-24 shows the predicted member responses of the retrofitted section: Figure 6-24(a) shows the shear-moment diagram indicating a failure in flexure. Figure 6-24(b) shows the predicted shear-displacement diagram. The maximum shear force resisted by the retrofitted column is 1235 kN, while the predicted shear force with the as-built spalled section and corroded reinforcement case is 1132 kN (Figure 6-11(b)). The moment-curvature relationships (sectional response) for three axial loads are shown in Figure 6-24(c). Finally, Figure 6-24(d) shows the axial load-moment interaction diagram for the cases of ultimate moment and general yielding moment, as used in Ruaumoko. It is noted that the retrofitted column is able to develop flexural yielding without major shear distress. Figure 6-25 shows the envelope of the hysteresis diagram used in this case.

A summary of the main parameters used in Ruaumoko for the case of the retrofitted column is presented in Table 6-1. The parameters for the beam remained the same for all the cases. Figure 6-26 shows the predicted IDA curves of the edge beam (Element 8) for the case of the retrofitted columns. Figure 6-27 shows the predicted IDA curves of the retrofitted edge column (Element 1) and retrofitted middle column (Element 3). It can be observed that the after-yielding slope of the IDA curves of the retrofitted case is larger than the curves of the as-built cases (Figure 6-17 and Figure 6-18). The combined median IDA values of the three elements of the retrofitted column case are shown in Figure 6-28. As expected, it can be observed that the spectral acceleration level at which the retrofitted columns start to yield is 0.65 g, that is larger than the spectral acceleration of 0.60 g when the unretrofitted columns fail in shear (see Figure 6-20(b)). The retrofitted structure can achieve spectral acceleration levels of 0.80 g; that is greater than the value specified by the CHBDC (I = 1.5) of 0.70 g.

Figure 6-29 shows the variation in the median values of the maximum and minimum axial loads for the retrofitted edge and middle columns. It can be observed that the relationship of the variation of the axial load versus the spectral acceleration remains linear up to a higher acceleration value of 0.65 g.

The objective of avoiding a premature shear failure on the columns while increasing the strength of the element has been accomplished.

6.8 Summary

The main moment-resisting frame of one of the two-span structures of the St-Jean Blvd. overpass crossing Autoroute 40 has been evaluated using the Incremental Dynamic Analysis technique. Two cases that represent possible conditions for the as-built columns were studied: one with the columns unspalled, and another opposite with spalled columns with corroded reinforcement. The seven-column frame was subjected to a wide range of earthquakes and scale factors as part of the IDA technique, to evaluate and compare the response with the spectral acceleration levels specified by the CHBDC and UHS for Montreal. The insufficient shear reinforcement in the columns resulted in a shear failure before any flexural yielding could occur. An equivalent yielding moment versus axial load interaction diagram was calculated for the expected range of axial load on the columns (Figure 6-12). Similar diagrams were developed for the beams, but in these cases, the beams were predicted to yield in flexure without failing in shear.

The maximum curvatures and axial loads of three representative elements (edge column, middle column, and edge beam) were retrieved during the IDA. A comparison between the median IDA curves in each case for the three elements showed that the early shear failure of the columns dominate the overall behaviour of the frame (Figure 6-20). The spectral acceleration level at which the columns fail (approximately 0.60 g) is lower than the spectral acceleration level of the CHBDC (0.70 g), even for an emergency route bridge

(I = 1.5). However, it is higher than the level that corresponds to the 2% in 50 years (50th percentile) of the Uniform Hazard Spectra for Montreal (0.424 g).

The chosen retrofitting strategy involves the introduction of additional shear reinforcement in the form of T-headed bars in the concrete columns to avoid shear failure. The columns would experience flexural yielding before any flexural yielding or shear distress in the beams. The columns of the retrofitted frame can sustain higher levels of spectral acceleration (0.65 g) before starting to yield (Figure 6-28).

An approach using minimum intervention was studied as part of the retrofitting strategy. The retrofit of the columns improves the performance of the frame. The as-built frame suffers a shear failure at a predicted spectral acceleration of 0.60 g whereas the retrofitted frame is predicted to experience general yielding of the columns at 0.65 g, with the ability to undergo spectral accelerations in excess of 0.8 g.

Although the localized spalling and corrosion of some of the column ties should be addressed with corrective measures, this study indicates that this minimal deterioration has not significantly affected the expected seismic performance.

Table 6-1 Main Parameters Used by Ruaumoko in the Analysis per case

Parameter \ Case	Unspalled Column Case	Spalled - Corroded Column Case	Retrofitted Column Section
Reinforced Concrete Column (Elements 1 to 7)			
Elastic Section Properties			
Cross Sectional Area [m^2]	1.0740	1.0740	1.0740
Moment of Inertia [m^4]	0.05916	0.05916	0.05916
Inertia Cracking Factor	0.3686	0.3245	0.3245
Element Properties			
Rigid Block at top end [m]	0.5588	0.5588	0.5588
Member Hinge Lengths at bottom end [m]	0.05	0.05	0.05
Member Hinge Lengths at top end [m]	0.172	0.172	0.172
Concrete Interaction Parameters (*)			
Factor for Flexural terms (α)	1.16	1.246	1.45
Factor for Axial terms (β)	1.287	1.225	1.115
Axial Compression Yield Force (PC) [KN]	-36222	-31977	-31977
Axial Compression Force at Balance Point (PB) [KN]	-10298	-8839	-8839
Yield Moment at Balance Point around the z-z axis (MBz) [KN.m]	5165	4430	4605
Axial Tension Yield Force (PT) [KN]	11022	9828	10442
Strength Degradation Data			
Ductility at which degradation begins	1.33	1.34	3.90
Ductility at which degradation stops	8	8	11.90
Reduction in strength due to degradation	0.048	0.048	0.049
Ductility at 0.01 strength	n/a	n/a	n/a
Reinforced Concrete Beam (Elements 8 to 23)			
Elastic Section Properties			
Cross Sectional Area [m^2]		1.9515	
Moment of Inertia [m^4]		0.18515	
Inertia Cracking Factor		0.3631	
Element Properties			
Rigid Block at top end [m]		0.4064	
Member Hinge Lengths [m]		0.1	
Member Initial Distributed Loads [kN/m]		-411.39	
Concrete Interaction Parameters (*)			
Factor for Flexural terms (α)		1.305	
Factor for Axial terms (β)		1.379	
Axial Compression Yield Force (PC) [KN]		-55975	
Axial Compression Force at Balance Point (PB) [KN]		-20643	
Yield Moment at Balance Point around the z-z axis (MBz) [KN.m]		8864	
Axial Tension Yield Force (PT) [KN]		6413	
Strength Degradation Data			
Ductility at which degradation begins		25.84	
Ductility at which degradation stops		28.43	
Reduction in strength due to degradation		0.17	
Ductility at 0.01 strength		45.78	

Note: (*) The yield interaction surface is $\left\{\frac{P-PB}{PC,PT-PB}\right\}^{\beta}+\left\{\frac{Mz}{MBz}\right\}^{\alpha}+\left\{\frac{My}{MBy}\right\}^{\alpha}=1$ (Carr, 2001).

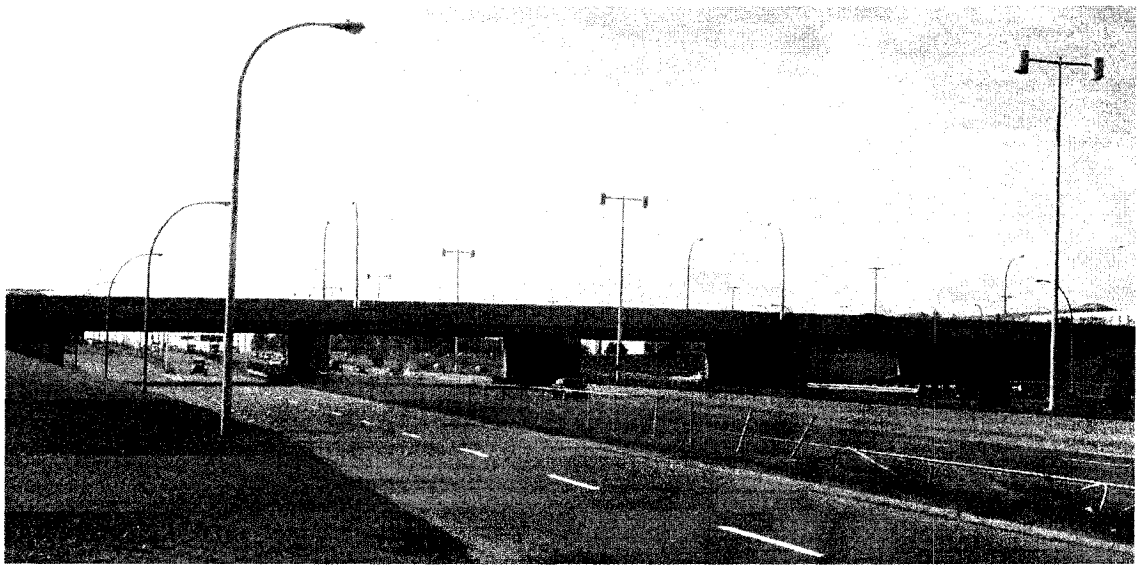

Figure 6-1 East view of St-Jean Blvd. overpass crossing Autoroute 40

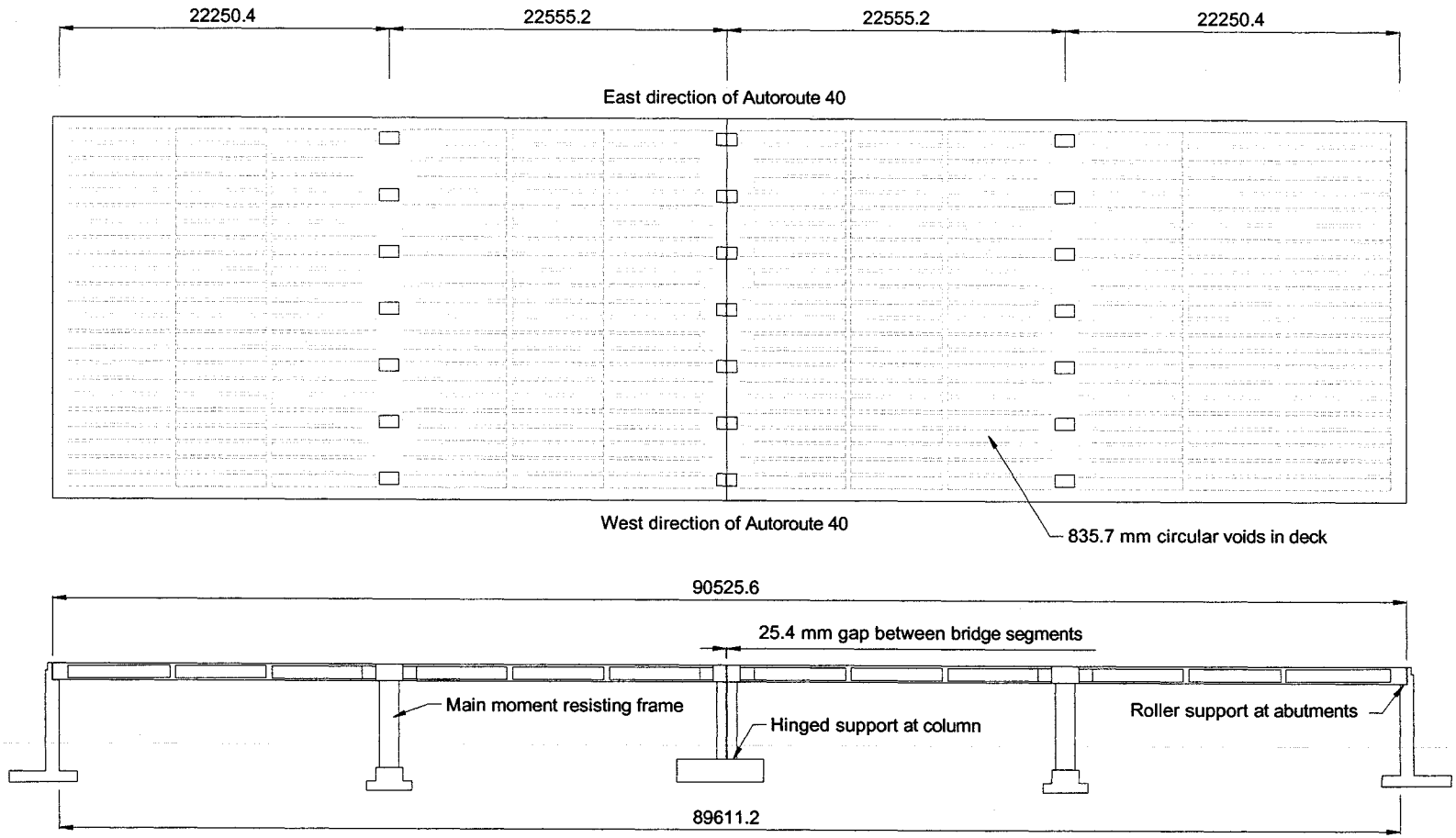

Figure 6-2 Plan and elevation of bridge

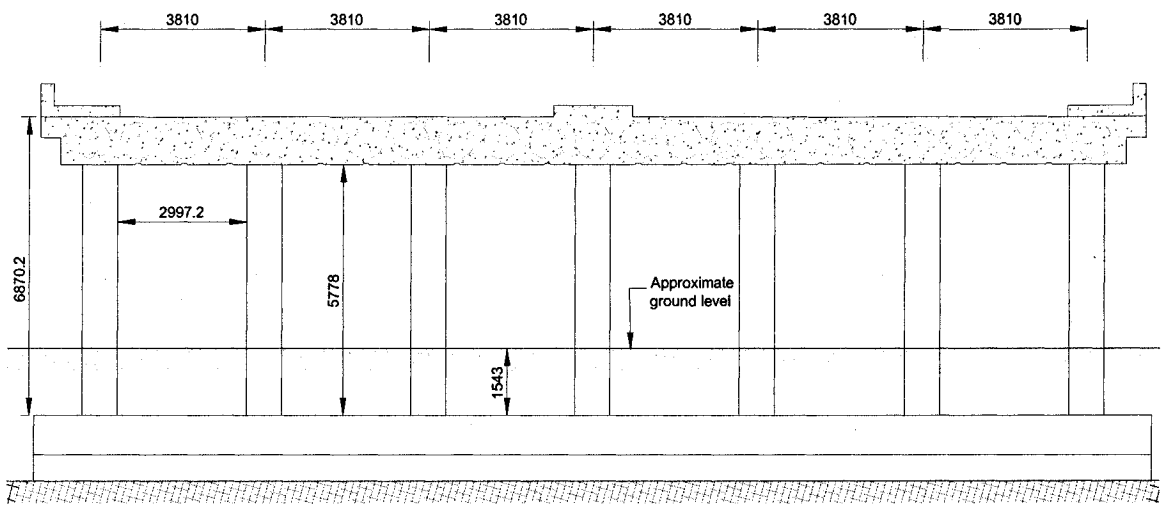

(a) Frame elevation

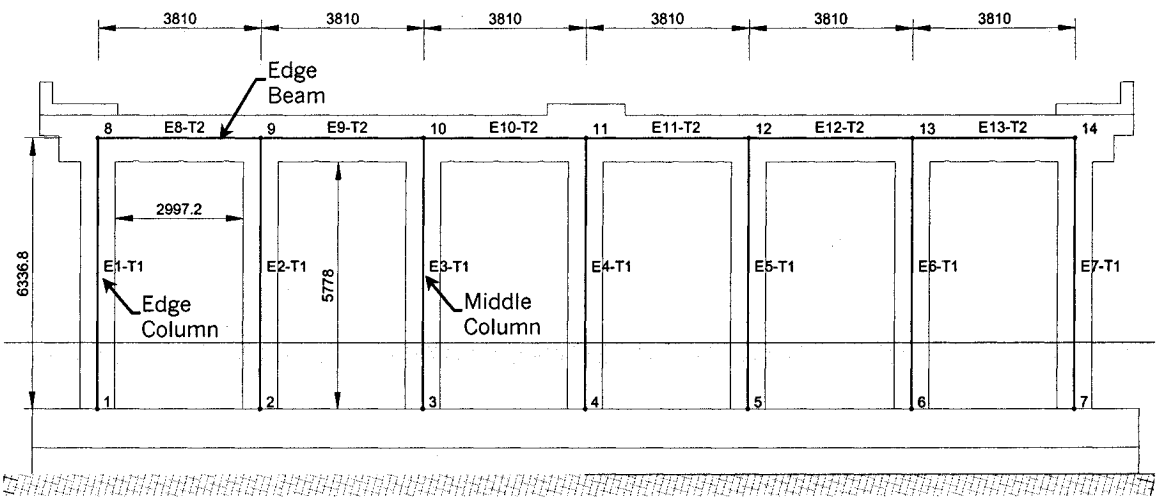

(b) Frame model

Figure 6-3 Structural idealization of main moment-resisting frame

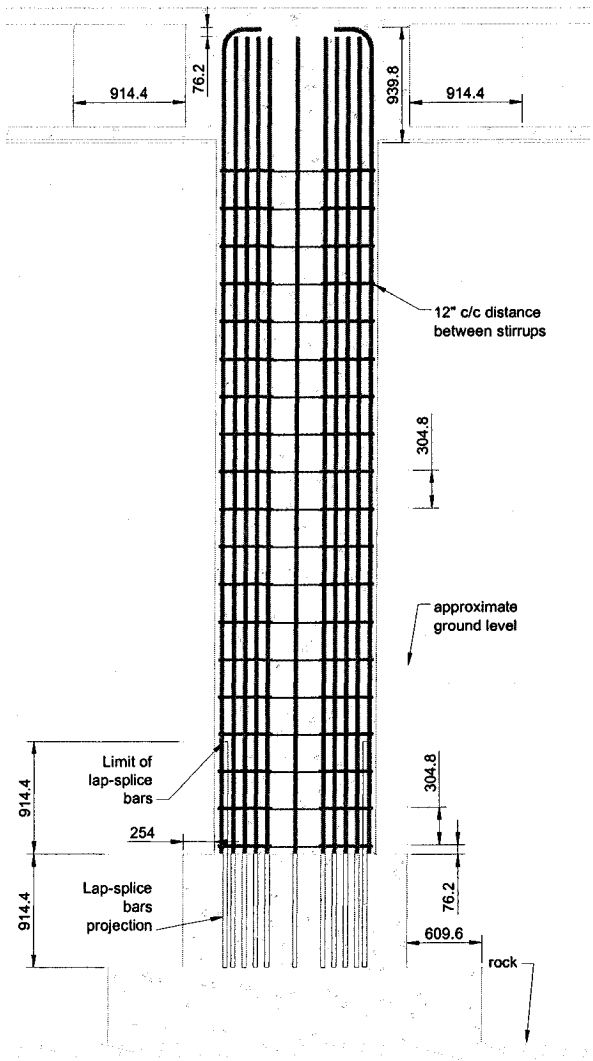

(a) Details of column elevation

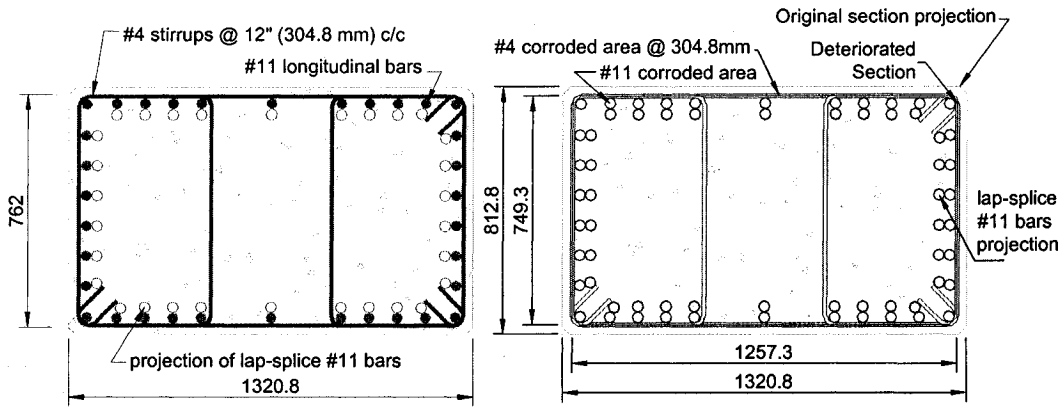

(b) Column section: unspalled and spalled – corroded cases

Figure 6-4 Details of as-built column

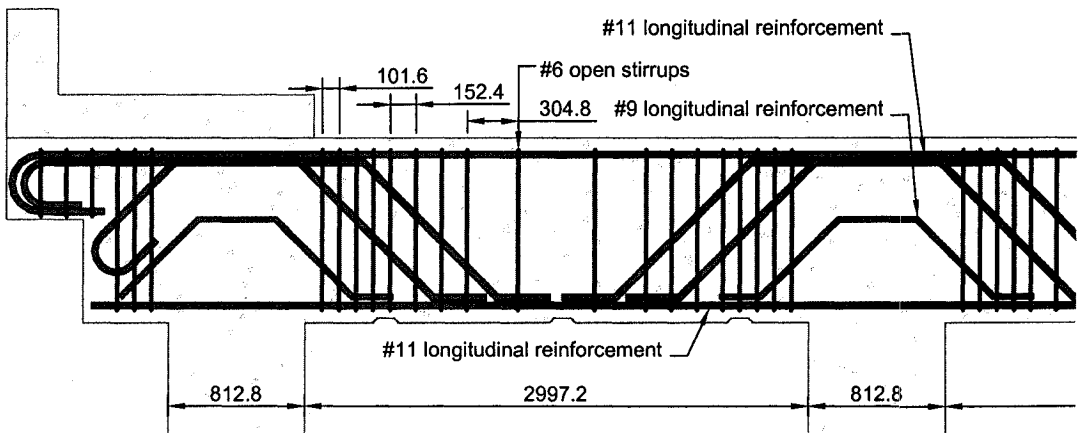

(a) Details of beam

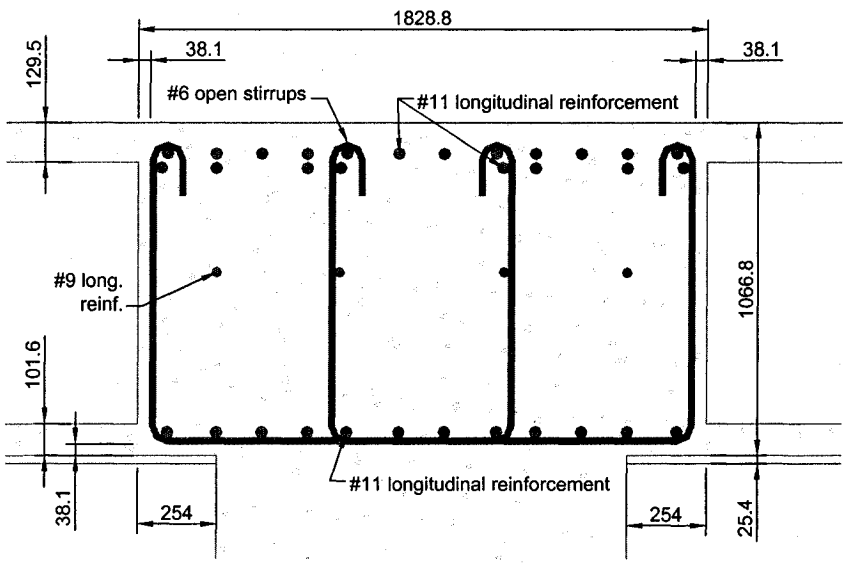

(b) Beam section

Figure 6-5 Details of as-built beam

Figure 6-6 Deterioration of one of the exterior columns

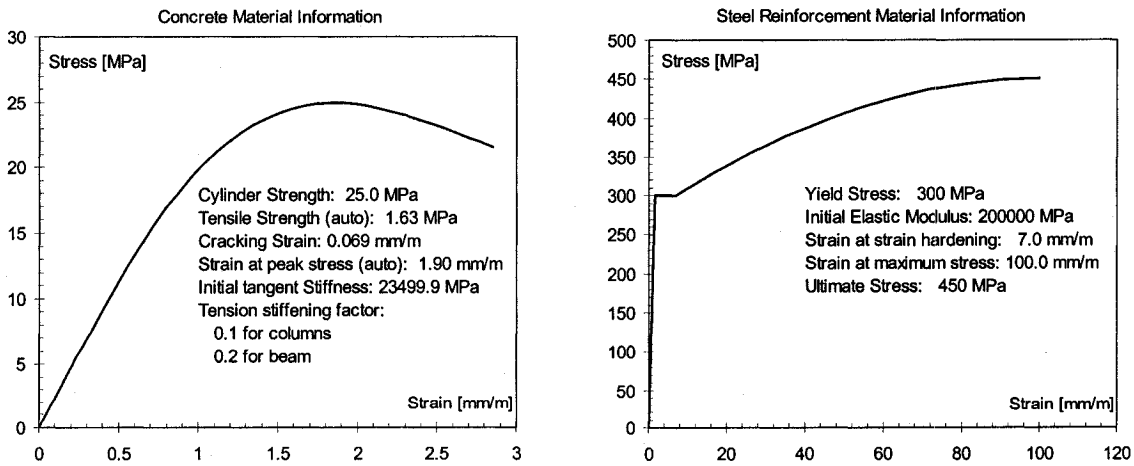

(a) Concrete (b) Steel Reinforcement

Figure 6-7 Assumed stress-strain relationships

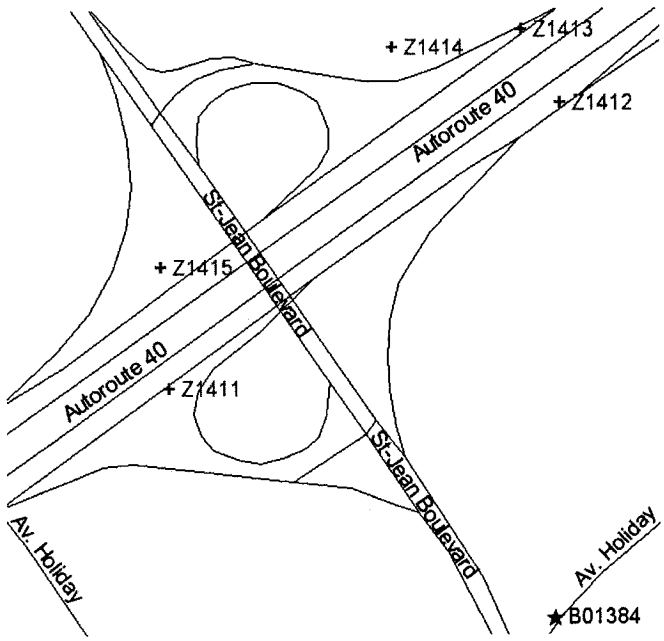

Figure 6-8 Location of GAN recordings and borehole near St-Jean overpass crossing Autoroute 40

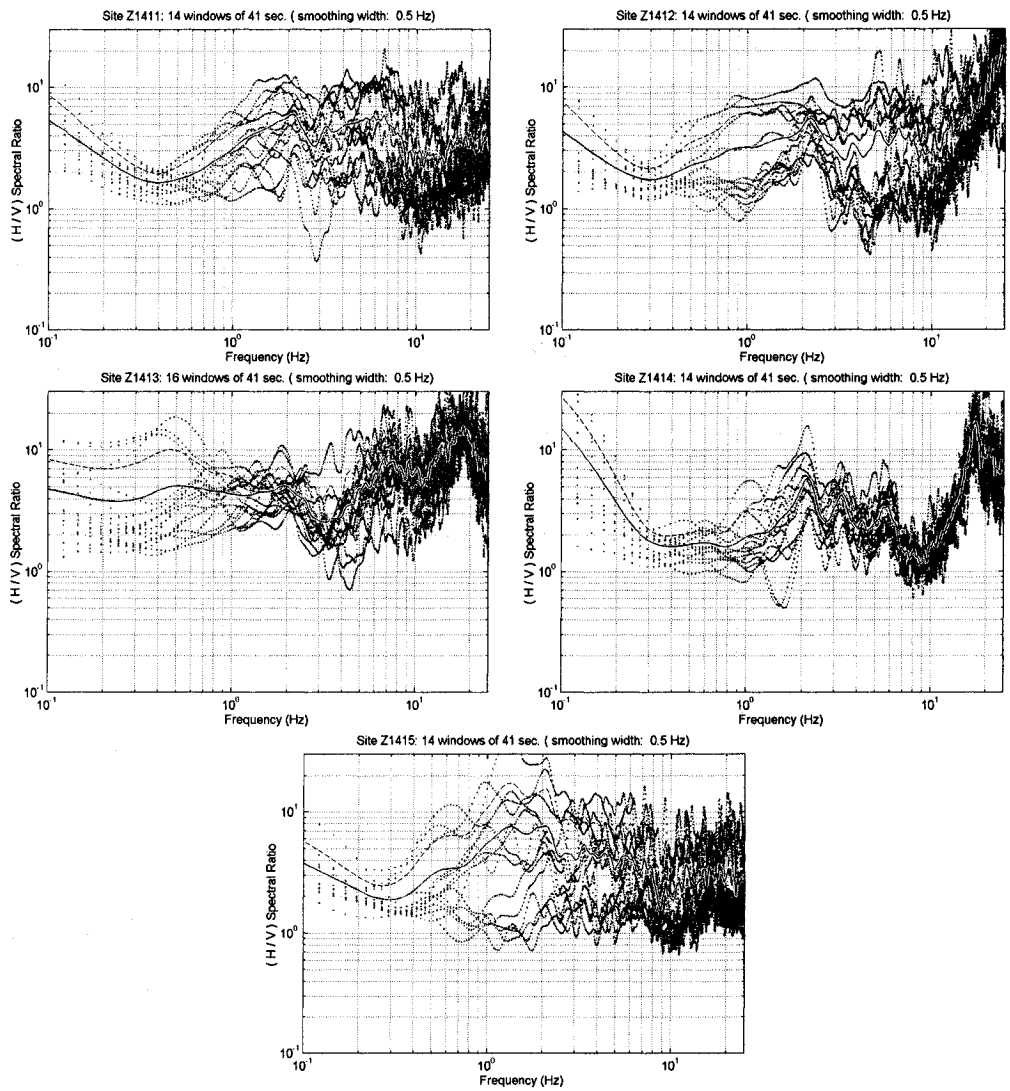

Figure 6-9 HVSR of GAN recordings near St-Jean overpass crossing Autoroute 40

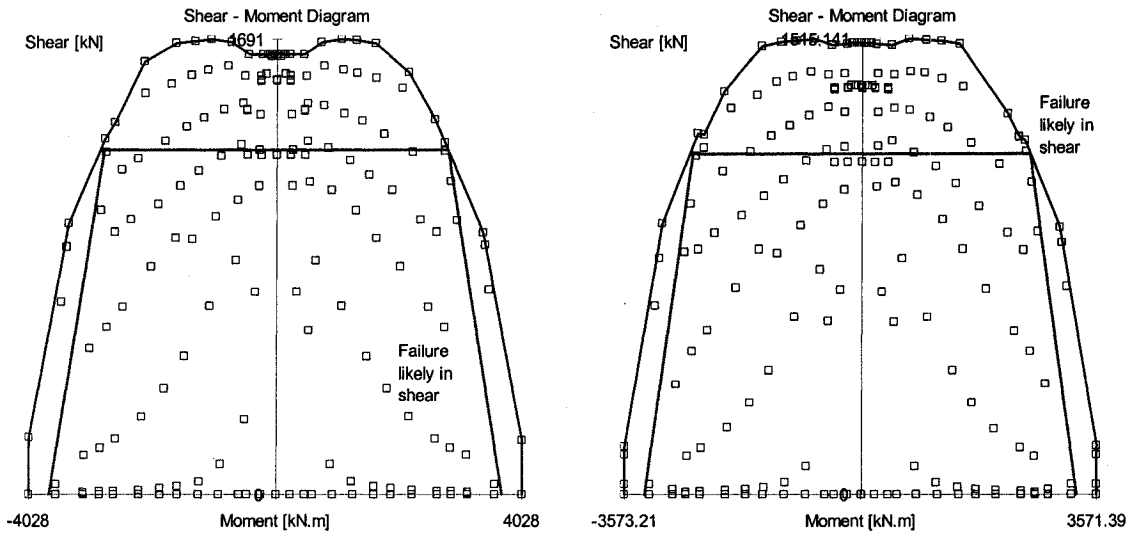

(a) Unspalled column section (b) Spalled-corroded column section

Figure 6-10 Shear-moment diagram of as-built column with different section configurations

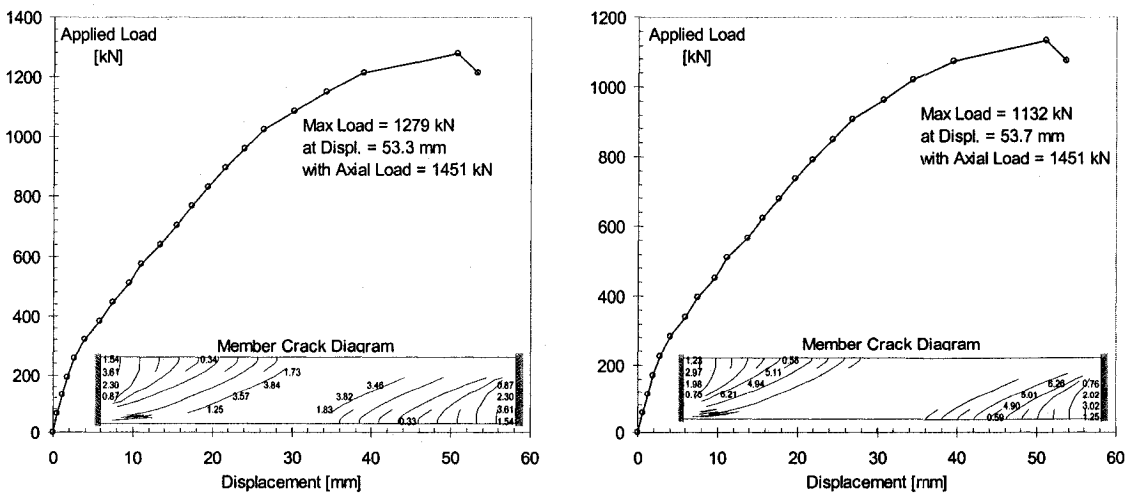

(a) Unspalled column section (b) Spalled-corroded column section

Figure 6-11 Predicted shear-displacement responses of as-built column with different section configurations

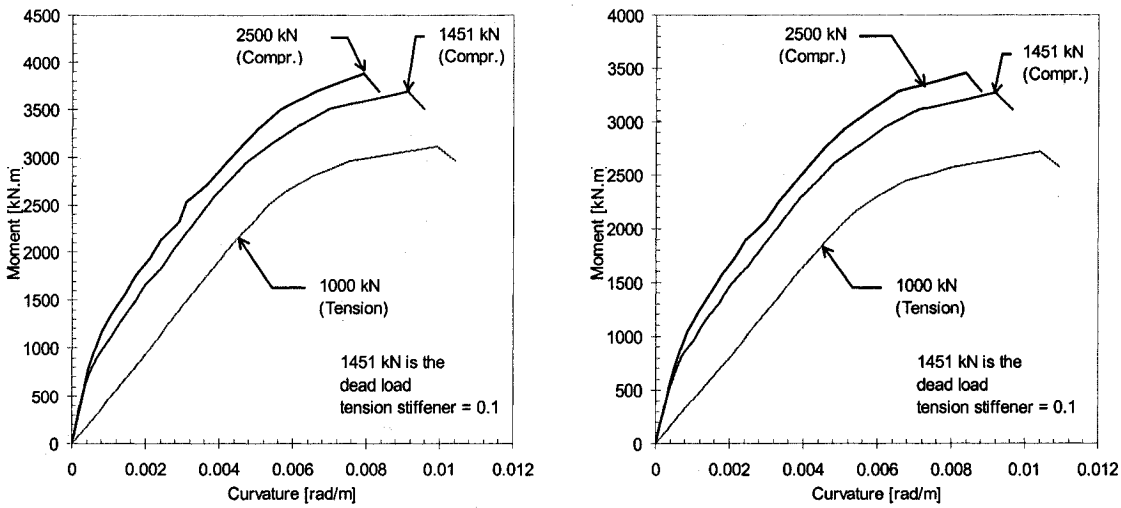

(a) Unspalled column section (b) Spalled-corroded column section

Figure 6-12 Predicted moment-curvature responses of as-built column with different section configurations

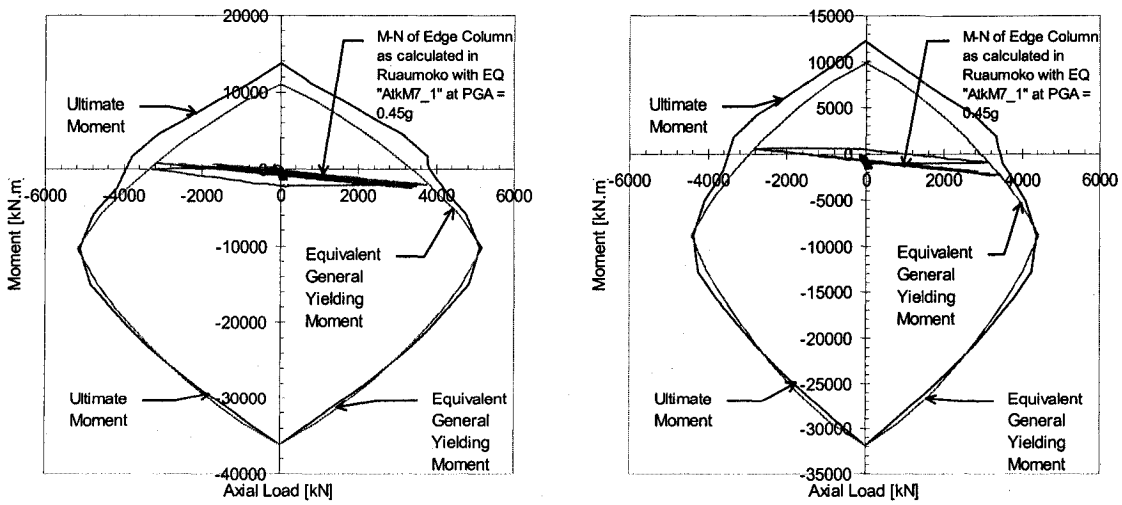

(a) Unspalled column section (b) Spalled-corroded column section

Figure 6-13 Predicted axial load - moment interaction diagrams for as-built columns with different section configurations

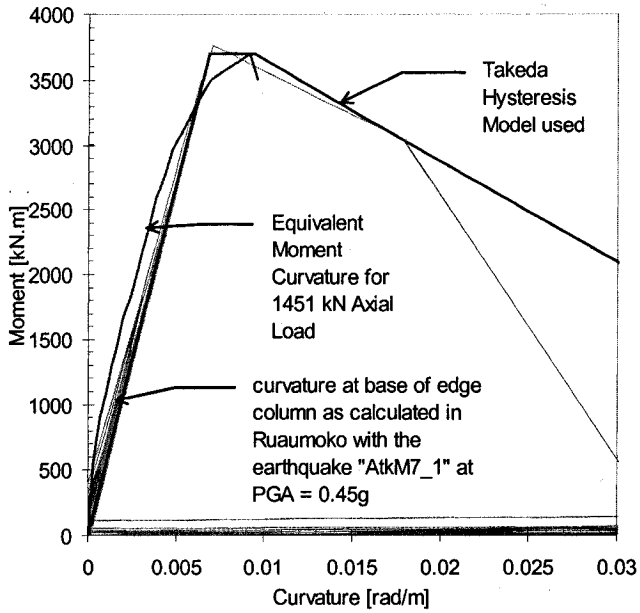

(a) Unspalled column section

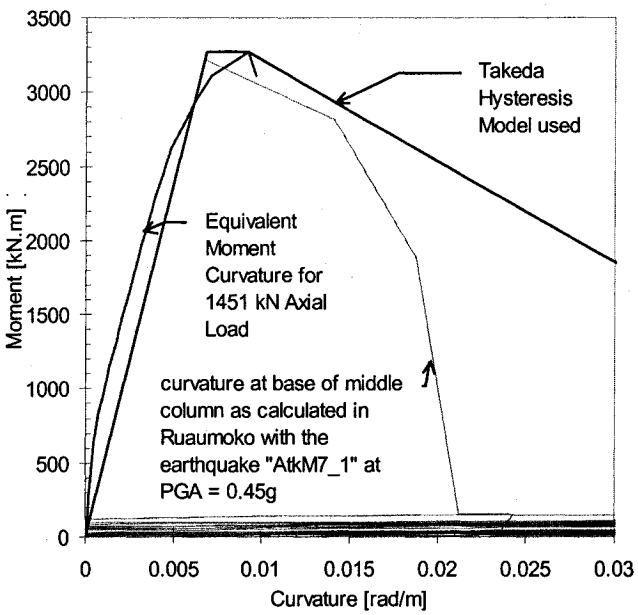

(b) Spalled-corroded column section

Figure 6-14 Envelope of hysteresis diagrams used in Ruaumoko and moment-curvature predicted using Response for column sections

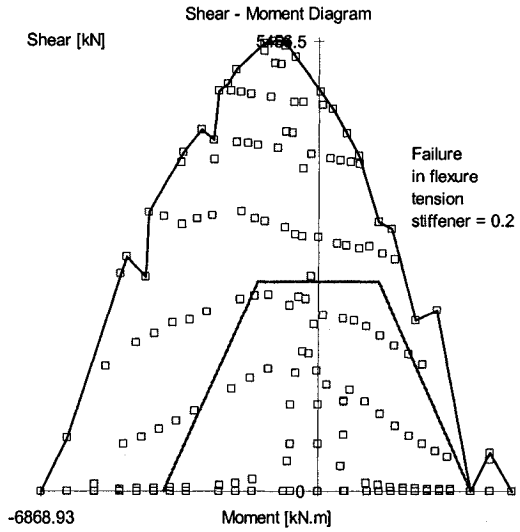

(a) Shear-moment diagram

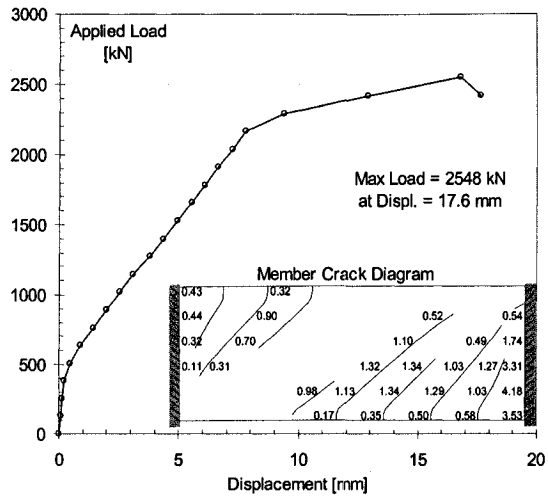

(b) Force displacement response

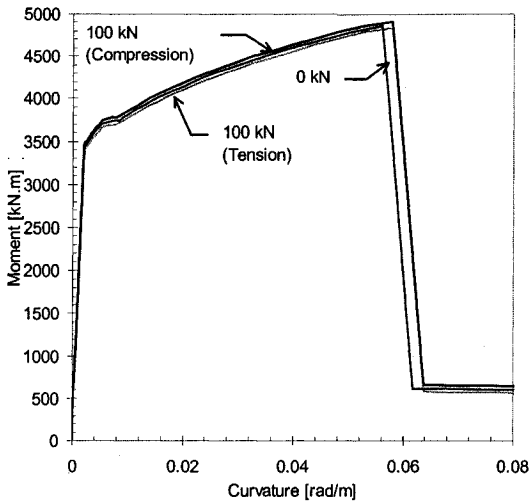

(c) Moment-curvature responses

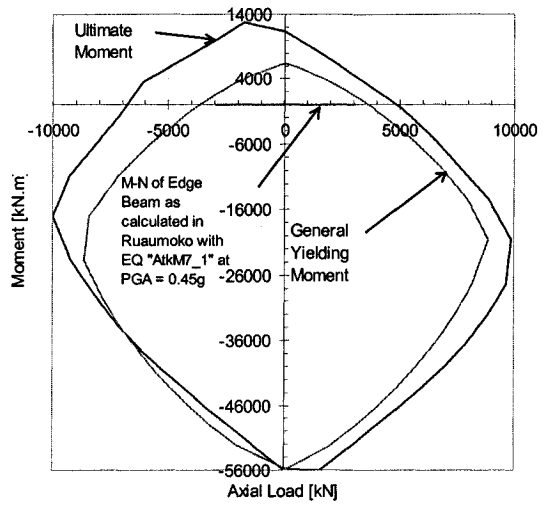

(d) Axial load-moment interaction diagram

Figure 6-15 Predicted member responses of as-built beam.

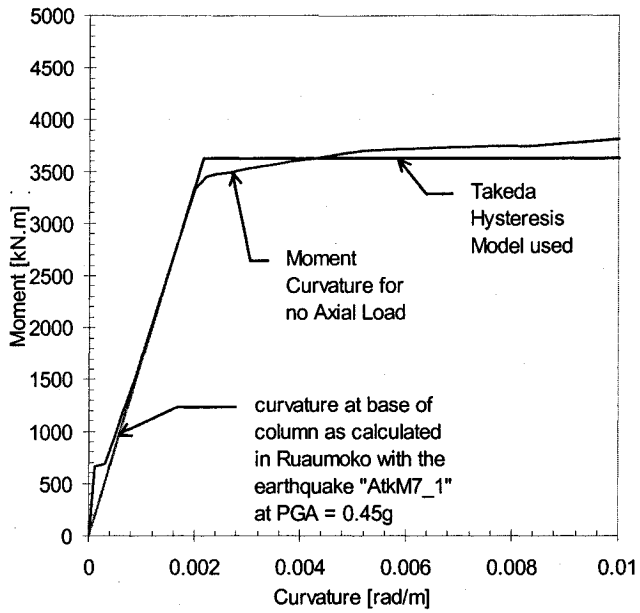

Figure 6-16 Envelope of hysteresis diagrams used in Ruaumoko and the moment-curvature from Response for the beam section

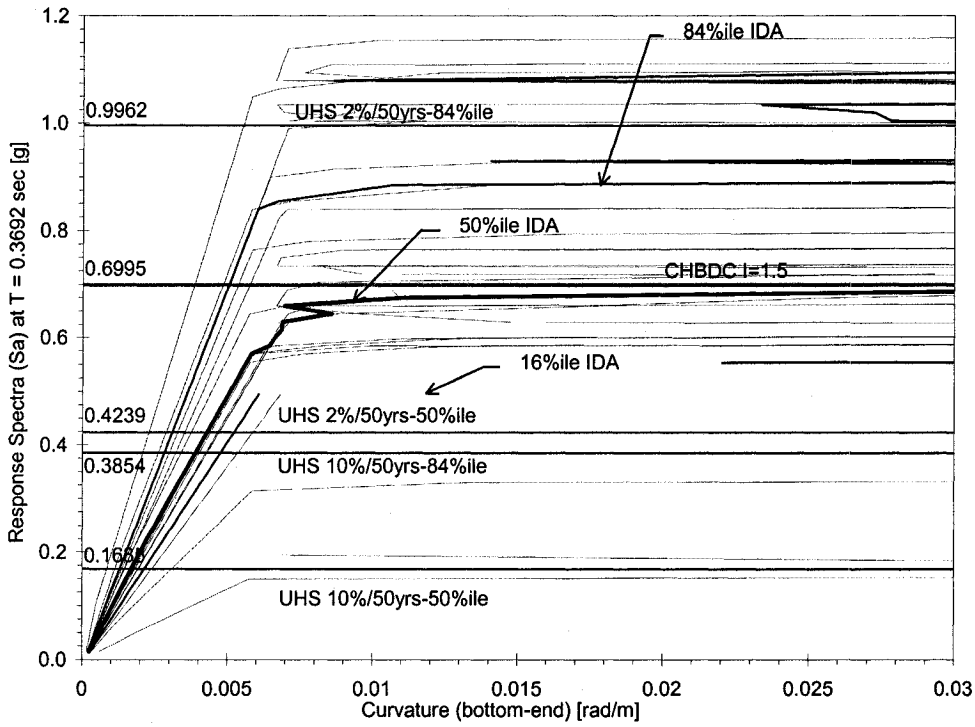

(a) Curvatures of edge column (Element 1)

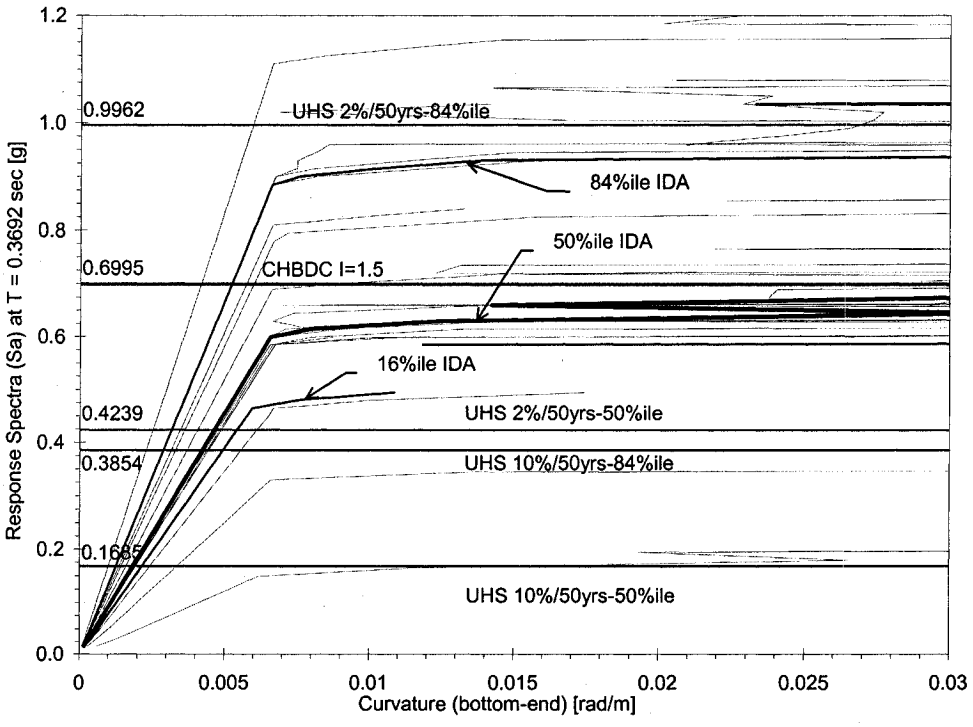

(b) Curvatures of middle column (Element 3)

Figure 6-17 Predicted IDA curvatures at bottom of columns, unspalled column case

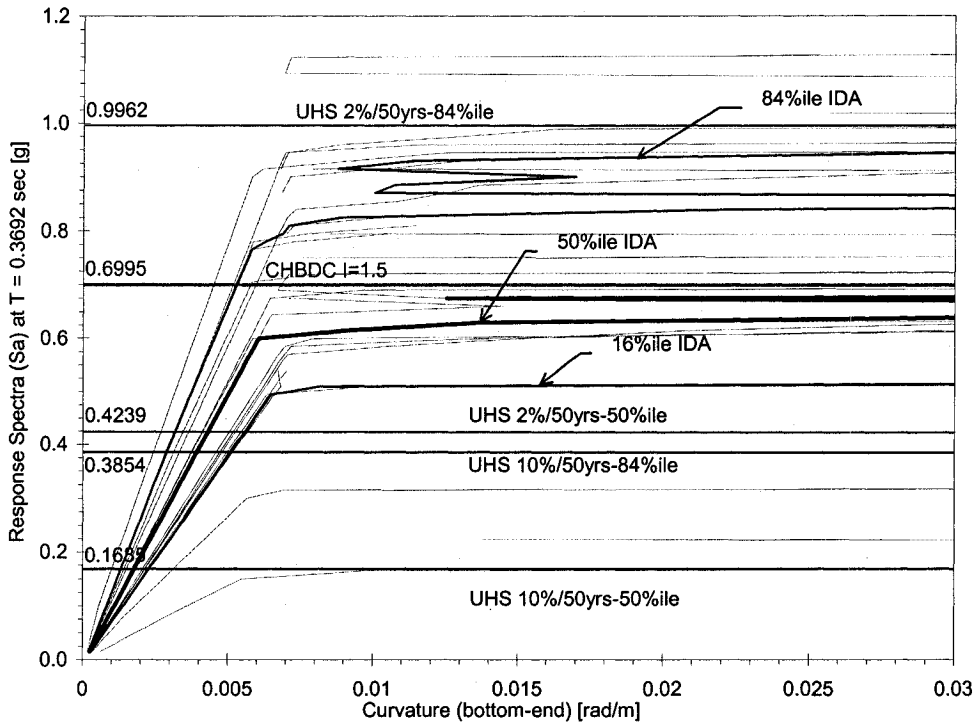

(a) Curvatures of edge column (Element 1)

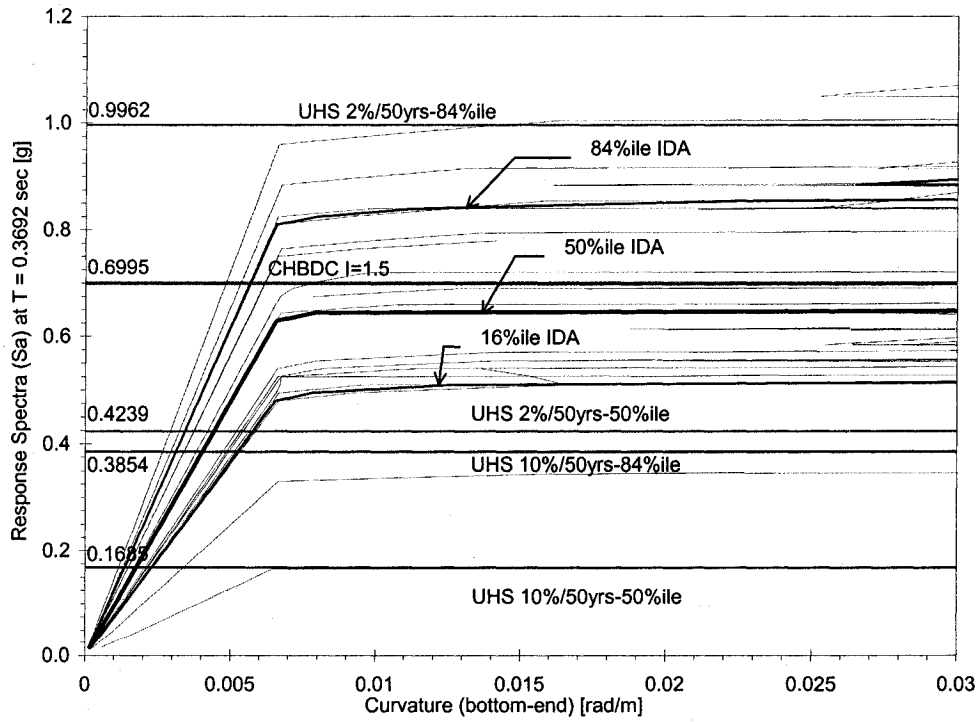

(b) Curvatures of middle column (Element 3)

Figure 6-18 Predicted IDA curvatures at bottom of columns, spalled-corroded column case

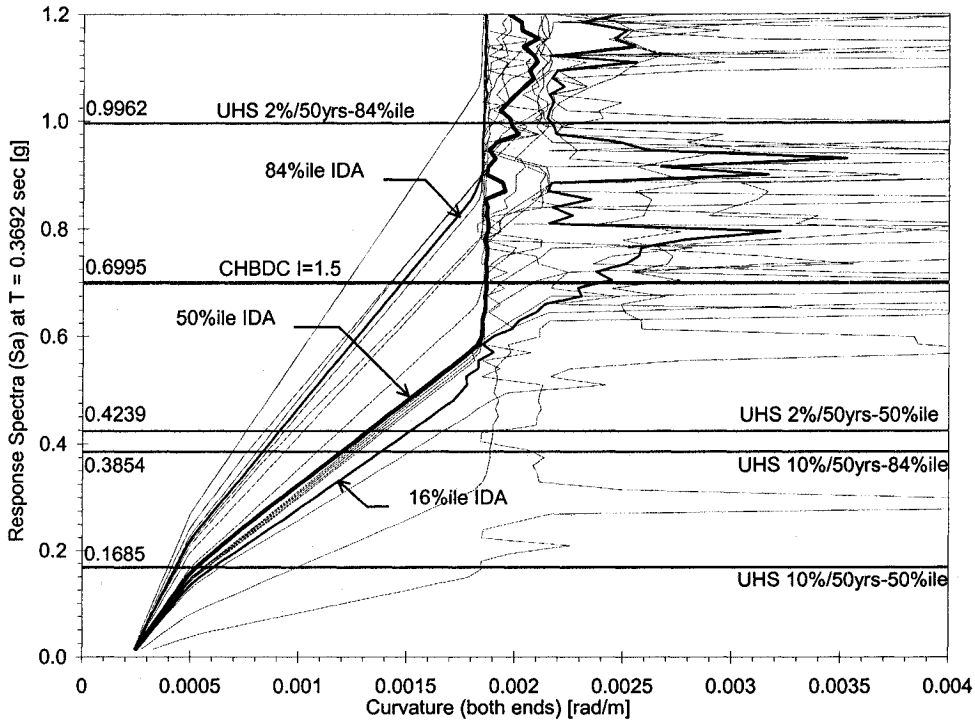

(a) Unspalled column case

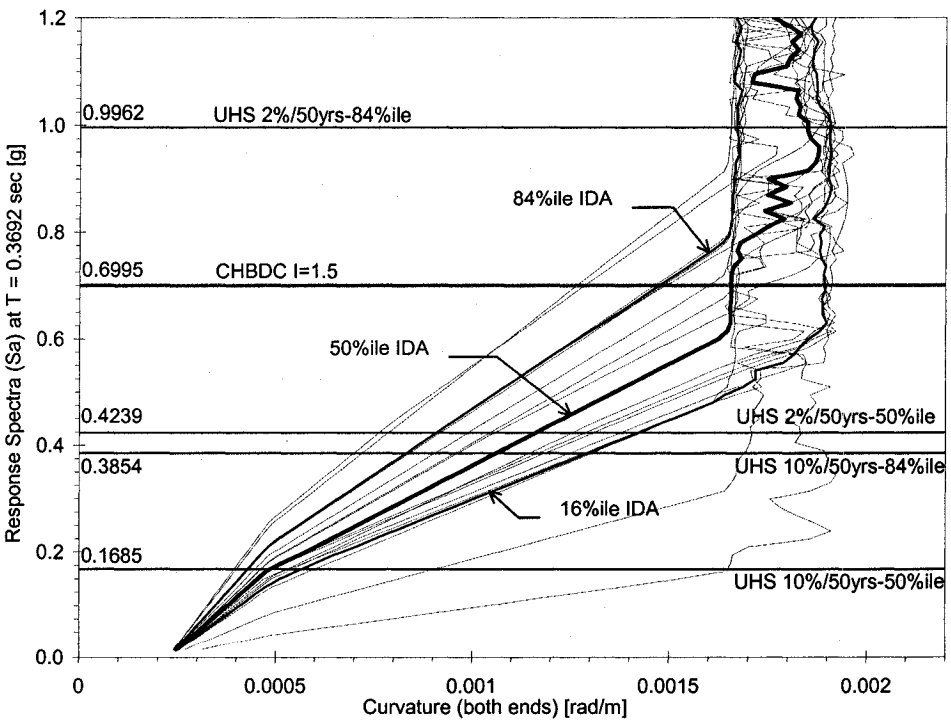

(b) Spalled-corroded column case

Figure 6-19 Predicted IDA curvatures at edge beam (Element 8) for different cases

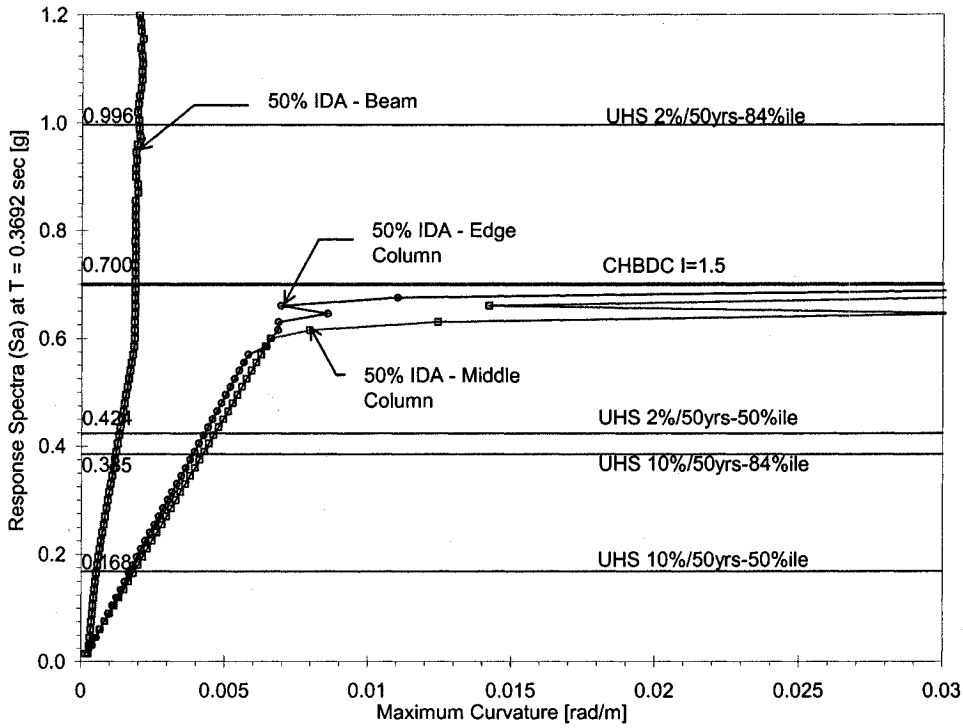

(a) Unspalled column case

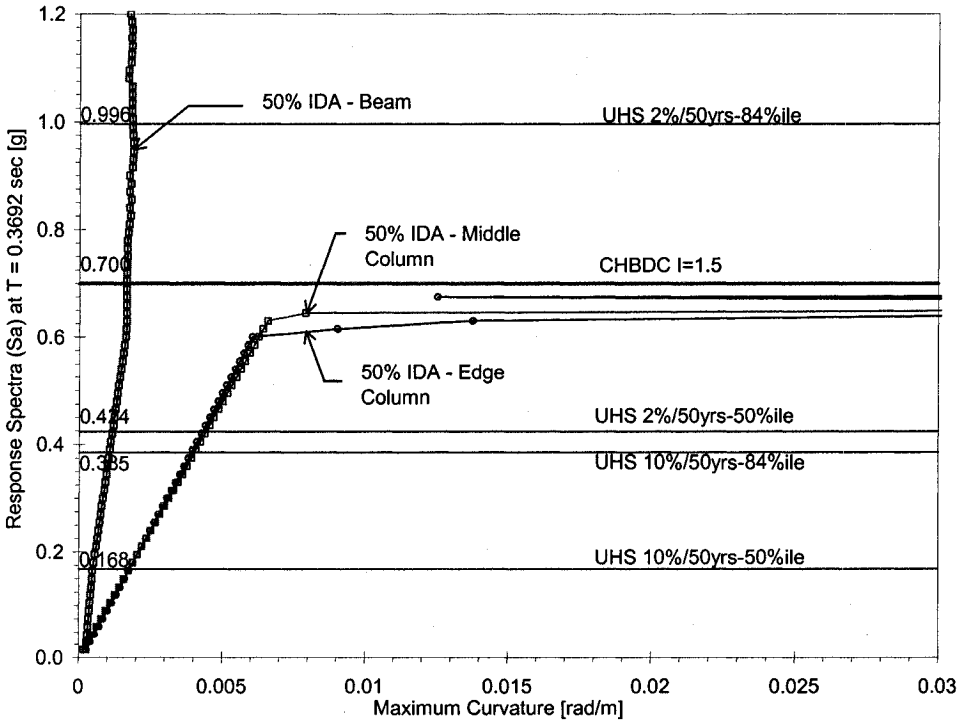

(b) Spalled-corroded column case

Figure 6-20 Predicted IDA median values of maximum curvatures for different cases (as-built)

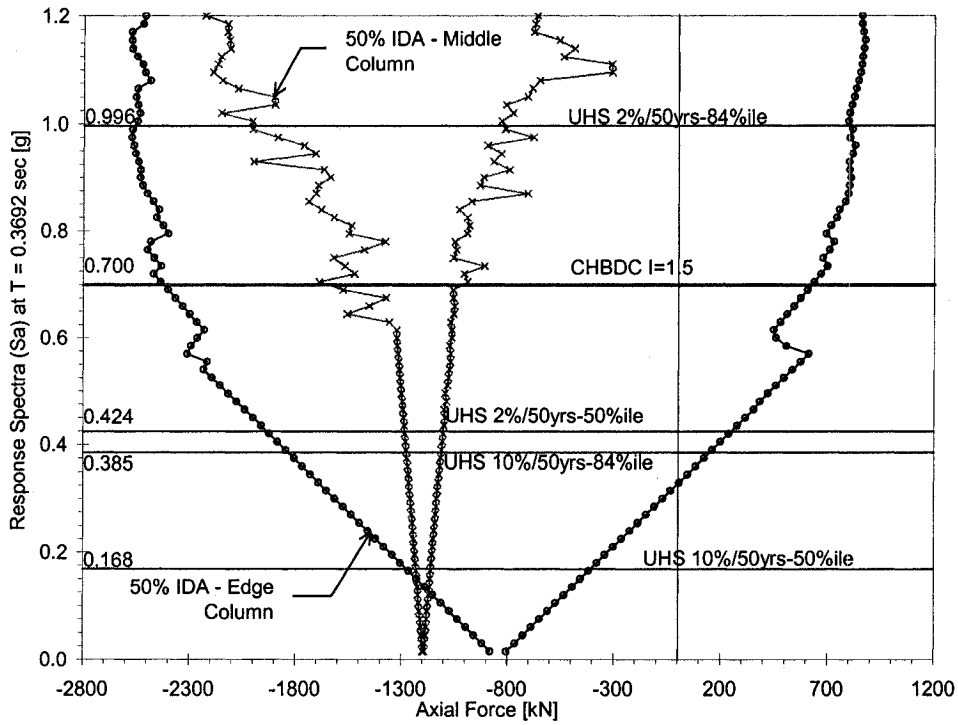

(a) Unspalled column case

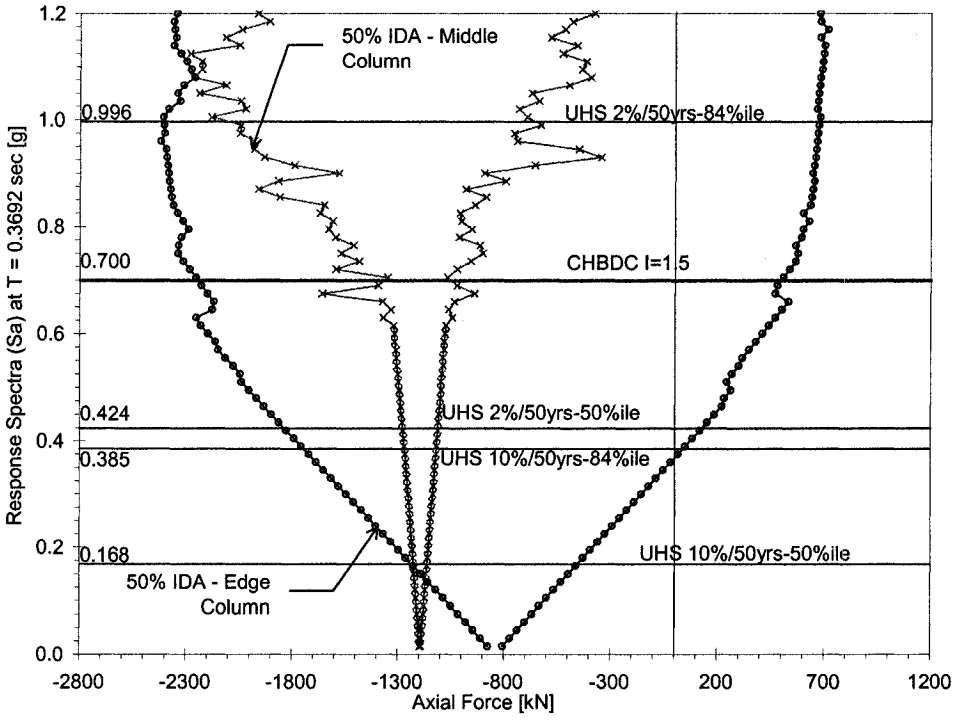

(b) Spalled corroded column case

Figure 6-21 Predicted IDA median values of axial force variation for different cases (as-built)

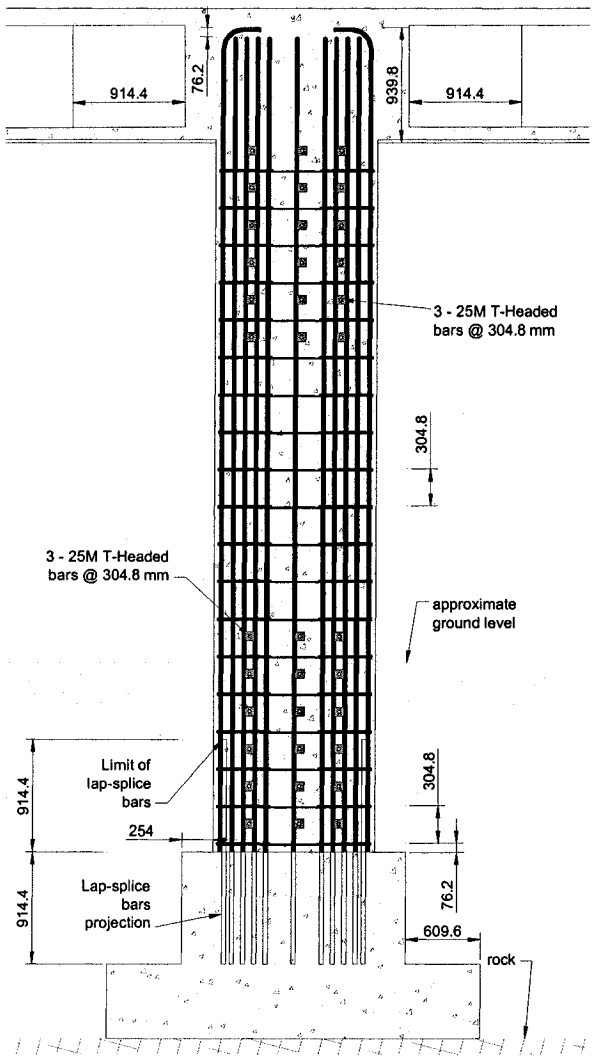

(a) Details of retrofitted column elevation

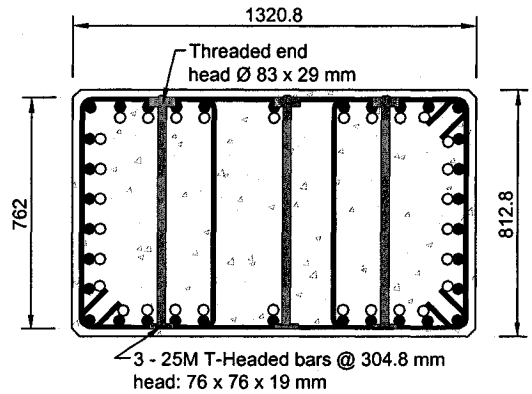

(b) Retrofitted column section

Figure 6-22 Details of column retrofitting

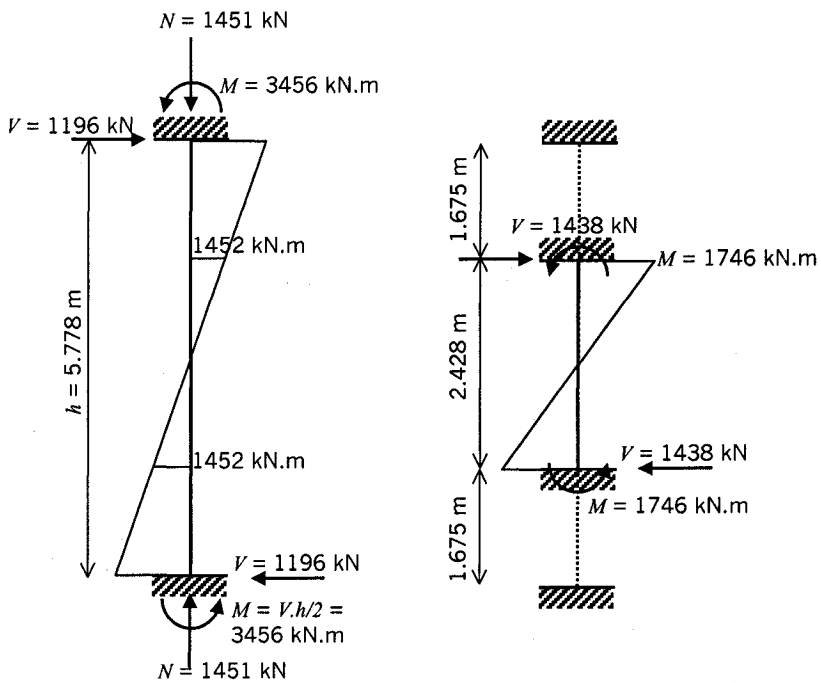

Figure 6-23 Diagrams of predicted shear forces and flexural moments on retrofitted column

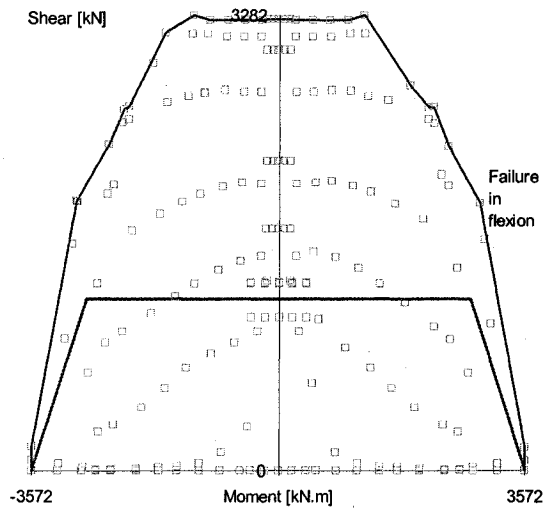

(a) Shear-moment diagram

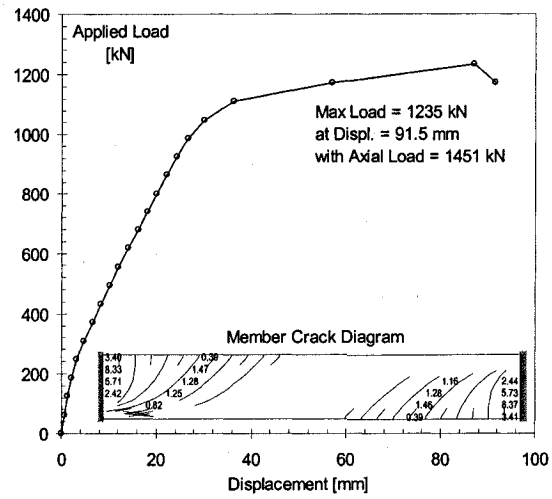

(b) Predicted shear-displacement responses

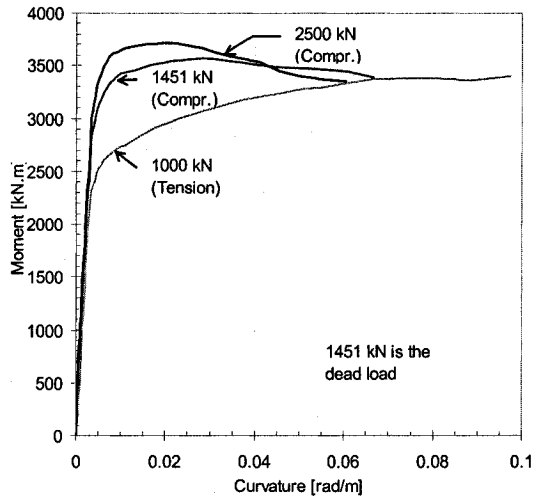

(c) Moment-curvature responses

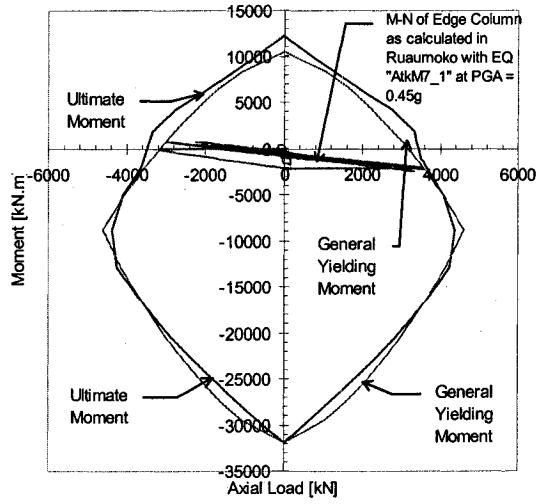

(d) Axial load-moment interaction diagram

Figure 6-24 Predicted member responses of retrofitted column

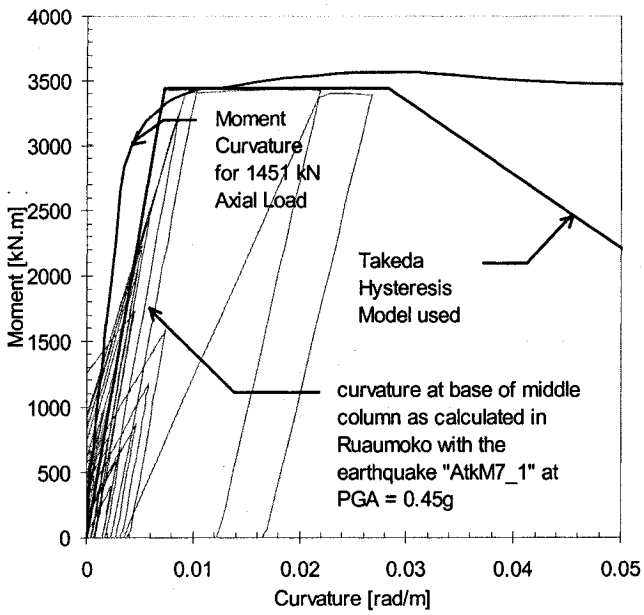

Figure 6-25 Envelope of hysteresis diagrams used in Ruaumoko and moment-curvature predicted using Response for the retrofitted column section

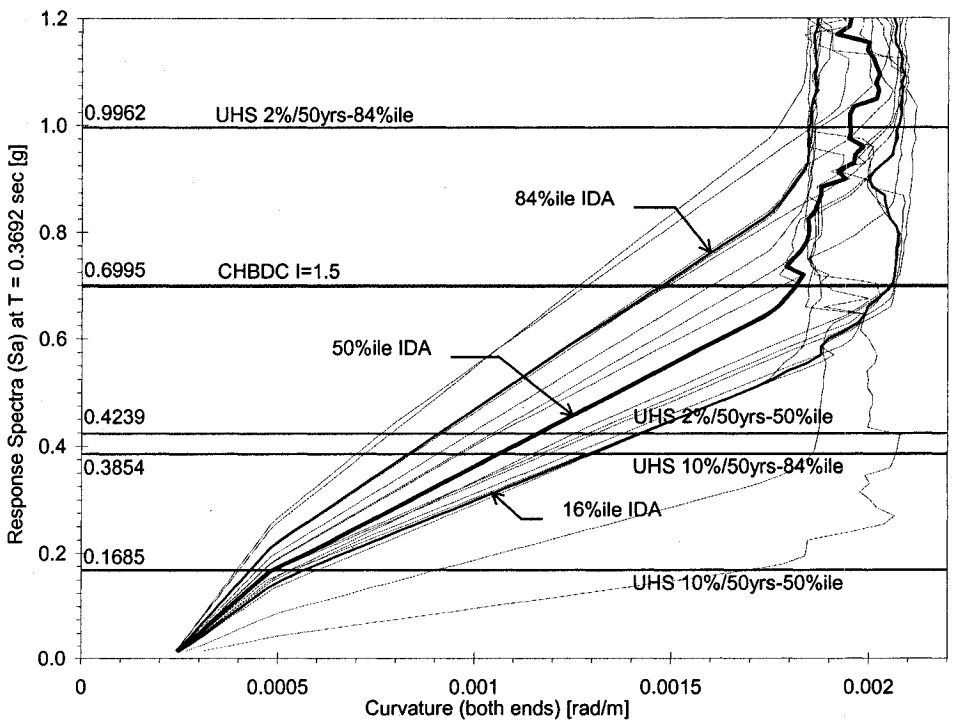

Figure 6-26 Predicted IDA curvatures at edge beam (Element 8) for the retrofitted column case

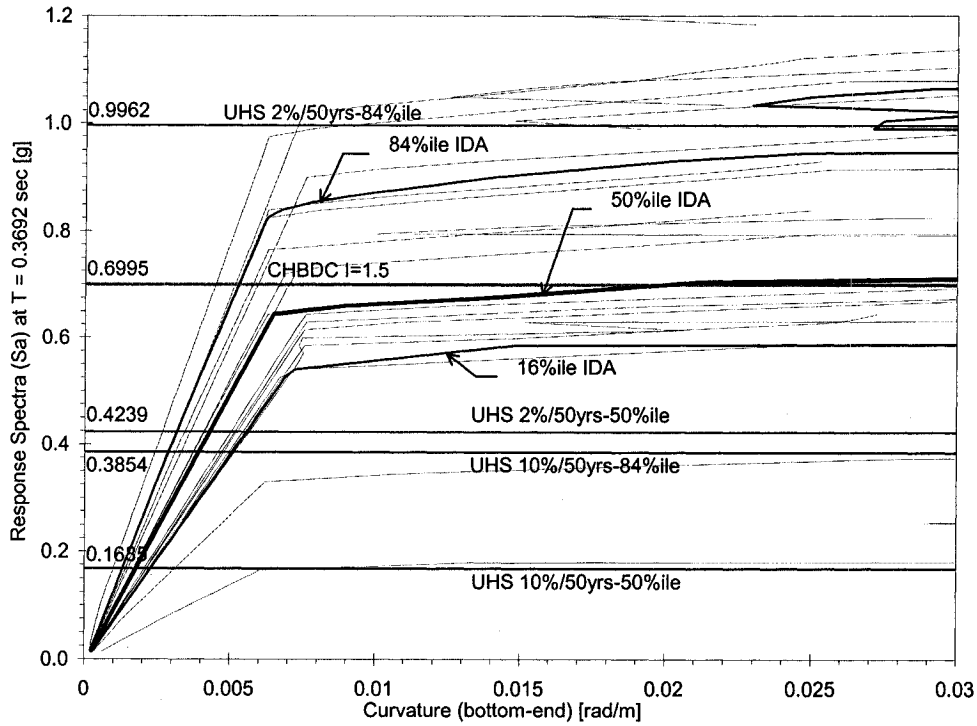

(a) Curvatures of edge column (Element 1)

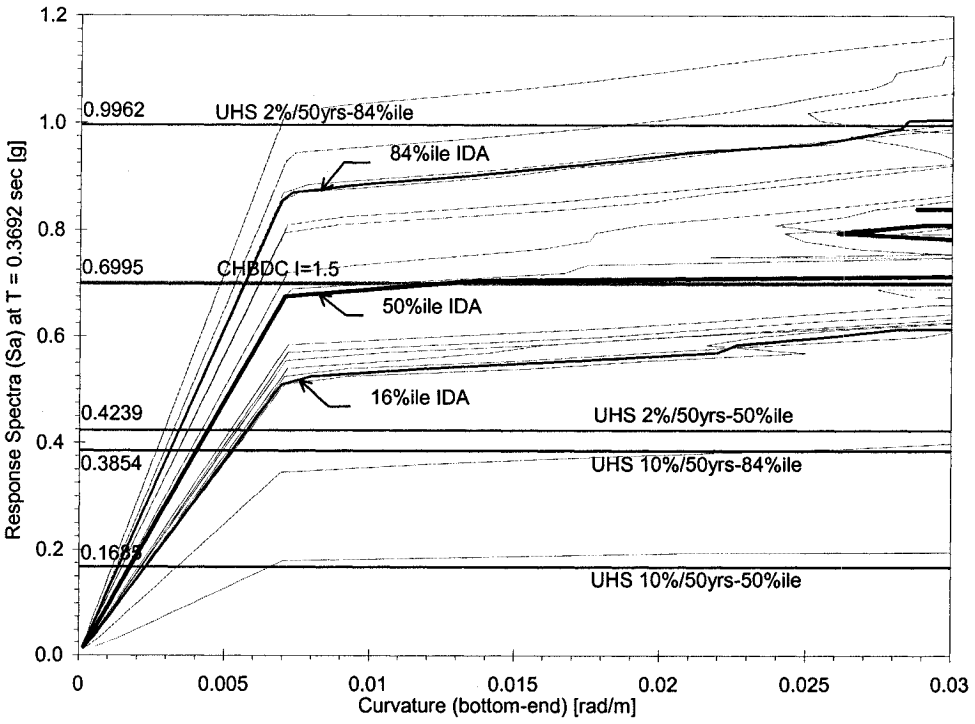

(b) Curvatures of middle column (Element 3)

Figure 6-27 Predicted IDA curvatures at bottom of columns, retrofitted column case

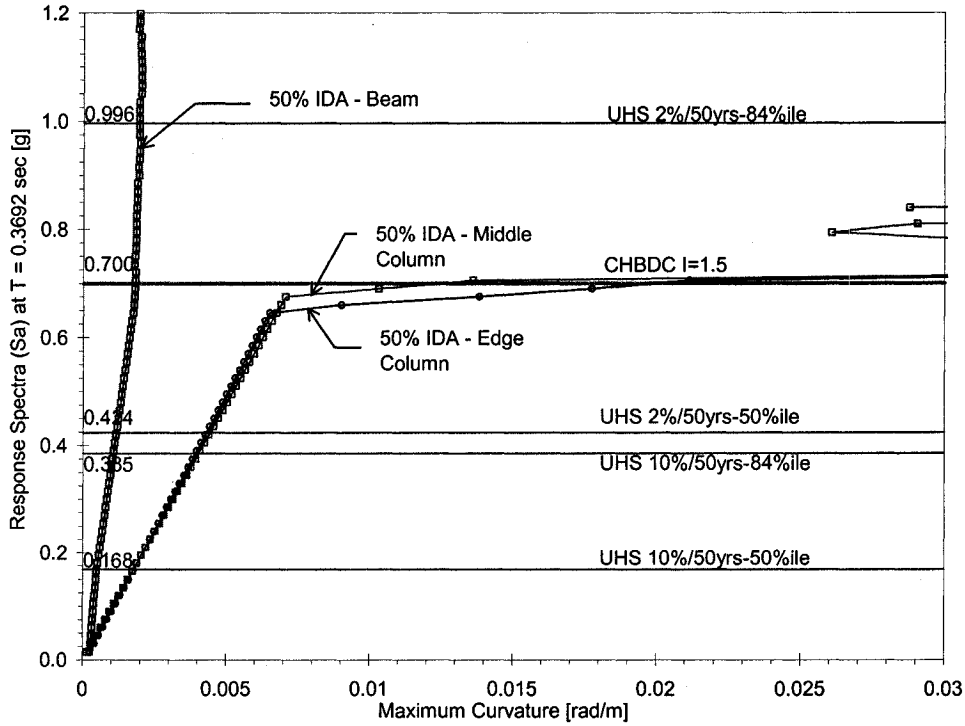

Figure 6-28 Predicted IDA median values of maximum curvatures for the retrofitted column case

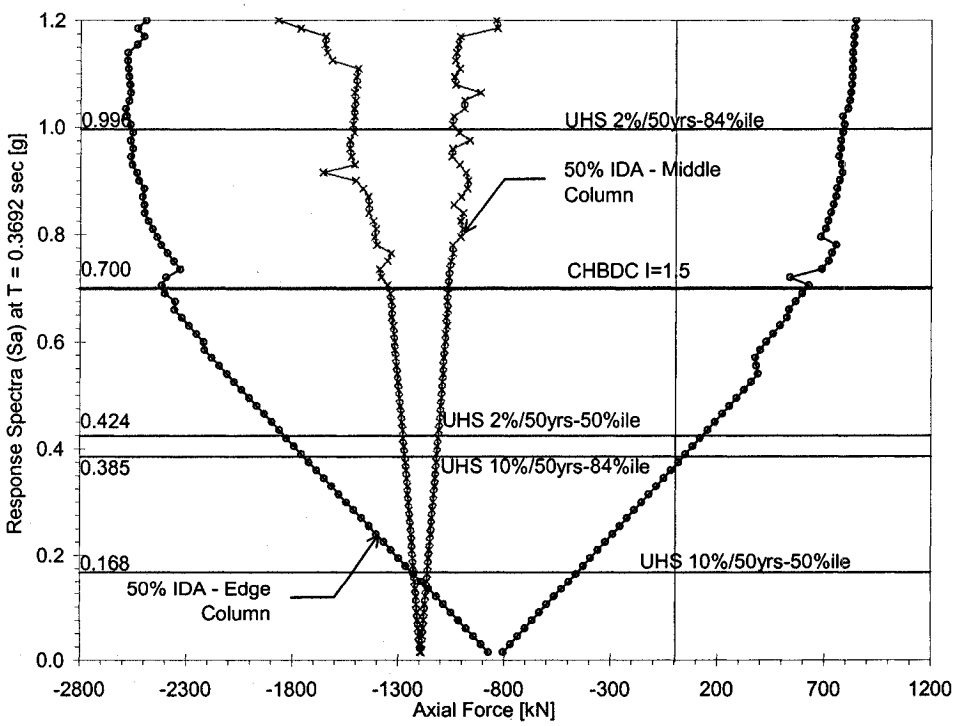

Figure 6-29 Predicted IDA median values of axial force variations for the retrofitted column case

Chapter 7

Conclusions

The two main objectives of this thesis are to:

i. Contribute to the seismic microzonation of the island of Montreal and

ii. Investigate the seismic vulnerability of representative highway overpass bridges under the provisions of the 2000 Canadian Highway Bridge Design Code

7.1 Seismic Microzonation of the island of Montreal

The predominant frequency of vibration of soils is used as the main parameter to define the seismic microzonation of the island of Montreal. The predominant frequency is determined using both a field method based on the Horizontal-to-Vertical Spectral Ratio of Ground Ambient Noise (GAN), and SHAKE analyses using borehole data.

The GAN investigations were performed based on a sampling plan that maximized the full coverage of the island while increasing the density of sampling points in areas that were identified a priori as soft soil locations. A total number of 820 records were obtained for the island of Montreal. The SHAKE analyses were performed with profile and borehole data at locations where the full soil profile was provided. A total of 1973 boreholes were used in the SHAKE analyses. The spatial coverage for the boreholes is not as uniformly distributed as for GAN results since their location often correspond to major infrastructure such as highways, sewer lines or water mains. A comparison of predominant frequency maps for both types of analyses indicates a very strong correlation, which demonstrates the good agreement between the field and numerical methods. The correlation is not as

good in areas where borehole data is sparse. This can be explained by the observation that predominant frequencies are highly variable in space and that interpolation between sparse data points may not be representative of actual conditions. The SHAKE analysis could be improved by further validating the dynamic soil properties for the typical soils encountered in the island of Montreal. In addition, more boreholes could be added over some areas in order to obtain a better spatial resolution of the seismic site response. The maps were compared qualitatively with the surface geology map of the island of Montreal and the position of ancient rivers and streams.

The correlation with the surface geology features such as ancient streams and rivers shows good correspondence in some areas such as the location of the ancient Lac à la loutre, l'Anse à l'orme and la baie de Valois. The correlation with the location of other ancient rivers and streams could not be established due to lack of data in those specific areas. Maps were obtained for both the GAN and SHAKE results by using spatial interpolation techniques. Three interpolation methods were originally investigated: Kriging, Triangulation with a linear interpolation, and Inverse distance to a power. The best results were obtained with the Triangulation with a Linear Interpolation Method.

Finally, the data from GAN and SHAKE were combined in order to increase the sample size and maximise the spatial resolution of the seismic site response with the available data. This map integrates the results from the abundant but non-uniformly distributed boreholes and the relative well distributed GAN recordings.

From this map, twelve zones of soft to medium soil, generally associated with significant seismic amplification, were identified from the contour lines for frequencies below 10 Hz. This limit was selected since it corresponds to the fundamental frequency of vibration of soils that may adversely affect structures of one or more storeys during earthquakes. Box plots of the fundamental frequencies in each zone confirm the homogeneity of the zones. These plots indicate that more than 75% of the boreholes

inside the zones have a fundamental frequency less than 10 Hz, while more than 75% of boreholes outside these zones have frequencies above 10Hz.

The ratio between the median response spectra acceleration and the acceleration from the Uniform Hazard Spectra (UHS) was calculated for the four zones with the lowest average fundamental frequency. The largest ratios were obtained in the zone located at the eastern tip of the island of Montreal where deep clay deposits are predominant. The fundamental period for the zone is in the long-range spectrum, from 0.29 to 0.74 seconds, which may match the natural periods of two or more storeys buildings.

7.2 St-Jean and Railways Overpass

The Incremental Dynamic Analysis (IDA) approach was used to study the seismic vulnerability of one of the 12-column frames of the St-Jean Blvd. overpass crossing the CN and CP railways. The frame components were studied and evaluated for three cases reflecting the condition of the concrete columns: unspalled columns, spalled columns, and spalled columns with corroded reinforcement. From the lack of transverse reinforcement in the beam, it was evident that it would fail in shear before the yielding of the beams or the columns. However, the columns were capable of reaching yielding before failing in shear. For the evaluation, yielding-moment versus axial load interaction diagrams were calculated for these elements.

In each column case, the IDA approach scaled to seventeen different earthquakes and the frame responses were compared with the spectral acceleration levels specified by the UHS and Canadian Highway Bridge Design Code (CHBDC). The analysis of the maximum curvatures and axial loads of three representative elements (edge column, middle column, and edge beam) showed that the predicted shear failure in the beam occurs at a spectral acceleration level of approximately 0.15 g. This level is much lower than that specified by the CHBDC (0.49g, $I = 1.5$) and that corresponding to the spectral

acceleration for the 2% in 50 years UHS (0.288g) for Montreal. Therefore, a retrofit strategy is required.

In deciding upon the retrofitting strategy, an approach using minimum intervention was studied. This consists of the strengthening of the concrete beam to avoid shear failure and to provide sufficient flexural resistance so that yielding occurs in the columns rather than in the beams. Additional shear reinforcement was provided in the edge beams due to the greater moment and shear demands in those beam segments.

The overall behaviour of the retrofitted frame shows clearly the beams do not suffer any shear distress or any flexural yielding. The columns of the retrofitted frame can sustain higher levels of spectral acceleration before starting to yield. The retrofit of the beam completely changes the performance of the frame. The as-built frame suffers a brittle shear failure at a predicted spectral acceleration of 0.15 g whereas the retrofitted frame is predicted to experience general yielding of the columns at 0.35 g, with the ability to undergo spectral accelerations in excess of 0.8 g.

Although the localized spalling and corrosion of some of the column ties should be addressed with corrective measures, this study indicates that this minimal deterioration has not significantly affected the expected seismic performance.

7.3 St-Jean and Autoroute 40 Overpass

The Incremental Dynamic Analysis technique was used to evaluate the seven-column main moment resisting frame of one of the two span structures of the St Jean Blvd. overpass crossing Autoroute 40. Two different cases that represent possible conditions for the columns were studied: unspalled columns, spalled columns with corroded reinforcement. In a similar fashion to the previous overpass, the frame was subjected to a wide range of earthquakes and scale factors as part of the IDA technique, to

evaluate and compare the response with the spectral acceleration levels specified by the CHBDC and UHS for Montreal.

An early shear failure, due to insufficient shear reinforcement, was predicted in the column before any flexural yielding. An equivalent yielding moment versus axial load interaction diagram was calculated for the expected range of axial load on the columns. A similar diagram was developed for the beam, but in this case, the beam was predicted to yield in flexure without failing in shear.

The analysis of the maximum curvatures and axial loads of three representative elements (edge column, middle column, and edge beam) retrieved during the IDA showed that the predicted shear failure of the columns dominates the behaviour of the frame occurring at a spectral acceleration level of approximately 0.60 g. This value is lower than the spectral acceleration level of the CHBDC (0.70 g), even for an emergency route bridge (I = 1.5). However, it is higher than the level that corresponds to the 2% in 50 years (50th percentile) of the Uniform Hazard Spectra for Montreal (0.424 g).

An approach using minimum intervention was studied as part of the retrofitting strategy. This involves the introduction of additional shear reinforcement in the form of T-headed bars in the concrete columns to avoid shear failure. The columns would experience flexural yielding before any flexural yielding or shear distress in the beams. The retrofitted frame can sustain higher levels of spectral acceleration (0.65 g) before the columns start to yield, resulting in the frame being able to undergo spectral acceleration levels above 0.8g.

Similarly to the previous study, although the localized spalling and corrosion of some of the column ties should be addressed with corrective measures, this study indicates that this minimal deterioration has not significantly affected the expected seismic performance.

7.4 Future Research

On the topic of the seismic microzonation of Montreal, suggestions for future research are given below:

- In order to improve the results of numerical modeling of boreholes, more research is necessary to accurately determine soil properties used in computer program SHAKE for at least the most common soil types present in Montreal. The suggested minimum list of soil properties is: curves of percentage of damping versus strain; curves of shear modulus versus strain; unit weight versus depth; and maximum shear wave velocity versus depth. The latter two are accompanied by a more detailed representation of the borehole layers in the form of more sub layers.
- In order to better correlate the results between the field method and the numerical method, more Ground Ambient Noise (GAN) recordings must be made on top or very close to existing boreholes, having more extensive soil property data. Additionally, the interpolation grids from the two data sets can be compared with the used of more advanced geo statistical methods.
- In order to decrease the sparseness of data points, more boreholes and GAN recordings are required, preferable one close to another to validate the results. In addition, with the advent of more reliable data, better mapping techniques must be investigated to correctly interpolate the desired microzonation parameters.

On the topic of the analysis the seismic vulnerability of overpasses, the following suggestions are given:

- The continuous increase in affordable computer power makes it attractive to extend the use of techniques such as the Incremental Dynamic Analysis (IDA) to larger structures. In addition, improvements can be made to integrate programs such as Ruaumoko and Response 2000 (or another behavioural analysis program) to better model the non-linear behaviour, in the form of hysteresis rules for concrete frame elements.

However, even for modern computers, the IDA for large non-linear models of structures can take a large amount of time and resources. It is recommended, if that research path is pursued, that special code be developed to optimize the memory and CPU usage.

- Although the influence of corrosion on the overall behaviour of the overpasses has been accounted for in the form of a reduced steel area, more research is required in order to assess the real extent of the corrosion in the reinforcement, and hence its influence on the behaviour of the bridges.

- The concrete compressive strengths for the existing overpasses were estimated as a function of standard practise at the time of construction in accordance with the Canadian Highway Bridge Design Code. More research is necessary to verify these estimations. This can be accomplished by core sampling of the concrete in the existing structure.

- The best evidence to the feasibility of a retrofitting solution is through experimentation. Laboratory testing of scaled portions of the overpasses' retrofitted frames can be carried out to verify results and to suggest other retrofitting approaches.

Appendix A – Excel Shake

Excel-Shake is a spreadsheet application created to help to the execution of SHAKE91 under user-specified circumstances. The use of some intermediate worksheets and macros allow Excel-Shake to manage a large database of sites where the predominant frequency, outcrop acceleration, amplification factor, and other parameters are of interest. The main advantage of this approach is, when using open Visual Basic code on the macros, it allows the user to modify the spreadsheet and the macros to meet the needs of a specific project where hundreds of boreholes are involved.

The source code of the macros and a extensive description of the use of each worksheet can be found in the user manual (De la Puente and Rosset, 2002).

A.1 SHAKE and site effects

It is widely know that soft soil deposits may amplify the effects of earthquakes. In general, the ground motions of soft soil deposit sites are larger than those of nearby rock outcrops. *SHAKE91* is a computer program for conducting equivalent linear seismic response analyses of horizontally layered soil deposits, created by I.M. Idriss and Joseph I. Sun in 1992 (Idriss and Sun, 1992). This program is the modification of the original *SHAKE* program, published by Per Schnabel, John Lysmer and H. Bolton Seed in 1972 (Schnabel *et al*, 1972).

SHAKE idealizes the soil profile as a system of homogeneous, viscous-elastic layers of infinite horizontal extent. The response of the system is calculated considering vertically propagating shear waves (Idriss and Sun, 1992). The algorithm, based on the wave-equation solution is explained in Chapter 2. *SHAKE91* accounts for the non-linearity of the soil by using an iterative equivalent linear analysis procedure to obtain values for the

modulus and damping in each layer based on the shear strain (Idriss and Sun, 1992). Each layer requires a set of properties to be assigned (maximum shear wave velocity, initial damping, and unit weight), in addition to the non-linear shear modulus and damping ratio versus shear strain. The information of a single borehole can be summarized in layers each with only five parameters: soil thickness, soil type, soil unit weight, initial damping, and maximum shear wave velocity, while additional properties such as shear modulus and damping versus strain can be specified separately.

SHAKE in its original form performs a complete analysis for one site at a time. Since around 2000 boreholes had to be analyzed, each of them with seventeen different earthquakes records (making a potential 34000 computations), it was obvious that another approach was needed. Hence *Excel-Shake* was developed.

A.2 Description of Excel-Shake

Excel-Shake, a workbook application in *Microsoft Excel* ®, uses Visual Basic macros to create input files and to read the output files after the execution of *SHAKE* has been completed. The screenshots of the most important worksheets are shown in Figure A-1.

The main characteristics of *Excel-Shake* are:

- Up to ten soil layers per borehole (including the bedrock) can be stored in the database. More layers can be added after modification of certain parts of the application.
- The transfer function and the response spectra of each site subjected to a particular earthquake can be saved in their respective text files for further analysis.
- Up to 31 earthquakes can be used in the earthquake database.
- The maximum number of type of soils with different dynamic soil properties is eight, including the bedrock layer.
- Up to eleven points can be used to define the strain and damping curves.

- Graphical representations of the response spectra, acceleration at outcrop and bedrock levels, as well as the transfer function (amplification spectra) can be plotted.

A.3 Flow diagram of Excel-Shake

The procedure followed by *Excel-Shake* when processing, in batch mode, the borehole database for all the earthquakes of the list is illustrated in Figure A-2. In each execution, *SHAKE91* produces two output result files: one mainly containing general information such as fundamental frequency and amplification factors, and the other that includes mainly the response spectra and outcrop acceleration. *Excel-Shake*, in batch mode, collects the results (fundamental frequency, amplification factor, maximum outcrop acceleration, response spectra 5% damping, and amplification spectra) and saves them in the results sheet or, for the case of the spectra, in specific text files, one per each earthquake employed. The process is repeated until all the boreholes in the database have been analyzed before selecting a new earthquake.

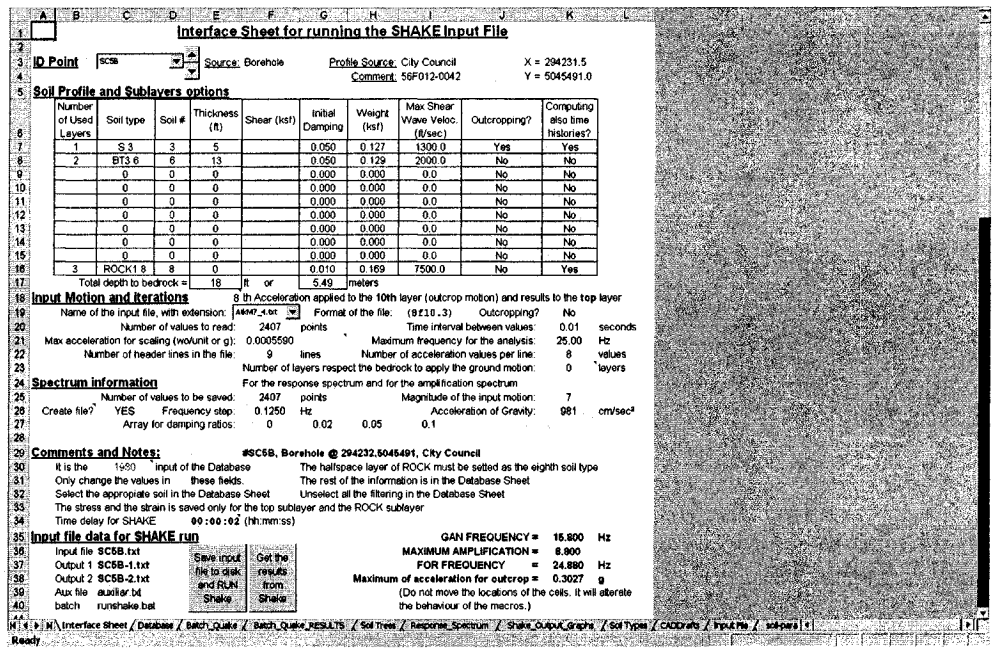

Interface Sheet for running the SHAKE Input File

ID Point: SC5B — Source: Borehole — Profile Source: City Council — Comment: 56F012-0042 — X = 294231.5 — Y = 5045491.0

Soil Profile and Sublayers options

Number of Used Layers	Soil type	Soil #	Thickness (ft)	Shear (ksf)	Initial Damping	Weight (ksf)	Max Shear Wave Veloc. (ft/sec)	Outcropping?	Computing also time histories?
1	S 3	3	5		0.050	0.127	1300.0	Yes	Yes
2	BT3.6	6	13		0.050	0.129	2000.0	No	No
	0	0	0		0.000	0.000	0.0	No	No
	0	0	0		0.000	0.000	0.0	No	No
	0	0	0		0.000	0.000	0.0	No	No
	0	0	0		0.000	0.000	0.0	No	No
	0	0	0		0.000	0.000	0.0	No	No
	0	0	0		0.000	0.000	0.0	No	No
	0	0	0		0.000	0.000	0.0	No	No
3	ROCK1.8	8	0		0.010	0.169	7500.0	No	Yes
Total depth to bedrock =			18	ft or	5.49	meters			

Input Motion and iterations — 8 th Acceleration applied to the 10th layer (outcrop motion) and results to the top layer

Name of the input file, with extension: A6k47_4.txt — Format of the file: (9f10.3) — Outcropping? No

Number of values to read: 2407 points — Time interval between values: 0.01 seconds

Max acceleration for scaling (wo/unit or g): 0.0005590 — Maximum frequency for the analysis: 25.00 Hz

Number of header lines in the file: 9 lines — Number of acceleration values per line: 8 values

Number of layers respect the bedrock to apply the ground motion: 0 layers

Spectrum information — For the response spectrum and for the amplification spectrum

Number of values to be saved: 2407 points — Magnitude of the input motion: 7

Create file? YES — Frequency step: 0.1250 Hz — Acceleration of Gravity: 981 cm/sec²

Array for damping ratios: 0 0.02 0.05 0.1

Comments and Notes: — #SC5B, Borehole @ 294232.5045491, City Council

It is the 1+80 input of the Database — The halfspace layer of ROCK must be setted as the eighth soil type

Only change the values in these fields — The rest of the information is in the Database Sheet

Select the appropriate soil in the Database Sheet — Unselect all the filtering in the Database Sheet

The stress and the strain is saved only for the top sublayer and the ROCK sublayer

Time delay for SHAKE 00:00:02 (hh:mm:ss)

Input file data for SHAKE run

Input file SC5B.txt — Output 1 SC5B-1.txt — Output 2 SC5B-2.txt — Aux file auxiliar.txt — batch runshake.bat

Save input file to disk and RUN Shake — Get the results from Shake

GAN FREQUENCY = 15.800 Hz

MAXIMUM AMPLIFICATION = 8.900

FOR FREQUENCY = 24.880 Hz

Maximum of acceleration for outcrop = 0.3027 g

(Do not move the locations of the cells. It will alterate the behaviour of the macros.)

Interface Sheet / Database / Batch_Quake / Batch_Quake_RESULTS / Soil Types / Response_Spectrum / Shake_Output_Graphs / Soil Types / CADDrafts / Input File / soil-para

Ready

(a) Main interface sheet

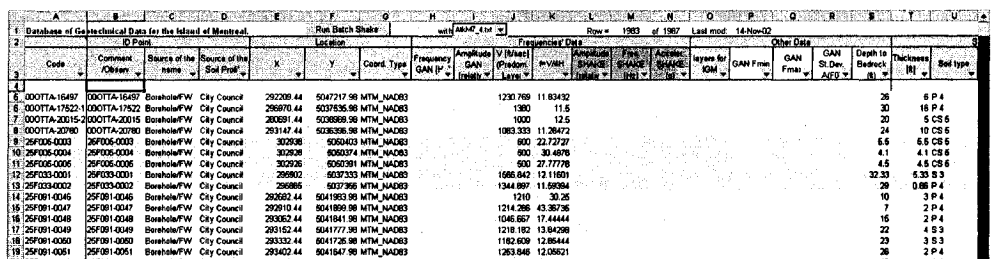

Database of Geotechnical Data for the Island of Montreal — Run Batch Shake — with A6k47_4.txt — Row = 1983 of 1987 — Last mod: 14-Nov-02

Code	Comment /Observ.	Source of the name	Source of the Soil Prof.	X	Y	Coord. Type	Frequency GAN [F	Amplitude GAN [Hz]	V [ft/sec] (Predom. Layer)	n=V/4H	Amplitude SHAKE [Hz]	Fre. SHAKE [Hz]	Amplitud. SHAKE [g]	layers for IGM	GAN Fmax	GAN St.Dev. A/F0	Depth to Bedrock (ft)	Thickness [ft]	Soil type
000TTA-16497	000TTA-16497	Borehole/FW	City Council	292208.44	5047217.98	MTM_NAD83			1230.769	11.83432							26	6	P 4
000TTA-17522-1	000TTA-17522	Borehole/FW	City Council	296970.44	5037635.98	MTM_NAD83			1380	11.5							30	10	P 4
000TTA-20015-2	000TTA-20015	Borehole/FW	City Council	280691.44	5036869.98	MTM_NAD83			1000	12.5							20	5	CS 5
000TTA-20760	000TTA-20760	Borehole/FW	City Council	293147.44	5036396.98	MTM_NAD83			1083.333	11.26472							24	10	CS 5
25F005-0003	25F005-0003	Borehole/FW	City Council	302938	5050403	MTM_NAD83			600	22.72727							5.5	5.5	CS 5
25F005-0004	25F005-0004	Borehole/FW	City Council	302928	5050374	MTM_NAD83			600	30.4878							4.1	4.1	CS 5
25F005-0005	25F005-0005	Borehole/FW	City Council	302926	5050391	MTM_NAD83			600	27.77778							4.5	4.5	CS 5
25F033-0001	25F033-0001	Borehole/FW	City Council	296902	5037333	MTM_NAD83			1666.842	12.11601							32.33	5.33	S 3
25F033-0002	25F033-0002	Borehole/FW	City Council	296865	5037366	MTM_NAD83			1344.897	11.59394							29	0.66	P 4
25F091-0046	25F091-0046	Borehole/FW	City Council	292682.44	5041993.98	MTM_NAD83			1210	30.25							10	3	P 4
25F091-0047	25F091-0047	Borehole/FW	City Council	292910.44	5041899.98	MTM_NAD83			1214.286	43.35795							7	2	P 4
25F091-0048	25F091-0048	Borehole/FW	City Council	293052.44	5041841.98	MTM_NAD83			1046.667	17.44444							15	2	P 4
25F091-0049	25F091-0049	Borehole/FW	City Council	293152.44	5041777.98	MTM_NAD83			1218.182	13.84298							22	4	S 3
25F091-0050	25F091-0050	Borehole/FW	City Council	293332.44	5041725.98	MTM_NAD83			1162.609	12.85444							23	3	S 3
25F091-0051	25F091-0051	Borehole/FW	City Council	293402.44	5041647.98	MTM_NAD83			1263.846	12.05621							26	2	P 4
25F091-0052	25F091-0052	Borehole/FW	City Council	293980.44	5041611.98	MTM_NAD83			1345.455	10.19284							33	4	P 4
25F091-0055	25F091-0055	Borehole/FW	City Council	294194.44	5041251.98	MTM_NAD83			1221.053	18.08648							19	5	P 4
25F108-0001	25F108-0001	Borehole/FW	City Council	295249.44	5035978.98	MTM_NAD83			1872.727	4.256198							110	9	S 3
31F002-44-1	31F002-44	Borehole/FW	City Council	297746	5042270	MTM_NAD83			787.1795	25.23011							7.8	2	S 3
40F001-0011	40F001-0011	Borehole/FW	City Council	293398	5036715	MTM_NAD83			600	4.807692							26	26	CS 5
44OTTA-16896-1	44OTTA-16896	Borehole/FW	City Council	303036.44	5047576.98	MTM_NAD83			1123.188	4.098523							69	2	P 4
45OTTA-15431	45OTTA-15431	Borehole/FW	City Council	292843.44	5041513.98	MTM_NAD83			807.6923	15.53254							13	2	P 4
50OTTA-10708-1	50OTTA-10708	Borehole/FW	City Council	299665.44	5047986.98	MTM_NAD83			553.3333	9.222222							15	14	CS 5
51OTTA-20587-1	51OTTA-20587	Borehole/FW	City Council	294848.44	5039605.98	MTM_NAD83			1260	26.04167							12	2	P 4
52F002-0001-2	52F002-0001	Borehole/FW	City Council	293130	5045335	MTM_NAD83			1473.333	12.27778							30	6	P 4
52OTTA-10701	52OTTA-10701	Borehole/FW	City Council	299669.5	5048264.9	MTM_NAD83			922.2222	12.80864							18	8	CS 5
52OTTA-10709-1	52OTTA-10709	Borehole/FW	City Council	299701.3	5048063.3	MTM_NAD83			638.0952	9.977324							21	9	CS 5
52OTTA-10726-1	52OTTA-10726	Borehole/FW	City Council	299730.4	5048050.5	MTM_NAD83			904.3478	9.829868							23	9	CS 5
52OTTA-14796	52OTTA-14796	Borehole/FW	City Council	295011.44	5041903.98	MTM_NAD83			1035.714	18.4949							14	7	P 4
52OTTA-14797-1	52OTTA-14797	Borehole/FW	City Council	296030.44	5041882.98	MTM_NAD83			600	12.5							10	10	CS 5
53F002-0005	53F002-0005	Borehole/FW	City Council	292485	5047098	MTM_NAD83			1262.5	39.45313							8	1	P 4
53OTTA-14701-1	53OTTA-14701	Borehole/FW	City Council	292196.44	5039034.98	MTM_NAD83			1132	11.32							25	1	S 3
53OTTA-14709	53OTTA-14709	Borehole/FW	City Council	292215.44	5038994.98	MTM_NAD83			1342.742	13.5357							24.8	1	P 4
54F001-0047	54F001-0047	Borehole/FW	City Council	293115	5043177	MTM_NAD83			1234.783	28.8431							11.5	2.5	P 4
54F001-0048	54F001-0048	Borehole/FW	City Council	293056	5043034	MTM_NAD83			1377.313	10.27848							33.5	1.7	P 4
54F001-0053	54F001-0053	Borehole/FW	City Council	292619	5043037	MTM_NAD83			1300	26							13	13	S 3
54F001-0054	54F001-0054	Borehole/FW	City Council	292539	5041872	MTM_NAD83			1300	65							5	5	S 3
54F001-0055	54F001-0055	Borehole/FW	City Council	292473	5041732	MTM_NAD83			1300	36.11111							9	2.5	S 3
54F001-0056	54F001-0056	Borehole/FW	City Council	292412	5041562	MTM_NAD83			1300	16.25							20	7	S 3
54F001-0057	54F001-0057	Borehole/FW	City Council	292362	5041412	MTM_NAD83			1363.636	15.49587							22	10	S 3
54F001-0062	54F001-0062	Borehole/FW	City Council	292062	5040912	MTM_NAD83			1087.097	17.53282							15.5	11	P 4
54F001-0063	54F001-0063	Borehole/FW	City Council	292045	5040818	MTM_NAD83			1064.286	19.0051							14	11	P 4
54F001-0064	54F001-0064	Borehole/FW	City Council	292127	5041003	MTM_NAD83			1300	17.10526							19	9	S 3
54F001-0065	54F001-0065	Borehole/FW	City Council	292167	5041186	MTM_NAD83			1300	20.3125							16	6	S 3
54F003-0001	54F003-0001	Borehole/FW	City Council	291110	5038827	MTM_NAD83			1561.636	11.48599							33.99	3	P 4
54F003-0004	54F003-0004	Borehole/FW	City Council	291116	5038815	MTM_NAD83			1694.444	11.07253							36	2	P 4
54F003-0005	54F003-0005	Borehole/FW	City Council	291127	5038803	MTM_NAD83			1657.576	11.79982							33	2	P 4
54F003-0008	54F003-0008	Borehole/FW	City Council	291145	5038794	MTM_NAD83			1245.455	28.30579							11	2	P 4

Interface Sheet / Database / Batch_Quake / Batch_Quake_RESULTS / Soil Types / Response_Spectrum / Shake_Output_Graphs / Soil Types / CADDrafts / Input File / soil-para

Ready

(b) Database sheet

Figure A-1 Screenshots of *Excel-Shake*

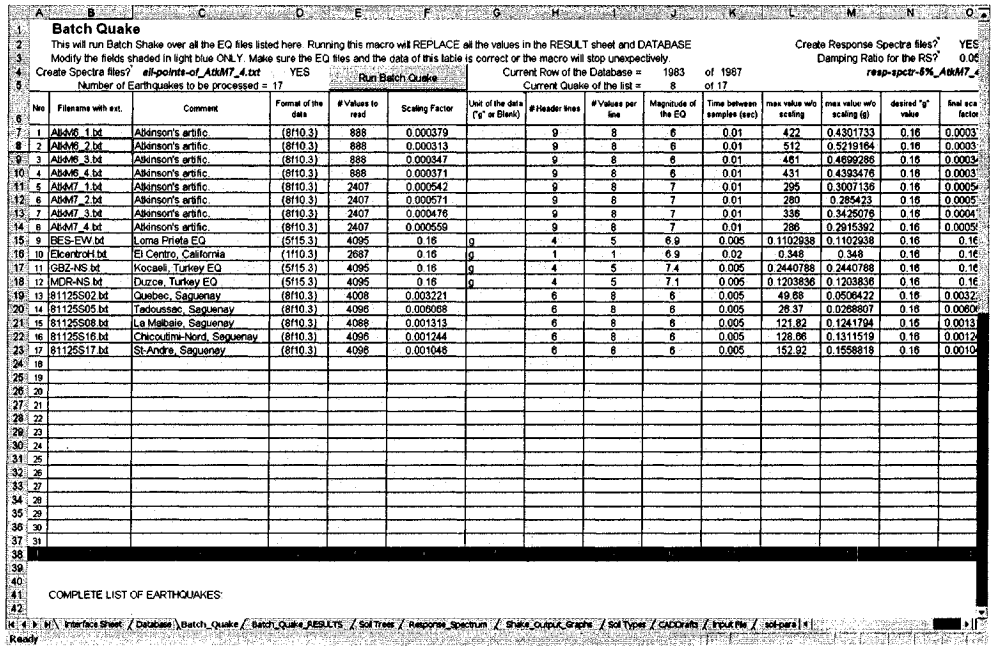

Batch Quake

This will run Batch Shake over all the EQ files listed here. Running this macro will REPLACE all the values in the RESULT sheet and DATABASE

Modify the fields shaded in light blue ONLY. Make sure the EQ files and the data of this table is correct or the macro will stop unexpectively.

Create Spectra files? *all-points-of_AtkM7_4.txt* YES — Run Batch Quake — Current Row of the Database = 1983 of 1967 — Current Quake of the list = 8 of 17

Create Response Spectra files? YES — Damping Ratio for the RS? 0.05 — *resp-spctr-5%_AtkM7_4*

Number of Earthquakes to be processed = 17

No	Filename with ext.	Comment	Format of the data	# Values to read	Scaling Factor	Unit of the data ("g" or Blank)	# Header lines	# Values per line	Magnitude of the EQ	Time between samples (sec)	max value w/o scaling	max value w/o scaling (g)	desired "g" value	final sca factor
1	AtkM6_1.txt	Atkinson's artific.	(8f10.3)	888	0.000379		9	8	6	0.01	422	0.4301733	0.16	0.0003
2	AtkM6_2.txt	Atkinson's artific.	(8f10.3)	888	0.000313		9	8	6	0.01	512	0.5219164	0.16	0.0003
3	AtkM6_3.txt	Atkinson's artific.	(8f10.3)	888	0.000347		9	8	6	0.01	461	0.4699286	0.16	0.0003
4	AtkM6_4.txt	Atkinson's artific.	(8f10.3)	888	0.000371		9	8	6	0.01	431	0.4393476	0.16	0.0003
5	AtkM7_1.txt	Atkinson's artific.	(8f10.3)	2407	0.000542		9	8	7	0.01	295	0.3007136	0.16	0.0005
6	AtkM7_2.txt	Atkinson's artific.	(8f10.3)	2407	0.000571		9	8	7	0.01	280	0.285423	0.16	0.0005
7	AtkM7_3.txt	Atkinson's artific.	(8f10.3)	2407	0.000476		9	8	7	0.01	336	0.3425076	0.16	0.0004
8	AtkM7_4.txt	Atkinson's artific.	(8f10.3)	2407	0.000559		9	8	7	0.01	286	0.2915392	0.16	0.0005
9	BES-EW.txt	Loma Prieta EQ	(5f15.3)	4095	0.16	g	4	5	6.9	0.005	0.1102938	0.1102938	0.16	0.16
10	ElcentroH.txt	El Centro, California	(1f10.3)	2687	0.16	g	1	1	6.9	0.02	0.348	0.348	0.16	0.16
11	GBZ-NS.txt	Kocaeli, Turkey EQ	(5f15.3)	4095	0.16	g	4	5	7.4	0.005	0.2440788	0.2440788	0.16	0.16
12	MDR-NS.txt	Duzce, Turkey EQ	(5f15.3)	4095	0.16	g	4	5	7.1	0.005	0.1203836	0.1203836	0.16	0.16
13	81125S02.txt	Quebec, Saguenay	(8f10.3)	4008	0.003221		6	8	6	0.005	49.88	0.0506422	0.16	0.0032
14	81125S05.txt	Tadoussac, Saguenay	(8f10.3)	4096	0.006068		6	8	6	0.005	26.37	0.0268807	0.16	0.0060
15	81125S08.txt	La Malbaie, Saguenay	(8f10.3)	4068	0.001313		6	8	6	0.005	121.82	0.1241794	0.16	0.0013
16	81125S16.txt	Chicoutimi-Nord, Saguenay	(8f10.3)	4096	0.001244		6	8	6	0.005	128.86	0.1311519	0.16	0.0012
17	81125S17.txt	St-Andre, Saguenay	(8f10.3)	4098	0.001046		6	8	6	0.005	152.92	0.1558819	0.16	0.0010

COMPLETE LIST OF EARTHQUAKES:

Interface Sheet / Database / Batch_Quake / Batch_Quake_RESULTS / Soil Trees / Response Spectrum / Shake_Output_Graphs / Soil Types / CADCrafts / Input File / soil-para

Ready

(c) Earthquake database sheet

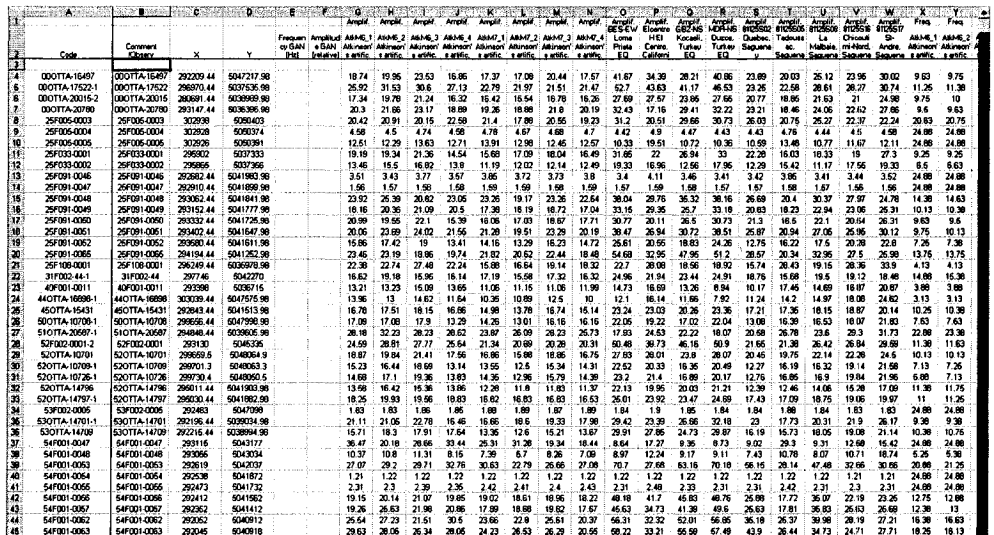

Code	Comment (Query	X	Y	Frequency (Hz)	Amplitude (Relative)	Ampl. AtkM6_1 Atkinson's artific	Ampl. AtkM6_2 Atkinson's artific	Ampl. AtkM6_3 Atkinson's artific	Ampl. AtkM6_4 Atkinson's artific	Ampl. AtkM7_1 Atkinson's artific	Ampl. AtkM7_2 Atkinson's artific	Ampl. AtkM7_3 Atkinson's artific	Ampl. AtkM7_4 Atkinson's artific	Ampl. BES-EW Loma Prieta EQ	Ampl. ElcentroH Elcentro HEI	Ampl. GBZ-NS Kocaeli, Turkey EQ	Ampl. MDR-NS Duzce, Turkey EQ	Ampl. 81125S02 Quebec, Saguena y	Ampl. 81125S05 Tadoussac, Saguenay	Ampl. 81125S08 La Malbaie, Saguenay	Ampl. 81125S16 Chicoutimi-Nord, Saguenay	Ampl. 81125S17 St-Andre, Saguenay	Freq. AtkM6_1 Atkinson's artific	Freq. AtkM6_2 Atkinson's artific
000TTA-16497	000TTA-16497	292209.44	5047217.98			18.74	19.95	23.53	16.85	17.37	17.08	20.44	17.57	41.67	34.39	28.21	40.85	23.89	20.03	25.12	23.95	30.02	9.83	9.75
000TTA-17522-1	000TTA-17522	296870.44	5037535.98			25.92	31.53	30.6	27.13	22.79	21.97	21.51	21.47	52.7	43.63	41.17	46.53	23.26	22.58	28.64	26.27	30.74	11.25	11.38
000TTA-20015-2	000TTA-20015	280691.44	5038969.98			17.34	19.78	21.24	16.32	16.42	16.54	16.78	16.26	27.69	27.57	23.85	27.66	20.77	18.85	21.63	21	24.98	9.75	10
000TTA-20780	000TTA-20780	293147.44	5036396.98			20.3	21.66	23.17	18.89	19.26	18.88	21.8	20.19	32.43	17.16	29.41	32.22	23.21	18.46	24.05	22.62	27.66	9.6	9.63
25F005-0003	25F005-0003	302938	5050403			20.42	20.91	20.15	22.58	21.4	17.89	20.55	19.23	31.2	20.51	29.66	30.73	26.03	20.75	25.37	22.37	22.24	20.63	20.75
25F005-0004	25F005-0004	302928	5050374			4.68	4.5	4.74	4.68	4.78	4.67	4.68	4.7	4.42	4.9	4.47	4.43	4.43	4.76	4.44	4.6	4.68	24.88	24.88
25F005-0005	25F005-0005	302926	5050391			12.51	12.29	13.63	12.71	13.91	12.98	12.45	12.57	10.33	19.51	10.72	10.36	10.59	13.48	10.77	11.67	12.11	24.88	24.88
25F033-0001	25F033-0001	295902	5037333			19.19	19.34	21.36	14.54	15.68	17.09	18.04	16.49	31.65	22	26.94	33	22.28	16.03	18.33	19	27.3	9.25	9.25
25F033-0002	25F033-0002	295865	5037366			13.46	15.5	16.92	13.8	11.19	12.02	12.14	12.49	19.33	16.96	12.56	17.95	12.29	15.42	11.17	17.56	19.33	6.6	6.63
25F091-0046	25F091-0046	292682.44	5041980.98			3.51	3.43	3.77	3.57	3.85	3.72	3.73	3.8	3.4	4.11	3.46	3.41	3.42	3.95	3.41	3.44	3.52	24.88	24.88
25F091-0047	25F091-0047	292910.44	5041898.98			1.56	1.57	1.58	1.58	1.59	1.59	1.58	1.59	1.57	1.59	1.58	1.57	1.57	1.58	1.57	1.58	1.56	24.88	24.88
25F091-0048	25F091-0048	293062.44	5041841.98			23.92	26.39	20.62	23.05	23.26	19.17	23.26	22.64	38.04	28.76	36.32	38.16	26.69	20.4	30.37	27.97	24.76	14.38	14.63
25F091-0049	25F091-0049	293152.44	5041777.98			16.16	20.36	21.09	20.5	17.38	18.19	18.72	17.04	33.16	29.35	25.7	33.18	20.63	18.23	22.94	23.06	25.31	10.13	10.38
25F091-0050	25F091-0050	293332.44	5041725.98			20.99	19.55	22.1	15.39	16.06	17.03	18.67	17.71	30.77	20.11	26.5	30.73	21.3	16.5	22.1	20.64	26.31	9.63	9.6
25F091-0051	25F091-0051	293402.44	5041647.98			20.06	23.89	24.02	21.56	21.28	19.51	23.29	20.19	39.47	26.94	30.72	38.51	25.87	20.54	27.06	25.96	30.12	9.75	10.13
25F091-0052	25F091-0052	293680.44	5041611.98			15.86	17.42	19	13.41	14.16	13.29	16.23	14.72	26.61	20.95	18.83	24.26	12.75	16.22	17.5	20.28	22.8	7.26	7.38
25F091-0065	25F091-0065	294194.44	5041252.98			23.46	23.19	18.86	19.74	21.82	20.62	22.44	18.48	54.69	32.95	47.95	51.2	28.57	20.34	32.95	27.5	25.98	13.75	13.75
25F108-0001	25F108-0001	296249.44	5036978.98			22.36	22.74	27.48	22.24	15.88	16.64	19.14	18.32	22.7	38.08	18.56	19.92	15.74	26.43	19.15	28.36	33.9	4.13	4.13
31F002-44-1	31F002-44	297746	5042270			16.62	19.18	15.96	16.14	17.19	15.58	17.32	16.32	24.96	21.94	23.44	24.91	18.75	15.68	19.5	19.12	18.46	14.88	15.38
40F001-0011	40F001-0011	293398	5036715			13.21	13.23	15.09	13.65	11.05	11.15	11.06	11.99	14.73	16.89	13.26	6.94	10.17	17.45	14.69	18.07	20.87	3.88	3.88
44OTTA-16598-1	44OTTA-16598	301319.44	5047575.98			13.95	13	14.57	11.64	10.35	10.89	12.5	10	12.1	16.4	11.65	7.92	11.24	14.2	14.97	18.08	24.82	3.13	3.13
45OTTA-15431	45OTTA-15431	292843.44	5041513.98			16.78	17.51	18.15	16.66	14.98	13.78	16.74	15.14	23.24	23.03	20.26	23.36	17.21	17.36	18.15	18.87	20.14	10.25	10.38
50OTTA-10708-1	50OTTA-10708	298656.44	5047998.98			17.08	17.08	17.9	13.29	14.26	13.01	16.16	16.16	22.05	19.22	17.02	22.04	13.08	16.39	16.53	18.07	21.83	7.63	7.63
51OTTA-20587-1	51OTTA-20587	294848.44	5039605.98			26.18	32.23	28.23	26.62	23.87	26.09	28.23	25.73	17.93	24.53	22.22	18.07	20.68	26.78	23.6	29.3	31.73	22.88	23.38
52F002-0001-2	52F002-0001	293130	5046335			24.59	28.81	27.77	25.64	21.34	20.69	20.26	20.31	50.48	39.73	46.16	50.9	21.65	21.38	26.42	26.84	29.69	11.38	11.63
52OTTA-10701	52OTTA-10701	298669.6	5048084.9			18.87	19.84	21.41	17.56	16.86	15.88	18.85	16.75	27.83	29.01	23.8	26.07	20.45	19.75	22.14	22.26	24.5	10.13	10.13
52OTTA-10709-1	52OTTA-10709	299701.3	5048063.3			15.23	16.44	18.69	13.14	13.55	12.5	15.34	14.31	22.52	20.33	16.35	20.49	12.27	16.19	16.32	19.14	21.58	7.13	7.25
52OTTA-10726-1	52OTTA-10726	299730.4	5048060.5			14.68	17.1	19.36	13.83	14.35	12.96	15.79	14.39	23.2	21.4	16.89	20.17	12.75	16.85	16.9	19.84	21.96	6.88	7.13
52OTTA-14796	52OTTA-14796	296011.44	5041993.98			13.58	16.42	15.36	13.86	12.28	11.8	11.83	11.37	22.13	19.95	20.03	21.21	12.39	12.46	14.06	15.28	17.09	11.38	11.75
52OTTA-14797-1	52OTTA-14797	296030.44	5041862.98			18.25	19.83	19.56	18.83	16.62	16.83	16.63	16.53	26.01	23.92	23.47	24.89	17.43	17.09	18.75	19.06	19.97	11	11.25
53F002-0005	53F002-0005	292463	5047098			1.83	1.83	1.86	1.86	1.88	1.89	1.87	1.89	1.84	1.9	1.85	1.84	1.84	1.88	1.84	1.83	1.83	24.88	24.88
53OTTA-14701-1	53OTTA-14701	292196.44	5039034.98			21.11	21.05	22.78	16.46	16.66	18.6	19.33	17.98	29.42	23.39	26.66	32.18	23	17.73	20.31	21.9	26.17	9.38	9.38
53OTTA-14709	53OTTA-14709	292216.44	5038994.98			15.71	18.3	17.91	17.64	13.35	12.6	15.21	13.67	29.91	27.86	24.73	29.87	16.19	15.73	18.05	19.08	21.14	10.38	10.75
54F001-0047	54F001-0047	293116	5043177			36.47	30.18	29.66	33.44	26.31	31.28	19.34	18.44	8.64	17.27	9.35	8.73	9.02	29.3	9.31	12.69	15.42	24.88	24.88
54F001-0048	54F001-0048	293066	5043034			10.37	10.8	11.31	8.15	7.39	6.7	8.26	7.09	8.97	12.24	9.17	9.11	7.43	10.78	8.07	10.71	18.74	6.25	6.38
54F001-0053	54F001-0053	292619	5042037			27.07	29.2	29.71	32.76	30.63	22.79	26.66	27.06	70.7	27.68	63.16	70.18	56.15	29.14	47.48	32.66	30.66	20.88	21.25
54F001-0064	54F001-0064	292538	5041872			1.21	1.22	1.22	1.22	1.22	1.22	1.22	1.22	1.22	1.22	1.22	1.22	1.22	1.22	1.22	1.21	1.21	24.88	24.88
54F001-0065	54F001-0065	292473	5041732			2.31	2.3	2.39	2.35	2.42	2.41	2.4	2.43	2.31	2.48	2.33	2.31	2.31	2.42	2.31	2.3	2.31	24.88	24.88
54F001-0066	54F001-0066	292412	5041562			19.15	20.14	21.07	19.65	19.02	18.61	19.96	18.22	48.18	41.7	45.83	48.76	26.88	17.72	36.07	22.19	23.26	12.75	12.88
54F001-0067	54F001-0067	292352	5041412			19.26	26.83	21.98	20.86	17.89	18.88	19.62	17.67	45.63	34.73	41.39	49.5	25.63	17.81	35.93	25.63	26.69	12.38	13
54F001-0062	54F001-0062	292052	5040912			25.64	27.23	21.51	30.5	23.66	22.9	25.81	20.37	56.31	32.32	52.01	56.85	36.19	26.37	39.98	28.19	27.21	16.38	16.63
54F001-0063	54F001-0063	292045	5040918			29.63	28.06	26.34	28.05	24.23	26.53	26.29	20.55	68.22	33.21	55.59	57.49	43.9	26.44	34.73	24.71	27.71	18.25	18.13
54F001-0064	54F001-0064	292127	5041003			22.03	20.81	17.89	18.6	20.27	19.64	20.86	17.18	51.21	31.54	42.39	48.11	27.14	19.2	31.11	26.38	24.64	13.75	13.63
54F001-0065	54F001-0065	292167	5041188			23.72	24.58	20.5	27.62	22.09	21.18	24.04	19.02	56.26	32.78	52.26	54.82	39.54	23.53	35.9	27	26.73	18.6	16.75
54F003-0001	54F003-0001	291110	5038827			24.42	29.78	28.96	28.64	19.97	20.79	22.92	21	56.76	43.91	42	51.2	24.61	24.74	28.67	28.04	30.92	10.63	11
54F003-0004	54F003-0004	291115	5038815			25.74	26.12	27.93	28.27	21.09	19.69	24.07	21.09	51.51	42.83	35.15	50.92	26.37	25.88	29.62	30.37	35.31	10.38	10.5
54F003-0005	54F003-0005	291127	5038803			24.43	29.86	29.91	27.39	19.08	20.83	22.15	20.14	52.76	43.48	39.5	50.69	22.94	22.23	27.44	27.67	29.02	10.88	11.13
54F003-0008	54F003-0008	291145	5038794			6.55	6.09	8.38	6.26	9.09	7.23	7.03	7.18	5.4	24.56	5.84	5.44	5.49	8.39	6.56	5.89	8.49	24.88	24.88
54F003-0009	54F003-0009	291163	5038813			24.44	29.88	29.9	27.51	19.05	20.88	22.17	20.14	52.61	43.34	39.63	51.62	22.99	22.27	27.51	27.81	29.12	10.88	11.13

Interface Sheet / Database / Batch_Quake / Batch_Quake_RESULTS / Soil Trees / Response Spectrum / Shake_Output_Graphs / Soil Types / CADCrafts / Input File / soil-para

Ready

(d) Batch results sheet

Figure A-1(cont) Screenshots of *Excel-Shake*

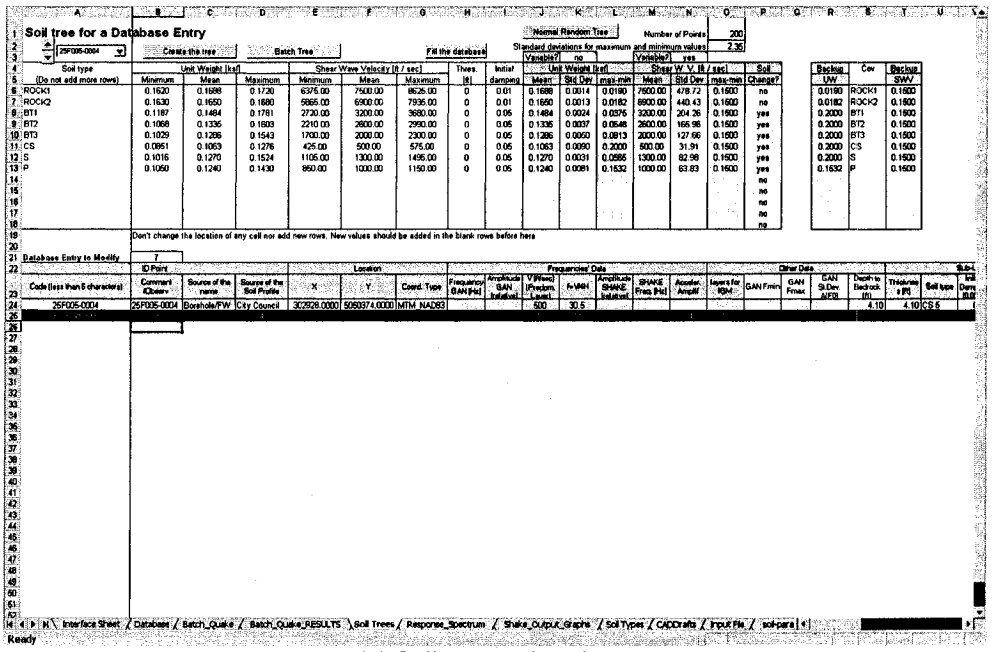

(e) Soil properties sheet

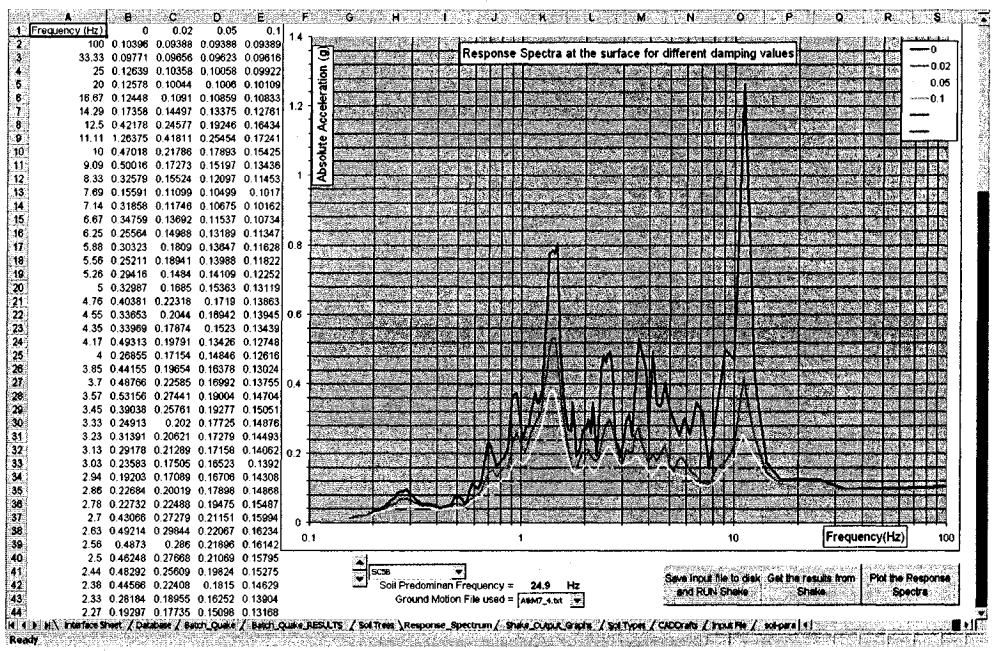

(f) Response spectra sheet

Figure A-1(cont) Screenshots of *Excel-Shake*

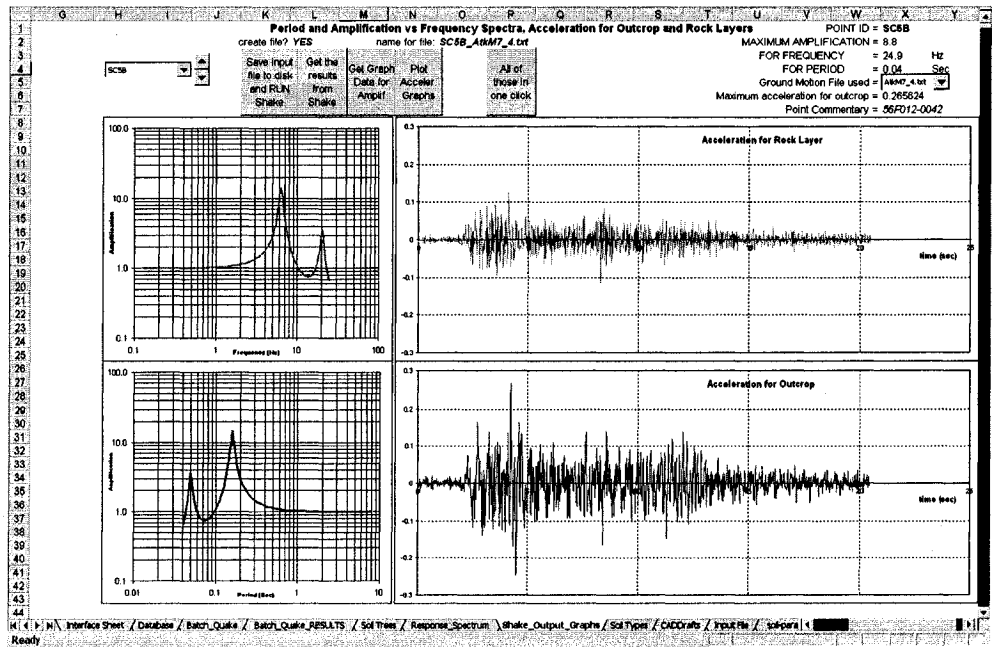

(g) Acceleration and transfer function graphs sheet

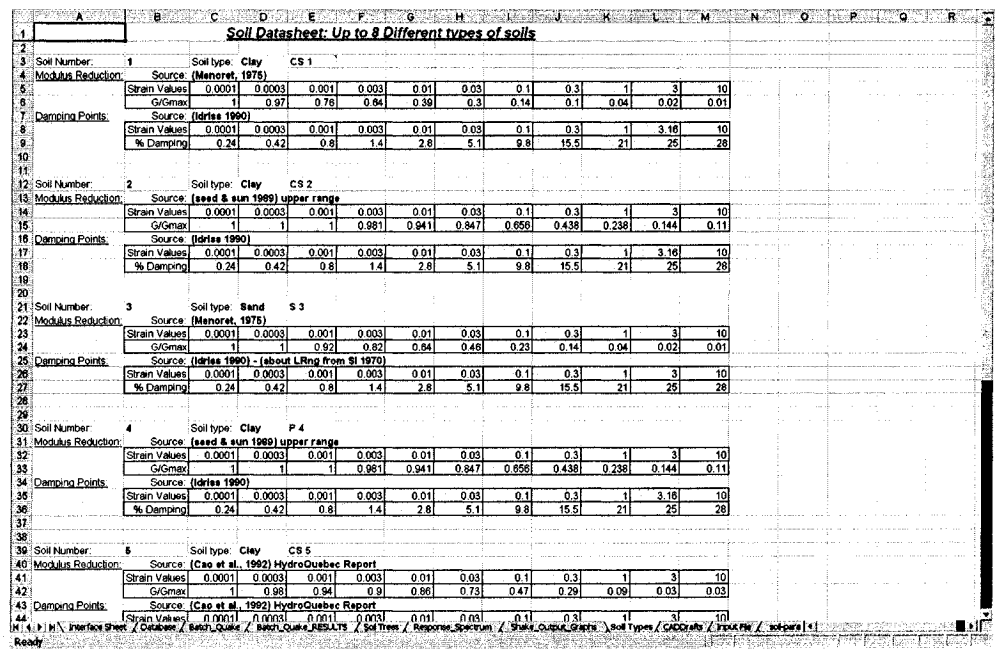

Soil Datasheet: Up to 8 Different types of soils

Soil Number:	1	Soil type: Clay	CS 1										
Modulus Reduction:		Source: (Menoret, 1975)											
	Strain Values	0.0001	0.0003	0.001	0.003	0.01	0.03	0.1	0.3	1	3	10	
	G/Gmax	1	0.97	0.76	0.64	0.39	0.3	0.14	0.1	0.04	0.02	0.01	
Damping Points:		Source: (Idriss 1990)											
	Strain Values	0.0001	0.0003	0.001	0.003	0.01	0.03	0.1	0.3	1	3.16	10	
	% Damping	0.24	0.42	0.8	1.4	2.8	5.1	9.8	15.5	21	25	28	
Soil Number:	2	Soil type: Clay	CS 2										
Modulus Reduction:		Source: (seed & sun 1989) upper range											
	Strain Values	0.0001	0.0003	0.001	0.003	0.01	0.03	0.1	0.3	1	3	10	
	G/Gmax	1	1	1	0.981	0.941	0.847	0.656	0.438	0.238	0.144	0.11	
Damping Points:		Source: (Idriss 1990)											
	Strain Values	0.0001	0.0003	0.001	0.003	0.01	0.03	0.1	0.3	1	3.16	10	
	% Damping	0.24	0.42	0.8	1.4	2.8	5.1	9.8	15.5	21	25	28	
Soil Number:	3	Soil type: Sand	S 3										
Modulus Reduction:		Source: (Menoret, 1975)											
	Strain Values	0.0001	0.0003	0.001	0.003	0.01	0.03	0.1	0.3	1	3	10	
	G/Gmax	1	1	0.92	0.82	0.64	0.46	0.23	0.14	0.04	0.02	0.01	
Damping Points:		Source: (Idriss 1990) - (about LRng from SI 1970)											
	Strain Values	0.0001	0.0003	0.001	0.003	0.01	0.03	0.1	0.3	1	3	10	
	% Damping	0.24	0.42	0.8	1.4	2.8	5.1	9.8	15.5	21	25	28	
Soil Number:	4	Soil type: Clay	P 4										
Modulus Reduction:		Source: (seed & sun 1989) upper range											
	Strain Values	0.0001	0.0003	0.001	0.003	0.01	0.03	0.1	0.3	1	3	10	
	G/Gmax	1	1	1	0.981	0.941	0.847	0.656	0.438	0.238	0.144	0.11	
Damping Points:		Source: (Idriss 1990)											
	Strain Values	0.0001	0.0003	0.001	0.003	0.01	0.03	0.1	0.3	1	3.16	10	
	% Damping	0.24	0.42	0.8	1.4	2.8	5.1	9.8	15.5	21	25	28	
Soil Number:	5	Soil type: Clay	CS 5										
Modulus Reduction:		Source: (Cao et al., 1992) HydroQuebec Report											
	Strain Values	0.0001	0.0003	0.001	0.003	0.01	0.03	0.1	0.3	1	3	10	
	G/Gmax	1	0.98	0.94	0.9	0.86	0.73	0.47	0.29	0.09	0.03	0.03	
Damping Points:		Source: (Cao et al., 1992) HydroQuebec Report											
	Strain Values	0.0001	0.0003	0.001	0.003	0.01	0.03	0.1	0.3	1	3	10	

(h) Soil dynamic properties sheet

Figure A-1(cont) Screenshots of *Excel-Shake*

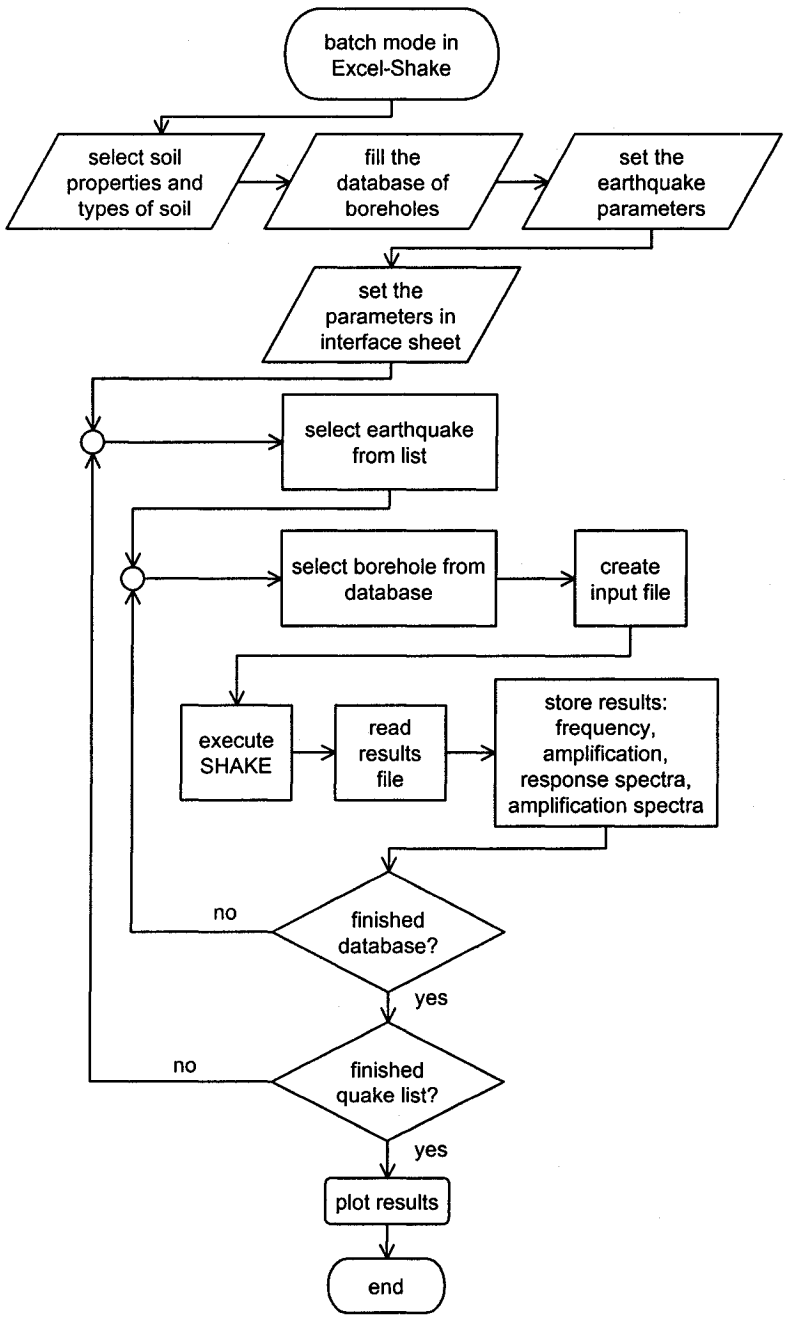

Figure A-2 Flow chart for *Excel-Shake*

Appendix B – Ruaumoko Helper

Ruaumoko Helper is an application developed within *Microsoft Excel* ® Visual Basic, to perform systematic calculations using *Ruaumoko 3D* (Carr, 2001) for a user-defined structural model. The main feature of the program is the batch computation of a finite number of structural analyses to be used under the Incremental Dynamic Analysis approach.

B.1 Ruaumoko 3D and Incremental Dynamic Analysis

The program *Ruaumoko 3D*, developed by Carr (2001), is a useful tool for the inelastic dynamic analysis of three-dimensional structures. It can also permit performing: static analysis, modal analysis, dynamic analysis (with either input ground motions or dynamic forces), and pushover analysis, among other things. The program analyses structures under reversed cyclic loading, including the influence of P-Delta effects in the analysis. The program can model a large variety of elements (frame, spring, damper, tendon, masonry, etc). Nevertheless, one of the most powerful features is the introduction of 43 different hysteresis rules for frame and spring elements. This research project focused in one of the most widely accepted hysteresis rule: Takeda.

An application of the Incremental Dynamic Analysis (IDA) method was described in Chapter 5 and Chapter 6. The method, described in Chapter 2, can be summarized as:

(1) A non-linear structural model is developed. The fundamental period of the structure is calculated.

(2) A set of performance parameters is selected for key structural elements. Typical parameters are: maximum curvature, maximum axial loads (tension and compression), maximum moments, and maximum ductility.

(3) A set of accelerograms or input ground motions is selected. Their response spectra (5% damping) are calculated.

(4) An increasing target spectral acceleration is selected from within a pre-defined range (e.g., 0.015 g to 1.6 g). The accelerograms are scaled to match the target spectral acceleration evaluated at the fundamental period of the structure.

(5) The structure is repeatedly analyzed with each scaled accelerogram. The analysis is repeated until the desired spectral acceleration range has been covered. The performance parameters are extracted from the results.

(6) The results for each accelerogram are graphically presented, with the performance parameters (i.e., maximum curvature) in the X-axis and the spectral accelerations in the Y-axis. A median curve, from the median values at each spectral acceleration level, is plotted from the combination of all the accelerograms in the set.

B.2 Description of Ruaumoko Helper

The application *Ruaumoko Helper* is a workbook of *Microsoft Excel*®, which by using Visual Basic macros interacts with Ruaumoko 3D in creating the input files, running the program, and reading the output files. Visual Basic was chosen for its simplicity of use and openness for modification. New modules and modifications can be added quickly to suit the problem being solved. A copy of *Ruaumoko 3D* and *Microsoft Excel*, as well as some input ground motion files, are necessary to run the application.

The main functions of the *Ruaumoko Helper* application are:

- Store the information of a structural model in the workbook.
- Construct the input file for Ruaumoko 3D based on the structural model.
- Specify the type of loading, loads, and the ground motion files from a pre-selected list.
- Execute Ruaumoko 3D within Excel and read the results file.

- Execute a set of analysis of the same structure using pre-scaled ground motion records.
- Perform the above as part of the IDA; store the main results in a table and in output files. This process is performed with minimum user intervention.
- Plot selected IDA graphs.
- Create the script commands necessary for plotting the structure layout in *AutoCAD*.

The main worksheets of the *Ruaumoko Helper* application are shown in Figure B-1. The information relative to the project is stored in the different sheets: the files and directories, the analysis parameters, the nodes and elements locations, the element properties, the ground motion record information, and the information relative to the IDA are defined in the sheets.

B.3 Flow diagram for Ruaumoko Helper

The procedure followed by *Ruaumoko Helper* when performing batch IDA is illustrated in Figure B-2. The process follows the procedure described for the IDA. In every execution, *Ruaumoko Helper* saves the input files and keeps the output files after running *Ruaumoko 3D*. The output file is then read and the parameters of interest are stored separately in a worksheet and text file before going to the next iteration. The output files are kept after the analysis to allow the post processing of the results or the reading of new information without the need to perform the IDA again.

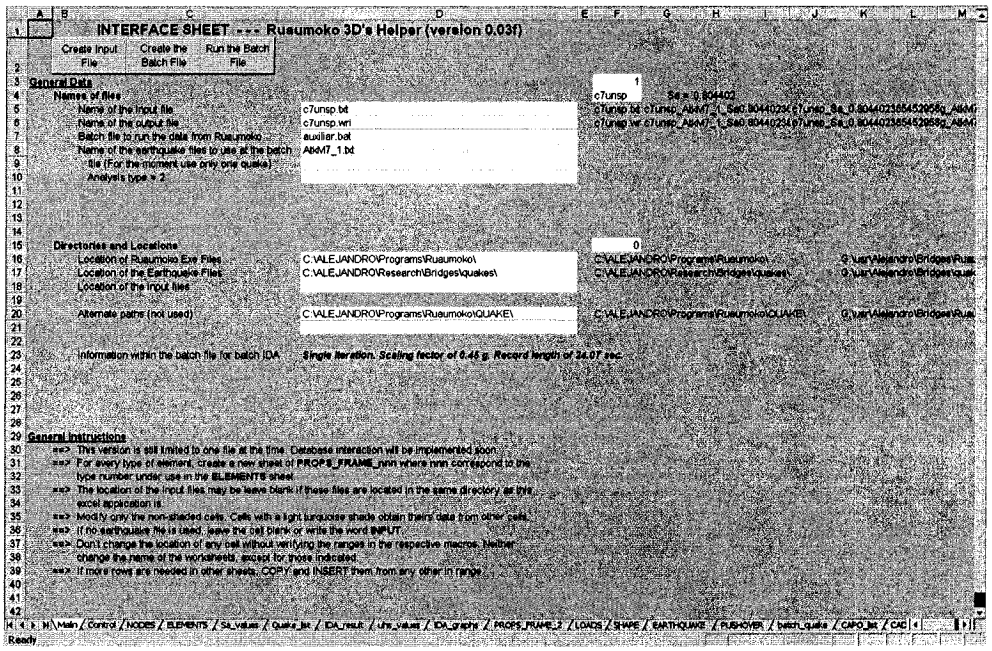

(a) Main interface and file sheet

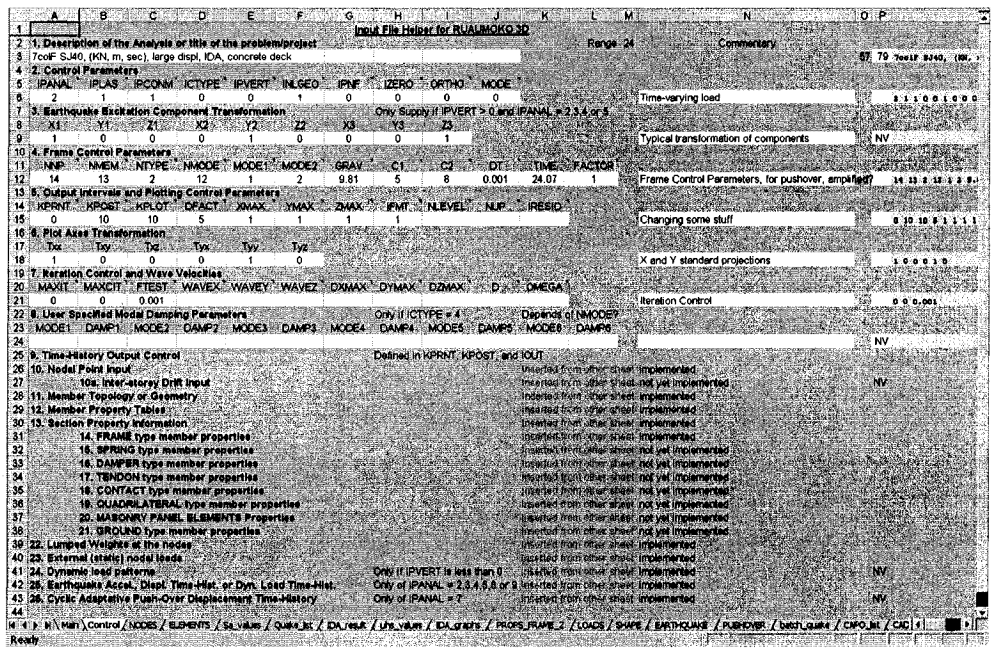

(b) Model input definition sheet

Figure B-1 Screenshots of *Ruaumoko Helper*

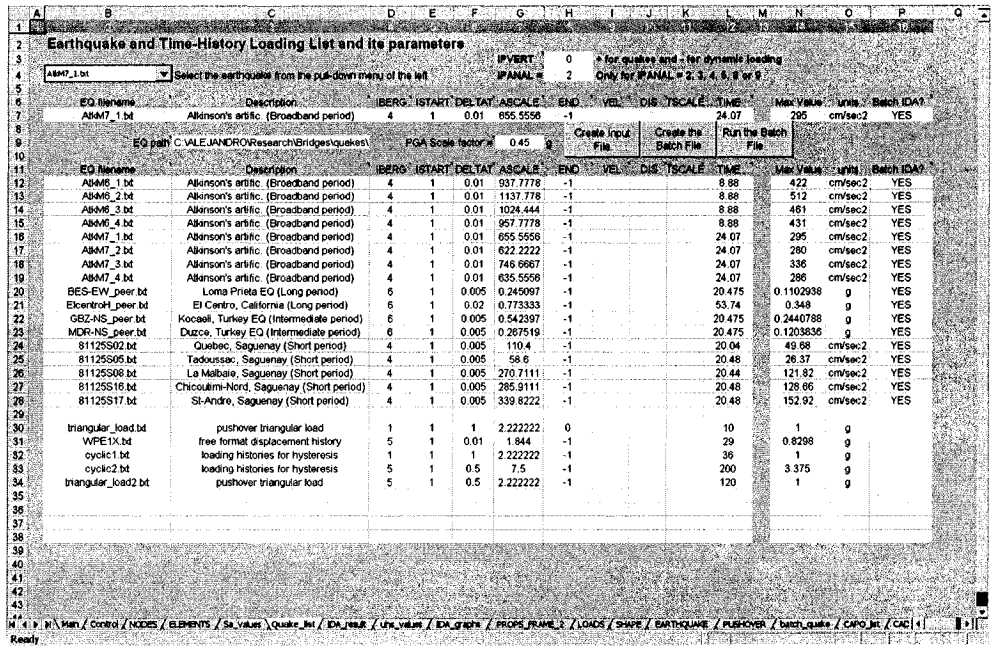

Earthquake and Time-History Loading List and its parameters

IPVERT = 0 + for quakes and - for dynamic loading

IPANAL = 2 Only for IPANAL = 2, 3, 4, 5, 6 or 9

Select the earthquake from the pull-down menu of the left

EQ path: C:\ALEJANDRO\Research\Bridges\quakes\

PGA Scale factor = 0.45 g

Create Input File | Create the Batch File | Run the Batch File

EQ filename	Description	IBERG	ISTART	DELTAT	ASCALE	END	VEL	DIS	TSCALE	TIME	Max Value	units	Batch IDA?
AtkM7_1.txt	Atkinson's artific. (Broadband period)	4	1	0.01	655.5556	-1				24.07	295	cm/sec2	YES
AtkM6_1.txt	Atkinson's artific. (Broadband period)	4	1	0.01	937.7778	-1				8.88	422	cm/sec2	YES
AtkM6_2.txt	Atkinson's artific. (Broadband period)	4	1	0.01	1137.778	-1				8.88	512	cm/sec2	YES
AtkM6_3.txt	Atkinson's artific. (Broadband period)	4	1	0.01	1024.444	-1				8.88	461	cm/sec2	YES
AtkM6_4.txt	Atkinson's artific. (Broadband period)	4	1	0.01	957.7778	-1				8.88	431	cm/sec2	YES
AtkM7_1.txt	Atkinson's artific. (Broadband period)	4	1	0.01	655.5556	-1				24.07	295	cm/sec2	YES
AtkM7_2.txt	Atkinson's artific. (Broadband period)	4	1	0.01	622.2222	-1				24.07	280	cm/sec2	YES
AtkM7_3.txt	Atkinson's artific. (Broadband period)	4	1	0.01	746.6667	-1				24.07	336	cm/sec2	YES
AtkM7_4.txt	Atkinson's artific. (Broadband period)	4	1	0.01	635.5556	-1				24.07	286	cm/sec2	YES
BES-EW_peer.txt	Loma Prieta EQ (Long period)	6	1	0.005	0.245097	-1				20.475	0.1102938	g	YES
ElcentroH_peer.txt	El Centro, California (Long period)	6	1	0.02	0.773333	-1				53.74	0.348	g	YES
GBZ-NS_peer.txt	Kocaeli, Turkey EQ (Intermediate period)	6	1	0.005	0.542397	-1				20.475	0.2440788	g	YES
MDR-NS_peer.txt	Duzce, Turkey EQ (Intermediate period)	6	1	0.005	0.267519	-1				20.475	0.1203836	g	YES
81125S02.txt	Quebec, Saguenay (Short period)	4	1	0.005	110.4	-1				20.04	49.68	cm/sec2	YES
81125S05.txt	Tadoussac, Saguenay (Short period)	4	1	0.005	58.6	-1				20.48	26.37	cm/sec2	YES
81125S08.txt	La Malbaie, Saguenay (Short period)	4	1	0.005	270.7111	-1				20.44	121.82	cm/sec2	YES
81125S16.txt	Chicoutimi-Nord, Saguenay (Short period)	4	1	0.005	285.9111	-1				20.48	128.66	cm/sec2	YES
81125S17.txt	St-Andre, Saguenay (Short period)	4	1	0.005	339.8222	-1				20.48	152.92	cm/sec2	YES
triangular_load.txt	pushover triangular load	1	1	1	2.222222	0				10	1	g	
WPE1X.txt	free format displacement history	5	1	0.01	1.844	-1				29	0.8298	g	
cyclic1.txt	loading histories for hysteresis	1	1	1	2.222222	-1				36	1	g	
cyclic2.txt	loading histories for hysteresis	5	1	0.5	7.5	-1				200	3.375	g	
triangular_load2.txt	pushover triangular load	5	1	0.5	2.222222	-1				120	1	g	

Main / Control / NODES / ELEMENTS / Sa_values / Quake_txt / IDA_result / uns_values / IDA_graphs / PROPS_FRAME_2 / LOADS / SHAPE / EARTHQUAKE / PUSHOVER / batch_quake / CAPO_txt / CAC

Ready

(c) Earthquake and time-history loading list sheet

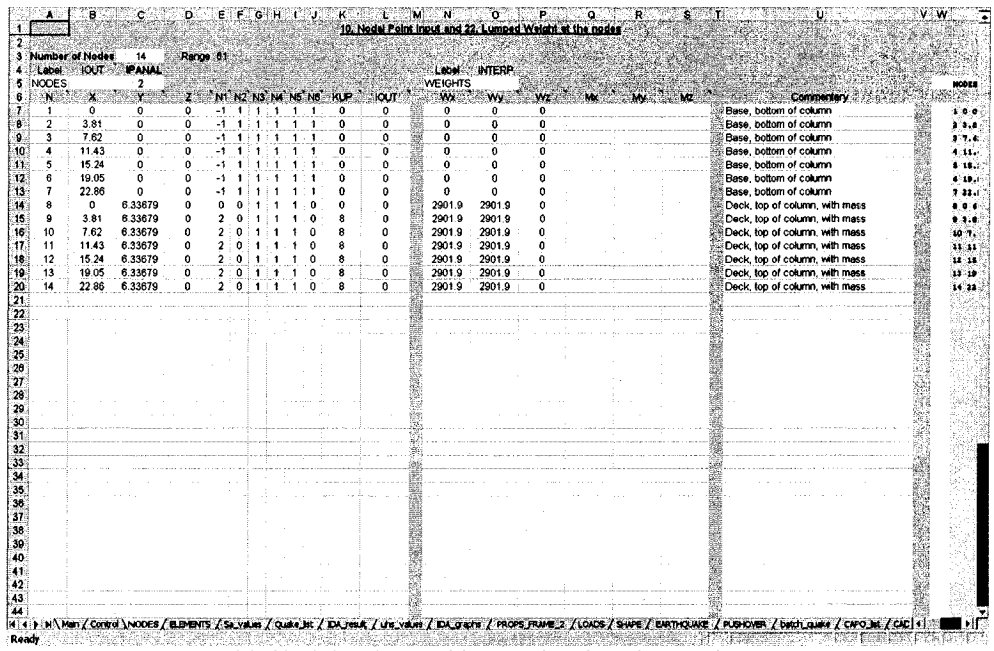

10. Nodal Point Input and 22. Lumped Weight at the nodes

Number of Nodes 14 Range 61

Label IOUT IPANAL

NODES 2

Label INTERP

WEIGHTS

N	X	Y	Z	N1	N2	N3	N4	N5	N6	KUP	IOUT	Ww	Wy	Wz	Mx	My	Mz	Commentary
1	0	0	0	-1	1	1	1	1	1	0	0	0	0	0				Base, bottom of column
2	3.81	0	0	-1	1	1	1	1	1	0	0	0	0	0				Base, bottom of column
3	7.62	0	0	-1	1	1	1	1	1	0	0	0	0	0				Base, bottom of column
4	11.43	0	0	-1	1	1	1	1	1	0	0	0	0	0				Base, bottom of column
5	15.24	0	0	-1	1	1	1	1	1	0	0	0	0	0				Base, bottom of column
6	19.05	0	0	-1	1	1	1	1	1	0	0	0	0	0				Base, bottom of column
7	22.86	0	0	-1	1	1	1	1	1	0	0	0	0	0				Base, bottom of column
8	0	6.33679	0	0	0	1	1	1	0	0	0	2901.9	2901.9	0				Deck, top of column, with mass
9	3.81	6.33679	0	2	0	1	1	1	0	8	0	2901.9	2901.9	0				Deck, top of column, with mass
10	7.62	6.33679	0	2	0	1	1	1	0	8	0	2901.9	2901.9	0				Deck, top of column, with mass
11	11.43	6.33679	0	2	0	1	1	1	0	8	0	2901.9	2901.9	0				Deck, top of column, with mass
12	15.24	6.33679	0	2	0	1	1	1	0	8	0	2901.9	2901.9	0				Deck, top of column, with mass
13	19.05	6.33679	0	2	0	1	1	1	0	8	0	2901.9	2901.9	0				Deck, top of column, with mass
14	22.86	6.33679	0	2	0	1	1	1	0	8	0	2901.9	2901.9	0				Deck, top of column, with mass

Main / Control / NODES / ELEMENTS / Sa_values / Quake_txt / IDA_result / uns_values / IDA_graphs / PROPS_FRAME_2 / LOADS / SHAPE / EARTHQUAKE / PUSHOVER / batch_quake / CAPO_txt / CAC

Ready

(d) Nodal point and lumped weight input sheet

Figure B-1(cont) Screenshots of *Ruaumoko Helper*

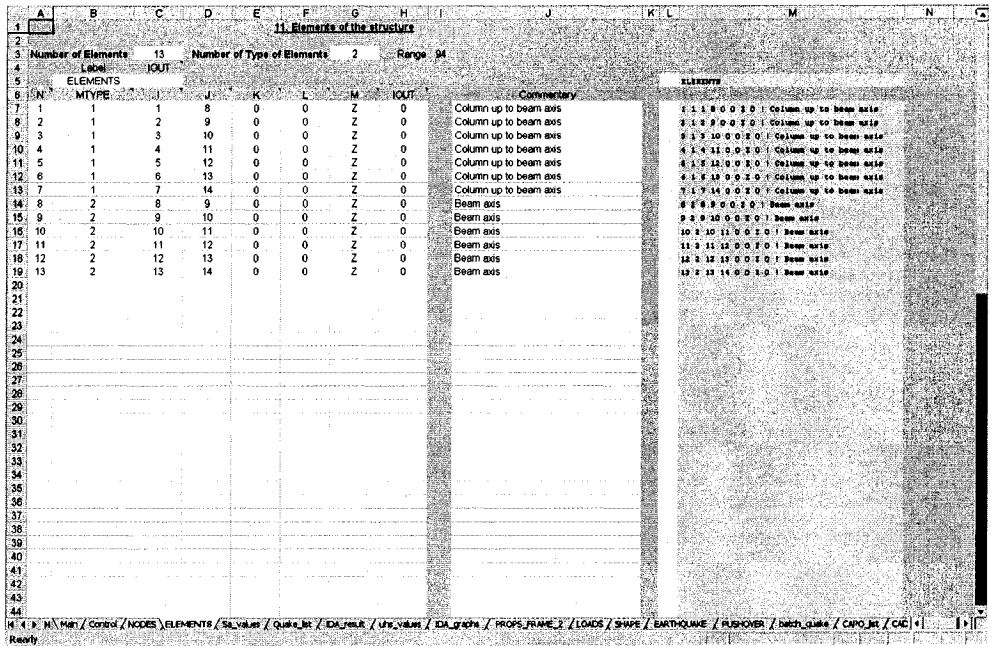

(e) Element assignation sheet

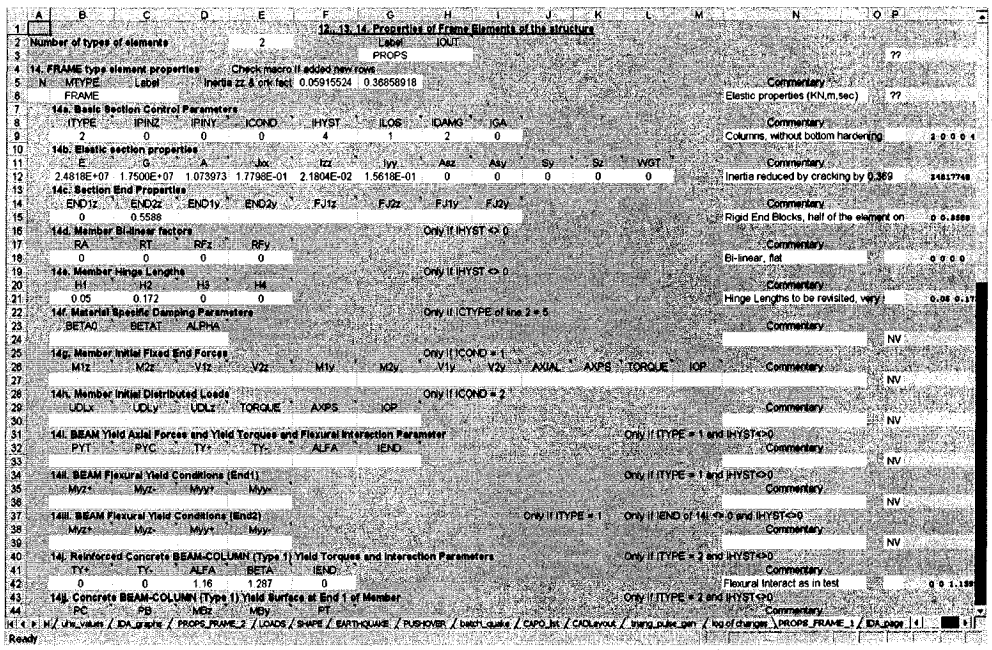

(f) Element properties sheet (one per type of element)

Figure B-1(cont) Screenshots of *Ruaumoko Helper*

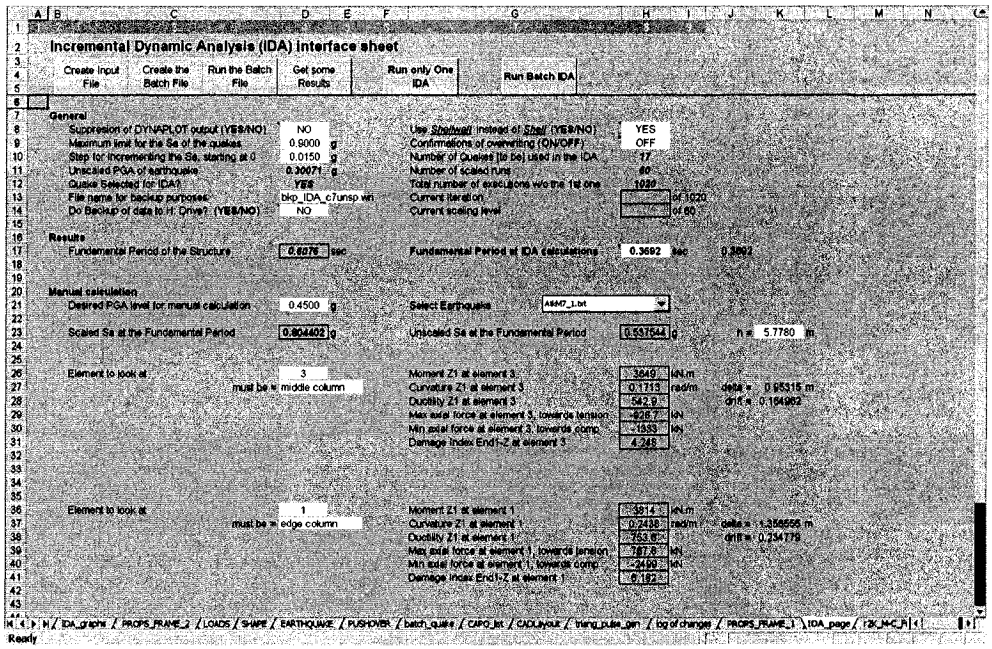

(g) IDA interface sheet

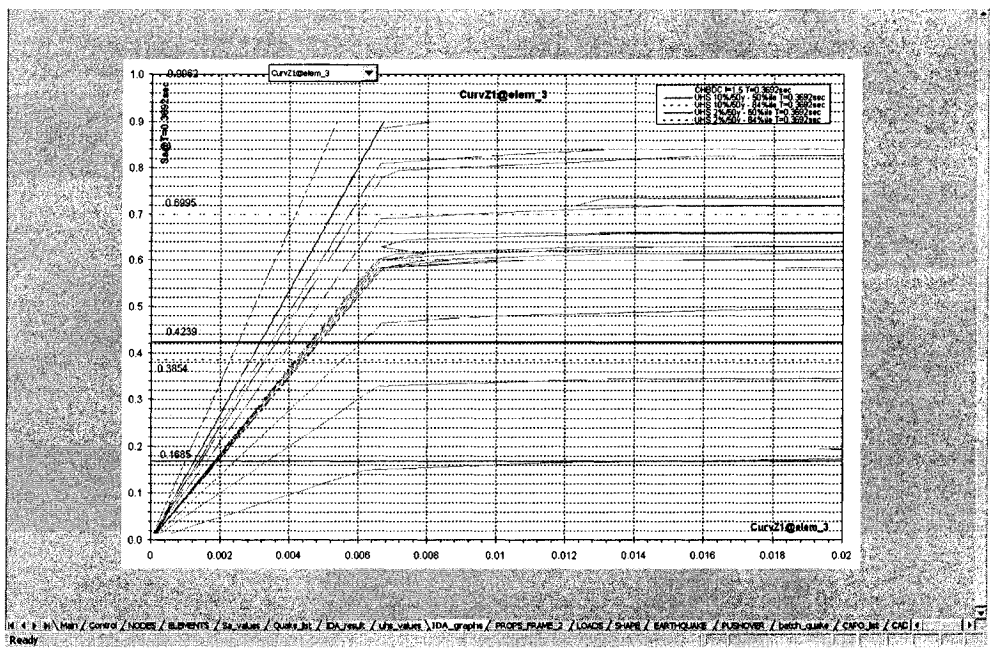

(h) IDA graph sheet

Figure B-1(cont) Screenshots of *Ruaumoko Helper*

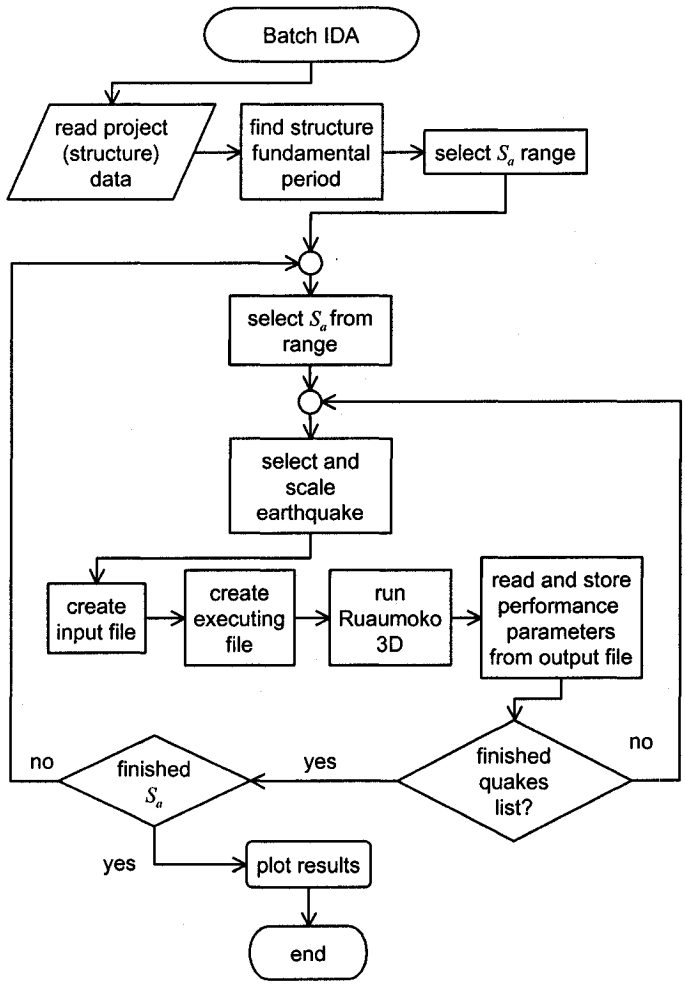

Figure B-2 Flow chart of batch IDA in *Ruaumoko Helper*

Bibliography

Adams, J.; and Atkinson, G. M. (2003). "Development of seismic hazard maps for the proposed 2005 edition of the National Building Code of Canada." *Canadian Journal of Civil Engineering*, 30(2), 255-271.

Adams, J.; Rogers, G.; Halchuk, S.; McCormack, D.; and Cassidy, J. (2002) "The Case for an Advanced National Earthquake Monitoring System for Canada's Cities at Risk." *Seventh U.S. National Conference on Earthquake Engineering (7NCEE)*, Boston, Massachusetts, USA, July 21-25, 2002.

Adams, J.; Weichert, D. H.; and Halchuk, S. (1999). "Trial Seismic Hazard Maps of Canada - 1999 2%/50 Year Values for Selected Canadian Cities." *Open File 3724*, Geological Survey of Canada.

Aguilar, Z.; Salas, L.; and Moreno, R. (2004) "Seismic Microzonation of Moquegua City, Peru." *13th World Conference on Earthquake Engineering*, Vancouver, B.C., Canada, August 1-6, 2004.

Arai, H.; and Tokimatsu, K. (2004). "S-Wave Velocity Profiling by Inversion of Microtremor H/V Spectrum." *Bulletin of the Seismological Society of America*, 94(1), 53-63.

Atakan, K.; Duval, A.-M.; Theodulidis, N.; Guillier, B.; Chatelain, J.-L.; Bard, P.-Y.; and the SESAME Team. (2004) "The H/V Spectral Ratio Technique: Experimental Conditions, Data Processing and Empirical Reliability Assessment." *13th World Conference on Earthquake Engineering*, Vancouver, B.C., Canada, August 1-6, 2004.

Atkinson, G. M.; and Beresnev, I. A. (1998). "Compatible Ground-Motion Time Histories for New National Seismic Hazard Maps." *Canadian Journal of Civil Engineering*, 25(2), 305-318.

Atkinson, G. M.; and Boore, D. M. (1995). "Ground-Motion Relations for Eastern North America." *Bulletin of the Seismological Society of America*, 85(1), 17-30.

Bard, P.-Y.; and SESAME participants. (2004) "The SESAME Project: An Overview and Main Results." *13th World Conference on Earthquake Engineering*, Vancouver, B.C., Canada, August 1-6, 2004.

Bardet, J. P.; Ichii, K.; and Lin, C. H. (2000). "EERA: A Computer Program for Equivalent-linear Earthquake site Response Analyses of Layered Soil Deposits." Department of Civil Engineering, University of Southern California, Los Angeles.

Basheer, P. A. M.; Chidiac, S. E.; and Long, A. E. (1996). "Predictive Models for Deterioration of Concrete Structures." *Construction and Building Materials*, 10(1), 27-37.

Bentz, E. (2001). *Response-2000, Shell-2000, Triax-2000, Membrane-2000: User Manual*, Department of Civil Engineering, University of Toronto, Toronto, Ontario, Canada.

Canadian Standards Association. (2000). *Canadian Highway Bridge Design Code*, CSA International, Toronto.

Carr, A. J. (2001). *RUAUMOKO -- The Maori God of Volcanoes and Earthquakes 3-Dimensional Version*, Department of Civil Engineering - University of Canterbury, Christchurch, New Zealand.

Cornell, C. A. (1968). "Engineering Seismic Risk Analysis." *Bulletin of the Seismological Society of America*, 58(5), 1583-1606.

De la Puente, A.; and Rosset, P. (2002). "Excel Shake Interface User's Manual." *Structural Engineering Series Report No. 2002-02*, Department of Civil Engineering and Applied Mechanics, McGill University, Montreal.

Dimitriu, P.; Kalogeras, I.; and Theodulidis, N. (1999). "Evidence of nonlinear site response in horizontal-to-vertical spectral ratio from near-field earthquakes." *Soil Dynamics and Earthquake Engineering*, 18(6), 423-435.

Dolsek, M.; and Fajfar, P. (2004) "IN2 - A Simple Alternative for IDA." *13th World Conference on Earthquake Engineering*, Vancouver, B.C., Canada, August 1-6, 2004.

Fajfar, P. (2000). "A Nonlinear Analysis Method for Performance-Based Seismic Design." *Earthquake Spectra*, 16(3), 573-592.

Field, E. H.; Hough, S. E.; and Jacob, K. H. (1990). "Using Microtremors to Assess Potential Earthquake Site Response: A Case Study in Flushing Meadows, New York City." *Bulletin of the Seismological Society of America*, 80(6), 1456-1480.

Filiatrault, A.; Tremblay, R.; and Kuan, S. (2004). "Generation of floor accelerations for seismic testing of operational and functional building components." *Canadian Journal of Civil Engineering*, 31(4), 646-663.

Finn, W. D. L.; and Wightman, A. (2003). "Ground motion amplification factors for the proposed 2005 edition of the National Building Code of Canada." *Canadian Journal of Civil Engineering*, 30(2), 272-278.

Frischknecht, C.; Gonzenbach, M.; Rosset, P.; and Wagner, J.-J. (1998) "Estimation of Site Effects in an Alpine Valley. A Comparison Between Ground Ambient Noise Response and 2D Modeling." *11th European Conference on Earthquake Engineering*, Balkema, Rotterdam.

Frischknecht, C.; Rosset, P.; and Wagner, J.-J. (2005). "Toward Seismic Microzonation - 2-D Modeling and Ambient Seismic Noise Measurements: The Case of an Embanked, Deep Alpine Valley." *Earthquake Spectra*, 21(3), 635-651.

Golden Software Inc. (1996). "Surfer 6.04 - Surface Mapping System." http://www.goldensoftware.com/, Golden, Colorado.

Griezic, A. (1996). "Seismic Evaluation and Retrofit of Concrete Bridge Columns and Joints." Ph.D. Thesis, Dept. of Civil Engineering and Applied Mechanics, McGill University, Montreal.

Griezic, A.; Cook, W. D.; and Mitchell, D. (1996) "Seismic Retrofit of Bridge Column-Footing Connections." *11th World Conference on Earthquake Engineering*, Mexico, July 1996.

Griezic, A.; Cook, W. D.; and Mitchell, D. (1999). "Seismic Retrofit of Existing Bridge Columns with Hinges." ACI Special Publication 187 "Seismic Response of Concrete Bridges", August 1999, 205-233.

Guralp. (2000). *Güralp CMG-40T Broadband Seismometer Fact Sheet*, Güralp Systems Limited, Reading, UK.

Idriss, I. M.; and Sun, J. I. (1992). *User's Manual for SHAKE91*, Center for Geotechnical Modeling, Department of Civil & Environmental Engineering, University of California, Davis, California.

Itagawa, W. (2005). "Seismic Response of a Concrete Bridge Bent." Master of Engineering Thesis, Dept. of Civil Engineering and Applied Mechanics, McGill University, Montreal.

Jacob, K. H. (1999). "Site Conditions Effecting Earthquake Loss Estimates for New York City." NYCEM: The New York City Area Consortium for Earthquake Loss Mitigation, New York.

Johnston, J. (1872). "Map of the island and city of Montreal." Bibliothèque nationale du Québec, http://www4.bnquebec.ca/cargeo/htm/TRBA0161.htm, Montreal.

Lacave, C.; Bard, P.-Y.; and Koller, M. G. (1999). "Microzonation: Techniques and Examples." Block 15: Naturgefahren-Erdbebenrisiko, at www.ndk.ethz.ch/downloads/publ/publ_Bl15/Koller.pdf.

Lermo, J.; and Chavez-Garcia, F. J. (1994). "Are microtremors useful in site response evaluation?" *Bulletin of the Seismological Society of America*, 84(5), 1350-1364.

Luco, N.; and Bazzurro, P. (2004). "Effects of Earthquake Record Scaling on Nonlinear Structural Response." *Report on PEER-LL Program Task 1G00 Addendum (Sub-Task 1 of 3)*, Pacific Earthquake Engineering Research Center (PEER).

Luco, N.; and Cornell, C. A. (2001). "Structure-Specific Scalar Intensity Measures for Near-Source and Ordinary Earthquake Ground Motions." *Earthquake Spectra*, Submitted April 2001, http://www.stanford.edu/group/rms/RMS_Papers/pdf/nico/EQ_Spectra01.pdf.

Mackie, K.; and Stojadinovic, B. (2002) "Relation between Probabilistic Seismic Demand Analysis and Incremental Dynamic Analysis." *Seventh U.S. National Conference on Earthquake Engineering (7NCEE)*, Boston, Massachusetts, USA, July 21-25, 2002.

Madriz, R. (2004). "Microzonation of the Island of Montreal." Master of Engineering Thesis, Dept. of Civil Engineering and Applied Mechanics, McGill University, Montreal.

Martirosyan, A.; Dutta, U.; Biswas, N.; Papageorgiou, A.; and Combellick, R. (2002). "Determination of Site Response in Anchorage, Alaska, on the Basis of Spectral Ratio Methods." *Earthquake Spectra*, 18(1), 85-104.

McGuire, R. K. (1995). "Probabilistic Seismic Hazard Analysis and Design Earthquakes: Closing the Loop." *Bulletin of the Seismological Society of America*, 85(5), 1275-1284.

Mitchell, D.; Tinawi, R.; and Law, T. (1989). "The 1988 Saguenay Earthquake - A site visit Report." National Research Council of Canada.

Motamed, R.; and Ghalandarzadeh, A. (2004) "Seismic Microzonation of Urmia City by Means of Microtremor Measurements." *13th World Conference on Earthquake Engineering*, Vancouver, B.C., Canada, August 1-6, 2004.

Mucciarelli, M.; and Gallipoli, M. R. (2004) "The HVSR Technique from Microtremor to Strong Motion: Empirical and Statistical Considerations." *13th World Conference on Earthquake Engineering*, Vancouver, B.C., Canada, August 1-6, 2004.

Nakamura, Y. (1989). "A Method for Dynamic Characteristics Estimation of Subsurface Using Microtremor on the Ground Surface." *Quarterly Report of Railway Technical Research Institute*, 30(1), 25-33.

Nakamura, Y. (2000) "Clear Identification of Fundamental Idea of Nakamura's Technique and Its Applications." *12th World Conference on Earthquake Engineering*, Auckland, New Zealand, 2000.

Nanometrics Inc. (2001). *Orion Manual*, Nanometrics Inc., Ontario, Canada.

NBCC. (2005). *National Building Code of Canada, 2005*, National Research Council of Canada, Ottawa, Ontario.

Newmark, N. M. (1959). "A method of computation for structural dynamic." *Journal of the Engineering Mechanics Division*, 85(EM 3), 67-94.

Ordonez, G. A. (2004). "SHAKE2000: A Computer Program for the 1-D Analysis of Geotechnical Earthquake Engineering Problems." Gustavo A. Ordóñez, http://www.shake2000.com/.

Park, R. (1989). "Evaluation of Ductility of Structures and Structural Assemblages from Laboratory Testings." *Bulletin of the New Zealand National Society for Earthquake Engineering*, 22(3), 155-166.

Prest, V. K.; and Hode Keyser, J. (1977). *Geology and Engineering Characteristics of Surficial Deposits, Montreal Island and vicinity, Quebec*, Energy Mines and Resources Canada, Ottawa.

Previllon, E.; Jacques, M.; Hébert, M.; Campeau, A.; Richard, J.; and Perreault, R. (1979). "Etude Geotechnique Quartier Riviere-des-Prairies (In french)." *Rapport No 78F-25A*, Service Des Travaux Publics, Division Technique, Laboratoire de Controle et Recherche, Ville de Montréal, Montreal.

Priestley, M. J. N.; Seible, F.; and Calvi, G. M. (1996). *Seismic Design and Retrofit of Bridges*, Wiley, New York.

Reiter, L. (1990). *Earthquake Hazard Analysis: Issues and Insights*, Columbia University Press, New York.

Rosset, P. (2002). "SPCRATIO User's Manual: A Tool To Analyse Ambient Noise Records." *Structural Engineering Series Report No. 2002-01*, Department of Civil Engineering and Applied Mechanics, McGill University, Montreal.

Rosset, P.; De la Puente, A.; Chouinard, L.; Mitchell, D.; and Adams, J. (2002) "Seismic Zoning at small scales in urban areas: A tool for preparedness and mitigation." *Improving Post-Disaster Reconstruction In Developing Countries*, Université de Montréal, Montreal, May 25-27 2002.

Rosset, P.; De la Puente, A.; Madriz, R.; Chouinard, L.; Mitchell, D.; and Adams, J. (2003). "Identification of site effects in the Montreal Urban Community, Canada: Pilot study and methodological developments." *Open File Report 3724*, Geological Survey of Canada, Montreal.

Schnabel, P. B.; Lysmer, J.; and Seed, H. B. (1972). "SHAKE, A Computer Program for Earthquake Response Analysis of Horizontally layered sites." *EERC72-12*, University of California, Berkeley, California.

Seed, H. B.; and Idriss, I. M. (1982). *Ground Motions and Soil Liquefaction During Earthquakes*, Earthquake Engineering Research Institute, Berkeley, California.

Shome, N. (1999). "Probabilistic Seismic Demand Analysis of Nonlinear Structures." Ph.D. Thesis, Department of Civil and Environmental Engineering, Stanford university, Stanford, CA.

Siddiqqi, J.; and Atkinson, G. M. (2002). "Ground-Motion Amplification at Rock Sites across Canada as Determined from the Horizontal-to-Vertical Component Ratio." *Bulletin of the Seismological Society of America*, 92(2), 877-884.

Stein, M. L. (1999). *Interpolation of spatial data : some theory for kriging*, Springer, New York.

Studer, J. A.; Koller, M. G.; Loew, S.; and Lateltin, O. (2004) "Classification of Soil Profiles with Corresponding Earthquake Design Spectra for Specific Conditions in Switzerland." *13th World Conference on Earthquake Engineering*, Vancouver, B.C., Canada, August 1-6, 2004.

Theodulidis, N.; Bard, P.-Y.; Archuleta, R.; and Bouchon, M. (1996). "Horizontal-to-Vertical Spectral Ratio and Geological Conditions: The Case of Garner Valley Downhole Array in Southern California." *Bulletin of the Seismological Society of America*, 86(2), 306-319.

Theodulidis, N.; Cultrera, G.; Tento, A.; Faeh, D.; Atakan, K.; Bard, P.-Y.; Panou, A.; Haghshenas, E.; and Team, t. S. (2004) "Empirical Evaluation of the Horizontal-To-Vertical Spectral Ratio Technique: Results from the "SESAME" Project." *13th World Conference on Earthquake Engineering*, Vancouver, B.C., Canada, August 1-6, 2004.

Tinawi, R.; Mitchell, D.; and Law, T. (1990). "Les Dommages dus au Tremblement de Terre du Saguenay du 25 Novembre 1988." *Canadian Journal of Civil Engineering*, 17(3), 366-394.

Tokeshi, J. C.; Karkee, M. B.; Cuadra, C. H.; Sunuwar, L.; and Sugimura, Y. (2004) "Estimation of Amplification Characteristics of the Ground During Moderate Earthquakes Using Simulated Microtremors." *13th World Conference on Earthquake Engineering*, Vancouver, B.C., Canada, August 1-6, 2004.

Tokimatsu, K.; Arai, H.; and Yamazaki, M. (2004) "Multi-Dimensional vs Profiling with Microtremor H/V and Array Techniques." *13th World Conference on Earthquake Engineering*, Vancouver, B.C., Canada, August 1-6, 2004.

Tremblay, R.; and Atkinson, G. M. (2001). "Comparative Study of the Inelastic Seismic Demand of Eastern and Western Canadian Sites." *Earthquake Spectra*, 17(2), 333-358.

Tuladhar, R.; Cuong, N. N. H.; and Yamazaki, F. (2004) "Seismic Microzonation of Hanoi, Vietnam Using Microtremor Observations." *13th World Conference on Earthquake Engineering*, Vancouver, B.C., Canada, August 1-6, 2004.

Uebayashi, H.; Kawabe, H.; and Takeuchi, Y. (2004) "A High-Resolution Modeling Technique of Irregular Subsurface Structures Using H/V Spectral Ratio of Long-Period Microtremors." *13th World Conference on Earthquake Engineering*, Vancouver, B.C., Canada, August 1-6, 2004.

Vamvatsikos, D. (2002). "Seismic Performance, Capacity and Reliability of Structures As Seen through Incremental Dynamic Analysis." Ph.D. Thesis, Department of Civil and Environmental Engineering, Stanford university, Stanford, CA.

Vamvatsikos, D.; and Cornell, C. A. (2002). "Incremental Dynamic Analysis." *Earthquake Engineering and Structural Dynamics*, 31(3), 491-514.

Vanmarcke, E. H. (1979). "Representation of Earthquake Ground Motion: Scaled Accelerograms and Equivalent Response Spectra, State-of-the-Art for Assesing Earthquake Hazards in the United States." *Report 14, Miscellaneous Paper 5-73-1*, U.S. Army Engineer Waterways Experiment Station, Vicksburg, MS.

Wathelet, M.; Jongmans, D.; and Ohrnberger, M. (2004). "Surface-wave inversion using a direct search algorithm and its application to ambient vibration measurements." *Near Surface Geophysics*, 2004(2), 211-221.

Zembaty, Z.; and Rutenberg, A. (2002). "Spatial response spectra and site amplification effects." *Engineering Structures*, 24(11), 1485-1496.

Zhao, J. X.; Irikura, K.; Zhang, J.; Fukushima, Y.; Somerville, P. G.; Asano, A.; Saiki, T.; Okada, H.; and Takahashi, T. (2004) "Site Classification for Strong-Motion Stations in Japan Using H/V Response Spectral Ratio." *13th World Conference on Earthquake Engineering*, Vancouver, B.C., Canada, August 1-6, 2004.

Statement of Originality

To the best of the Author's knowledge, the Original Contributions of this research include:

- ✓ The Microzonation of Montreal, with combined use of field and numerical methods
- ✓ The development of computer program tools (*Excel-Shake*) to help determine the diverse parameters employed in the assessment of the Microzonation of Montreal, especially in the computation of large borehole databases with multiple earthquake scenarios
- ✓ The creation of preliminary maps with the predominant frequency, and the response spectral accelerations, based on the Uniform Hazard Spectra
- ✓ The development of a methodology for the study of the seismic response of two existing highway overpass bridges, using the seismic evaluation method of the Canadian Highway Bridge Design Code and the Incremental Dynamic Analysis approach, including assessment of the influence of spalling of the concrete cover and corrosion of the reinforcement
- ✓ The study of minimum-intervention techniques for the seismic retrofit of two lifeline bridges containing deficiencies typical of bridges built in the 1960's
- ✓ The development of computer program tools (*Ruaumoko Helper*) to help calculate and interpret the seismic response of structures, with the capability of linking the non-linear responses with Incremental Dynamic Analysis